

LOW CYCLE FATIGUE EFFECTS IN THE DAMAGE CAUSED BY
THE MARMARA EARTHQUAKE OF AUGUST 17, 1999

A THESIS SUBMITTED TO
THE GRADUATE SCHOOL OF NATURAL AND APPLIED SCIENCES
OF
MIDDLE EAST TECHNICAL UNIVERSITY

BY

FÝKRÝ ACAR

IN PARTIAL FULFILLMENT OF THE REQUIREMENTS
FOR
THE DEGREE OF DOCTOR OF PHILOSOPHY
IN
CIVIL ENGINEERING

SEPTEMBER 2004

Approval of the Graduate School of Natural and Applied Sciences

Prof. Dr. Canan Özgen
Director

I certify that this thesis satisfies all the requirements as a thesis for the degree of Doctor of Philosophy.

Prof. Dr. Erdal Çokça
Head of Department

This is to certify that we have read this thesis and that in our opinion it is fully adequate, in scope and quality, as a thesis for the degree of Doctor of Philosophy.

Assoc.Prof. Dr. Uður Polat
Co-Supervisor

Prof. Dr. Polat Gülkan
Supervisor

Examining Committee Members:

Prof. Dr. Haluk Sucuođlu (METU,C.E.) _____

Prof. Dr. Polat Gülkan (METU,C.E.) _____

Prof. Dr. Yalçын Mengi (METU,E.S.) _____

Asst.Prof. Dr. Ahmet Yakut (METU,C.E.) _____

Asst.Prof. Dr. Burcu Güneđ (Atýlym University) _____

I hereby declare that all information in this document has been obtained and presented in accordance with academic rules and ethical conduct. I also declare that, as required by these rules and conduct, I have fully cited and referenced all material and results that are not original to this work.

Name, Last name : Fikri Acar

Signature :

ABSTRACT

LOW CYCLE FATIGUE EFFECTS IN THE DAMAGE CAUSED BY THE MARMARA EARTHQUAKE OF AUGUST 17, 1999

ACAR, Fikri

Ph.D., Department of Civil Engineering

Supervisor : Prof. Dr. Polat GÜLKAN

Co-Supervisor : Assoc.Prof. Dr. Uður POLAT

September 2004, 281 pages

This study mainly addresses the problem of estimating the prior earthquake damage on the response of reinforced concrete structures to future earthquakes. The motivation has arisen from the heavy damages or collapses that occurred in many reinforced concrete structures following two major earthquakes that recently occurred in the Marmara Region, Turkey.

The analysis tool employed for this purpose is the package named IDARC2D. Deterioration parameters of IDARC's hysteretic model have been calibrated using a search method. In the calibration process experimental data of a total of twenty-two beam and column specimens, tested under constant and variable amplitude displacement histories, has been used. Fine-tuning of deterioration parameters is essential for more realistic predictions about inelastic behavior and structural damage. In order to provide more realistic damage prediction, three ranges of parameters are proposed.

Some damage controlling structural parameters have been assessed via a large number of two-dimensional section analyses, inelastic time history and damage

analyses of SDOF systems and seismic vulnerability analyses of reinforced concrete buildings.

Inelastic time history and damage analyses of numerous SDOF systems have been carried out to determine whether the loading history has an effect on damage and dissipated hysteretic energy. Then this emphasis is directed to the analyses of MDOF systems. In the analyses of the SDOF systems, various forms of constant and variable amplitude inelastic displacement reversals and synthetic ground motions composed one of the four earthquake records preceded or followed by its modified records acted as a prior or successive earthquake, have been used. The analyses of two five-story R/C buildings have been carried out using synthetic accelerograms comprised of base input provided by the two recorded ground motions.

It is shown that both damage progression and cumulative hysteretic energy dissipated along a path seem to depend on the number and amplitude of cycles constituting the path. However, final damage and accumulated hysteretic energy dissipated along a loading path are independent of the ordering of the same number and amplitude cycles along the path. There is a nonlinear relationship between the earthquake excitation intensity and final damage attained in the end. Increase in the acceleration amplitude leads to exponential increase in damage. As the prior earthquake intensity increases the damage from the succeeding main earthquake decreases. A definite ground motion acting as prior and successive earthquake causes substantially different amounts of damage. Prior earthquake damage does not substantially affect the maximum drift response in future larger earthquakes. A MDOF frame type structure with a prior damage suffers less overall damage in an earthquake in comparison with the one without a prior damage.

Keywords: low cycle fatigue, prior earthquake damage, successive earthquakes, synthetic ground motion, performance based design, damage index, dissipated hysteretic energy, damage control parameter, cyclic loading, inelastic time history analysis, damage analysis, IDARC2D, Kocaeli earthquake, Düzce earthquake.

ÖZ

DÜPÜK DEVÝRLÝ YORULMANIN 17 ADUSTOS 1999 MARMARA DEPREMÝNÝN HASARLARI ÜZERÝNDEKÝ ETKÝLERÝ

ACAR, Fikri

Doktora, Ýnhat Mühendisliði Bölümü

Tez Yöneticisi: Prof. Dr. Polat GÜLKAN

Yardımcý Tez Yöneticisi: Doç. Dr. Uður POLAT

Eylül 2004, 281 sayfa

Bu arařtırmanın temel amacı, geçmiş deprem hasarlarının, betonarme yapıların sonradan maruz kalabilecekleri depremlerdeki davranışlarına olan etkilerini irdelemektir. Bu çalışmanın hareket noktası ise Marmara Bölgesinde en son meydana gelen iki büyük yıkıcı depreme maruz kalarak ağır hasar gören veya yıkılan betonarme yapılar olmuştur.

Bu çalışmada yapılan analizlerde IDARC2D adlı program kullanılmıştır. Programda kullanılan histeretik modelin hasar parametreleri Eđim Arařtırması Metodu ile kalibre edilmiştir. Kalibrasyon işleminde, sabit ve deđiken genlikli tersinir yüklemelere tabi tutulan toplam yirmi-iki adet kolon ve kirişin deney verileri kullanılmıştır. Yapı elemanının davranış ve hasar düzeyine ilişkin gerçekçi sonuçlar elde edilebilmesi için histeretik model hasar parametrelerinin hassas bir şekilde seçilmesi gerektiđi tespit edilmiştir. Gerçekçi hasarın belirlenebilmesi amacıyla farklı hasar durumlarının temsil eden üç ayrı hasar parametreleri kombinasyonu önerilmiştir.

Bazı yapısal özelliklerin hasar üzerindeki etkilerini belirleyebilmek için çok sayıda betonarme kesit analizi, tek dereceli sistemlerin elastik ötesi dinamik ve hasar

analizleri ile depreme maruz kalmıř betonarme sistemlerin sismik hasarlılık analizleri yapılmıřtır.

Yapısal sistemlerin maruz kaldıđı yüklemelerin enerjinin enerji tüketim kapasitesi ve hasar üzerinde etkisinin olup olmadıđını belirleyebilmek için de çok sayıda tek dereceli sistemin elastik ötesi dinamik ve hasar analizi yapılmıřtır. Aynı amaçla benzer etkilerin çok dereceli sistemlerdeki tesirleri de irdelenmiřtir. Tek dereceli sistem analizlerinde sabit ve deđik genlikli çeřitli elastik ötesi yüklemeler ve dört adet deprem kaydından biri ile kendisinden üretilen öncül veya ardçıl olarak etki eden kompozit deprem kayıtları kullanılmıřtır. Beřkatlı iki betonarme binanın analizlerinde ise kaydedilen bu iki yer hareketinin aynı yöndeki kayıtlarının birleřtirilmesiyle elde edilen kompozit yer hareketleri kayıtları kullanılmıřtır. Sözkonusu binalarda Düzce depreminde meydana gelen hasarın dađıllımları ile analitik olarak hesaplanan hasarların dađıllımlarının büyük oranda uyumlu olduđu gözlenmiřtir.

Hasar gelişimi ile tüketilen enerjinin yüklemenin devir sayısı ve genliđine bađlı olduđu görülmüřtür. Ancak, yüklemeye sonunda meydana gelen hasar ile tüketilen enerjinin, yüklemenin aynı genlik ve sayıdaki halkalarının sıralamasına bađlı olmadıđı anlaşılmıřtır. Deprem büyüklüđü ile dođurduđu hasar arasında dođrusal olmayan bir iliřki mevcuttur. Deprem ivme kaydının artmasıyla hasarda çok daha hızlı artıř meydana gelmektedir. Öncül deprem büyüdükçe daha sonra maruz kalınan ana depremdeki hasar azalmaktadır. Ana depremden önce ve sonra meydana gelen belli büyüklükteki bir deprem çok farklı hasarlar dođurmaktadır. Bir yapının öncül depremdeki hasarı, o yapının gelecekteki daha büyük bir depremdeki maksimum yanıl ötelenmesinin üzerinde büyük bir etkisi bulunmamaktadır. Bir depremde, çok dereceli bir yapı sisteminin önceden hasarlı hali, aynı sistemin hasarsız haline göre daha az hasar görmektedir.

Anahtar Kelimeler: düřik devirli yorulma, önceki deprem hasarı, ardıllık depremler, suni yer hareketi, performans tabanlı tasarım, hasar indeksi, tüketilen histeretik enerji, hasar kontrol parametresi, tersinir yüklemeye, elastik ötesi dinamik analiz, hasar analizi, IDARC2D, Kocaeli depremi, Düzce depremi

Dedicated to My Family

ACKNOWLEDGMENTS

I would like to express my deepest appreciation and sincere gratitude for the help, expert guidance, support, suggestions and continual supervision provided by my mentor, Prof. Dr. Polat Gülkan. Thanks are due to Assoc.Prof. Dr. Uður Polat for his suggestions and support.

I would like to offer my sincere thanks to advisory committee members Prof. Dr. Haluk Sucuođlu and Prof. Dr. Yalçýn Mengi for their valuable suggestions, contributions and criticism on the analytical aspects of the study.

I also owe thanks to Dr. Altuđ Erberik for providing experimental data of beam specimens tested by him. The assistance and support of Dr. Sinan Akkar is greatly appreciated.

To my wife, Vildan, I offer sincere thanks for her unshakable faith in me and her endless patience in sharing the vicissitudes of my endeavors. My children, Feyza Ebrar and Ömer Faruk and my brother Ferit, I also thank for understanding my frequent absences. Finally I would like to thank my family for their continuous motivation, support, trust and blessing.

TABLE OF CONTENTS

	Page
PLAGIARISM.....	iii
ABSTRACT.....	iv
ÖZ.....	vi
ACKNOWLEDGMENTS.....	ix
TABLE OF CONTENTS.....	x
LIST OF TABLES.....	xiv
LIST OF FIGURES.....	xvii
LIST OF SYMBOLS.....	xxxii
CHAPTER	
1 INTRODUCTION.....	1
1.1 General.....	1
1.2 Review of Past Work.....	3
1.2.1 Studies on Prior Damage Effects on Performance of Structures.....	4
1.2.2 Studies on Fatigue and Damage Models.....	8
1.3 Object and Scope.....	22
1.4 Description of Contents of Dissertation.....	24
2 LOW CYCLE FATIGUE.....	27
2.1 Introduction.....	27
2.2 Quantification of Damage Through Principles of Low Cycle Fatigue.....	28
2.3 IDARC’s Hysteresis Model Control Parameters.....	32
2.4 Quantification of Damage Using Park and Ang Damage Model.....	36
3 EVALUATION OF EXPERIMENTAL RESULTS.....	39
3.1 General.....	39
3.2 IDARC Hysteresis and Damage Models.....	40
3.3 Response Evaluation.....	41

3.3.1 Pujol Tests.....	43
3.3.1.1 Controlled Variable I: Hoop Spacing.....	46
3.3.1.2 Controlled Variable II: Axial Load Level.....	48
3.3.1.3 Controlled Variable III: Loading History.....	50
3.3.2 Erberik and Sucuođlu Tests.....	52
3.4 Systematic Assessment of Deterioration Parameters.....	59
3.4.1 Deterioration Parameters.....	59
3.4.1.1 Stiffness Degradation Parameter.....	59
3.4.1.2 Strength Deterioration Parameter.....	60
3.4.1.3 Pinching or Slip Parameter.....	60
3.4.2 Calibration of Deterioration Parameters.....	61
3.4.2.1 Method of Calibration.....	62
3.4.2.2 Discussion on Calibration Process.....	63
3.4.2.2.1 Error Variation in Hysteretic Energy Dissipation.....	86
3.4.2.2.2 Error Variation in Damage Index.....	88
3.4.2.3 Sensitivity of Deterioration Parameters to Structural Characteristics.....	91
3.4.2.3.1 Amount of Transverse Reinforcement.....	95
3.4.2.3.2 Axial Load Level.....	102
3.4.2.3.3 Concrete Strength.....	108
3.4.2.3.4 Loading History.....	115
3.4.3 Deterioration Parameters for Several Deterioration Levels.....	118
3.5 Concluding Remarks.....	121
4 ASSESSMENT OF CONTROLLING PARAMETERS ON DAMAGE.....	122
4.1 General.....	122
4.2 Factors Governing Damage.....	123
4.2.1 Effect of Axial Load Level.....	123
4.2.2 Effect of Longitudinal Reinforcement Ratio.....	126
4.2.3 Effect of Concrete Strength.....	127
4.2.4 Effect of Cross-Sectional Area of Load Carrying Members.....	133
4.3 Concluding Remarks.....	139
5 PRIOR AND SUCCESSIVE EARTHQUAKES DAMAGE.....	142
5.1 General.....	142

5.2	Constant Amplitude Loading.....	144
5.3	Variable Amplitude Loading.....	149
5.3.1	Displacement Path Consisting of Two Cycles.....	149
5.3.2	Displacement Path Consisting of Three Cycles.....	151
5.3.3	Variable Amplitude Cyclic Loading Generated from Earthquake Response.....	153
5.4	Successive Earthquake Ground Motions	156
5.4.1	Selected Ground Motions	157
5.4.2	Prior and Successive Earthquakes.....	159
5.4.2.1	Effects Foreshock and Aftershock Damage on Main Shock Damage.....	182
5.4.2.2	Effects Foreshock and Aftershock Damage on Total Damage.....	184
5.5	Concluding Remarks.....	185
6	DAMAGE EVOLUTION FOR SELECTED BUILDINGS SUBJECTED TO REPEATED EARTHQUAKES.....	188
6.1	General.....	188
6.2	Strong Ground Motions in 1999 Marmara and Düzce Earthquakes	189
6.3	Synthetic Ground Motions	192
6.4	Structural Damage.....	194
6.5	Case Study Buildings.....	196
6.5.1	The Ministry of Public Works and Settlement Building at Bolu	196
6.5.1.1	Observed Damage	200
6.5.1.2	2D Modeling and Inelastic Time History and Damage Analyses.....	210
6.5.1.2.1	Transverse (East-West) Direction of Building.....	210
6.5.1.2.2	Longitudinal (North-South) Direction of Building.....	216
6.5.1.3	Discussions on Calculated and Observed Damages	222
6.5.2	Five-Story Private Building in Düzce	223
6.5.2.1	Observed Damage.....	226
6.5.2.2	2D Modeling and Inelastic Time History and Damage Analyses.....	235
6.5.2.2.1	Transverse (East-West) Direction of Building.....	235
6.5.2.2.2	Longitudinal (North-South) Direction of Building.....	244
6.5.2.3	Discussions on Calculated and Observed Damages	247

7 CONCLUSIONS	248
7.1 Summary.....	248
7.2 Conclusions.....	251
7.3 Possible Future Work.....	257
APPENDICES	
A. TABLES OF HYSTERETIC MODEL PARAMETERS TABULATED SEARCH STUDY RESULTS	259
B. STRUCTURAL PROPERTIES AND ENGINEERING AND ARCHITECTURAL DRAWINGS OF THREE BUILDINGS.....	261
C. ENGINEERING AND ARCHITECTURAL DRAWINGS OF FIVE STORY BUILDING.....	268
REFERENCES	272
VITA.....	281

LIST OF TABLES

TABLE	Page
3.1 Properties of R/C beam column test specimens and experimental program.....	42
3.2 Properties of R/C beam column test specimens and appropriate parameter values.....	89
3.3. Proposed range of parameters for deterioration levels of structural systems.....	119
4.1 Effect of concrete strength on seismic performance and damage	129
4.2 Comparison of the sum of the cross-sectional areas of vertical load carrying members to the floor area in both directions of the buildings.....	137
5.1 Damage variation and dissipated energy for VH-111, VH-222 and VH-333.....	144
5.2 Ductility and equivalent number of cycles to failure (N_{eq}) for various concrete strength.....	148
5.3 Damage variation and dissipated energy for VH-12 and VH-21	150
5.4 Damage variation and dissipated energy for VH-123, VH-132 and VH-321.....	151
5.5 Total damage and total damage values for the specimens VH-2 and VH-3.....	154
5.6 Ground motion intensity parameters.....	159
5.7 Synthetic ground motions generated from selected earthquake records.....	160
5.8 Damage values for Pujol column subjected to synthetic ground acceleration histories (El Centro 1940, NS component and its various amplitude foreshocks).....	165

5.9	Damage values for Pujol column subjected to synthetic ground acceleration histories (El Centro 1940, NS component and its various amplitude aftershocks).....	165
5.10	Damage values for Pujol column subjected to synthetic ground acceleration histories (17 August 1999 Marmara Earthquake, Sakarya-EW component and its various amplitude foreshocks).....	170
5.11	Damage values for Pujol column subjected to synthetic ground acceleration histories (17 August 1999 Marmara Earthquake, Sakarya-EW component and its various amplitude aftershocks).....	170
5.12	Damage values for Pujol column subjected to synthetic ground acceleration histories (17 August 1999 Marmara Earthquake, YPT (Yarýmca Petrochemical Complex) Station, NS component and its various amplitude foreshocks).....	175
5.13	Damage values for Pujol column subjected to synthetic ground acceleration histories (17 August 1999 Marmara Earthquake, YPT (Yarýmca Petrochemical Complex) Station, NS component and its various amplitude aftershocks).....	175
5.14	Damage values for Pujol column subjected to synthetic ground acceleration histories (12 November 1999 Düzce Earthquake, Düzce Station, NS component and its various amplitude foreshocks).....	180
5.15	Damage values for Pujol column subjected to synthetic ground acceleration histories (12 November 1999 Düzce Earthquake, Düzce Station, NS component and its various amplitude aftershocks).....	180
5.16	Contribution of foreshock damage to main ground motion damage	183
5.17	Contribution of aftershock damage to main ground motion damage.....	183
5.18	Contribution of foreshock damage to total damage.....	184
5.19	Contribution of aftershock damage to total damage.....	185
6.1	Ground motion intensity parameters.....	192
6.2	Deformation limits (ATC 40, 1996).....	195
6.3	Maximum response values for the transverse (EW) direction of the building.....	214
6.4	Maximum response parameters in the transverse (EW) direction of the building.....	214

6.5	Modal period variations in the transverse (EW) direction of the building.....	216
6.6	Maximum response values for the longitudinal (NS) direction of the building.....	220
6.7	Maximum response parameters in the longitudinal (NS) direction of the building.....	220
6.8	Modal period variations in the longitudinal (NS) direction of the building.....	221
6.9	Maximum response values for the transverse (EW) direction of the building.....	239
6.10	Maximum response parameters in the transverse (EW) direction of the building.....	239
6.11	Modal period variations in the transverse (EW) direction of the building.....	240
6.12	Maximum response values for the longitudinal (NS) direction of the building.....	244
6.13	Maximum response parameters in the longitudinal (NS) direction of the building.....	244
6.14	Modal period variations in the longitudinal (NS) direction of the building.....	246
A.1	Analytical results of dissipated hysteretic energy and damage index for varied values of Hysteretic Model Parameters α , β and γ - Pujol column test specimen C10-2-3N.....	260

LIST OF FIGURES

FIGURE	Page
1.1 Evolving Takeda models	7
1.2 Effect of parameter m on damage index	10
1.3 Column and wall ratios required to limit drift	21
1.4 Prior earthquake damage	23
1.5 Successive earthquake damage	23
2.1 Modeling of IDARC's hysteresis model control parameters	34
3.1 Description of test assembly (dimensions in mm)	44
3.2 Deformed shape of test assembly	44
3.3 Comparison of loading histories and force-drift ratio relationships (Hoop spacing–Test specimen Set 1)	46
3.4 Comparison of loading histories and force-drift ratio relationships (Hoop spacing–Test specimen Set 2)	47
3.5 Comparison of loading histories and force-drift ratio relationships (Axial load-Test specimen Set 1)	48
3.6 Loading history and force-drift ratio relationship (Axial load)	49
3.7 Loading histories and force-drift ratio relationships (Displacement history – Test specimen Set 1)	50
3.8 Loading histories and force-drift ratio relationships (Displacement history – Test specimen Set 2)	51
3.9 Details of beam test specimen (dimensions in mm)	53
3.10 Deformed shape of test specimen	54
3.11 Experimental force-displacement relationships for the specimens ($f_c=20\text{MPa}$) tested under constant amplitude displacement histories	55

3.12	Experimental force-displacement relationships for the specimens ($f_c=13\text{MPa}$) tested under constant amplitude displacement histories.....	56
3.13	Loading histories and experimental force-displacement relationships for the specimens tested under variable amplitude displacement histories.....	57
3.14	Pujol column test specimen C10-2-3 North: a) Surfaces of variation in the dissipated hysteretic energy error ratio for $\alpha=5.0$ and β and γ parameters, b) Surfaces of variation in the damage index error for $\alpha=5.0$ and β and γ parameters, c) Comparison of the experimental (gray curve) and analytical (black curve) force-deformation relationships, d) Analytical progressive damage curve.....	64
3.15	Pujol column test specimen C10-3-1.5 South: a) Surfaces of variation in the dissipated hysteretic energy error ratio for $\alpha=5.0$ and β and γ parameters, b) Surfaces of variation in the damage index error for $\alpha=5.0$ and β and γ parameters, c) Comparison of the experimental (gray curve) and analytical (black curve) force-deformation relationships d) Analytical progressive damage curve.....	65
3.16	Pujol column test specimen C10-3-3 North: a) Surfaces of variation in the dissipated hysteretic energy error ratio for $\alpha=5.0$ and β and γ parameters, b) Surfaces of variation in the damage index error for $\alpha=5.0$ and β and γ parameters, c) Comparison of the experimental (gray curve) and analytical (black curve) force-deformation relationships, d) Analytical progressive damage curve.....	66
3.17	Pujol column test specimen C10-3-2.25 North: a) Surfaces of variation in the dissipated hysteretic energy error ratio for $\alpha=5.0$ and β and γ parameters, b) Surfaces of variation in the damage index error for $\alpha=5.0$ and β and γ parameters, c) Comparison of the experimental (gray curve) and analytical (black curve) force-deformation relationships, d) Analytical progressive damage curve.....	67
3.18	Pujol column test specimen C20-3-3 South: a) Surfaces of variation in the dissipated hysteretic energy error ratio for $\alpha=3.0$ and β and γ parameters, b) Surfaces of variation in the damage index error for $\alpha=3.0$ and β and γ parameters, c) Comparison of the experimental (gray curve) and analytical (black curve) force-deformation relationships, d) Analytical progressive damage curve.....	68
3.19	Pujol column test specimen C10-2-2.25 North: a) Surfaces of variation in the dissipated hysteretic energy error ratio for $\alpha=5.0$ and β and γ parameters, b) Surfaces of variation in the damage index error for $\alpha=5.0$ and β and γ parameters, c) Comparison of the experimental	

(gray curve) and analytical (black curve) force-deformation relationships, d) Analytical progressive damage curve	69
3.20 Pujol column test specimen C10-1-2.25 South: a) Surfaces of variation in the dissipated hysteretic energy error ratio for $\alpha=5.0$ and β and γ parameters, b) Surfaces of variation in the damage index error for $\alpha=5.0$ and β and γ parameters, c) Comparison of the experimental (gray curve) and analytical (black curve) force-deformation relationships, d) Analytical progressive damage curve	70
3.21 Erberik and Sucuođlu beam test specimen CH-1: a) Surfaces of variation in the dissipated hysteretic energy error ratio for $\alpha=7.0$ and β and γ parameters, b) Surfaces of variation in the damage index error for $\alpha=7.0$ and β and γ parameters, c) Comparison of the experimental (gray curve) and analytical (black curve) force-deformation relationships, d) Analytical progressive damage curve	71
3.22 Erberik and Sucuođlu beam test specimen CH-2: a) Surfaces of variation in the dissipated hysteretic energy error ratio for $\alpha=7.0$ and β and γ parameters, b) Surfaces of variation in the damage index error for $\alpha=7.0$ and β and γ parameters, c) Comparison of the experimental (gray curve) and analytical (black curve) force-deformation relationships, d) Analytical progressive damage curve	72
3.23 Erberik and Sucuođlu beam test specimen CH-3: a) Surfaces of variation in the dissipated hysteretic energy error ratio for $\alpha=7.0$ and β and γ parameters, b) Surfaces of variation in the damage index error for $\alpha=7.0$ and β and γ parameters, c) Comparison of the experimental (gray curve) and analytical (black curve) force-deformation relationships, d) Analytical progressive damage curve	73
3.24 Erberik and Sucuođlu beam test specimen CH-4: a) Surfaces of variation in the dissipated hysteretic energy error ratio for $\alpha=7.0$ and β and γ parameters, b) Surfaces of variation in the damage index error for $\alpha=7.0$ and β and γ parameters, c) Comparison of the experimental (gray curve) and analytical (black curve) force-deformation relationships, d) Analytical progressive damage curve	74
3.25 Erberik and Sucuođlu beam test specimen CH-5: a) Surfaces of variation in the dissipated hysteretic energy error ratio for $\alpha=5.0$ and β and γ parameters, b) Surfaces of variation in the damage index error for $\alpha=5.0$ and β and γ parameters, c) Comparison of the experimental (gray curve) and analytical (black curve) force-deformation relationships, d) Analytical progressive damage curve	75
3.26 Erberik and Sucuođlu beam test specimen CH-6: a) Surfaces of variation in the dissipated hysteretic energy error ratio for $\alpha=7.0$ and β and γ parameters, b) Surfaces of variation in the damage index error	

for $\alpha=7.0$ and β and γ parameters, c) Comparison of the experimental (gray curve) and analytical (black curve) force-deformation relationships, d) Analytical progressive damage curve	76
3.27 Erberik and Sucuođlu beam test specimen CL-1: a) Surfaces of variation in the dissipated hysteretic energy error ratio for $\alpha=5.0$ and β and γ parameters, b) Surfaces of variation in the damage index error for $\alpha=5.0$ and β and γ parameters, c) Comparison of the experimental (gray curve) and analytical (black curve) force-deformation relationships, d)Analytical progressive damage curve	77
3.28 Erberik and Sucuođlu beam test specimen CL-2: a) Surfaces of variation in the dissipated hysteretic energy error ratio for $\alpha=5.0$ and β and γ parameters, b) Surfaces of variation in the damage index error for $\alpha=5.0$ and β and γ parameters, c) Comparison of the experimental (gray curve) and analytical (black curve) force-deformation relationships, d) Analytical progressive damage curve	78
3.29 Erberik and Sucuođlu beam test specimen CL-3: a) Surfaces of variation in the dissipated hysteretic energy error ratio for $\alpha=3.0$ and β and γ parameters, b) Surfaces of variation in the damage index error for $\alpha=3.0$ and β and γ parameters, c) Comparison of the experimental (gray curve) and analytical (black curve) force-deformation relationships, d) Analytical progressive damage curve	79
3.30 Erberik and Sucuođlu beam test specimen CL-4: a) Surfaces of variation in the dissipated hysteretic energy error ratio for $\alpha=3.0$ and β and γ parameters, b) Surfaces of variation in the damage index error for $\alpha=3.0$ and β and γ parameters, c) Comparison of the experimental (gray curve) and analytical (black curve) force-deformation relationships, d) Analytical progressive damage curve	80
3.31 Erberik and Sucuođlu beam test specimen CL-5: a) Surfaces of variation in the dissipated hysteretic energy error ratio for $\alpha=2.0$ and β and γ parameters, b) Surfaces of variation in the damage index error for $\alpha=2.0$ and β and γ parameters, c) Comparison of the experimental (gray curve) and analytical (black curve) force-deformation relationships, d) Analytical progressive damage curve	81
3.32 Erberik and Sucuođlu beam test specimen VH-1: a) Surfaces of variation in the dissipated hysteretic energy error ratio for $\alpha=7.0$ and β and γ parameters, b) Surfaces of variation in the damage index error for $\alpha=7.0$ and β and γ parameters, c) Comparison of the experimental (gray curve) and analytical (black curve) force-deformation relationships, d) Analytical progressive damage curve	82
3.33 Erberik and Sucuođlu beam test specimen VH-2: a) Surfaces of variation in the dissipated hysteretic energy error ratio for $\alpha=7.0$ and β	

and γ parameters, b) Surfaces of variation in the damage index error for $\alpha=7.0$ and β and γ parameters, c) Comparison of the experimental (gray curve) and analytical (black curve) force-deformation relationships, d) Analytical progressive damage curve	83
3.34 Erberik and Sucuođlu beam test specimen VH-3: a) Surfaces of variation in the dissipated hysteretic energy error ratio for $\alpha=7.0$ and β and γ parameters, b) Surfaces of variation in the damage index error for $\alpha=7.0$ and β and γ parameters, c) Comparison of the experimental (gray curve) and analytical (black curve) force-deformation relationships, d) Analytical progressive damage curve	84
3.35 Erberik and Sucuođlu beam test specimen VL-1: a) Surfaces of variation in the dissipated hysteretic energy error ratio for $\alpha=5.0$ and β and γ parameters, b) Surfaces of variation in the damage index error for $\alpha=5.0$ and β and γ parameters, c) Comparison of the experimental (gray curve) and analytical (black curve) force-deformation relationships, d) Analytical progressive damage curve	85
3.36 Effect of various characteristics (transverse reinforcement, axial load level and loading history) a) Dissipated hysteretic energy vs. deterioration parameters α , β and γ , b) Dissipated hysteretic energy error ratio vs. deterioration parameters α , β and γ	93
3.37 Effect of various characteristics (transverse reinforcement, axial load level and loading history) a) Damage index vs. deterioration parameters α , β and γ , b) Damage index error ratio vs. deterioration parameters α , β and γ	94
3.38 Effect of amount of transverse reinforcement-Set I a) Dissipated hysteretic energy vs. deterioration parameters α , β and γ , b) Dissipated hysteretic energy error ratio vs. deterioration parameters α , β and γ	96
3.39 Effect of amount of transverse reinforcement-Set I a) Damage index vs. deterioration parameters α , β and γ , b) Damage index error ratio vs. deterioration parameters α , β and γ	97
3.40 Effect of amount of transverse reinforcement-Set II a) Dissipated hysteretic energy vs. deterioration parameters α , β and γ , b) Dissipated hysteretic energy error ratio vs. deterioration parameters α , β and γ	98
3.41 Effect of amount of transverse reinforcement-Set II a) Damage index vs. deterioration parameters α , β and γ , b) Damage index error ratio vs. deterioration parameters α , β and γ	99
3.42 Effect of axial load level a) Dissipated hysteretic energy vs. deterioration parameters α , β and γ , b) Dissipated hysteretic energy error ratio vs. deterioration parameters α , β and γ	100

3.43	Effect of axial load level a) Damage index vs. deterioration parameters α , β and γ , b) Damage index error ratio vs. deterioration parameters α , β and γ	101
3.44	Effect of axial load level on damage	103
3.45	Effect of concrete strength and loading history-Set I a) Dissipated hysteretic energy vs. deterioration parameters α , β and γ , b) Dissipated hysteretic energy error ratio vs. deterioration parameters α , β and γ	104
3.46	Effect of concrete strength and loading history-Set I a) Damage index vs. deterioration parameters α , β and γ , b) Damage index error ratio vs. deterioration parameters α , β and γ	105
3.47	Effect of concrete strength and loading history-Set II a) Dissipated hysteretic energy vs. deterioration parameters α , β and γ , b) Dissipated hysteretic energy error ratio vs. deterioration parameters α , β and γ	106
3.48	Effect of concrete strength and loading history-Set II a) Damage index vs. deterioration parameters α , β and γ , b) Damage index error ratio vs. deterioration parameters α , β and γ	107
3.49	Damage curves for Erberik and Sucuođlu beam test specimens ($f_c=20\text{MPa}$) obtained by using damage model developed by a) Erberik and Sucuođlu and b) Park and Ang.....	110
3.50	Damage curves for Erberik and Sucuođlu beam test specimens ($f_c=13\text{MPa}$) obtained by using Park and Ang damage model.....	110
3.51	Effect of loading history-Set I a) Dissipated hysteretic energy vs. deterioration parameters α , β and γ , b) Dissipated hysteretic energy error ratio vs. deterioration parameters α , β and γ	111
3.52	Effect of loading history-Set I a) Damage index vs. deterioration parameters α , β and γ , b) Damage index error ratio vs. deterioration parameters α , β and γ	112
3.53	Effect of loading history-Set II a) Dissipated hysteretic energy vs. deterioration parameters α , β and γ , b) Dissipated hysteretic energy error ratio vs. deterioration parameters α , β and γ	113
3.54	Effect of loading history-Set II a) Damage index vs. deterioration parameters α , β and γ , b) Damage index error ratio vs. deterioration parameters α , β and γ	114
3.55	Progressive damage curves for the two sets of specimens subjected to variable-amplitude displacement histories (Pujol column specimens).....	116

3.56	Effect of loading history (Erberik and Sucuođlu specimens) a) variable-amplitude displacement histories b) Experimental (gray) and analytical (black) force-displacement curves c) Damage curves.....	117
3.57	Sensitivity analysis of three-parameter model: a) Experiment, b) Simulation using $\alpha=10$, $\beta=0.1$ and $\gamma=0.8$, Mild deteriorating system (MLD), c) Simulation using $\alpha=6$, $\beta=0.3$ and $\gamma=0.5$, Moderate deteriorating system (MOD), d) Simulation using $\alpha=3$, $\beta=0.6$ and $\gamma=0.3$, Severe deteriorating system (SVD).....	120
4.1	Effect of axial load level on moment curvature relationships.....	124
4.2	Strength and ductility of column sections with different values of reinforcement ratio a) Interaction diagrams b) Axial load level versus curvature c) Curvature ductility versus axial load level.....	125
4.3	Effect of concrete strength and longitudinal reinforcement ratio on moment curvature relationships	127
4.4	Cantilever column model properties.....	128
4.5	Effect of concrete strength on drift ratio histories in time domain.....	129
4.6	Effect of concrete strength on base shear histories in time domain.....	130
4.7	Effect of concrete strength on damage; a) progressive damage variation curves, b) total damage and their components.....	132
4.8	Moment curvature relationships for various cross-sectional areas.....	133
4.9	The ground acceleration histories of May 1, 2003 Bingöl earthquake, Bingöl Ministry of Public Work and Settlement Office Station records.....	134
4.10	Location of the epicenter (star), the strong motion record station (circle) and the investigated buildings (square).....	135
4.11	Key plan showing locations of buildings	135
4.12	Damage data for the principal directions of three buildings.....	138
5.1	Constant amplitude loading histories, damage progression curves and force-displacement relationships.....	145
5.2	Damage progression curves for constant amplitude displacement cycles of various ductilities and concrete grades.....	147
5.3	Failure lines under constant amplitude displacement reversals.....	148

5.4	Variable amplitude loading histories, damage progression curves and force-displacement relationships.....	150
5.5	Variable amplitude loading histories, damage progression curves and force-displacement relationships.....	152
5.6	Force-displacement relationships, imposed loading histories and damage curves of the specimens VH-2 and VH-3.....	153
5.7	Description of test assembly (dimensions in mm).....	156
5.8	The ground motions used in this study. a) El Centro 1940, NS component, b) 17 August 1999 Marmara Earthquake, Sakarya Station, EW component, c) 17 August 1999 Marmara Earthquake, Yarıymca Petrochemical Complex (YPT) Station, NS component, d)12 November 1999 Düzce Earthquake, Düzce Station, NS component.....	158
5.9	Synthetic ground acceleration histories (El Centro 1940, NS component preceded by various amplitude foreshocks) and damage variation curves for Pujol column.....	162
5.10	Synthetic ground acceleration histories (El Centro 1940, NS component followed by various amplitude aftershocks) and damage variation curves for Pujol column.....	163
5.11	Comparison of damage curves for Pujol column subjected to the synthetic ground acceleration histories comprising El Centro 1940, NS component and its various amplitude a) foreshocks and b) aftershocks.....	164
5.12	Effect of foreshock and aftershock damage on the damage sustained by the main ground motion, El Centro 1940, NS component.....	164
5.13	Effect of foreshock and aftershock damage on the total damage sustained by the synthetic ground acceleration histories originated from El Centro 1940, NS component.....	164
5.14	Synthetic ground acceleration histories (17 August 1999 Marmara Earthquake Sakarya-EW component preceded by various amplitude foreshocks) and damage variation curves for Pujol column.....	167
5.15	Synthetic ground acceleration histories (17 August 1999 Marmara Earthquake Sakarya-EW component followed by various amplitude aftershocks) and damage variation curves for Pujol column.....	168
5.16	Comparison of damage curves for Pujol column subjected to the synthetic ground acceleration histories comprising 17 August 1999 Marmara Earthquake, Sakarya station, EW component and its various amplitude a) foreshocks and b) aftershocks.....	169

5.17	Effect of foreshock and aftershock damage on the damage sustained by the main ground motion, 17 August 1999 Marmara Earthquake, Sakarya station, EW component	169
5.18	Effect of foreshock and aftershock damage on the total damage sustained by the synthetic ground acceleration histories originated from 17 August 1999 Marmara Earthquake, Sakarya station, EW component	169
5.19	Synthetic ground acceleration histories (17 August 1999 Marmara Earthquake YPT (Yarýmca Petrochemical Complex) Station, NS component preceded by various amplitude foreshocks) and damage variation curves for Pujol column	172
5.20	Synthetic ground acceleration histories (17 August 1999 Marmara Earthquake, YPT (Yarýmca Petrochemical Complex) Station, NS component followed by various amplitude aftershocks) and damage variation curves for Pujol column	173
5.21	Comparison of damage curves for Pujol column subjected to the synthetic ground acceleration histories comprising 17 August 1999 Marmara Earthquake, YPT (Yarýmca Petrochemical Complex) Station, NS component and its various amplitude a)foreshocks and b)aftershocks	174
5.22	Effect of foreshock and aftershock damage on the damage sustained by the main ground motion, 17 August 1999 Marmara Earthquake, YPT (Yarýmca Petrochemical Complex) Station, NS component	174
5.23	Effect of foreshock and aftershock damage on the total damage sustained by the synthetic ground acceleration histories originated from 17 August 1999 Marmara Earthquake, YPT (Yarýmca Petrochemical Complex) Station, NS component	174
5.24	Synthetic ground acceleration histories (12 November 1999 Düzce Earthquake, Düzce Station, NS component preceded by various amplitude foreshocks) and damage variation curves for Pujol column	177
5.25	Synthetic ground acceleration histories (12 November 1999 Düzce Earthquake, Düzce Station, NS component followed by various amplitude aftershocks) and damage variation curves for Pujol columns	178
5.26	Comparison of damage curves for Pujol column subjected to the synthetic ground acceleration histories comprising 12 November 1999 Düzce Earthquake, Düzce Station, NS component and its various amplitude a) foreshocks and b) aftershocks	179
5.27	Effect of foreshock and aftershock damage on the damage sustained by the main ground motion, 12 November 1999 Düzce Earthquake,	

Düzce Station, NS component	179
5.28 Effect of foreshock and aftershock damage on the total damage sustained by the synthetic ground acceleration histories originated from 12 November 1999 Düzce Earthquake, Düzce Station, NS component	179
5.29 Effect of foreshock and aftershock damage on the main ground motion damage	182
5.30 Effect of foreshock and aftershock damage on the total damage	184
6.1 The ground motion acceleration histories of 17 August 1999 Marmara earthquake, Düzce records	190
6.2 The ground motion acceleration histories of the 12 November 1999 Düzce earthquake, Düzce and Bolu records	191
6.3 Synthetic ground acceleration histories used in the analyses of the building located at Bolu	193
6.4 Synthetic ground acceleration histories used in the analyses of the building located at Düzce	193
6.5 Damage state of the case study building	197
6.6 Key plan showing locations of buildings	197
6.7 Ground floor plan	198
6.8 Front and rear elevations of the building after Düzce earthquake	200
6.9 Diagonal crack in column D8 at the ground story	201
6.10 Diagonal crack in column D9 at the ground story	201
6.11 Failed D10 columns at the ground and first stories	201
6.12 Failed column D10 at the ground story	202
6.13 Column D12 at the ground story	202
6.14 Shear cracks in column E8 at the ground story	202
6.15 Diagonal crack in column E9 at the ground story	202
6.16 Diagonal cracks in column E10 at the ground story	203
6.17 Diagonal cracks in column E12 at the ground story	203

6.18	Cracked masonry infill walls between D9 and D12 columns at the ground and first story levels (rear elevation)	203
6.19	Diagonal crack in column F8 at the ground story.....	204
6.20	Diagonal crack in column F9 at the ground story.....	204
6.21	Crack observed in column F10 at the ground story	204
6.22	Diagonal crack in column F12 at the ground story.....	204
6.23	Diagonal crack in column G8 at the ground story.....	205
6.24	Diagonal crack in column G9 at the ground story.....	205
6.25	Column G10 at the ground story.....	205
6.26	Flexural cracks in the beam spanning between D10 and D12 at the ground story.....	205
6.27	Severely damaged column D10 at the first story.....	206
6.28	Column G12 at the first story.....	206
6.29	Diagonal cracks in column E9 at the first story.....	206
6.30	D9 columns at the first and second stories.....	207
6.31	G12 and F12 columns at the first story	207
6.32	Collapsed infill wall between columns D10 and E10 at the first story.....	207
6.33	Severely damaged infill wall between columns F9 and F7 at the first story.....	208
6.34	Severely damaged infill wall between columns D12 and F12 at the first story.....	208
6.35	Severely damaged infill wall between columns G12 and F12 at the first story.....	208
6.36	Column G9 at the second story.....	209
6.37	Diagonal crack in column F9 at the second story.....	209
6.38	Diagonal crack in column G10 at the second story.....	209
6.39	2D Frame model used in the inelastic analyses in transverse (EW)	

direction.....	211
6.40 Damaged state of 2D Frame model used in the inelastic analyses in transverse (EW) direction after Marmara earthquake (x : crack, o:yield, * : failure).....	211
6.41 Damaged state of 2D frame model used in the inelastic analyses in transverse (EW) direction after Düzce earthquake (x : crack , o : yield, * : failure).....	211
6.42 Synthetic ground acceleration history, roof drift ratio variation, base shear ratio variation and damage curve for transverse (east-west) direction model of the building located at Bolu.....	212
6.43 Interstory drift ratio histories for transverse (east-west) direction model of the building located at Bolu.....	213
6.44 2D Frame model used in the inelastic analyses in longitudinal (NS) direction.....	217
6.45 Damaged state of 2D Frame model used in the inelastic analyses in longitudinal (north-south) direction after Marmara earthquake (x:crack, o : yield, * : failure).....	217
6.46 Damaged state of 2D frame model used in the inelastic analyses in longitudinal (north-south) direction after Düzce earthquake (x : crack, o : yield, * : failure).....	217
6.47 Synthetic ground acceleration history, roof drift ratio variation, base shear ratio variation and damage curve for longitudinal (north-south) direction model of the building located at Bolu.....	218
6.48 Interstory drift ratio histories for longitudinal (north-south) direction model of the building located at Bolu.....	219
6.49 General view of the building after Düzce earthquake.....	224
6.50 Location of the strong motion record station (solid star) and the investigated building (solid circle).....	224
6.51 Key plan showing location of building.....	225
6.52 Ground floor plan.....	226
6.53 Rear elevation of the building after Düzce earthquake of 12 November 1999.....	227
6.54 Columns F3 and F5 at the ground story	227

6.55	Columns F8 and F10 at the ground story	228
6.56	Cracking on the second story exterior infill wall at the back side (east-west direction) of the building.....	228
6.57	Cracking on of the second story exterior infill walls at the right-side (south) of the building.....	229
6.58	Diagonal cracks on the web portion of the shear wall P1 at the ground story.....	229
6.59	Diagonal cracks on the web portion of the shear wall P2 and horizontal crack along the slab level of the ground story.....	230
6.60	Diagonal crack about 60 cm away from the end of beam spanning between E5 and E6 at the ground story.....	230
6.61	Diagonal crack in the beam spanning between B2 and C2 at the ground story.....	231
6.62	Flexural crack at the end of the beam spanning between A6 and B6 at the ground story.....	231
6.63	Flexural crack at the end of the beam spanning between B8 and C8 at the ground story.....	232
6.64	Flexural crack at the end of the beam spanning between B9 and C9, where it spans into the shear wall P2, at the ground story.....	232
6.65	Flexural crack, about 80 cm away from the end of the beam spanning between A8 and A11 at the ground story.....	233
6.66	Flexural crack, about 30 cm away from the end of the beam spanning between D12 and F12 at the ground story.....	233
6.67	Flexural crack, about 50 cm away from the left end of the beam spanning between B7 and B8 at the ground story.....	234
6.68	Flexural crack at the right end of the beam spanning between B7 and B8 at the ground story.....	234
6.69	2D Frame model used in the inelastic analyses in transverse (EW) direction.....	236
6.70	Damaged state of 2D Frame model used in the inelastic analyses in transverse (EW) direction after Marmara earthquake (x : crack, o : yield, * : failure).....	236
6.71	Damaged state of 2D frame model used in the inelastic analyses in	

transverse (EW) direction after Düzce earthquake (x : crack , o : yield, * : failure)	236
6.72 Synthetic ground acceleration history, roof drift ratio variation, base shear ratio variation and damage curve for transverse (east-west) direction model of the building located at Düzce	237
6.73 Interstory drift ratio histories for transverse (east-west) direction model of the building located at Düzce	238
6.74 2D Frame model used in the inelastic analyses in longitudinal (NS) direction	241
6.75 Damaged state of 2D frame model used in the inelastic analyses in longitudinal (NS) direction after Marmara earthquake (x : crack , o : yield, * : failure)	241
6.76 Damaged state of 2D frame model used in the inelastic analyses in longitudinal (NS) direction after Düzce earthquake (x : crack , o : yield, * : failure)	241
6.77 Synthetic ground acceleration history, roof drift ratio variation, base shear ratio variation and damage curve for longitudinal (north-south) direction model of the building located at Düzce	242
6.78 Interstory drift ratio histories for longitudinal (north-south) direction model of the building located at Düzce	243
B.1 Three dimensional elevation of the dormitory building	262
B.2 Ground story plan of the dormitory building	263
B.3 Three dimensional elevation of the school building	264
B.4 Ground, first and second stories plan of the school building	265
B.5 Ground story plan of the residential building	266
B.6 Photographs of the Çeltiksuyu Regional Primary Education School buildings after Bingöl earthquake of May 1, 2003	267
C.1 Three dimensional elevation of the building	269
C.2 Ground floor beams and slabs details	270
C.3 Ground Floor Columns Details	271

LIST OF SYMBOLS

A	Cycle displacement amplitude
A_c	Net concrete area of column cross section
A_g	Gross cross-sectional area of a column or beam section
A_p	Plan area of building
A_{st}	Cross sectional area of longitudinal reinforcement of a column
A_w	The cross-sectional area of the shear walls at a story of building
A_{fore}	Amplitude of foreshock ground acceleration history
A_{after}	Amplitude of aftershock ground acceleration history
A_{main}	Amplitude of main shock ground acceleration history
$a(g)$	Earthquake ground acceleration
b	Column cross sectional dimension in the transverse direction of bending
b	Fatigue strength component
c	fatigue ductility exponent
D	Damage index
D_{def}	Deformation component of total damage
D_{str}	Strength component of total damage
D_{total}	Total damage
D_{fore}	The resultant damage of foreshock
D_{after}	The resultant damage of aftershock
D_{main}	The resultant damage of main shock
d'	Clear cover of a cross section
$d\ddot{a}_m$	magnitude of the horizontal offset
E	Modulus of elasticity of concrete
E_{hyst}	Energy dissipation index
F_y	Yield strength of a structural component
f_c, f_{ck}	Characteristic compressive cylinder strength of concrete
f_{cd}	Design compressive strength of concrete

f_{ctd}	Design tensile strength of concrete
f_y, f_{yk}	Characteristic yield strength of longitudinal reinforcement
f_{yd}	Design yield strength of longitudinal reinforcement
h	Column cross sectional dimension in the bending direction
h_i	Height of i 'th storey
H	Height of building
l_i	i^{th} story column length, measured from axis to axis
M	Bending moment
M_b	Beam end bending moment
M_c	Column end moment
N	Axial force calculated under vertical and/or seismic loads
N_0	Axial load capacity of a cross section of column
N_b	Balanced axial load level
N_{cycle}	Number of applied cycles
n	Number of storey
n_i	Number of load reversals corresponding to the i 'th constant stress amplitude
N_f	Number of load cycles,
N_{fi}	Number of load cycles to failure the i 'th constant stress amplitude
PGA	Peak ground acceleration
PGV	Peak ground velocity
T_{eff}	Effective duration
R	Structural behavior factor
S_a	Spectral acceleration
S_d	Spectral displacement
T	Building natural vibration period
T_{modal}	Building modal vibration period
TEC	Turkish Earthquake Code
ACI	American Concrete Institute
UBC	Uniform Building Code
V	Shear strength of a cross section of column, beam or wall
V/W	Total base shear ratio acting on a building
W	Total weight of building
$\dot{\iota}$	Classical ductility ratio

$\dot{\delta}$	Curvature ductility
$\dot{\delta}_a$	Displacement ductility
f_u	Ultimate curvature
f_y	Yield curvature
Δd_p	Amplitude of plastic deformation
$\Delta \dot{\epsilon}_e/2$	Elastic strain amplitude
$\Delta \dot{\epsilon}_p/2$	Plastic strain amplitude
$\Delta \dot{\epsilon}/2$	Total strain amplitude
$\dot{\epsilon}_f'$	Fatigue ductility coefficient
δ_i	Lateral displacement at the ends of any column or wall at i'th storey
δ_m	Maximum displacement of a column or beam
δ_y	Yield displacement of a column or beam
d_u	Ultimate displacement of a column or beam
d_c	Calculated displacement of a column or beam (Powell and Allahabadi model)
d_t	Threshold displacement of a column or beam (Powell and Allahabadi model)
ρ_l	Longitudinal reinforcement ratio
ρ_s	Ratio of transverse reinforcement of column to the gross area of column
ρ_c	Ratio of column area to floor area
ρ_w	Ratio of wall area to floor area
α	Stiffness degradation parameter
β	Strength deterioration parameter
γ	Pinching or slip parameter
λ	Energy weighting factor

CHAPTER 1

INTRODUCTION

1.1 General

Engineering structures, built in areas where earthquakes quite often occur, may be subjected to successive strong earthquake excitations. The damage sustained during a prior earthquake excitation may significantly affect the response of a structure to a succeeding earthquake. Accumulation of damage due to low cycle fatigue may play a role in this sequence. Structural damage caused by successive earthquakes or long duration strong earthquakes can not only be attributed to defects in design or construction, but also to low cycle fatigue effects due to accumulation of damage. It is not unusual for this accumulation to lead to collapse during the successive events. But how the damage from each of these events could be predicted and which intensity of these excitations may cause noteworthy increase in the following earthquake damage? The prior earthquake or foreshock of what intensity may substantially affects the damage to be sustained during the major earthquake ground motions is another question.

Effects of damage from prior earthquakes on the response of reinforced concrete structures to a successive design-level earthquake can be assessed by means of two different approaches.

To imitate the prior damage-causing earthquake, the structural system can be exposed to a synthetic ground motion record that comprises a prior ground motion record and a succeeding ground motion record. Naturally, the synthetic composite ground motion record should be comprised of at least two successive ground motions, on the condition that the first ground motion causes a pre-determined seismic structural damage. The seismic inputs are provided successively as a

continuous ground motion without a quiescent period in which the structure comes to rest. Hence the effect of the prior event is carried forth to the next without returning the system to undamaged conditions. It is believed that this approach simulates the real conditions and provides the most realistic response of the structure. The difficulty of this method is to observe or monitor the intermediate damage state in between the ground motions.

In the second approach, the prior damage can be modeled as reductions in the initial mechanical characteristics of a structural member, namely, stiffness, strength and hysteresis. This is possible in case of changes in the structural properties could be estimated. In this approach, the structural properties (stiffness, strength and hysteresis loops) of a structural component are simulated by prescriptively modifying the component's force-deformation relation. Experiencing the first event, the weakened structural system with damaged elements is explicitly modeled and subjected to the succeeding ground motion. Estimated final values of the structural properties attained at the end of the first event, constitute for the starting properties of the damaged system at the start of the second event that is going to be experienced. The local (element) or global (overall) damage indices of the damaged structural system that has exposed to succeeding ground motions are compared with that of a companion structural system which is initially undamaged and subjected to only second earthquake excitation.

The second approach, compared with the first one, is rather complicated, tedious and time consuming, especially for MDOF frame type of structural systems as modeling is required for each member. It is believed that the second approach could not validate the inelastic behavior of a structural system as the first. Attempts to model the prior damage as reductions in the initial structural properties (stiffness and strength) of a structural member must be based on assumptions about structural behavior and may be handicapped by the lack of the proper analysis tools.

In the last decade, two destructive successive ground shaking, with magnitudes exceeding 7.0, have been experienced nearly 3 months apart in the north-western region of Turkey. The distance between the epicenters of the successive

ground motions, occurred on 17 August and 12 November 1999 in Marmara region, is about 110 km. These repeated destructive earthquakes provide a unique possibility to verify the effect of prior earthquake damage on the structural performance to future earthquakes. It was the first time that such strong successive earthquakes hit structures, in certain cities producing either accumulated extensive damage or collapse. It is worthwhile to note that this event is a benchmark to shed light on accumulation of damage.

The east part of the Marmara region and especially surroundings of Düzce and Bolu cities has served as an excellent laboratory in order to observe the effects of successive earthquake on structural damage. Many of the reinforced concrete structures had suffered light-to-moderate damage during the Marmara earthquake, on August 17, 1999 (also called the Kocaeli earthquake) then sustained further damage or partly/completely collapsed during the succeeding Düzce earthquake, on November 12, 1999. Hundreds of additional buildings collapsed or damaged further during the second event. These unusual building failures observed in Marmara region, especially surroundings of Düzce and Bolu cities after these two major successive earthquakes attracted special attention of national and international earthquake engineering community (Sözen, 2000; Sucuođlu and Yýlmaz, 2001). Although most of the surviving structures did not satisfy the code regulations, they exhibited satisfactory performance. Hence the causative-reasons behind both observed unusual building failures and seismic performance of the structures may be expressed via bases of low cycle fatigue phenomenon.

1.2 Review of Past Work

Previous research is presented under two headings in the following paragraphs. A limited number of research related with the effects of prior earthquake damage on seismic performance of SDOF and MDOF systems are introduced first. Then the researchs related to fatigue phenomenon and damage models are presented.

1.2.1 Studies on Prior Damage Effects on Performance of Structures

The main concern of the earthquake engineering community is the assessment of the damage status of the structures before and after a destructive ground motion, in order to take necessary precautions. To assess the post-earthquake reliability, it is convenient to determine the physical damage state of the structures subjected to earthquake excitations.

Until present time, only a limited number of researches have been conducted on assessment of the prior earthquake damage effects. Analytical and experimental studies, performed in the past, mainly address the problem of prediction of the post-earthquake seismic performance and future reliability of damaged reinforced concrete structures. In almost all researches summarized below, attempts made to meet this main objective are based on the comparison of the displacement response of damaged and undamaged structural systems.

In the shake-table tests performed by Çeçen (1979), two identical ten-story three-bay reinforced concrete frame models were tested. The two models were subjected to sequences of ground motions with different intensity, followed by a final test using identical ground motions. When the structures were subjected to the repeated ground motion, the peak displacement response at each story was only slightly affected by the previous shaking of the same intensity. When the two structures were subjected to the same final motion, peak displacement response over the height of the two structures was only slightly affected by the different prior sequences. Floor acceleration response, however, was prone to more variation.

Mahin (1980) conducted an analytical study to investigate response of SDOF oscillators subjected to five synthetic ground motions, each having 60 seconds duration. For this purpose, a number of earthquake aftershock sequences were used. He stated that, duration of severe ground shaking has a significant effect on inelastic deformational and energy dissipation demands, especially for relatively weak, short period structures which may be expected to develop significant inelastic

deformations. For bilinear models with negative post-yield stiffness, increases in duration tend to cause relatively smaller increases in displacement ductility demand.

In the shake-table tests conducted by Araki et al (1990), the reinforced concrete wall and frame-wall structures were exposed to single and repeated synthetic ground motions. It was found that low-rise structures subjected to repeated shake-table tests displaced to approximately twice as much as they did in a test subjected to a single ground motion. However, in case of mid-rise and high-rise structures, repeated testing caused peak displacements that ranged from 0 to 10 percent larger than those obtained in single tests.

Wolschlag (1993) tested three-story reinforced concrete walls on a shake-table. In one test series, an undamaged structure was subjected to repeated ground motions of the same intensity. It was concluded that, in the repeated tests, the peak displacement response at each floor of the damaged specimen was hardly different from the response measured for the initially undamaged structure.

Hanson (1996) conducted a research to evaluate the structural damage of reinforced concrete members damaged by earthquakes. He asserted that the prior earthquake damage might be measured by estimating the loss of lateral load carrying capacity of the structure. The procedure in this study is based on global and component lateral force capacities. It was suggested that this loss can be related to the observed width and extent of concrete and masonry cracks in the damaged structure.

In the ATC 43 (1998) [FEMA 306, 307, 308] project, effects of prior damage on the displacement response of SDOF models subjected to earthquakes were investigated to verify and/or modify current methods of predicting displacement demand. The procedure presented in this project is based on global displacement and component deformation capacities rather than force capacities. It was stated that there was a widespread disagreement on the significance of cracking on capacity and skepticism on the suitability of force capacity as a parameter for measuring damage as maintained by Hanson (1996). It was concluded that, prior earthquake damage

does not affect maximum displacement response in future larger earthquakes in many instances. It was concluded that although it seems illogical it was particularly true in cases in which significant strength degradation did not occur during the prior smaller earthquake.

Aschheim and Black (1999) made a comparative analytical study, as part of ATC-43 project (1998) using three existing hysteresis models to investigate the effects of prior earthquake damage on the peak displacement response of simple oscillators. Prior damage was modeled as a reduction in initial stiffness under the assumption that residual displacements were negligible. The study was performed using over twenty thousand SDOF systems. The main variables considered in the analysis were oscillator strength, period of vibration, degree of prior damage, and load-deformation relation. To assess whether ground motion duration or the presence or absence of near-field pulses associated with the fault rupture propagating towards the recording station might affect the responses, a large enough sample of recorded ground motions was used. The selected simulated earthquakes were classified as: short duration (with magnitudes less than 7), long duration (with magnitudes more than 7) and forward directive.

Effect of damage was investigated considering three load-deformation relations:

1. Standard Takeda (Takeda *et. al.*1970) load deformation relation with positive post-yield stiffness, Figure 1.1a,
2. Standard Takeda load deformation model with negative post-yield stiffness, Figure 1.1b, and
3. Modified Takeda load deformation model incorporating pinched hysteretic response with conjunction with a form of cyclic strength degradation, Figure 1.1c.

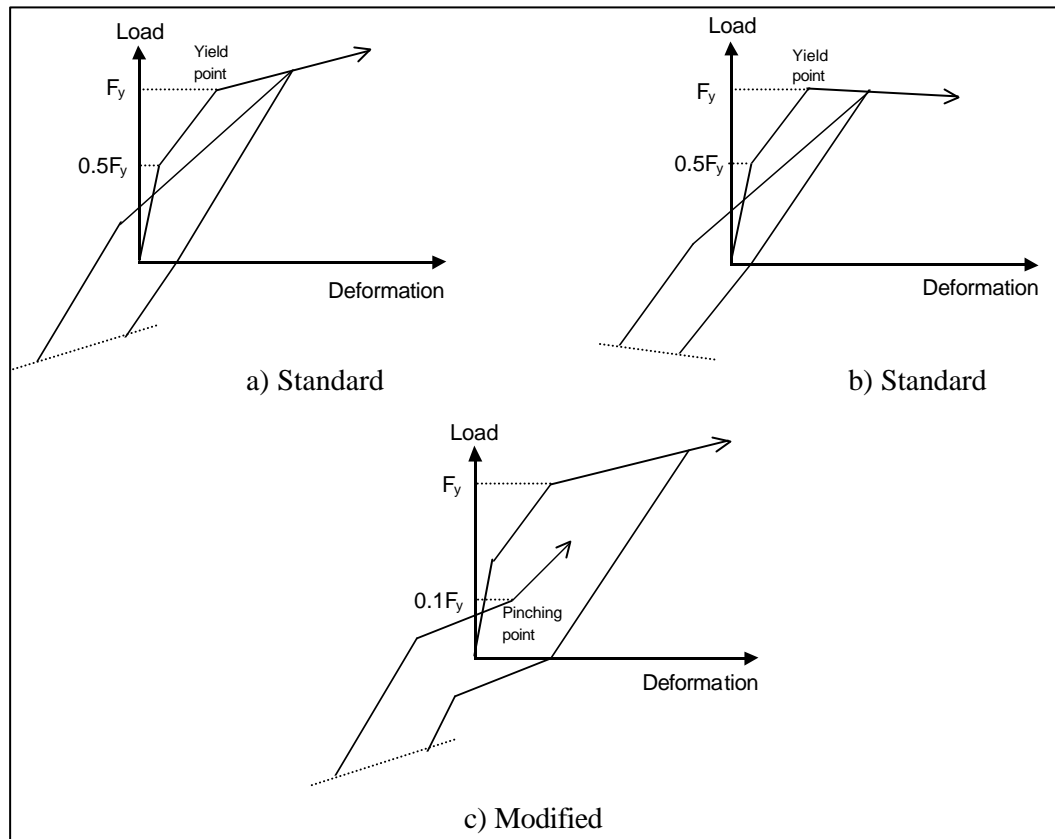


Figure 1.1 Evolving Takeda models

They concluded that prior damage has a minor influence on peak displacement response. This was observed for the full range of periods and ground motions investigated for SDOF oscillators exhibiting stiffness degradation and without dependence on the presence or absence of pinching of the hysteretic response. Load deformation relation with positive post-yield stiffness and modified load-deformation model incorporating pinched hysteretic response in conjunction with a form of cyclic strength degradation displayed satisfactory performance under the pre-specified seismic actions. It was concluded that a large number of collapses were found for the Takeda oscillators with negative post-yield stiffness, and regardless of prior damage, to prevent the collapse of these structures they should remain almost elastic.

Sözen (2000) made an analytical and statistical study on damage states of approximately 100 randomly selected buildings located in Düzce, shaken strongly by

two damaging ground motions in three months. Measurements of the frame members and nonstructural walls of these selected buildings were made by teams of engineers from Turkey and USA in December 1999 and June 2000. The majority of the buildings had four to six stories. They had variable beam and column sizes and founded on individual footings with grade beams. The compressive strength of concrete used ranged from 7 to 15 MPa.

It was emphasized that according to the direct observation there was no reason to conclude that the buildings that failed in November had been moderately damaged in August. It was stated that there was observational evidence that a considerable portion of the buildings damaged heavily in November had not been hurt in August and the ratio of the heavy damage in the November event to that in the August event is three. The crucial point of the study was exposed with the question asked by the author; “given the ground motion records and the damage for the August event as well as the ground motion records for the November event, could the damage in the November event have been estimated?”

As a result of the studies made by the author, the question was answered with respect to Düzce 1999; ‘without fore knowledge, a confident and convincing answer is not possible on the basis of direct or even indirect but simple procedures’. With this unsatisfactory answer, the author called attention to the connection between ground motion measurement and potential general damage. To assess the causative-reasons of such unusual damage caused by successive earthquakes, the author is of the opinion that there should be strong efforts made to connect ground motion measurement and potential damage.

1.2.2 Studies on Fatigue and Damage Models

Damage of a structural member accumulates with each displacement cycle. The accumulation of damage in a material up to the point of failure under repeated cyclic loading is known as ‘fatigue’. According to stress level it can be classified as ‘high-cycle’ and ‘low-cycle’ fatigue. In high-cycle fatigue the stresses are low, far below yielding strength. The structural component does not deform beyond elastic

stress level, so it may need a large number of cycles to failure. This is a matter of material science. In low-cycle fatigue the stresses are quite high to cause considerable plastic deformation.

In the basic fatigue process, the damage is assumed to increase incrementally with each cycle. High cycle fatigue is present when the individual cycles occur at an elastic stress level requiring many tens of thousands or millions of cycles to failure, whereas low cycle fatigue occurs when each cycle exceeds the yield stress. Then the number of cycles is far less. Basically, a monotonic test is a pseudo low-cycle fatigue test of one-half cycle (McCabe and Hall, 1989).

In earthquake engineering community, much theoretical and experimental research has been conducted on assessment of seismic damage in structural systems. By making use of damage indices, the damage in reinforced concrete structures sustained under earthquake loading is quantified numerically. The major research conducted on the assessment of structural damage has been concentrated especially on the development and application of damage indices. The structural damage indices are generally expressed as a function of one or more damage parameters. The damage models can be classified into three groups: non-cumulative, cumulative and combined. If the structural damage is quantified as a function of maximum structural response, such as the displacement, ductility or oscillation period this means the damage model is non-cumulative.

The earliest and simplest form of the non-cumulative damage is ductility-based. The ductility ratio can be defined using displacement, curvature or rotation. The displacement ductility can be written as;

$$\mu_{\delta} = \delta_{\max} / \delta_y \quad (1.1)$$

where δ_{\max} and δ_y refer to maximum plastic displacement and yield displacement of the component, respectively.

Failure occurs when the ductility demand exceeds the structural ductility (capacity). Powell and Allahabadi (1988) developed a more general form of the non-cumulative type of damage index. The damage expressed as follows:

$$DI = \left(\frac{\mathbf{d}_c - \mathbf{d}_t}{\mathbf{d}_u - \mathbf{d}_t} \right)^m \quad (1.2)$$

where \mathbf{d}_c , \mathbf{d}_t and \mathbf{d}_u are the calculated, threshold and ultimate values, respectively, for the damage parameter ranging between 0 and 1. The effect of the exponent, m , is shown in Figure 1.2. The value of the dimensionless damage index will be equal to 0, signifying no damage, if the calculated value of the parameter is less than the threshold value, \mathbf{d}_t . On the other hand, the index will be equal to 1 when the calculated value, \mathbf{d}_c , is equal to the ultimate value, signifying failure. Between threshold and ultimate values, damage index may take any value depending on the calculated value, \mathbf{d}_c , and the dimensionless parameter, m .

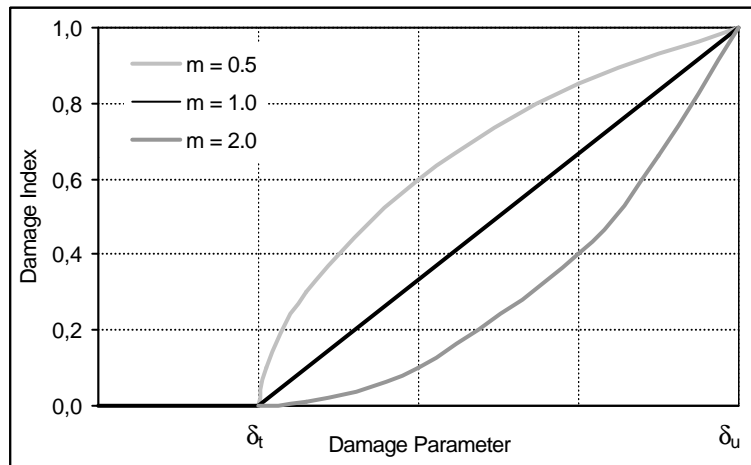


Figure 1.2 Effect of parameter m on damage index

The degradation procedure is based on the estimation of the undamaged (initial) and damaged state values of a property in a structure, substructure or member. The parameters like stiffness, strength, energy dissipation capacity and period can be considered for this procedure. This damage index is based on the variation of the first mode due to the stiffness and strength deterioration of the structure or member. For the degradation procedure, the value of the degrading

property will decrease progressively, and a suitable form of the softening or weakening in a structure or member is defined as (Powell and Allahabadi, 1988);

$$\mathbf{d} = 1 - \frac{P_d}{P_0} \quad (1.3)$$

where \mathbf{d} is damage parameter, P_d is the degraded final value of the structural property in the damaged state and P_0 is the value in the undamaged state.

It should be emphasized that each load cycle caused a certain amount of irreversible structural damage. Basically obtaining a cumulative value of the damage is to accumulate the damage caused by plastic deformations. If the damage procedure is to consider the accumulated damage sustained under cyclic loading, then the parameter used to assess the damage is based on cumulative damage. Modeling of the accumulation of damage which occurs under cyclic loading is usually performed either by means of a low-cycle fatigue formulation in which damage is taken as a function of the accumulated plastic deformation, or by incorporating a term related to the hysteretic energy absorbed during the loading (Williams and Sexsmith, 1995).

Investigations related to fatigue life of the engineering components are focused on metals and steel components, and it was first introduced in the 1860's by Wöhler (Suresh, 1991). The fatigue life of the engineering components is defined as the total number of cycles to induce fatigue damage. The fatigue life theory was extended further, and a fatigue-based cumulative damage rule was developed (Palmgren, 1924; Miner, 1945). For years, Palmgren-Miner cumulative damage rule was considered as a simple criterion for predicting the extent of fatigue damage induced by a certain constant amplitude loadings. In this linear damage rule, it was assumed that; (i) the number of stress cycles imposed on a component, expressed as a percentage of the total number of stress cycles of the same amplitude necessary to cause failure, gives the fraction of expanded fatigue life, and (ii) the order in which the stress or strain blocks of different amplitudes are imposed does not affect the fatigue life (Suresh, 1991).

Based on these assumptions, for a cyclic excursion having k different stress amplitudes the accumulated damage is expressed linearly as follows (Miner, 1945);

$$DI = \sum_{i=1}^k \frac{n_i}{N_{fi}} \quad (1.4)$$

where, n_i is number of load reversals corresponding to the i 'th constant stress amplitude, and N_{fi} is number of load reversals to failure for the i 'th constant stress amplitude.

In the extreme case where failure takes place, the summation given in the linear damage rule formulation becomes equal to 1.0. As the most primitive fatigue damage model, it is only relevant for constant amplitude fatigue loading. In reality, however, engineering components are invariably subjected to varying cyclic loading amplitudes.

Kasiraj and Yao (1968) studied the low-cycle fatigue failure of structures and stated that the failure of a structure subjected to a strong ground motion with high damage potential could be more influenced by the damage caused by low-cycle fatigue rather than by maximum displacement (response) of the structure.

Krawinkler and Zohrei (1983) proposed a more suitable expression for number of (constant amplitude cycling) reversals to failure of structural components as a result of experimental studies on steel components,

$$N_f = C^{-1}(\Delta \mathbf{d}_p)^{-c} \quad (1.5)$$

where $\Delta \mathbf{d}_p$ is the amplitude of plastic deformation and c and C are material constants to be determined experimentally. In the low cycle fatigue tests of steel components the failure modes of local buckling in beam flanges and fracture at weldments are taken into consideration, and they proposed linear damage models. They conducted some experiments including monotonic and constant-amplitude cyclic loading and

used them to develop cumulative damage models for the fatigue life prediction under variable amplitude cyclic loading patterns. The proposed damage model considers different amounts of the plastic displacements using the following expression for cumulative damage;

$$D_F = A \sum_{i=1}^n (\mathbf{m}_i - 1)^a \quad (1.6)$$

where A and a are parameters which depend on the properties of the structural component, n is the number of reversals and \mathbf{m}_i is the ductility at the i^{th} plastic cycle. The parameter A is derived applying the equation 1.6 to monotonic loading.

$$D_F = \sum_{i=1}^n \left(\frac{\mathbf{m}_i - 1}{\mathbf{m}_{l,mon} - 1} \right)^a \quad (1.7)$$

McCabe and Hall (1989) proposed a damage index based on the concept of equivalent hysteretic cycles of deformation, and stated that counting the number of hysteresis cycles that occurred during response would provide a measure of damage. The shortcoming in this proposal is that cycles are not identical nor are they full-cycles. To cope with this deficiency they introduced the concept of equivalent hysteresis cycle in which the total dissipated energy is divided by the amount of energy in a standard hysteretic cycle to obtain the number of equivalent cycles required to dissipate this same amount of energy. The number of equivalent cycles is expressed as:

$$N = \frac{H_t}{(R_y)(\Delta U)} \quad (1.8)$$

where N : number of equivalent hysteretic cycles,
 R_y : yield resistance,
 ΔU : displacement, and
 H_t : total dissipated hysteretic energy.

They suggested three different methods to calculate the ΔU term;

1. Using maximum deformation encountered during response,

$$\Delta U = U_m - U_y \quad (1.9)$$

2. Using displacement defined by the strain energy at yield,

$$\Delta U = \frac{U_y}{2}, \quad (1.10)$$

3. Using a weighted deformation computed from the response values,

$$\Delta U = U_{wt} - U_y, \text{ and} \quad (1.11)$$

$$U_{wt} = \frac{\sum_i H_i \Delta U_i}{H_t} \quad (1.12)$$

where H_i is hysteretic energy at i^{th} cycle, ΔU_i is displacement magnitude for a particular yield excursion and H_t is total dissipated hysteretic energy up to current time.

Among these, weighted deformation is in good agreement with the actual observed test data. In this approach equivalent deformation cycle was defined using a weighted deformation computed from the response values that were responsible for generating most of the hysteretic energy.

The best known and widely used damage index is developed by Park and Ang (1985). In this damage index, suitable for reinforced concrete members when bending plays the major role, the structural damage expressed as a linear combination of the normalized deformation and dissipated hysteretic energy.

$$D = \frac{\mathbf{d}_m}{\mathbf{d}_u} + \mathbf{b} \frac{\int dE}{F_y \mathbf{d}_u} \quad (1.13)$$

where \mathbf{d}_m : maximum deformation under earthquake,

\mathbf{d}_u : ultimate deformation under monotonic loading,

F_y : calculated yield strength (defined as the first yielding in tension reinforcement, or when the extreme fiber compressive strain in concrete exceeds 1.5 times the crushing strain, ϵ_o ,

$\int dE$: accumulated hysteretic energy during the response history (enclosed area of force-deformation loops),

\mathbf{b} : strength degradation parameter (function of structural parameters)

The first term on the right-hand side of equation (1.13) represents damage due to increased deformation whereas the second term represents the damage due to history of deformations. The advantages of this model are its simplicity and the facts that it has been calibrated against significant amount of observed seismic damage, including some instances of shear and bond failures (Kunnath et al, 1990). It should be noted that, this damage index yields normalized values between zero and unity. A damage index in the neighborhood of unity signifies partial or complete collapse of the component.

The effect of cyclic loading on structural damage is represented by this parameter, β . The strength deterioration parameter is empirically formulated from regression analysis of 140 monotonic and 261 cyclic test data of beams and columns (Park and Ang, 1985; Kunnath et al, 1990);

$$\mathbf{b} = [0.37n_0 + 0.36(k_p - 0.2)^2] * 0.9^{r_w} \quad (1.14)$$

where n_0 : normalized axial stress, k_p : normalized steel ratio and r_w : transverse reinforcement ratio. The equation shows a negative correlation between the deterioration parameter and the transverse reinforcement ratio, and also weak positive correlations between this parameter and normalized axial stress and steel ratio.

The absorbed hysteretic energy was integrated up to the failure point for these large set of cyclic test data and this low-cycle damage based model was calibrated with these experimental data for reinforced concrete members. Park, Ang and Wen (1985) suggested damage index of 0.4 as a threshold value between repairable and irreparable damage. Then in 1987, the same authors suggested the following detailed damage classification (Williams and Sexsmith, 1995):

$D < 0.1$	No damage or localized minor cracking,
$0.1 \leq D < 0.25$	Minor damage - minor cracks throughout, partial crushing of concrete in columns,
$0.25 \leq D < 0.4$	Moderate damage-extensive large cracks, localized spelling,
$0.4 \leq D < 1.0$	Severe damage-crushing of concrete, reinforcement exposed,
$D \geq 1.0$	Collapse-total or partial collapse of building.

The damage classification and lower/upper limits of the damage levels may change for the other damage indices.

The index was implemented in the original release of IDARC (Park, Reinhorn and Kunnath, 1997). The recent release of IDARC (Kunnath et al, 1992) uses a slightly modified form of fatigue based Park and Ang (1985) damage index. The only difference is that instead of force and displacement they used moment and curvature and the recoverable deformation has been removed from the damage index formulation;

$$D = \frac{\mathbf{f}_m - \mathbf{f}_y}{\mathbf{f}_u - \mathbf{f}_y} + \mathbf{b} \frac{\int dE}{M_y \mathbf{f}_u} \quad (1.15)$$

where \mathbf{f}_m is the maximum curvature attained during the loading history, \mathbf{f}_u is the ultimate curvature capacity of the section, \mathbf{f}_y is the yield curvature, M_y is the yield moment and E_h is the dissipated energy in the section. Then, the biggest damage index of the end sections of a component is selected as the damage index of the component (Valles et al, 1996).

Calibration of the index was performed by Stone and Taylor (1993) and the following damage classification is proposed:

$D < 0.11$	No damage (localized minor cracking),
$0.11 \leq D < 0.4$	Repairable (extensive spelling but inherent stiffness remains),
$0.4 \leq D < 0.77$	Irreparable (still standing but failure imminent),
$D \geq 0.77$	Collapsed.

As a result of evaluation of several local damage indices against the results of a series of cyclic combined shear and flexural tests, Williams et al (1995) stated that Park and Ang index is one of the most consistent indicators of severe damage and failure. On the basis of comparisons against one set of shear-dominated tests, they stated that, it appeared that the damage sustained is primarily depends on the deformation level, with the number of cycles of loading having only a small effect. This means that the relatively simple, predominantly deformation-based measures, such as ductility, stiffness degradation and modified Park and Ang damage index formulations, provide a more reliable indication of the various damage levels than many of the apparently more sophisticated indices.

An experimental study was carried out by Lew (1997) to assess the relationship between the state of damage and low-cycle fatigue characteristics. In this study, a series of reinforced concrete columns were tested under monotonic and cyclic loading histories. The amplitudes of the constant cyclic loading histories were selected as two, three, four and five times of the yield displacement, δ_y . As a result, it was concluded that at failure stage the accumulated energy dissipation is definitely path dependent.

El-Bahy et al (1999) tested relatively slender columns (ratio of shear span to diameter of 4.5) in two stages. In the first stage, a series of identical quarter-scale concrete circular cross-sections bridge columns were tested under displacement cycles of monotonic and constant amplitude loading to establish the monotonic force-deformation envelope and low-cycle fatigue characteristics. In the second stage, the specimens were tested under variable amplitude loading to observe the effects of load path on cumulative damage. The former failure mode was associated with relatively large displacement amplitudes in excess of 4 percent lateral drift, while the latter was associated with a large number of smaller amplitude cycles. Buckling and fracture of the longitudinal reinforcement dominate observed failure modes. The total number of cycles of constant amplitude that a column could sustain before failure was observed to decrease with increasing cycle amplitude. A fatigue life expression was developed that could be used in damage based seismic design of circular, flexural bridge columns expressed as;

$$\mathbf{d}=10.6 (N_{2f})^{-0.285} \quad (\text{percent}) \quad (1.16)$$

where \mathbf{d} is the lateral drift and N_{2f} is the number of complete cycles to failure. They used Miner's linear damage model to define cumulative damage in the form;

$$D = \sum_{i=1}^n \frac{1}{(N_{2f})_i} \quad (1.17)$$

where $(N_{2f})_i$ is computed for each imposed drift amplitude using Equation 1.16 and the summation is performed over the entire cyclic history. Finally they stated that the computed damage is in reasonable agreement with test observations.

Erberik and Sucuođlu (2001) conducted an experimental and analytical study to determine energy dissipation and low cycle fatigue characteristics of reinforced concrete components. A total of 17 beam specimens were tested under monotonic, constant-amplitude and variable-amplitude cyclic loading. A two-parameter fatigue model was developed for deteriorating systems;

$$E_{nn} = \mathbf{a} + (1 - \mathbf{a}) e^{b(1-N)} \quad (1.18)$$

where $1-\mathbf{a}$: the level of reduction in dissipated energy,

\mathbf{b} : the rate of the reduction in dissipated energy ($\mathbf{b}=0$ refers to an ideal system with no degradation, and $\mathbf{b} = \infty$ refers to a system that lose all of its energy dissipation capacity in the very first cycle),

\mathbf{a} : constant parameter that ranges between zero and unity. (A severely degrading structural system with $\mathbf{a}=0$ loses all of its energy dissipation capacity while $N \rightarrow \infty$. A structural system with $\mathbf{a}=1$ never loses its energy dissipation capacity, for instance elasto-plastic systems).

This model was employed for prediction of the energy dissipation under variable-amplitude displacement cycles. An energy-based hysteresis and damage

models were developed for structural members, and they are based on stiffness and strength degradation, but not pinching.

Total damage expression for the n^{th} full-cycle is given as follows;

$$D_{e,n} = \frac{m-1}{m-1} + \left(\frac{m}{m-1} \right) \cdot \left(\frac{4}{5\bar{E}_{h,n}} - 1 \right) \quad (1.19)$$

The first term represents damage due to maximum effective ductility, and the second term due to low cycle fatigue at $i_{eq,n}$ cycles.

They stated that energy dissipation is memory dependent. The cumulative energy dissipated along a completed displacement path governs the energy dissipation capacity in the following displacement cycle. They also concluded that, energy dissipation is path dependent, and the cumulative energy dissipated along a path depends on the number and amplitude of cycles constituting the path.

Another tool widely used for damage measurement is the inter-story drift. Attempts have been made to relate damage to maximum inter-story drift. The importance of drift control is established when it is accepted that the earthquake induced displacements are the main causes and measure tool of seismic structural distortion and damage. Seismic drift calculation is required by the several seismic codes such as TEC (1998), UBC, ACI. Seismic drift control procedure is based on imposing limits on maximum seismic drift or its relative values.

Sözen (1981) proposed a drift-control-based damage model to determine the damage level at a story. As a measure tool of damage, he used the inter-story drift ratio, difference in maximum drift response between two consecutive stories divided by the story height. A drift ratio value smaller than 1 percent corresponds to damage in non-structural components while values of drift ratio greater than 4 percent may lead to irreparable structural damage or collapse. Failure is considered to occur when the value of drift ratio exceeds 6 percent.

The percentage of damage in the structure is given by the equation given below:

$$\text{Percentage of damage} = 50 \times (\text{maximum interstorey drift in percent}) - 25 \quad (1.20)$$

In accordance with equation (1.20) an inter-story drift value of 2.5 percent corresponds to the percentage of damage of 100, implying failure.

Similarly, ATC 40 (1996) prescribes performance levels with imposing limits to the maximum drift ratio. Maximum drift ratio of 1 percent is the upper limit of the *immediate occupancy* performance level, while the value of maximum drift ratio ranging from 1 percent to 2 percent corresponds to *damage control* level. And the requirement of the *life safety* performance level can be satisfied whenever the value of drift ratio does not exceed 2 percent. In accordance with Turkish Earthquake Code (TEC, 1998), structures to be used as residential buildings should be designed for *life safety* performance level under the extreme loading.

Gülkan and Sözen (1999) developed a hypothesis and proposed a procedure similar to Sözen (1981) to quantify the seismic structural vulnerability at the ground story level in reinforced concrete frame buildings with and without masonry filler walls. The method requires only the dimensions of the structure as input and is based on defining the ranking on a two dimensional plot using column and masonry wall ratios. In their study, Gülkan and Sözen take the ‘relative ground story drift’ as the primary indicator for structural damage and formulate a rational expression to calculate drift in relation to the dimensions of the structure only. They give an expression for *mean ground story drift* denoted by MGSD.

$$MGSD = \frac{n_s^{4/3}}{h_s^{1/3}} \sin \frac{\mathbf{P}}{2n} \left\{ \frac{\mathbf{h}}{\frac{c_c E_c p_c}{\mathbf{I}^2} + \frac{E_w p_w}{(h_s / l_w)^2 + \frac{2.5}{c_{wc}}}} \right\}^{2/3} \quad (1.21)$$

where n is the number of stories, \mathbf{h} is the building unit mass, E_c and E_w are the material properties of elements contributing to lateral resistance including non-

structural walls c_{wc} , c_{wa} are type and fixity conditions of masonry units, c_c is the relative size of beam and column elements and fixity the at base of columns, λ is column slenderness, and h_s and l_w gives the wall geometry. In this formulation the column ratio, denoted by r_c , is defined simply as *the ratio of the sum of the column areas at the base of a building to the floor area above the base*. It was stated that, the wall columns can be included within this sum. Similarly the wall ratio, denoted by r_w , is *the ratio of the effective masonry wall area in a given direction at the base to the floor area above the base*. In this definition, the ratios based on total floor area are obtained by dividing the ratio by the number of floors.

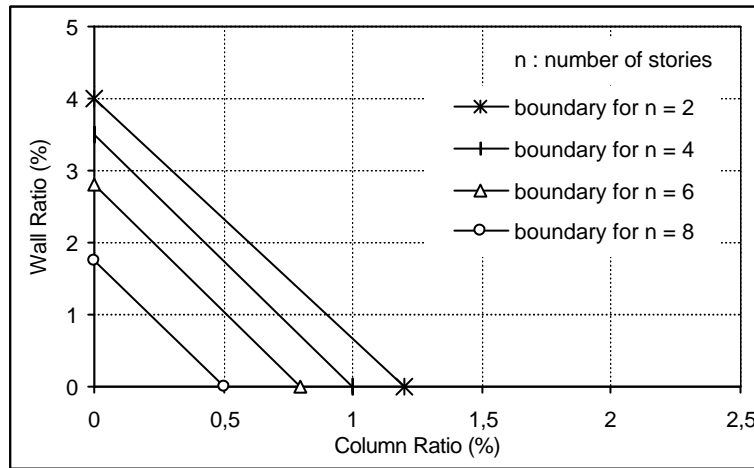


Figure 1.3 Column and wall ratios required to limit drift

They stated that if the two indices (the column and wall ratios) define a point inside a triangular region, drawn considering the effect of number of stories as shown in Figure 1.3, a particular building is judged to have heavy damage.

They made a verification analysis with field data gathered from Erzincan (1992) earthquake, to depict the accuracy of the model. The data from 46 buildings were identified as no damage, light damage, moderate damage and severe damage. They concluded that the data of broad spectrum of workmanship quality, materials and designs was in good agreement with the proposed model that was served as a convenient identifier of seismic vulnerability for existing buildings.

1.3 Object and Scope

Post-earthquake reliability depends on the determination of the physical damage state of a structure that has experienced one or more earthquakes with magnitudes smaller than that of performance earthquake.

The objective of the study described in this dissertation is to determine whether the prior earthquake damage has an effect on the future performance of damaged buildings. The motivation of this study arisen from the observed building failures in recent successive earthquakes. Many reinforced concrete structures have sustained light-to-moderate damage in the Kocaeli earthquake, August 17, 1999 and then suffered heavy damage or partly/completely collapsed in the following Düzce earthquake, November 12, 1999. This phenomenon has been estimated that these are probably resulted from local or global damages that had been caused by the first long duration of severe damaging earthquake having a magnitude of 7.4 and could not withstand the destructive effects of the following (Düzce) strong ground motion having a magnitude of 7.2. The accumulation of damage may lead to collapse during the later successive events. But how the damage from each of the successive events could be predicted and what intensity of these events may cause to substantial increase in the following earthquake damage? Prior earthquake of what intensity substantially influences the damage sustained during the following major earthquake is another question. It has been estimated that failures of the buildings experiencing the successive earthquakes with high damage potential might be influenced substantially by the damage caused by low-cycle fatigue.

Rational damage prediction strongly depends on the selection of the hysteretic model parameters appropriately. To accomplish this purpose the parameters of the Park and Ang hysteresis model, incorporated into IDARC, are calibrated by means of experimental data obtained from the constant and variable amplitude cyclic tests of a total of 22 beam and column specimens. Three ranges of parameters are proposed for the three deterioration levels of structural components.

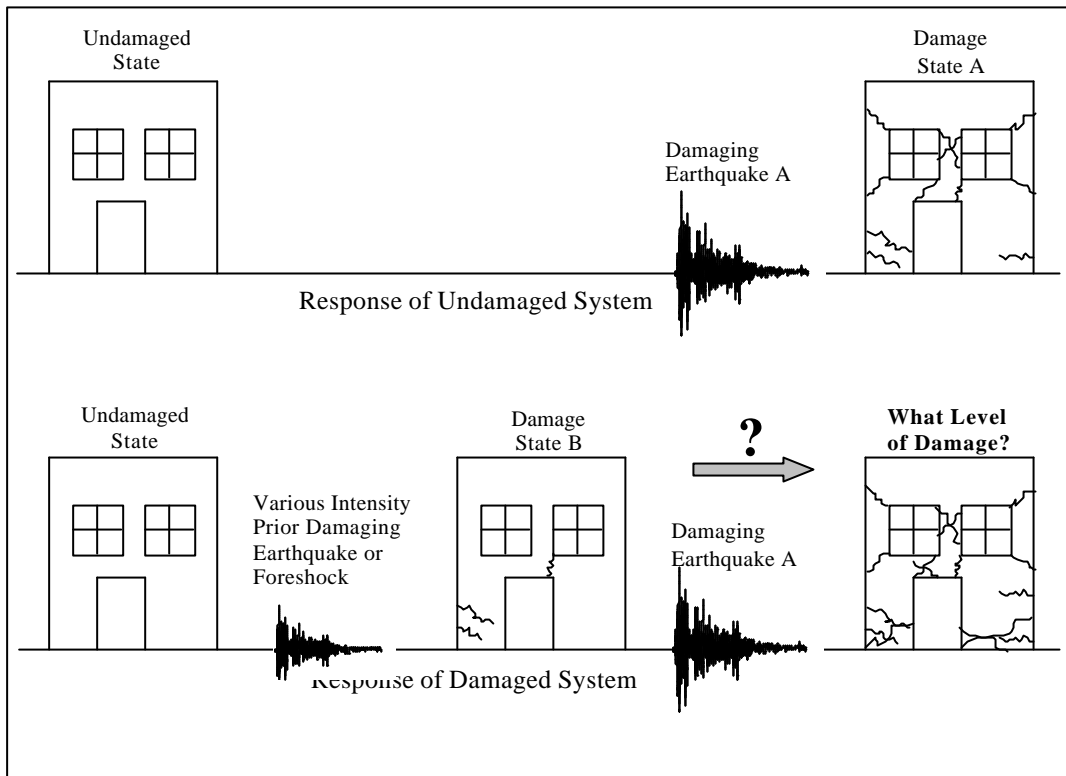


Figure 1.4 Prior earthquake damage

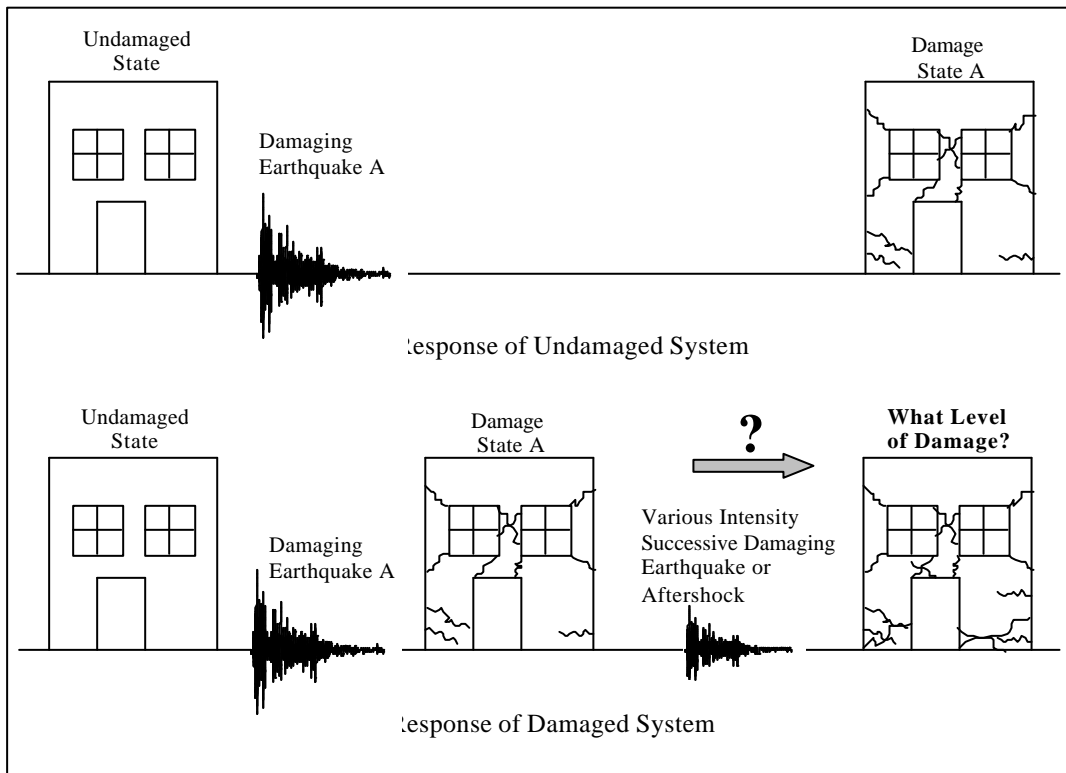


Figure 1.5 Successive earthquake damage

Work conducted in this study consists of analytical studies of representative SDOF and MDOF systems, and models of two selected buildings subjected to ranges of synthetic ground motions. The study was formulated so that the following two questions might be answered;

i) If a building has suffered damage in various intensities of prior earthquake or foreshock, and if that intermediate damage state could be assessed numerically, how this prior damage would influence the damage from a prescribed future successive earthquake (Figure 1.4), and

ii) If a building has suffered damage from a prescribed prior earthquake, and if that damage state could be assessed numerically, what would be the level of damage from future successive earthquakes or aftershocks (Figure 1.5).

For this purpose the inelastic time history and damage analyses of two five-storey buildings are performed. The buildings had experienced two major destructive earthquakes, namely 17 August 1999 Marmara and 12 November 1999 Düzce earthquakes. To assess the low cycle fatigue effects in the damage that is caused by the prior earthquake, these analyses have been carried out using the synthetic accelerograms comprised of base input provided by these two recorded successive ground motions. The proposed ranges of parameters are implemented on the models of the two buildings. To determine the prior earthquake damage effects, the overall structural damages caused by the following 12 November Düzce earthquake have been quantified using the overall structural damage index of the previous (Marmara) destructive ground motion.

The analysis tool employed for this purpose is the package named IDARC 2D V5.0 (A Program for the Inelastic Damage Analysis of Buildings) developed at SUNY Buffalo, as the extension of DRAIN-2D. The section analyses have been carried out using publicly available software (Bentz, 2000).

1.4 Description of Contents of Dissertation

The study is composed of seven chapters and three appendices. The first chapter gives the preliminaries of the study and also includes the literature survey

related with the effects of prior earthquake damage on seismic performance of SDOF and MDOF systems. The researches related to fatigue phenomenon and damage models are also presented.

Chapter 2 covers the quantification of damage using low cycle fatigue principles. Then the damage models developed especially for reinforced concrete components, especially Park and Ang damage model incorporated into IDARC, are introduced. The modeling of stiffness degradation, strength deterioration and pinching parameters of the three-parameter Park and Ang hysteresis model are also discussed.

Chapter 3 presents the search study related with the assessment of the most suitable combination of parameters α , β and γ , to permit predictions about inelastic behavior. First the deterioration parameters α , β and γ are introduced. Then, these parameters are calibrated by using the experimental database gathered from a total of 22 beam and column specimen tests drawn from two sources. Sensitivity of damage index and dissipated hysteretic energy to both hysteretic model deterioration parameters and main structural parameters is designated. For more rational damage prediction, necessity of the fine tuning of these parameters especially parameters β and γ is demonstrated. As a result, three ranges of parameters are proposed for three deterioration levels of structural components.

Chapter 4 includes the systematic assessment of the principal structural damage control parameters, such as axial load level, concrete strength and cross-sectional area. For this purpose, in addition to a large number of two dimensional reinforced concrete section analyses and inelastic time history and damage analyses of SDOF, seismic vulnerability analyses of MDOF frame type structural systems are performed.

In Chapter 5, effect of loading history on dissipated hysteretic energy and damage is investigated. To accomplish this purpose inelastic time history and damage analyses of SDOF systems have been conducted. In these analyses, in addition to various constant and variable amplitude inelastic displacement reversals

with increasing and decreasing order, synthetic ground motions composed of one of the four earthquake records preceded or followed by its various times amplitude-compressed record acting as a prior earthquake (or foreshock) and succeeding earthquake (or aftershock) are used.

Results of the inelastic time history and damage analyses of selected two five story buildings and discussions are presented in Chapter 6. The buildings had experienced the two major destructive earthquakes. To assess the low cycle fatigue effects in the damage caused by the prior earthquake, these analyses have been carried out using the created synthetic accelerograms comprised of base input provided by these two recorded successive ground motions. Comparison of the computed and observed damage is performed for both buildings.

Chapter 7, the last chapter, presents the conclusions and possible future extensions of the study.

Appendix A contains the sample table summarizing the results of the search study conducted for calibration of the deterioration parameters of the IDARC's hysteretic model.

Appendix B contains the engineering drawings of the Çeltiksuyu Regional Primary Education School buildings evaluated to demonstrate the substantial effect of *the ratio of the sum of the column areas at the base of a building to the sum of the floor area above the base* on the seismic performance and damageability of reinforced concrete structures. In addition to snapshots of 3D building models, photographs showing damaged state of the buildings after the experienced 1 May 2003 Bingöl earthquake are included in this appendix.

Appendix C includes the 3D model snapshots and sample engineering drawings of the branch office building of the Ministry of Public Works and Settlement located at Bolu, that experienced the August 17, 1999 Marmara and November 12, 1999 Düzce earthquakes.

CHAPTER 2

LOW CYCLE FATIGUE

2.1 Introduction

Earthquake loads cause a few plastic cycles at relatively large ductility combined with lots of cycles with much smaller deformation demands. The current seismic design philosophy accepts the possibility that the structures undergo a large number of inelastic cycles under shaking of destructive strong ground motions. Experimental and field evidence reveal that the mechanical characteristics of a structural component deteriorate, whenever it is introduced in its plastic range of behavior. Hence, low-cycle fatigue, denoted as a small number of inelastic reversals to failure, is believed to be indispensable especially during severe earthquakes in which structures are expected to undergo several significant reversals of inelastic deformation. Low cycle fatigue based modeling of damage is therefore reasonable. In spite of this, current seismic design procedures do not take into account explicitly the effect of low cycle fatigue reflecting the cumulative damage effect on failure of a structural member.

It should be emphasized that due to the cumulative plastic demands in the structural performance of earthquake-resistant reinforced concrete structures, it is important to include both the damage due to peak response and the damage accumulated through all non-peak plastic cycles. So, it is believed that to assess the damage state of reinforced concrete members, structural damage indices should consider both the peak deformation response and dissipated energy accumulated through plastic cycles underwent during an earthquake.

This chapter aims to present some important features relating to the quantification of damage using low cycle fatigue principles. In addition, damage models developed especially for reinforced concrete will be introduced.

2.2 Quantification of Damage Through Principles of Low Cycle Fatigue

‘Fatigue’ is generally stated as the progressive accumulation of damage in a material up to failure under cyclic loading applications. Assessment of total fatigue life to failure in terms of the cyclic stress or the strain range is the most important purpose of the fatigue design. The number of stress or strain cycles causing fatigue failure in initially uncracked material is estimated under controlled amplitudes of cyclic stresses and strains (Suresh, 1991). Each applied load cycle results in a certain amount of irreversible damage and forms a part of the total fatigue life of a material.

According to the stress level, fatigue can be classified as; ‘low cycle’ fatigue. In low cycle fatigue the stresses are quite high to cause considerable plastic deformations, and the number of cycles to failure is described in terms of strain range. Low cycle fatigue takes place when each load cycle exceeds the yield stress. The number of cycles is less. However, in high cycle fatigue the stresses are low and consequently the material deforms within elastic limits. The fatigue life is expressed in terms of the stress range and a large number of cycles is needed to failure.

‘Damage’ is a widely used term and expresses different phenomena. In reinforced concrete, ‘damage’ describes a certain level of deterioration in structural characteristics, such as, stiffness, strength, ductility, energy dissipation capacity, etc. Under intense ground motion the damage sustained by a reinforced concrete member is similar to the damage experienced in metal fatigue under large strain reversals. The term ‘damage’ when used in this dissertation refers to structural damage caused by an earthquake excitation.

A phenomenological model commonly used for the prediction of fatigue life of metals assumes that the damage process metals can be adequately characterized by

the total strain imposed by the cyclic loading process. The total strain amplitude is assumed to be consists of elastic and plastic strain components (Collins, 1993);

$$\frac{\Delta \mathbf{e}}{2} = \frac{\Delta \mathbf{e}_e}{2} + \frac{\Delta \mathbf{e}_p}{2} \quad (2.1)$$

where $\Delta \mathbf{e}/2$: total strain amplitude, $\Delta \mathbf{e}_e/2$: elastic strain amplitude, $\Delta \mathbf{e}_p/2$: plastic strain amplitude. The elastic strain amplitude represents the damage in the high cycle fatigue range, whereas the plastic strain amplitude represents the damage in the low cycle fatigue range. The fatigue life prediction, both strain amplitudes are commonly expressed in terms the number of load cycles using power-laws.

For high cycle fatigue, the elastic strain amplitude can be written as (Collins, 1993);

$$\frac{\Delta \mathbf{e}}{2} = \frac{\mathbf{s}_f'}{2} (2N_f)^b \quad (2.2)$$

where N_f : number of load cycles, E : Young's modulus of material, \mathbf{s}_f' : fatigue strength coefficient, and b : fatigue strength exponent. One load cycle is assumed to consist of two load reversals.

For low cycle fatigue, Coffin (1954) and Manson (1953) proposed a widely used formula to express the plastic strain amplitude representing low cycle fatigue. They stated that, the logarithm of plastic strain amplitude, $\Delta \mathbf{e}_p/2$, when plotted against the logarithm of load reversals to failure, $(2N_f)$, generates a linear relationship. This relationship can be written as;

$$\frac{\Delta \mathbf{e}_p}{2} = \mathbf{e}_f' (2N_f)^c \quad (2.3)$$

where $\Delta \mathbf{e}_p/2$: plastic strain amplitude, N_f : number of load cycles, \mathbf{e}_f' : fatigue ductility coefficient, and c : fatigue ductility exponent.

The parameters \mathbf{e}_f' , \mathbf{s}_f' , \mathbf{s}_f' and c may be determined from a series of uniaxial fatigue tests performed under constant strain amplitudes.

The strain based model representing low cycle fatigue, described by Equation (2.3) has been extensively calibrated, and for most metals, the exponent c varies between -0.5 and -0.8 (Suresh, 1991; Collins, 1993). An average value of this exponent as -0.6 is commonly assumed for steel. Note that the plastic strain component, $\Delta \mathbf{e}_p/2$, is sometimes referred to as the Coffin-Manson equation (Suresh, 1991).

One of the approaches to follow in the assessment of cumulative structural damage under intense ground motion is to assume that the damage sustained by the structure during a strong earthquake is similar to the damage experienced in metal fatigue under large strain reversals. (Kasiraj and Yao, 1969; Krawinkler and Zohrei, 1993; McCabe and Hall, 1989). Since the number of load cycles experienced during earthquakes is significantly smaller than the number of cycles needed for damage in high-cycle fatigue, seismic damage is normally assessed in terms of the plastic strain component. In structural application, however, characterization of damage in terms of the plastic strain amplitude is less convenient since the response displacement is the more commonly computed response parameter instead of strains. Although size effects may be important especially for members involving brittle fracture, a common approach assumes a correspondence between material and structural damage under large inelastic strain reversals (Krawinkler, 1987; McCabe and Hall, 1989);

$$\Delta_m - \Delta_y = (\Delta_{um} - \Delta_y)(2N_f)^c \quad (2.4)$$

where Δ_m : peak response displacement under cyclic loading; Δ_{um} : ultimate displacement under monotonic loading, and Δ_y : first yield displacement. The left hand side of Equation 2.4 represents the cyclic plastic displacement that is similar to

the plastic strain amplitude $\Delta \mathbf{e}_p / 2$ on the left side of Equation 2.3. The term $(\Delta_{um} - \Delta_y)$ on the right hand side of Equation 2.4 represents the monotonic plastic displacement and is similar to the fatigue ductility coefficient \mathbf{e}_f' which is on the right hand side of Equation 2.3. By adopting a definition for cyclic displacement ductility factor;

$$\mathbf{m}_e = \frac{\Delta_m}{\Delta_y} \quad (2.5)$$

and monotonic displacement ductility factor;

$$\mathbf{m}_m = \frac{\Delta_{um}}{\Delta_y} \quad (2.6)$$

Equation 2.4 can be written as;

$$\left[\frac{\mathbf{m}_e - 1}{\mathbf{m}_m - 1} \right]^{1/c} = 2N_f \quad (2.7)$$

Under a constant amplitude cyclic displacement condition, the number of load reversals ($2N_f$) that may be imposed on the structure decreases exponentially with the magnitude of the imposed displacement as characterized by the displacement ductility factor \mathbf{m}_e (Chai and Romstad, 1997).

The damageability of reinforced concrete members depends upon a large number of factors. When structural components subjected to cyclic inelastic deformations, exhibit both stiffness and strength degradation. Damage quantification of structural systems generally made via the degraded structural response quantities or structural characteristics such as displacement or curvature ductility, stiffness, strength and hysteretic energy.

The principles of stress based characterization of total fatigue life of a component are only relevant for constant amplitude fatigue loading. In reality, however, components are invariably subjected to variable amplitude cyclic loading (Suresh, 1991). The quantification of damage in reinforced concrete structures is usually made via ductility demands for individual members, as the most widely used indicator of damage. Although much effort has been spent on the computation of ductility in reinforced concrete frames, there is little research available which correlates ductility demand with actual observed damage in laboratory experiments. One major problem is that ductility alone may not be a good measurement of damage in reinforced concrete members. Low cycle fatigue type damage, which is caused by a number of inelastic cycles, is also important in failure of reinforced concrete member. Therefore, a combination of sudden high deformations (e.g., denoted by ductility demand) and cumulative fatigue damage may cause the member to fail. There are several alternative analytical damage models for prediction of damage in reinforced concrete frames (Banon et al, 1981).

Quantifying damage level, calculated damage index value measures the damage level between lower and upper limiting cases of the damage scale corresponding to 'no damage' and 'failure'.

2.3 IDARC's Hysteresis Model Control Parameters

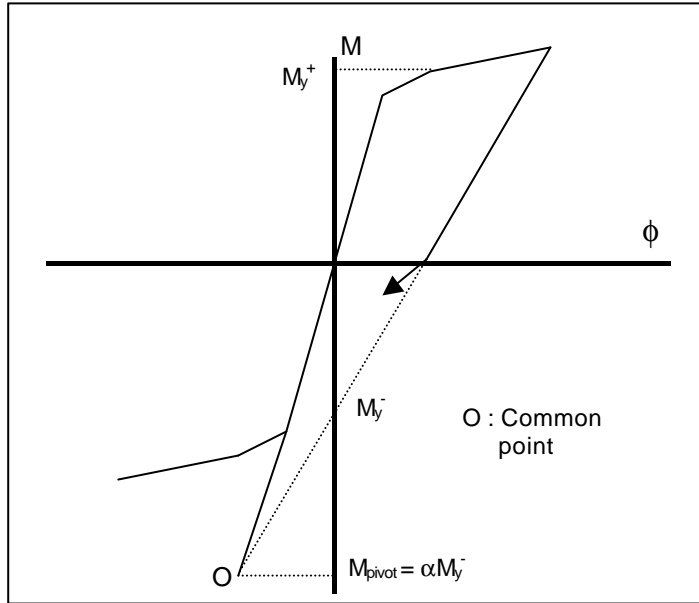
In the last three decades, a good deal of research has been focused on the prediction of post-earthquake seismic resistance and future reliability of damaged reinforced concrete structures. However, the number of research related with the assessment of prior damage effects on the post-earthquake response of structures is quite limited.

Since over the past twenty to thirty years, throughout the world, the earthquake engineering community have made a considerable effort to quantify the local and overall damage caused by shaking of ground motions. Till now, the research conducted on quantifying the structural damage has been concentrated exclusively on the development and application of damage indices. The structural

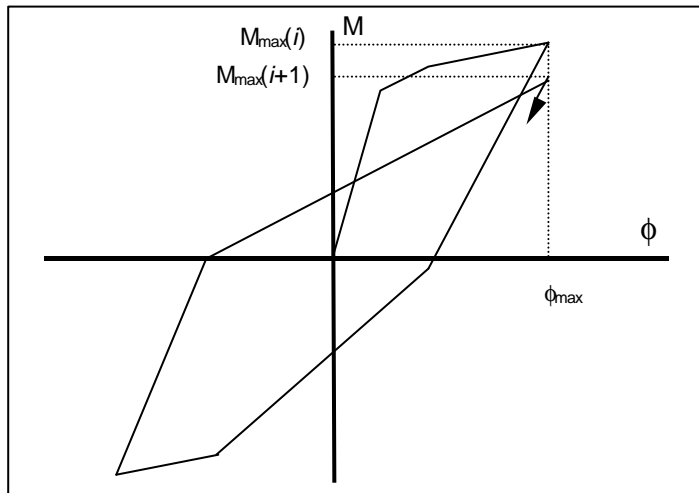
damage indices are generally expressed as a function of one or more damage parameters and many of them are of empirical nature and were originally derived from experimental and analytical studies on metals. It should be emphasized that, structural damage of reinforced concrete structures, substructures or members resulted from ground motion shaking is quantifiable numerically by means of damage indices. Several damage models have been developed by researchers to evaluate the seismic performance of structures. The first fatigue-based cumulative damage rule was developed for metals by Miner (1945) which is introduced in the previous chapter. For years, this cumulative damage rule was considered as a simple criterion for predicting the extent of fatigue damage induced by a certain constant amplitude loadings.

Comprehensive reviews of many of the proposed damage models can be found in the papers by Williams and Sexsmith (1995) and Powell and Allahabadi (1988). Since the non-homogeneous feature, most of these models are not directly applicable to reinforced concrete. The most frequently used models, including the model incorporated in IDARC, are introduced briefly in the first chapter. In this section, the hysteretic model implemented into IDARC will be introduced first. The modeling of deterioration parameters will be graphically expressed. Then quantification of reinforced concrete component damages will be discussed.

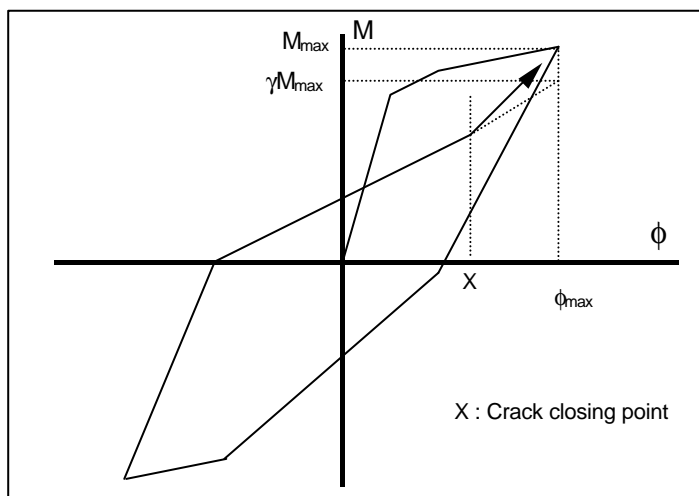
The original release of IDARC used the trilinear monotonic moment curvature relationship, together with a three-parameter hysteresis model developed by Park. The original version of the model is controlled by three parameters simulating the stiffness degradation, strength deterioration and slip or pinching behavior of a structural member. The new release of IDARC employed in this study incorporated the latest type of the Park hysteretic model with four deterioration parameters, namely stiffness degradation, ductility-based strength deterioration, hysteretic energy-based strength deterioration and pinching parameters. The geometric definition and modeling of these parameters are presented in Figure 2.1.



a) Stiffness degradation parameter (α)



b) Strength deterioration parameter (β)



c) Pinching parameter (γ)

Figure 2.1 Modeling of IDARC's hysteresis model control parameters

Stiffness degradation, represented by α , occurs due to geometric effects. The elastic stiffness degrades with increasing ductility. The phenomenon of stiffness degradation was modeled by the pivot rule (Kunnath et al, 1990). According to this rule, the load-reversal branches are assumed to target a common point on the initial elastic stiffness line at a distance of αP_y on the opposite side, where α is the stiffness degradation parameter. The rule assumes that unloading lines target this point until they reach the abscissa (deformation-axis), after which they aim the previous maximum or minimum points. It is recommended to be 2.0. The modeling of this parameter can be seen in Figure 2.1a.

Strength deterioration parameter, denoted by β , specifies the rate of strength degradation, as shown schematically in Figure 2.1b. This parameter represents the ratio of the incremental damage caused by the increase of the maximum response, specified as $d\mathbf{f}_m M_y$, to the normalized incremental hysteretic energy, dE , as follows (Park et al, 1985);

$$\mathbf{b} = \left(\frac{d\mathbf{f}_m}{\mathbf{f}_u} \right) \div \frac{dE}{\mathbf{f}_u M_y} = \frac{d\mathbf{f}_m M_y}{dE} \quad (2.8)$$

The same parameter is used in the definition of the IDARC's damage index. IDARC (Kunnath et al, 1992) requires a user-defined β (strength degradation parameter) with a default value of 0.1 (for well-detailed reinforced concrete sections) and recommends that it should not normally exceed 0.5.

In a new release of IDARC, the strength degradation modeled considering the hysteretic energy, the ductility or both. However, it has been shown that the energy-based strength degradation parameter is the dominant one in quantification of damage while ductility-based strength degradation parameter is almost ineffective. Hence, both parameters are taken as the same values in this study. For the sake of simplicity these parameters will be referred to as the 'strength deterioration parameter, β ,' for the rest of this study.

Pinching or slip occurs as a result of crack closure, bar slip, etc. Pinching or slip behavior is modeled by lowering the target extremum point to a straight level of γP_y along the previous unloading line, where γ is the pinching parameter. Reloading lines target this new point until they reach the crack-closing point. Such a pinching behavior leads to a general reduction of both the size of loops of hysteresis and the amount of dissipated hysteretic energy. For realistic pinching of beams and columns, the recommended value for γ is 0.5 unless poor confinement or other factors indicate high shear stresses leading to bond slip. Figure 2.1c demonstrates the modeling of this parameter. The general meaning of these deterioration parameters of the hysteretic model can be characterized as follows:

- An increase in stiffness degradation parameter slows down the degradation of stiffness,
- An increase in strength deterioration (ductility-based and energy-based) parameter, β , speeds up the strength deterioration, and
- An increase in pinching parameter, γ , decreases the amount of slip.

2.4 Quantification of Damage Using Park and Ang Damage Model

As mentioned in Chapter 1, important research efforts by several scientists have been carried out to develop accurate damage indices to quantify the response of structures.

The widely used, DRAIN-based and general features Park & Ang combined damage model, described by Equation 1.13, was introduced in the first release of IDARC (Park, Reinhorn and Kunnath, 1997). In this model, the structural damage expressed as a linear combination of the damage caused by peak deformation and damage resulted from energy dissipation due to cyclic loading.

IDARC incorporates the fatigue based Modified Park-Ang-Wen damage model, presented in the Equation 1.15, to calculate different damage indices: element, story and overall building damage. This program uses ultimate inter-story deformation and the corresponding story shear force, to calculate the story and overall damage indices. Note that, the element damage is selected as the biggest

damage index of the end sections. On the other hand, story and overall damage indices are computed using weighting factors based on the dissipated hysteretic energy at elements and story levels of the structure, respectively;

$$D_{story} = \sum (I_i)_{component} (D)_{component} \quad ; \quad (I_i)_{component} = \left(\frac{E_i}{\sum E_i} \right)_{component} \quad (2.9)$$

$$D_{overall} = \sum (I_i)_{story} (D)_{story} \quad ; \quad (I_i)_{story} = \left(\frac{E_i}{\sum E_i} \right)_{story} \quad (2.10)$$

where I_i are the energy weighting factors and E_i are the total absorbed energy by the component or story 'i'.

In the new release of IDARC provisions were made so that the user can request printing of the variation of the fundamental period of the structure as the analysis progresses. The program IDARC includes the option to determine the response of the structure at instants during the analysis. Several types of response snapshots can be specified:

- i) Displacement profile,
- ii) Element stress ratios,
- iii) Structural collapse state,
- iv) Damage indices, and
- v) Dynamic characteristics (eigenvalue analysis).

Response snapshots can be requested by the user during pushover, quasi-static or dynamic analysis (Valles et al, 1996).

This model has been shown to be capable of describing the behavior of a large number of laboratory models (Kunnath et al, 1990; Stone and Taylor 1993; Valles et al, 1996). Although the damage model has been calibrated against a large number of observed seismic damage (Kunnath et al, 1990), the need for tuning of the parameters for a particular structural type is the main drawback of this index. Some recommendations have been made for the selection of the stiffness degradation, strength deterioration and pinching parameters. Stone and Taylor (1993) suggest that appropriate values of the parameters vary with structural type, material properties, and construction quality, with the result that some tuning of the parameters is usually needed. On the other hand, Kunnath et al (1990) studied the sensitivity of the

stiffness and strength degradation parameters without considering the pinching parameter. They evaluated the experimental results of only one column specimen that was tested by Wight and Sözen (1973), and stated that for well-detailed sections, analyses results are insensitive to quite substantial changes in the parameter values. Valles et al (1996) proposed some typical ranges of values for these hysteretic parameters referring to deterioration levels of the reinforced concrete member. The major disadvantage of this tri-linear hysteresis model is the undesirable significant arbitrariness in choosing its parameters.

Consequently, the sensitiveness of tuning of the hysteresis model parameters α , β and γ , required for the more accurate damage prediction or measurement of damage sustained is still uncertain. Often, inelastic macro models have been calibrated on an as-needed basis. It is believed that, to overcome the difficulties stemming from these uncertainties in the prediction of damage, given the material properties, axial load, and geometry, one should be able to make reasonably accurate estimates of cyclic response for a prescribed path. Hence, to accomplish the purpose of more rational prediction of damage, the deterioration parameters of the model will be calibrated, using experimental database of a large number of beam and column specimen tests.

The major limitation of the existing damage indices is that they are formulated and validated almost exclusively on the basis of flexural response, neglecting the effect of shear as a cause of seismic damage (Williams et al, 1997). Williams et al (1997) compared eight damage indices using shear-dominated test data. On the basis of comparisons against one set of shear-dominated tests, they stated that the damage sustained was primarily dependent on the deformation level, with the number of cycles of loading having only a small effect. In conclusion, they maintained that the relatively simple, deformation-based damage indices such as modified Park and Ang damage model provide a more reliable indication of the various damage levels than many of the apparently more sophisticated models. However, experience in recent earthquakes suggests that structures often fail in shear or in combined shear and flexure. Therefore, it is convenient to use IDARC incorporating modified Park and Ang damage model in damage measurement.

CHAPTER 3

EVALUATION OF EXPERIMENTAL RESULTS

3.1 General

The need for both engineering understanding of complex behavior and interpretation of the overall inelastic response of reinforced concrete structures to severe earthquake action has brought the concepts of damage and damageability of such structural systems into the forefront of analytical modeling procedures. On the other hand, a rational prediction of damageability requires definition of damage that can be quantified and incorporated into a general analysis program and an analytical tool that is capable of reproducing the inelastic response of reinforced concrete structures and their components with reasonable accuracy (Kunnath et al, 1990).

In recent years, the earthquake engineering community has been interested in the performance based design methods for more rational earthquake resistant seismic design. The underlying general objective of such approaches is the quantitative prediction of the damage level in a structure subjected to earthquake ground motion. Therefore knowledge about structural behavior beyond the onset of damage is needed to bring such methods to maturity. Analyses must be conducted to correlate and quantify the stages of damage with respect to the level of ground shaking. The basic requirement of such analyses is the availability of accurate constitutive hysteretic models capable of representing deteriorating structural behavior and their implementation in computer programs to perform nonlinear structural analyses.

Numerous experimental studies have shown that repeated cyclic loading causes three important effects: stiffness degradation, strength deterioration and “pinching” which is a general reduction of the size of hysteresis loops. This indicates

diminished capacity to dissipate energy. Analytical modeling of the behavior of structural members through mathematical relationships must be based either on theoretical or empirical bases. Hysteresis curves are mathematical relationships commonly used in global seismic behavior calculation of structures. They vary from simple models to complex set of nonlinear equations in which changes in the physical state of the structure are taken into account.

3.2 IDARC Hysteresis and Damage Models

The damage index implemented in IDARC is closely related to the hysteretic behavior of the reinforced concrete member being studied. The IDARC model is a tri-linear monotonic force-deformation relationship, together with a hysteresis model controlled by three-parameters, namely stiffness degradation, strength deterioration and pinching parameters denoted by α , β and γ , respectively. The geometric definition and modeling of these parameters were presented in Chapter 2. Kunnath et al (1990) briefly reviewed the development of the concrete hysteresis model. This model has been shown to be capable of describing the behavior of a large number of laboratory models (Kunnath et al, 1990; Stone and Taylor 1993; Valles et al, 1996). However the sensitivity of tuning of the hysteresis model parameters α , β and γ , required for more accurate damage prediction or measurement of damage sustained is uncertain.

Although the damage model has been calibrated against a large number of observed seismic damage (Kunnath et al, 1990), the need for tuning of the parameters for a particular structural type is the main drawback of this index. Some recommendations have been made for the selection of the stiffness degradation, strength deterioration and pinching parameters. Stone and Taylor (1993) suggest that appropriate values of the parameters vary with structural type, material properties, and construction quality, with the result that some tuning of the parameters is usually needed. On the other hand, Kunnath et al (1990) studied the sensitivity of the stiffness and strength degradation parameters without considering the pinching parameter. They evaluated the experimental results of only one column specimen which was tested by Wight and Sözen (1973), and stated that for well-detailed

sections, analyses results are insensitive to quite substantial changes in the parameter values. Valles et al (1996) proposed some typical ranges of values for these hysteretic parameters referring to deterioration levels of the reinforced concrete members. The major disadvantage of this tri-linear hysteresis model is the undesirable significant arbitrariness in choosing its parameters.

The purpose of the exercise for determining the most suitable combination of parameters α , β and γ in a given case is to permit predictions rather than hindsight comments about inelastic behavior. Often, inelastic macro models have been calibrated on an as-needed basis. Given the material properties, axial load, and geometry, one should be able to make reasonably accurate estimates of cyclic response for a prescribed path. In the absence of such insight, damage models will not serve the purpose for which they have been utilized in the likely state of an intact building after a given ground shaking has shaken it.

3.3 Response Evaluation

This chapter covers a search study concentrated on a reasonable tuning of the stiffness degradation, strength deterioration and pinching parameters, via minimization of the difference between the amounts of experimentally and analytically dissipated total hysteretic energy. For this purpose, the recorded experimental data of a total of 22 reinforced concrete beam and column specimens, tested under constant and variable amplitude displacement histories, has been evaluated. The experiments draw from two sources.

Pujol (2002) tested sixteen cantilever columns at Purdue University under constant and variable amplitude inelastic displacement reversals to determine whether the displacement history has an effect on the drift capacity of reinforced concrete columns. An assembly consisted of two test specimens joined by a center stub through which cyclic transverse load was applied, so sixteen individual cantilever columns were tested. The main variables controlled in the specimens were (i) the spacing of the hoops, (ii) the axial load, and (iii) the displacement history. One of two components of each test assembly will be evaluated in this study.

The remaining fifteen cantilever 1/3 scale beam specimens were tested under constant and variable amplitude displacement histories, to assess the energy dissipation characteristics of structural members exhibiting stiffness degradation and strength deterioration under effects of displacement reversals in the inelastic range (Erberik and Sucuođlu, 2004).

Table 3.1 Properties of R/C beam column test specimens and experimental program

Specimen	LP	f_c (MPa)	r_l (%)	r_s (%)	s (mm)	N (kN)	$N/f_c A_g$	$[N_{cycle}]$ A (mm)	$[N_{cycle}]$ δh (%)	
Pujol (2002)	C10-2-3N	VA	33.7	2.4	0.55	76.2	136	0.087	[7]14+[7]21	[7]2+[7]3
	C10-3-3N	CA	29.9	2.4	0.55	76.2	136	0.098	[9]21	[9]3
	C20-3-3S	CA	36.4	2.4	0.55	76.2	272	0.161	[9]21	[9]3
	C10-1-2.25S	VA	36.5	2.4	0.73	57.2	136	0.080	[7]7+[20]21	[7]1+[20]3
	C10-2-2.25N	VA	34.9	2.4	0.73	57.2	136	0.084	[7]14+[16]21	[7]2+[16]3
	C10-3-2.25N	CA	27.4	2.4	0.73	57.2	136	0.107	[19]21	[19]3
	C10-3-1.5S	VA	32.1	2.4	1.1	38.1	136	0.091	[7]21+[11]27	[7]3+[11]4
	C20-3-1.5*	VA	27.4	2.4	1.1	38.1	272	0.214	[7]21+[10]27	[7]3+[10]4
Erberik and Sucuođlu (2004)	CH-1	CA	20.5	1.3	0.8	35	0	0	[5]28.8	[5]6.4
	CH-2	CA	20.6	1.3	0.8	35	0	0	[6]24.0	[6]5.3
	CH-3	CA	20.6	1.3	0.8	35	0	0	[12]20.8	[12]4.6
	CH-4	CA	20.6	1.3	0.8	35	0	0	[10]16.8	[10]3.7
	CH-5	CA	21.2	1.3	0.8	35	0	0	[12]13.2	[12]2.9
	CH-6	CA	20.6	1.3	0.8	35	0	0	[15]9.6	[15]2.1
	CL-1	CA	13.0	1.3	0.8	35	0	0	[7]15.6	[7]3.5
	CL-2	CA	13.0	1.3	0.8	35	0	0	[10]13.2	[10]2.9
	CL-3	CA	13.0	1.3	0.8	35	0	0	[15]7.6	[15]1.7
	CL-4	CA	13.0	1.3	0.4	70	0	0	[15]7.6	[15]1.7
	CL-5	CA	13.0	1.3	0.8	35	0	0	[20]3.6	[20]1.0
	VH-1	VA	20.6	1.3	0.8	35	0	0	28.8(max)	6.4(max)
	VH-2	VA	21.2	1.3	0.8	35	0	0	20.8(max)	4.6(max)
	VH-3	VA	21.2	1.3	0.8	35	0	0	20.8(max)	4.6(max)
VL-1	VA	13.0	1.3	0.8	35	0	0	15.6(max)	3.5(max)	

*This test failed in an unexpected mode and the cycles applied were limited before buckling of the longitudinal reinforcement at the joint face (Pujol, 2002).

Experimental results obtained from the reinforced concrete beam column specimens that have been evaluated in this study comprising both Pujol column specimens and Erberik and Sucuođlu beam specimens are tabulated in Table 3.1. The

first column indicates the labels of the specimens. The second column shows the loading pattern employed in the loading history: constant amplitude loading (CA) or variable amplitude loading (VA). The following columns are the compressive strength of concrete (f_c), longitudinal reinforcement ratio (ρ_l), transverse reinforcement ratio (ρ_s), hoop spacing (s), axial load (N) and axial load level ($N/f_c A_g$), respectively. The last two columns contain the complete experimental program, including the displacement histories imposed to specimens tested. Displacement history for each test specimen are described in terms of both displacement amplitude and drift ratio ranging from 1 percent to 6.4 percent. The values given in the parentheses are the number of applied constant amplitude cycles.

In the following two sections, the details of the experimental studies will be introduced. Then the sensitiveness of the dissipated hysteretic energy and damage index to the hysteretic model parameters controlling damage will be investigated by using the search method.

3.3.1 Pujol Tests

These tests were conducted to determine whether the displacement history has an effect on the capacity of reinforced concrete columns. For this purpose sixteen cantilever columns were tested under various inelastic displacement reversals. The experimental program included a total of eight tests assemblies. Each specimen was intended to represent a cantilever column under axial load and a point transverse load applied at its end. The center stub was intended to act as the base of the cantilevers (Pujol, 2002). The layout of the test assembly selected for experimental investigation is shown in Figure 3.1. The deformed shape and loading type of the test assembly is presented in Figure 3.2, where positive loads correspond to downward deflections.

The cross section of the specimens was 152 mm wide and 305 mm deep and the shear span (a , distance from the support point to the nearest face of the center stub) was 686 mm. The core area, A_c , was a half of the gross cross-sectional area A_g . The effective depth (d) was 254 mm, for a shear span to effective depth ratio (a/d) of 2.7 (Figure 3.1). The longitudinal reinforcement consisted of four continuous 19 mm

diameter deformed bars with the average yield strength of 453 MPa and an average ultimate strength of 642.6 MPa. Transverse reinforcement outside the center stub consisted of hoops made from plain 6.35 mm diameter bars with average yield strength of 411 MPa and an average ultimate strength of 526.8 MPa. The average concrete strength of 150x300 mm cylinder samples of each assembly ranged from 28.27 to 35.85 MPa.

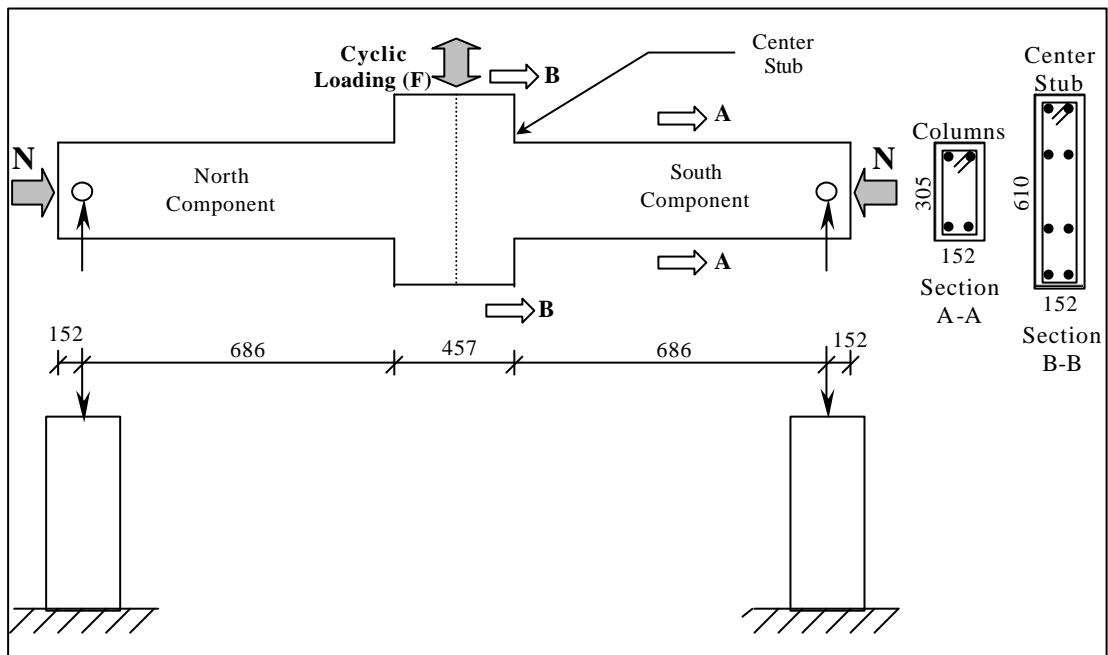


Figure 3.1 Description of test assembly (dimensions in mm)

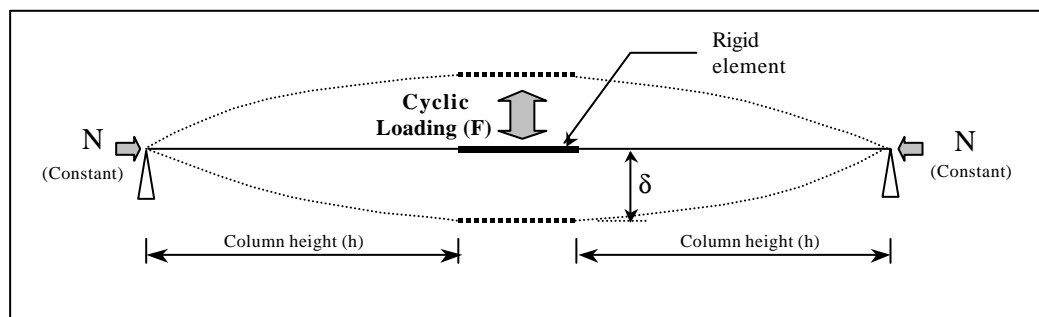


Figure 3.2 Deformed shape of test assembly

The spacing of the hoops outside the center stub was either 38.1, 57.2 or 76.2 millimeters. The axial load was either 136 or 272 kN. Displacement history for each test assembly described in terms of drift ratio (ratio of displacement to shear span) ranged from 1 percent to 4 percent. The displacement at mid-span was controlled so that the larger of the two specimen rotation did not exceed the target maximum drift ratio (Pujol, 2002).

The assemblies are designated using one letter and three numerals: the letter 'C' is the abbreviation of the 'Column'. The first numeral indicates the level of axial load as a percentage of the product $f_c A_g$ presented in the eighth column of Table 3.1 (where f_c is the compressive strength of the concrete and A_g is the gross cross-sectional area). The second numeral indicates the maximum drift ratio to be reached during the initial displacement cycles, and the last numeral is the hoop spacing in inches (Pujol, 2002).

All specimens reached their full flexural capacity and inelastic deformations. Columns susceptible to shear or bond failures before reaching the full flexural capacity were not considered. Although the transverse reinforcement of the specimens was designed to avoid buckling of longitudinal reinforcement during the test of specimen of C20-3-1.5 North (tested under a 272 kN or $0.214f_c A_g$ of axial load level), limited cycles could be applied before buckling of longitudinal reinforcement at the joint face. Test assembly of C20-3-1.5 failed in an unexpected mode under excessive axial load level.

Test results of seven of the test assemblies were taken into consideration. The ranges of the variables in the experiments are summarized in Table 3.1. The main variables controlled in the specimens were the spacing of the hoops outside the center stub, the axial load (kept constant in each test), and the displacement schedule.

Figures 3.3 to 3.8 show comparisons of these independent variables using the loading histories and force-drift ratio relationships recorded during the tests of each assembly. The response of the specimens was interpreted in terms of stiffness

reduction during subsequent cycles. Stiffness was defined as the slope of the line joining the peaks of the shear-drift ratio curve for a given cycle. The peaks of a displacement cycle were defined as the two points most distant to the origin on a shear force versus drift ratio plot (Pujol, 2002).

3.3.1.1 Controlled Variable I: Hoop Spacing

In these column test specimens, the hoop spacing ranged from 38.1 to 76.2 mm which corresponds to the transverse reinforcement ratio ranging from 1.1 percent to 0.6 percent. Two suites of experiments with similar specimens (specimens C10-3-2.25 and C10-3-3, and specimens C10-2-2.25 and C10-2-3) were tested under the same displacement schedule and axial load but with different amounts of transverse reinforcement to study whether the ratio of transverse reinforcement has an effect on drift capacity. Figures 3.3 and 3.4 show the loading histories and force-drift ratio relationships recorded during the tests of these suites of specimens.

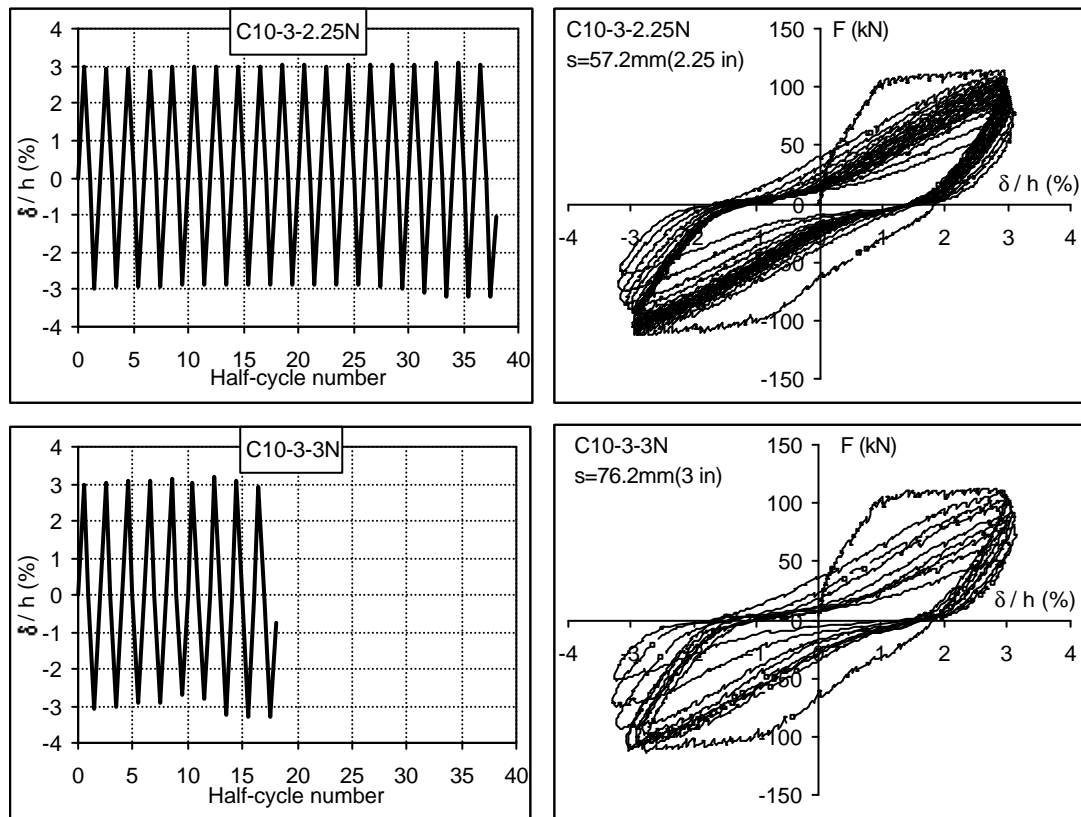


Figure 3.3 Comparison of loading histories and force-drift ratio relationships (Hoop spacing–Test specimen Set 1)

Figure 3.3 shows the displacement histories for specimens C10-3-2.25 North and C10-3-3 North. Both specimens were tested under 136 kN axial load. The hoops in specimen C10-3-2.25 North were placed at 57.2 mm, whereas the spacing of the hoops placed in specimen C10-3-3 North was at 76.2 mm.

Similarly, the loading histories and force-drift ratio relationships shown in Figure 3.4 are for specimens C10-2-2.25 North and C10-2-3 North, tested under the same displacement schedule and axial load but with different amounts of transverse reinforcement. Both specimens were tested under 136 kN axial load and both were subjected to seven displacement cycles at a maximum drift ratio of 2 percent before being displaced to a drift ratio of 3 percent. But the hoops in specimen C10-2-2.25 North were placed at every 57.2 mm, while the hoops in specimen C10-2-3 North were placed at every 76.2 mm.

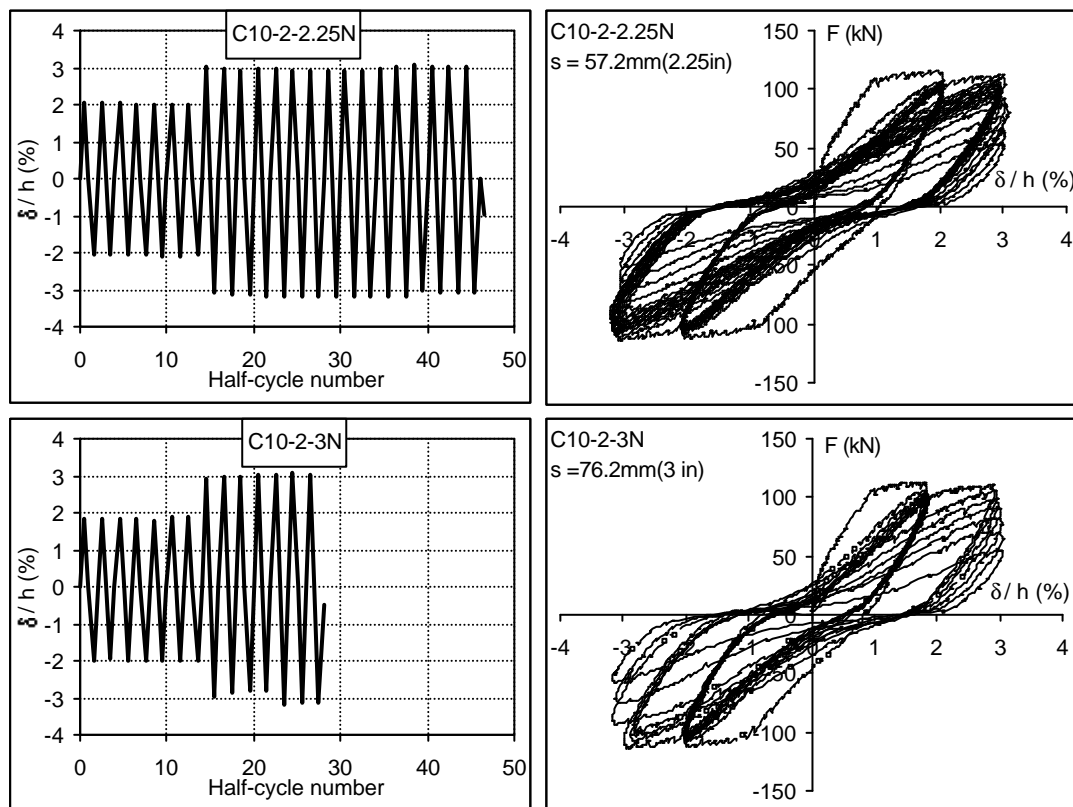


Figure 3.4 Comparison of loading histories and force-drift ratio relationships (Hoop spacing–Test specimen Set 2)

It was concluded that the spacing of the hoops affected the displacement response of the test specimens significantly. As can be shown from Figures 3.3 and

3.4, the smaller the hoop spacing, the larger was the number of cycles that could be sustained at a given maximum drift ratio.

3.3.1.2 Controlled Variable II: Axial Load Level

Two suites of experiments with similar specimens (specimens C10-3-3 and C20-3-3 and specimens C10-3-1.5 and C20-3-1.5) tested under the same displacement schedules and transverse reinforcements but with different axial load level to study whether the axial load has an effect on drift capacity.

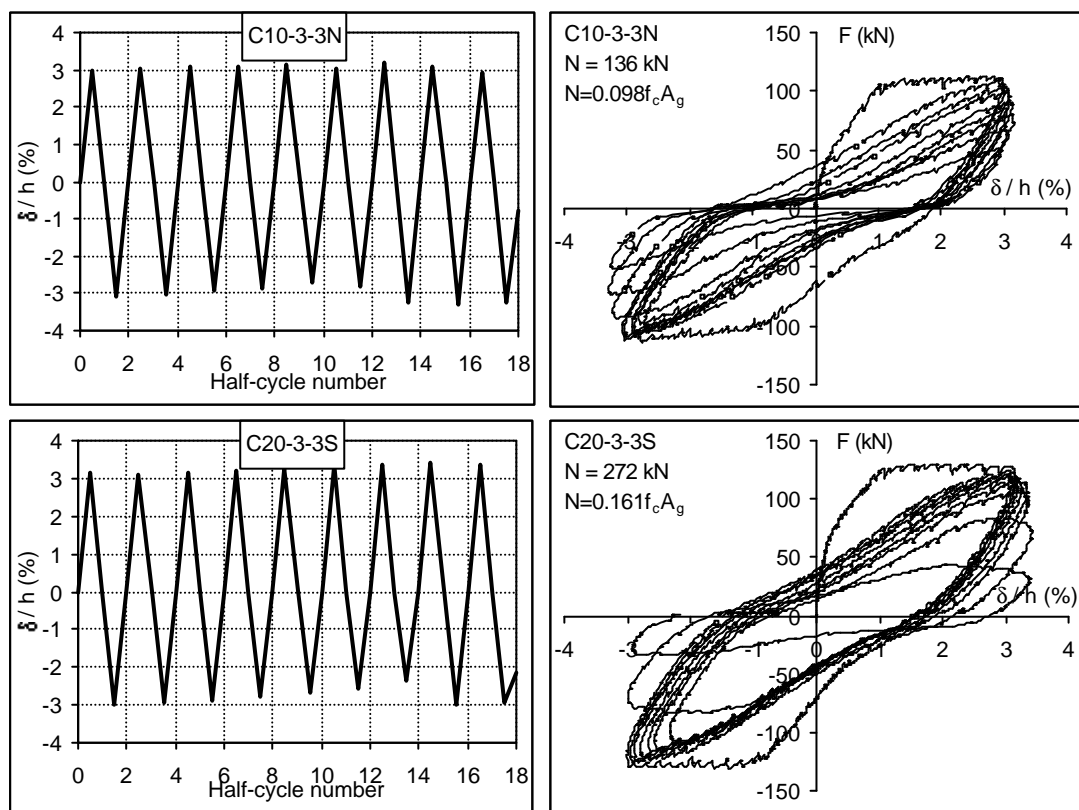


Figure 3.5 Comparison of loading histories and force-drift ratio relationships (Axial load-Test specimen Set 1)

The first pair of specimens was tested under displacement cycles to a drift ratio of 3 percent. Loading histories and force-drift ratio relationships recorded during tests of these specimens sets can be compared in Figure 3.5. The spacing of the hoops in both specimens is 76.2 mm. Specimen C20-3-3 South was tested under a 272kN ($0.161f_cA_g$) while the axial load applied to specimen C10-3-3 North was 136kN ($0.098f_cA_g$). The axial load applied on the specimen C20-3-3S is two times of

the specimen C10-3-3N. But the level of the axial load applied on the specimen C20-3-3S does not correspond to two times of the other component of the suite, due to small differences in their concrete compressive strengths. It was stated that the rate at which stiffness decreased during the final displacement cycles was much higher for the specimen with the higher axial load (C20-3-3 South).

Similarly, specimens C10-3-1.5 and C20-3-1.5 were tested under the same displacement schedule and transverse reinforcement but with different axial load level. The spacing of the hoops in both specimens is 38.1 mm. But specimen C20-3-1.5 North was tested under 272 kN ($0.214f_cA_g$) while the axial load applied to specimen C10-3-1.5 South was 136 kN ($0.091f_cA_g$). Both specimens were tested under displacement cycles at a drift ratio of 4 percent after 7 cycles at a drift ratio of 3 percent. The history of displacements recorded during test of the specimen C10-3-1.5 South is given in Figure 3.6. Although the transverse reinforcement was designed to avoid buckling of longitudinal reinforcement, during the tests of C20-3-1.5 North, a limited number of cycles could be applied before buckling of longitudinal reinforcement at the joint face. It was failed in an unexpected mode. Since the mode of failure did not correspond to phenomenon of Pujol (2002) study, the test data of this assembly was not taken into consideration.

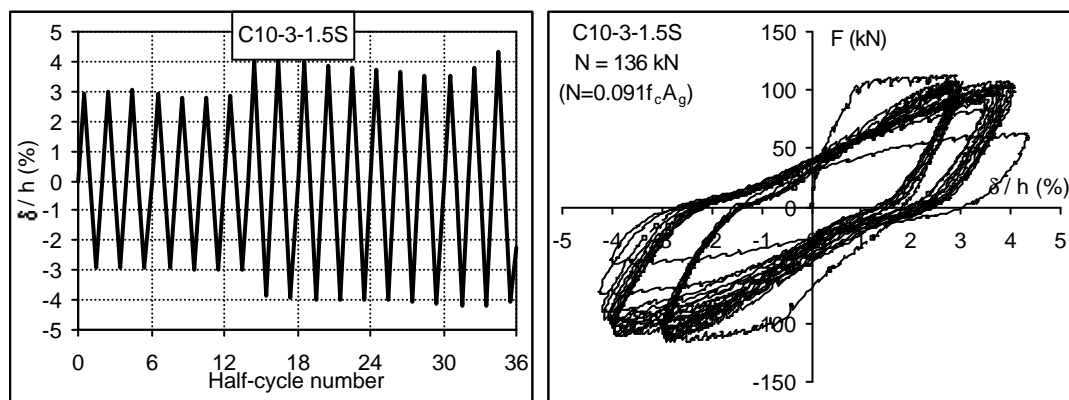


Figure 3.6 Loading history and force-drift ratio relationship (Axial load)

It was concluded that axial load did not affect significantly the number of cycles that could be sustained at given drift ratio before stiffness reduction. But axial load did affect the rate at which stiffness decreased during the final displacement cycles. It was stated that the higher the axial load, the more abrupt was the failure.

3.3.1.3 Controlled Variable III: Loading History

Two series of experiments with similar specimens (specimens C10-1-2.25, C10-2-2.25 and C10-3-2.25, and specimens C10-2-3 and C10-3-3) tested under different displacement schedules were carried out to study whether displacement history has an effect on drift capacity.

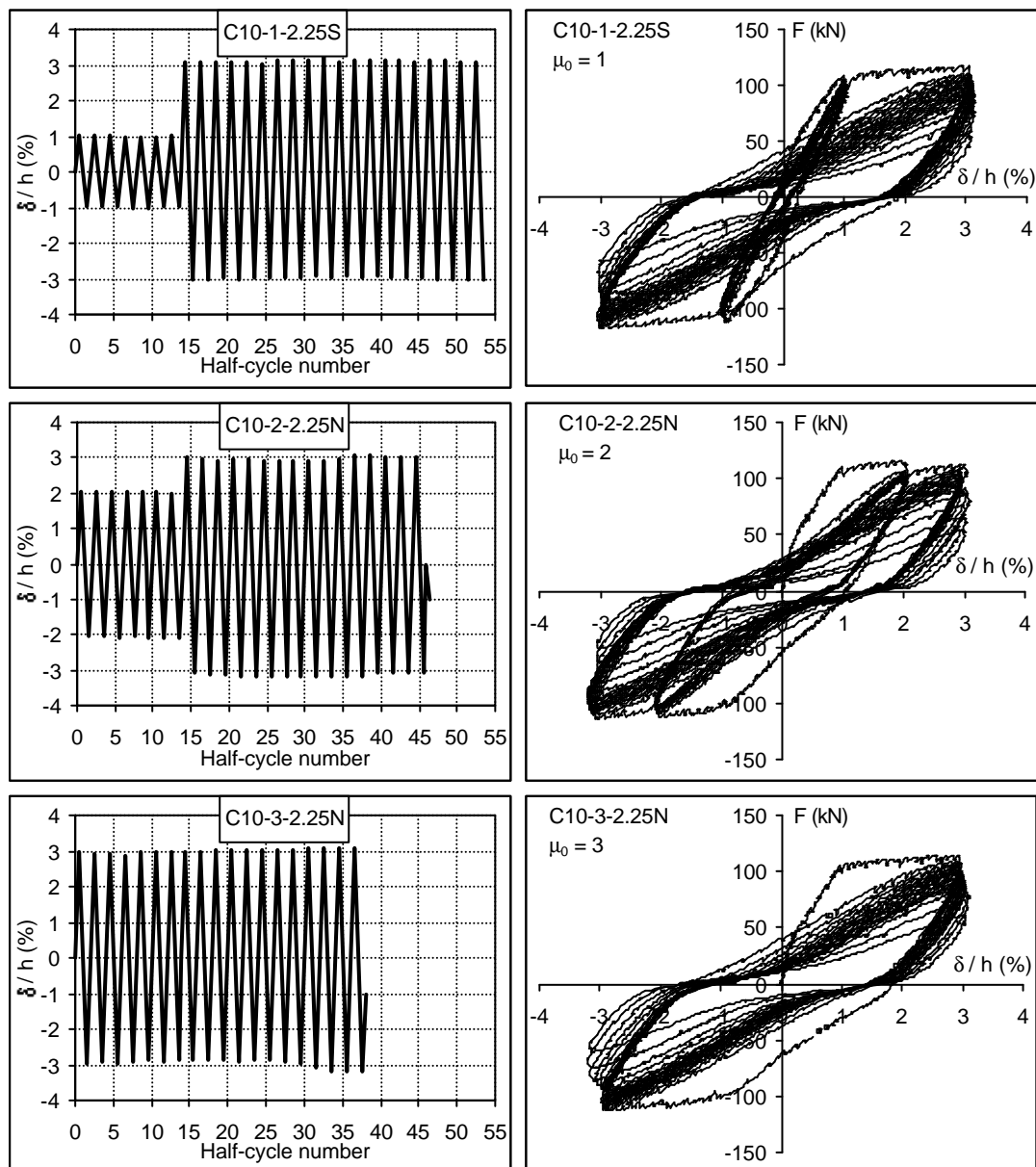


Figure 3.7 Loading histories and force-drift ratio relationships (Displacement history – Test specimen Set 1)

Specimens C10-1-2.25, C10-2-2.25 and C10-3-2.25 were subjected to the same axial load of 136 kN. The spacing of the hoops in all specimens is 57.2 mm. All three sets of specimens were tested at a drift ratio of 3 percent. Specimens C10-3-2.25 were displaced directly to a drift ratio of 3 percent. Specimens C10-1-2.25 were subjected to seven cycles at a drift ratio of 1 percent (approximately the drift ratio at yield) and specimens C10-2-2.25 were subjected to seven cycles at a drift ratio of 2 percent before application of cycles at 3 percent. The displacement histories recorded for the specimens that failed in these assemblies are shown in Figure 3.7. It was stated that the damage caused by cycles at a drift ratio of 2 percent affected the response at 3 percent. On the other hand, damage caused by the cycles at 1 percent did not accelerate the loss of stiffness with cycles at 3 percent.

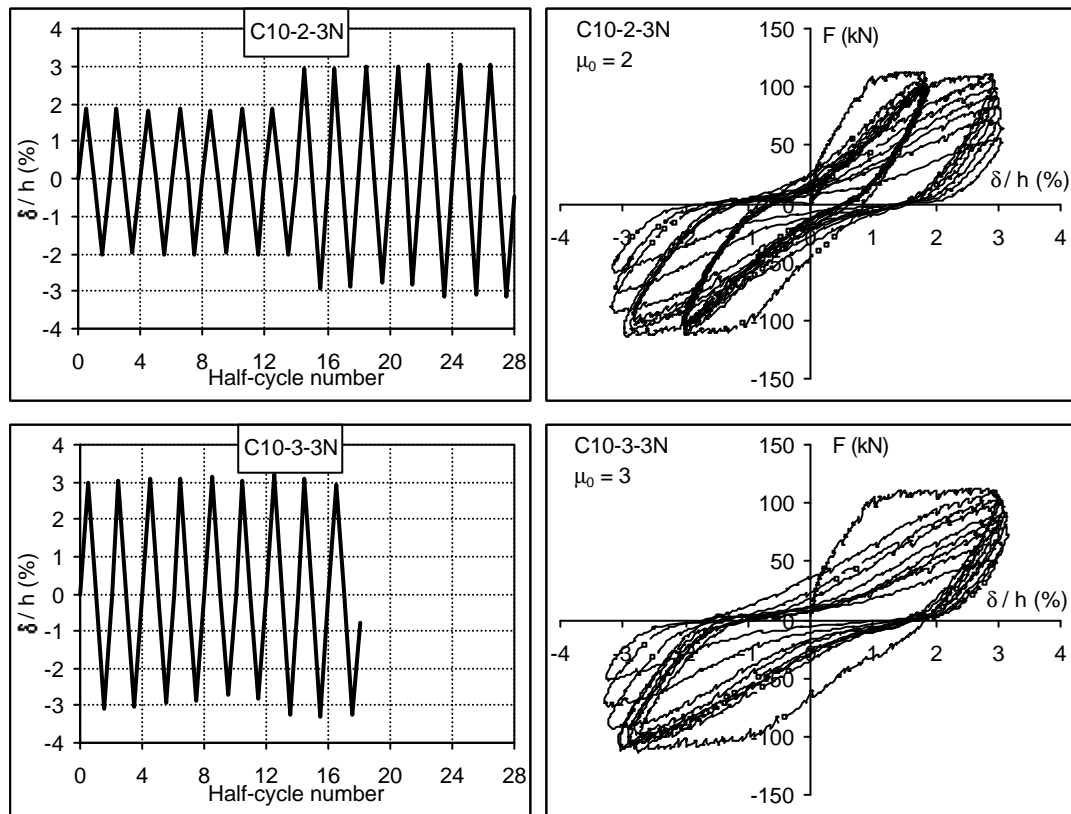


Figure 3.8 Loading histories and force-drift ratio relationships (Displacement history – Test specimen Set 2)

Similarly, specimens C10-2-3 and C10-3-3 had the same axial load of 136 kN and the same amount of transverse reinforcement (76.2 mm of hoop spacing) but

were tested under different displacement histories. Specimens C10-2-3 were subjected to seven cycles of a drift ratio of 2 percent before being tested at 3 percent. On the other hand C10-2-3 were tested directly at 3 percent. Again it was stated that the damage produced by the cycles at 2 percent drift ratio caused the stiffness decrease with cycles at 3 percent to accelerate.

It was concluded that these test series indicated categorically that the displacement history affected the response of reinforced concrete columns under cyclic loading, and the column drift capacity was found to be sensitive to displacement history. It was stated that the number of cycles that could be sustained at a given maximum drift ratio before a large reduction in stiffness, decreased with increasing number and amplitude of previous displacement cycles in the inelastic range of response.

3.3.2 Erberik and Sucuođlu Tests

This section covers the experimental study that concentrated on the assessment of the structural damage under seismic excitation via energy dissipation and low cycle fatigue characteristics of structural systems. For this purpose, a total of seventeen beam specimens were tested in METU, one with monotonic loading, twelve with constant amplitude cyclic loading and four with variable amplitude cyclic loading. The main variable controlled in the specimens was the displacement history.

The test specimen is a 500 mm long cantilever beam with a cross-section of 100x150 mm, a footing with a cross section of 150x250 mm, and a point transverse load applied at distance of 450 mm from the face of the footing. The effective depth (d) was 135 mm, for a shear span to effective dept ratio of 3.33. The dimensions and details of the test specimens were identical except for one in which the spacing of transverse reinforcement was not reduced at the plastic hinge region. The test set-up and the cross-sectional details of the beams can be seen in Figure 3.9. In these tests axial load was not taken into consideration. In eleven specimens the compressive

strength of concrete was 20 MPa representing moderate concrete grade, and it was 13 MPa in the remaining six specimens, representing low concrete grade. Plain bars were employed as longitudinal and transverse reinforcement. The longitudinal reinforcement consisted of four continuous 8 mm diameter plain bars with average yield strength of 330 MPa and average ultimate strength of 470 MPa. Transverse reinforcement outside the footing consisted of hoops made from plain 4 mm diameter bars with average yield strength 270 MPa and an average ultimate strength of 390 MPa. The spacing of the hoops outside the footing at the end region was 70 mm, except for one specimen with a hoop spacing of 35 mm. The properties of these beam test specimens including the experimental program followed are presented in Table 3.1.

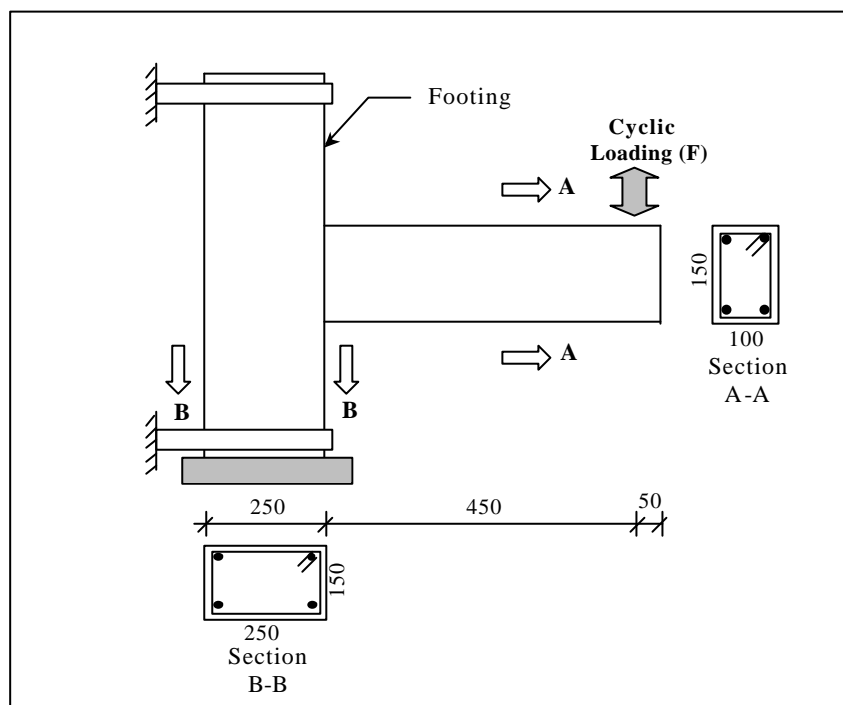


Figure 3.9 Details of beam test specimen (dimensions in mm)

The specimens were designated using two abbreviations and one numeral. The first letter is used for the tests: ‘C’ for constant amplitude tests and ‘V’ for variable amplitude tests. The second abbreviation represents the grade of concrete: ‘H’ stands for the specimens with relatively high target compressive concrete

strength of 20 MPa and 'L' for the specimens with low compressive concrete strength of 13 MPa. The numeral indicates the number of each specimen tested (Erberik and Sucuođlu, 2004).

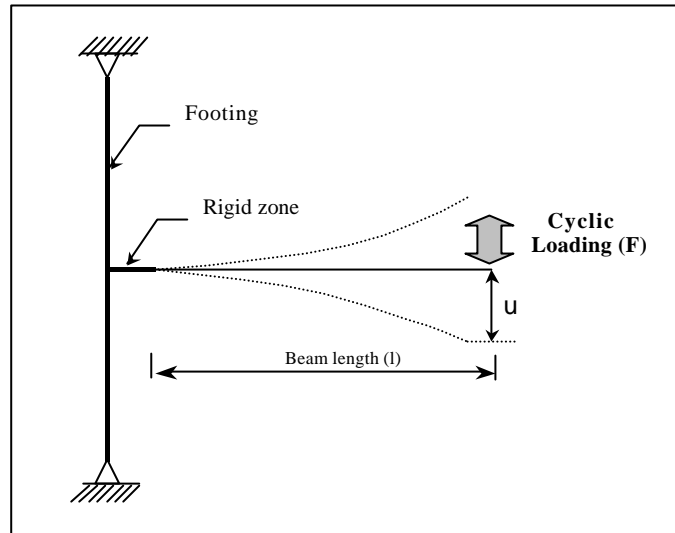


Figure 3.10 Deformed shape of test specimen

The deformed shape and loading type of the test specimens are presented in Figure 3.10 where positive loads correspond to downward deflections.

The main variable controlled in the specimens was the displacement history. All tests were conducted under displacement controlled loading histories. Twelve of the specimens were subjected to cyclic loads with constant amplitudes ranging from 3.6 mm to 28.8 mm, corresponding to ductility ratio of 1 to 8.6 or drift ratio of 1 to 6.4 percent. The remaining four specimens were tested under variable amplitude displacement histories derived from the displacement response histories of an inelastic SDOF system exposed to several recorded earthquake excitations.

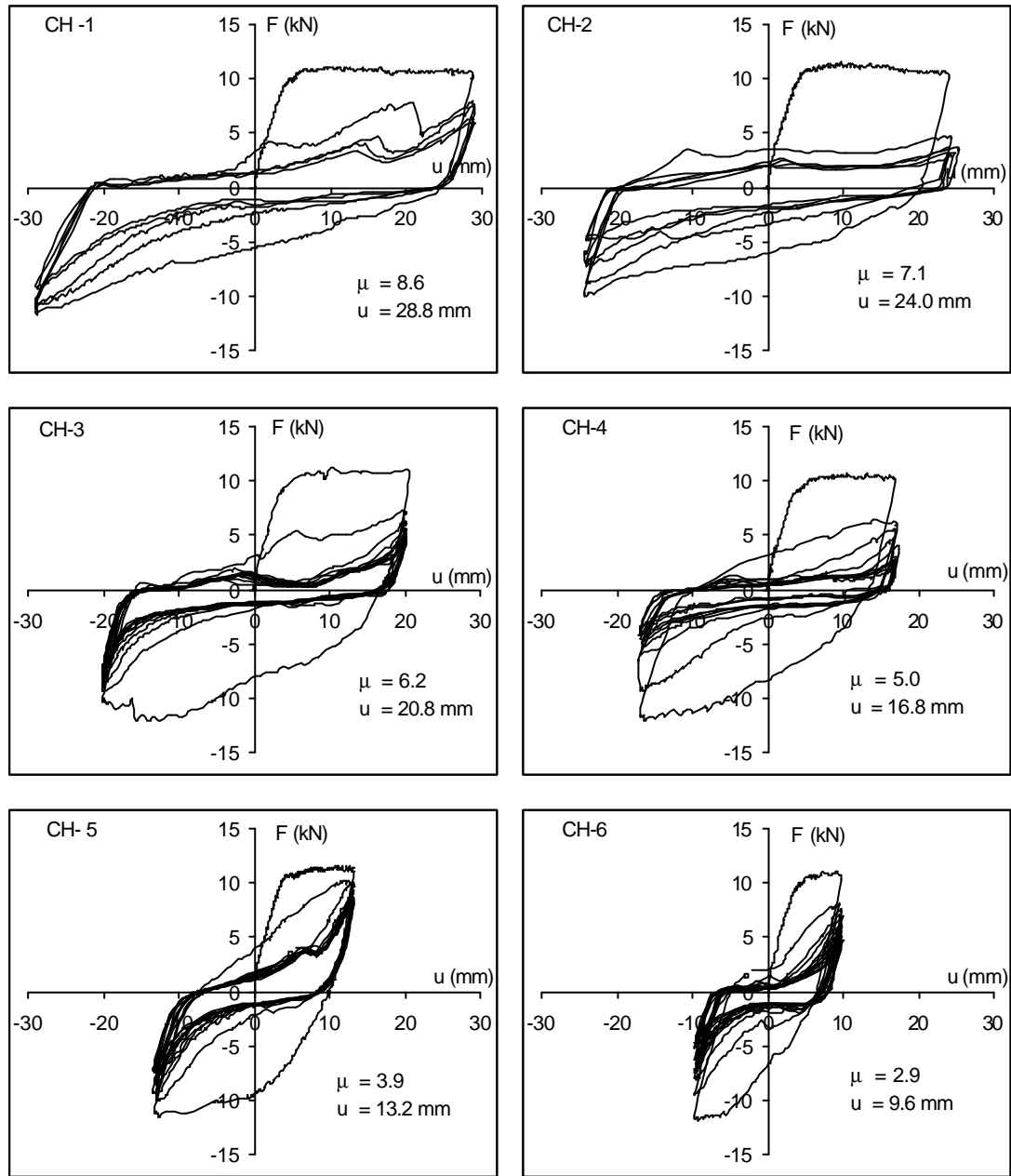


Figure 3.11 Experimental force-displacement relationships for the specimens ($f_c=20\text{MPa}$) tested under constant amplitude displacement histories

Force-displacement relationships for the six specimens with an average concrete compressive strength of 20 MPa and five specimens with an average concrete compressive strength of 13 MPa, tested under various constant amplitude displacement histories are shown in Figures 3.11 and 3.12.

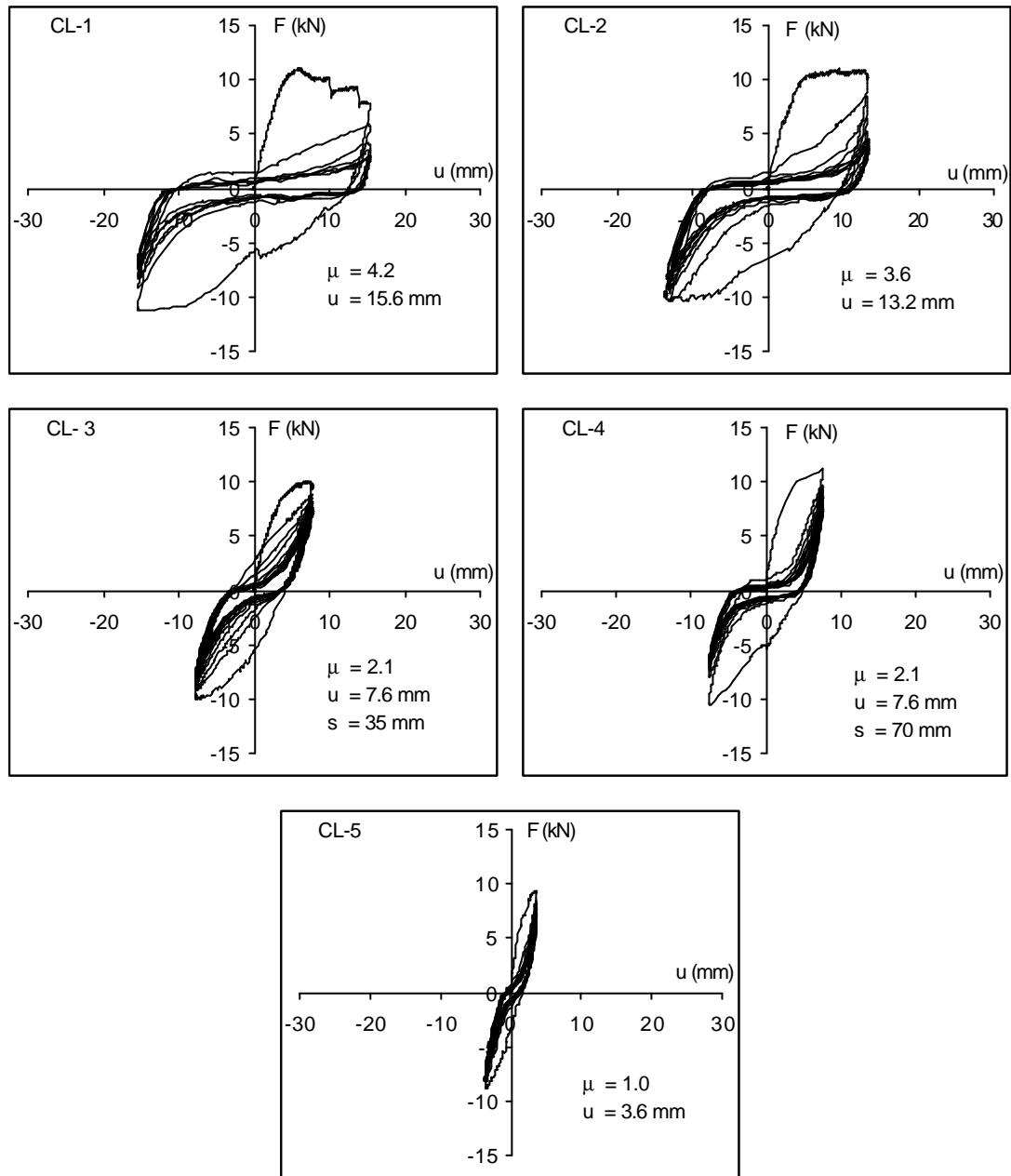


Figure 3.12 Experimental force-displacement relationships for the specimens ($f_c=13\text{MPa}$) tested under constant amplitude displacement histories

Figure 3.13 shows the loading histories and experimental force-displacement relationships for the specimens tested under variable amplitude displacement reversals.

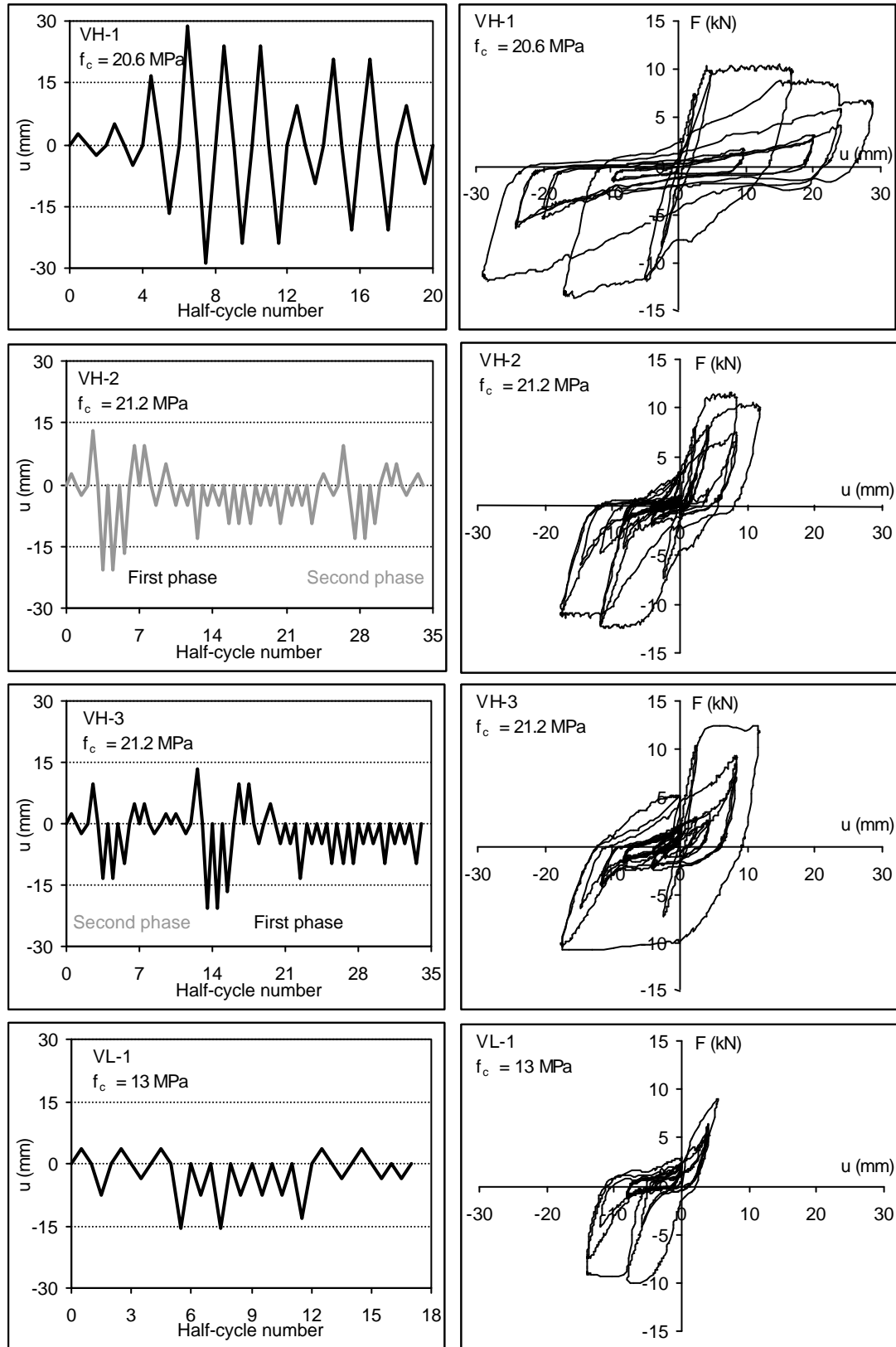


Figure 3.13 Loading histories and experimental force-displacement relationships for the specimens tested under variable amplitude displacement histories

Displacement history of specimen VH-1 was composed of ten symmetric cycles derived from the strong part of the displacement response history of an inelastic SDOF system exposed to NS component of El Centro earthquake record. The non-symmetric loading histories of specimens VH-2 and VH-3 were obtained from the displacement history of a SDOF system subjected to the L component of Bolu record during the 12 November 1999 Düzce earthquake. Displacement loading history of specimen VL-1 was derived from the displacement history of a SDOF system subjected to Düzce EW component of 12 November 1999 Düzce earthquake (Erberik, 2001).

Inspection of the general shape of the hysteresis loops of beam specimens tested by Erberik and Sucuođlu under constant and variable amplitude displacement histories, which are shown in Figures 3.11, 3.12 and 3.13, reveals that the energy dissipation capacity was reduced significantly immediately after the first half-cycle of loading. The loops narrowing initiated at the second half-cycle and influenced substantially the energy dissipation characteristics of the specimens. The area under the second and further half-cycle loops of the hysteresis reduced enormously compared to that of first half-cycle. Such behavior suggests a number of reasons. These small size specimens had a shear span ratio of 3.33, accentuating the effect of shear on the cyclic response which is governed also by a host of other parameters such a degree of confinement, anchorage, concrete properties and boundary conditions. Figures of the loops seem to be peculiar to those tests only, and lacking in universality. The authors are of the opinion that such unusual behavior mainly occurred due to the slip of the longitudinal plain reinforcement (Erberik, 2001; Erberik and Sucuođlu, 2004). It is evident that in the excessive deformations deterioration in strength and stiffness are dominant rather than pinching. While the energy criterion was successful in duplicating analytically the test results, applicability in a wide sense seems to be limited. The degree of transportability of these test results seems to be severely limited in comparison with the results reported by Pujol (2002).

3.4 Systematic Assessment of Deterioration Parameters

Numerous experimental studies have shown that repeated displacement cycles with inelastic range cause reduction in stiffness, deterioration in strength and pinching in reinforced concrete structural members. The three-parameter hysteretic model was first proposed by Park et al (1985) as part of the original release of IDARC (Valles et al, 1996). It incorporates stiffness degradation, strength deterioration, pinching, non-symmetric response and a tri-linear monotonic envelope. Furthermore the Park and Ang damage model implemented in IDARC has been demonstrated to be closely related to the hysteretic behavior of the reinforced concrete members, and it is an integral part of the hysteretic model with three-characteristics (parameters) of concrete hysteresis.

3.4.1 Deterioration Parameters

The three-parameter hysteretic IDARC model was introduced in the previous chapter in detail. In the following sections, the modeling of the stiffness degradation, strength deterioration and pinching or slip parameters will be briefly discussed.

3.4.1.1 Stiffness Degradation Parameter

Stiffness degradation, represented by α , occurs due to geometric effects. The elastic stiffness degrades with increasing ductility. The phenomenon of stiffness degradation was modeled by the pivot rule (Kunnath et al, 1990). According to this rule, the load-reversal branches are assumed to target a pivot point on the initial elastic stiffness line at a distance of αP_y on the opposite side, where α is the stiffness degradation parameter. The rule assumes that unloading lines target this point until they reach the abscissa (deformation-axis), after which they aim the previous maximum or minimum points. The modeling of this parameter can be seen in Figure 2.1a.

3.4.1.2 Strength Deterioration Parameter

Strength deterioration parameter, denoted by β , specifies the rate of strength degradation, as shown schematically in Figure 2.1b. This parameter represents the ratio of the incremental damage caused by the increase of the maximum response, specifying as $d\mathbf{d}_m P_y$, to the normalized incremental hysteretic energy, dE , as follows (Park et al, 1985):

$$\mathbf{b} = \left(\frac{d\mathbf{d}_m}{\mathbf{d}_u} \right) \div \frac{dE}{\mathbf{d}_u P_y} = \frac{d\mathbf{d}_m P_y}{dE} \quad (3.1)$$

Actually the same parameter is used in the definition of the IDARC damage index.

3.4.1.3 Pinching or Slip Parameter

Pinching or slip occurs as a result of crack closure, bar slip, etc. Pinching or slip behavior is modeled by lowering the target extremum point to a straight level of γP_y along the previous unloading line, where γ is the pinching parameter. Reloading lines target this new point until they reach the crack-closing point. Such a pinching behavior leads to a general reduction of both the size of loops of hysteresis and the amount of dissipated hysteretic energy. Figure 2.1c demonstrates the modeling of this parameter.

This IDARC hysteresis model has been shown to be capable of describing the behavior of a large number of laboratory tests (Kunnath et al, 1990; Valles et al, 1996; Stone and Taylor 1993). Stone and Taylor (1993) suggest that appropriate values of the parameters vary with structural type, material properties, and construction quality with the result that some tuning of the parameters is usually needed. Kunnath et al (1990) studied on the sensitivity of the stiffness and strength degradation parameters without considering the pinching parameter. They used experimental result of an only one column which had been tested by Wight and Sözen (1973), and stated that for well-detailed sections, the effect of varying these parameters does not significantly alter the response, and the use of three-parameter model does not require extensive calibration or correlation to estimate a reasonable

range of values for practical use in analysis. They claimed that, analyses results are insensitive to quite substantial changes in these parameter values.

However the amount of tuning of the hysteresis model parameters required for determination of damage with reasonable accuracy is uncertain. The simplicity of the damage model and its calibration against an extensive experimental data and a significant amount of observed seismic damage, included some instances of shear and bond failures are interpreted as the model main advantages compared to developed other damage models. Although some recommendations were made for the selection of the stiffness degradation, strength deterioration and pinching parameters, the need of their tuning for a particular structural type is its main drawback.

This section of the dissertation is an attempt to understand the sensitivity of both damage index and energy dissipation to deterioration parameters of the hysteresis model. For this purpose, the quasi-static analyses of a total of twenty-two beam column specimens, tested by Pujol (2002) and Erberik and Sucuođlu (2004) under cyclic loading, have been performed using the displacement histories recorded during the tests.

3.4.2 Calibration of Deterioration Parameters

A theoretical or empirical modeling of the complex behavior of structural members through mathematical relationships is an imaginary world; hence, experimental testing is a better indicator than complex analytical predictions based on approximate assumptions. Force-deformation relationships of the beam column specimens tested by Pujol (2002) and Erberik and Sucuođlu (2004) have shown that the hysteretic behavior of reinforced concrete structural members is dependent upon numerous structural parameters, such as amount of transverse and longitudinal reinforcement, axial load level, concrete strength, loading history, etc. These parameters affect considerably the deformation and energy dissipation characteristics of the members. It is, therefore, important to recognize that in order to reproduce closely the hysteretic behavior of various components, a highly versatile model is

required in which several significant aspects of hysteretic loops can be included, such as stiffness degradation, strength deterioration, pinching, and the variability of the energy dissipation capacities at different deformation levels under repeated cyclic loading. Moreover, the calibration of the model is essential since it will provide information about the sensitivity of the deterioration parameters on the component behavior and their possible range of numerical values for which the model reflects better the observed behavior. As the results of the calibration of the three parameters and their sensitivity evaluation, three ranges of parameter values are proposed for the defined three classes of structural performance.

The results of the analyses are expressed in terms of as damage indices and hysteretic energy dissipated by the reinforced concrete member being studied. The analyses tool used was the Park and Ang damage model based on dissipated hysteretic energy and ductility.

3.4.2.1 Method of Calibration

This section of the study covers a search focused on clarification of the significant arbitrariness in the hysteretic model parameters choice, which is undesirable. The damage model is a qualitative indicator of damageability and energy reserves in the overall structural system, and it should represent the damage state level to be predicted or observed in post-earthquake inspections of reinforced concrete structures and their components. It is estimated that, ‘the extent the structure has undergone damage’ and ‘whether the damage index is sensitive to tuning of deterioration parameters of the model or not’ are the unidentified points in need of clarification.

IDARC model expresses the structural damage as a linear combination of the damage caused by peak deformation and that contributed by hysteretic energy dissipation due to repeated cyclic loading. The amount of dissipated hysteretic energy is determined by accumulation of the enclosed area of force-displacement loops during the response history. It has been estimated that since the loading histories imposed on the specimens are displacement controlled, the energy

dissipation capacity is the model's remaining unique variable to be controlled by these three parameters. Hence, the total amount of the hysteretic energy dissipated by the member being studied has been considered as the main variable in the calibration process. The calibration of the parameters is performed by the minimization of the difference (denoted as 'error' in the following figures) between the amounts of experimentally and analytically computed dissipated hysteretic energy by using a search method. In other words, the results of the calibration process were sorted with respect to the error in the total amount of dissipated energy as each independent parameter was varied. The local minimum point is found by a search. Visually the strategy of a search is to pick the direction that is steepest uphill (or downhill) from the guessed point and move in that direction until the graph levels out. The level spot is the new guess to approach the solution point. The parameter values have been changed to find the minimum value. The search is continued up to the minimum positive or negative value closing to zero. Near the solution, the gradient approaches zero. The gradient is zero at the solution point whose coordinates are the best parameter values giving the most accurate damage state level of the particular component studied. For a fuller understanding of the role of the parameters, a systematic sweep procedure through all possible values of the range of controlling parameters was done here.

3.4.2.2 Discussion on Calibration Process

The three-dimensional drawings showing the variations of energy dissipated ratio error and damage index error, are presented in Figures 3.14a,b to 3.35a,b. In these figures ' E_{error}/E ' denotes the *error ratio* of the dissipated hysteretic energy, which is defined as the ratio of the total amount of hysteretic energy dissipated in each iteration to the experimentally dissipated hysteretic energy (given numerically in Figures 3.14c to 3.35c) for each specimen. The *damage index error* labeled as ' D_{error} ' in these figures is described as the difference between the damage indices obtained in each iteration and solution point that has coordinates constituting the most suitable combination of deterioration parameters. As a result of calibration process, numerical values obtained for the sample specimen (Pujol column specimen C10-2-3N) tabulated in Table A.1 in Appendix A.

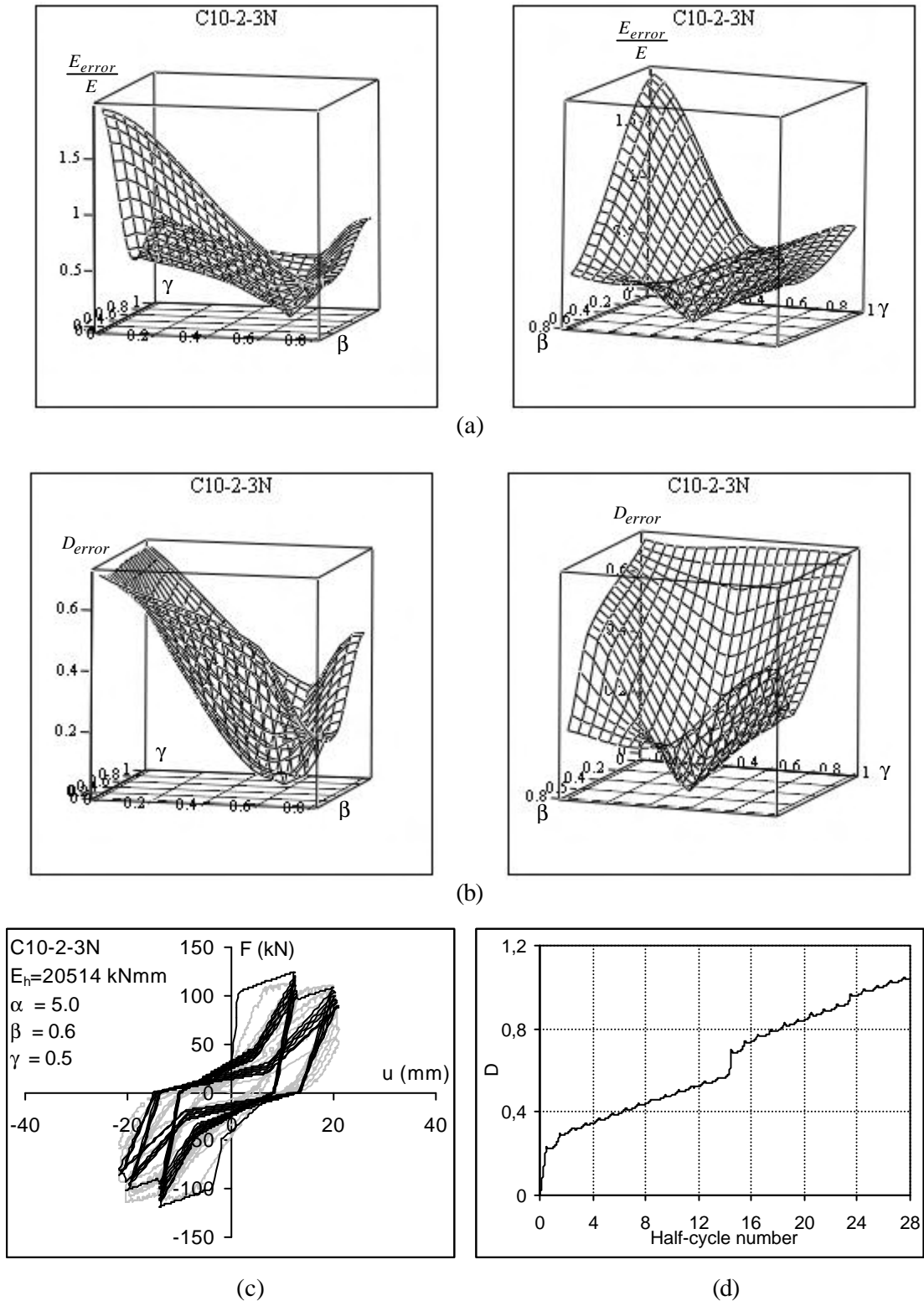
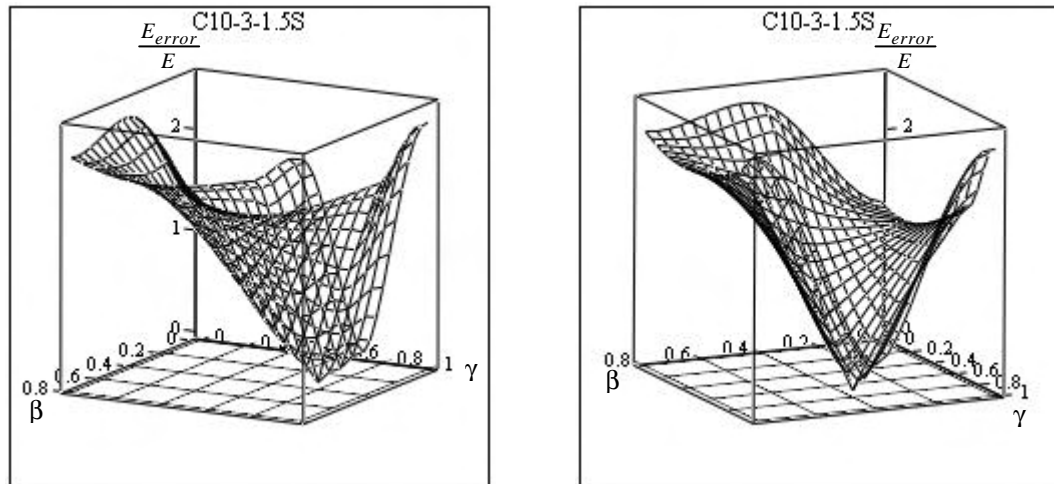
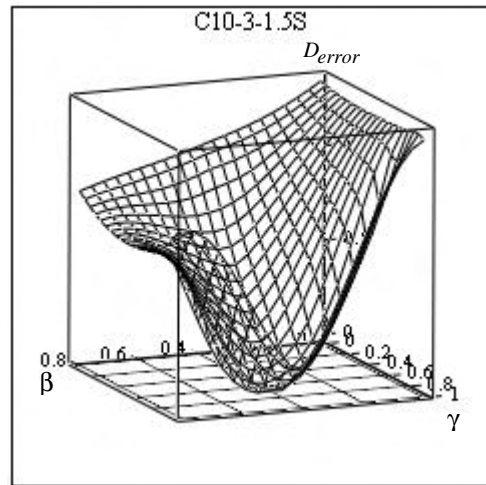
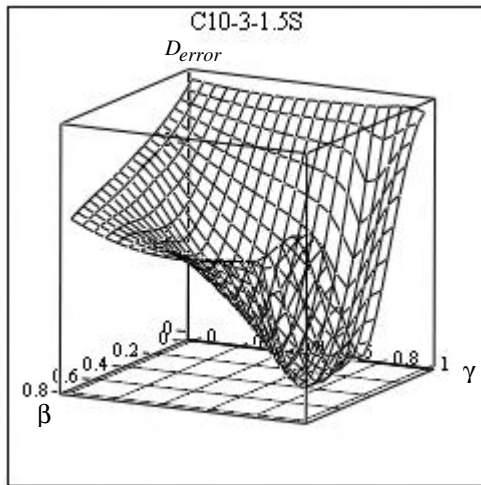


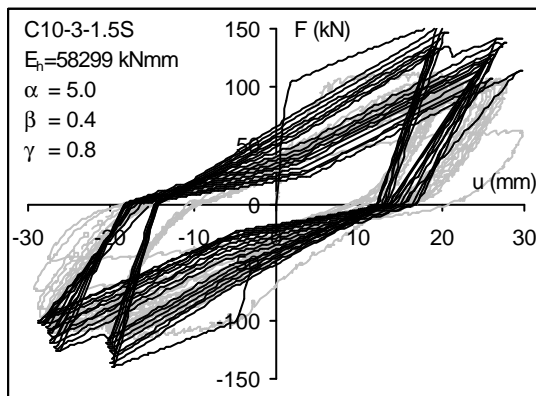
Figure 3.14 Pujol column test specimen C10-2-3 North: **a)** Surfaces of variation in the dissipated hysteretic energy error ratio for $\alpha=5.0$ and β and γ parameters, **b)** Surfaces of variation in the damage index error for $\alpha=5.0$ and β and γ parameters, **c)** Comparison of the experimental (gray curve) and analytical (black curve) force-deformation relationships, **d)** Analytical progressive damage curve



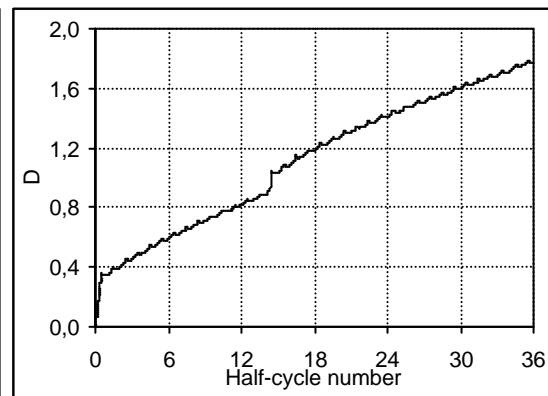
(a)



(b)



(c)



(d)

Figure 3.15 Pujol column test specimen C10-3-1.5 South: **a)** Surfaces of variation in the dissipated hysteretic energy error ratio for $\alpha=5.0$ and β and γ parameters, **b)** Surfaces of variation in the damage index error for $\alpha=5.0$ and β and γ parameters, **c)** Comparison of the experimental (gray curve) and analytical (black curve) force-deformation relationships **d)** Analytical progressive damage curve

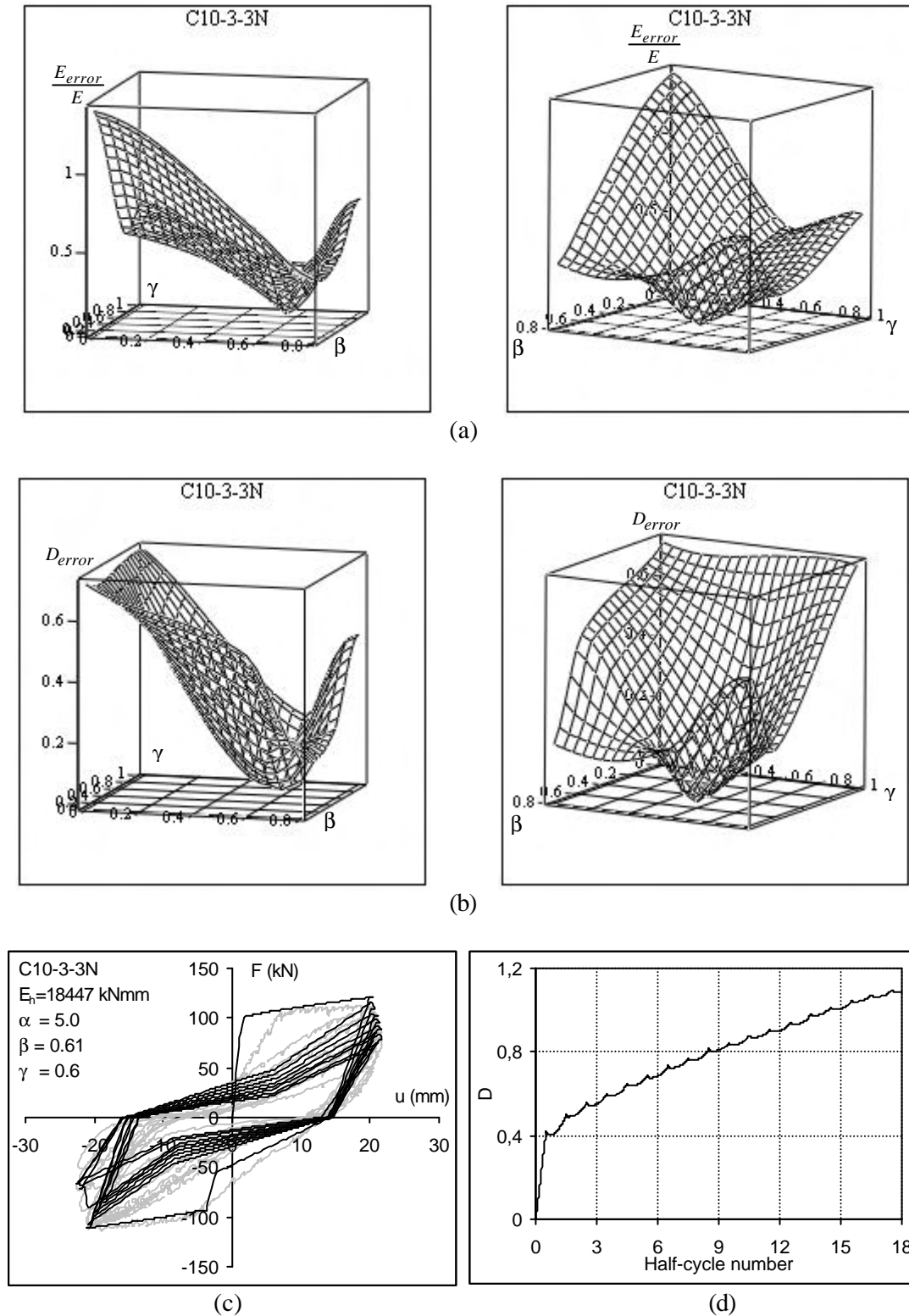


Figure 3.16 Pujol column test specimen C10-3-3 North: **a)** Surfaces of variation in the dissipated hysteretic energy error ratio for $\alpha=5.0$ and β and γ parameters, **b)** Surfaces of variation in the damage index error for $\alpha=5.0$ and β and γ parameters, **c)** Comparison of the experimental (gray curve) and analytical (black curve) force-deformation relationships, **d)** Analytical progressive damage curve

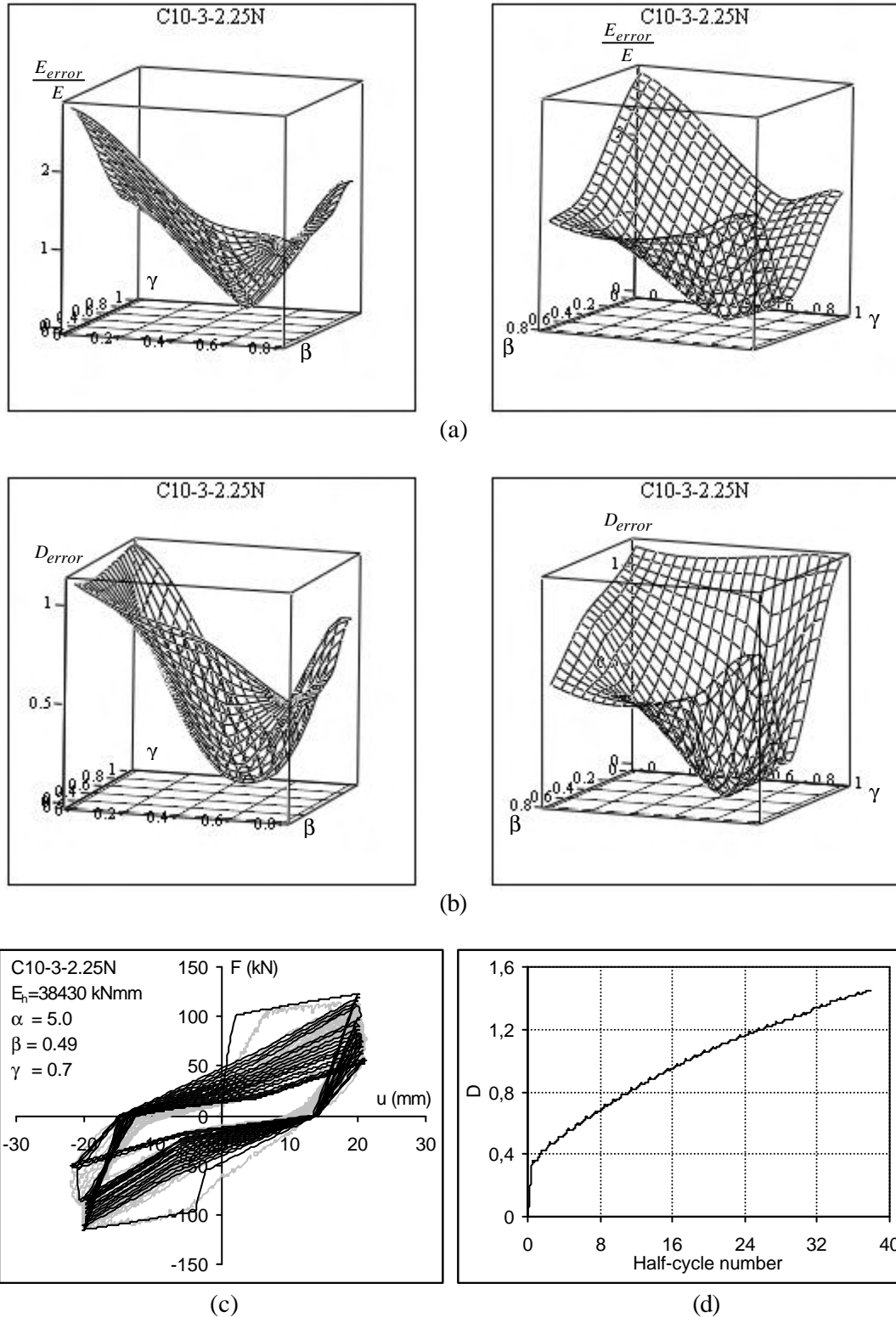


Figure 3.17 Pujol column test specimen C10-3-2.25 North: **a)** Surfaces of variation in the dissipated hysteretic energy error ratio for $\alpha=5.0$ and β and γ parameters, **b)** Surfaces of variation in the damage index error for $\alpha=5.0$ and β and γ parameters, **c)** Comparison of the experimental (gray curve) and analytical (black curve) force-deformation relationships, **d)** Analytical progressive damage curve

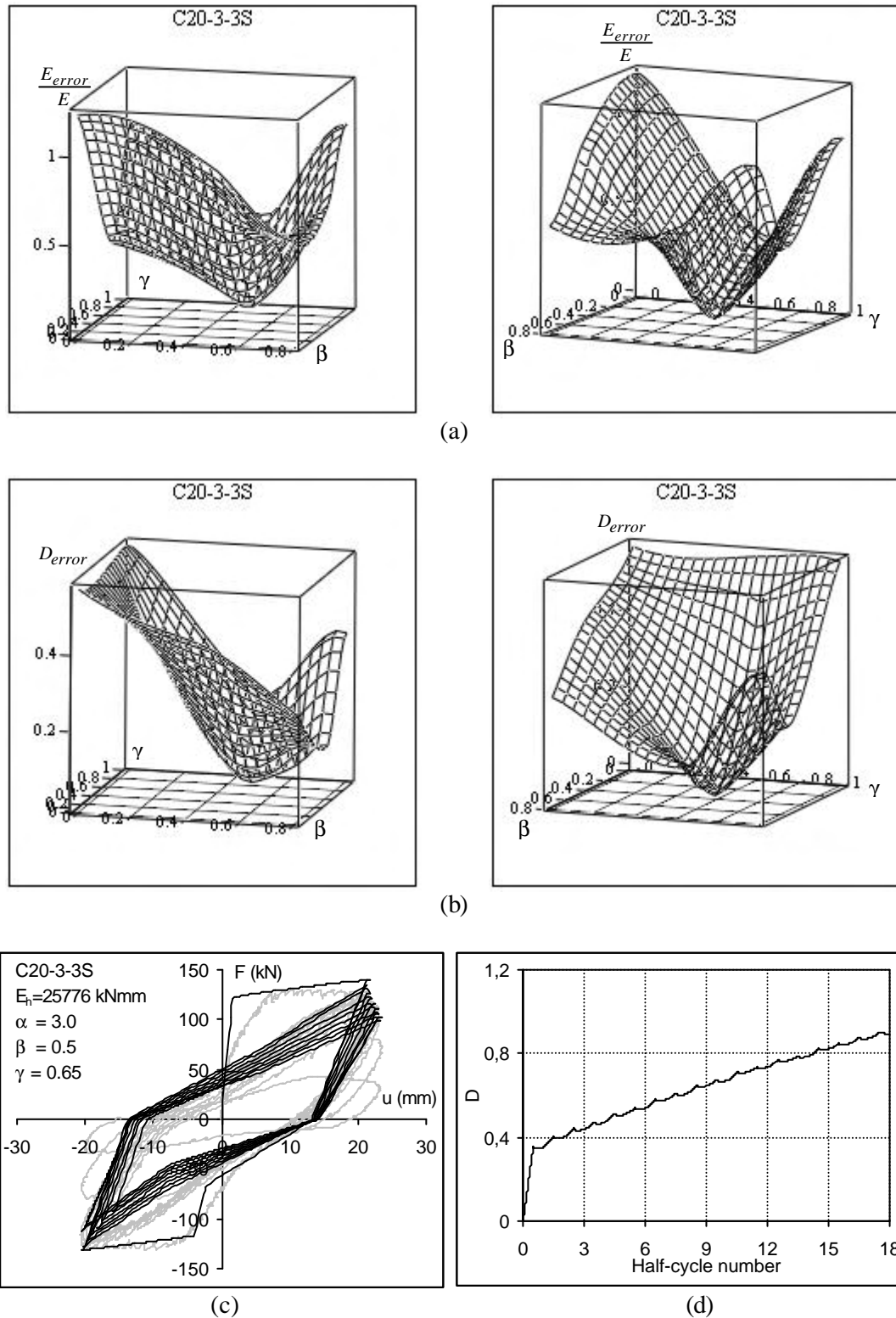


Figure 3.18 Pujol column test specimen C20-3-3 South: **a)** Surfaces of variation in the dissipated hysteretic energy error for $\alpha=3.0$ and β and γ parameters, **b)** Surfaces of variation in the damage index error for $\alpha=3.0$ and β and γ parameters, **c)** Comparison of the experimental (gray curve) and analytical (black curve) force-deformation relationships, **d)** Analytical progressive damage curve

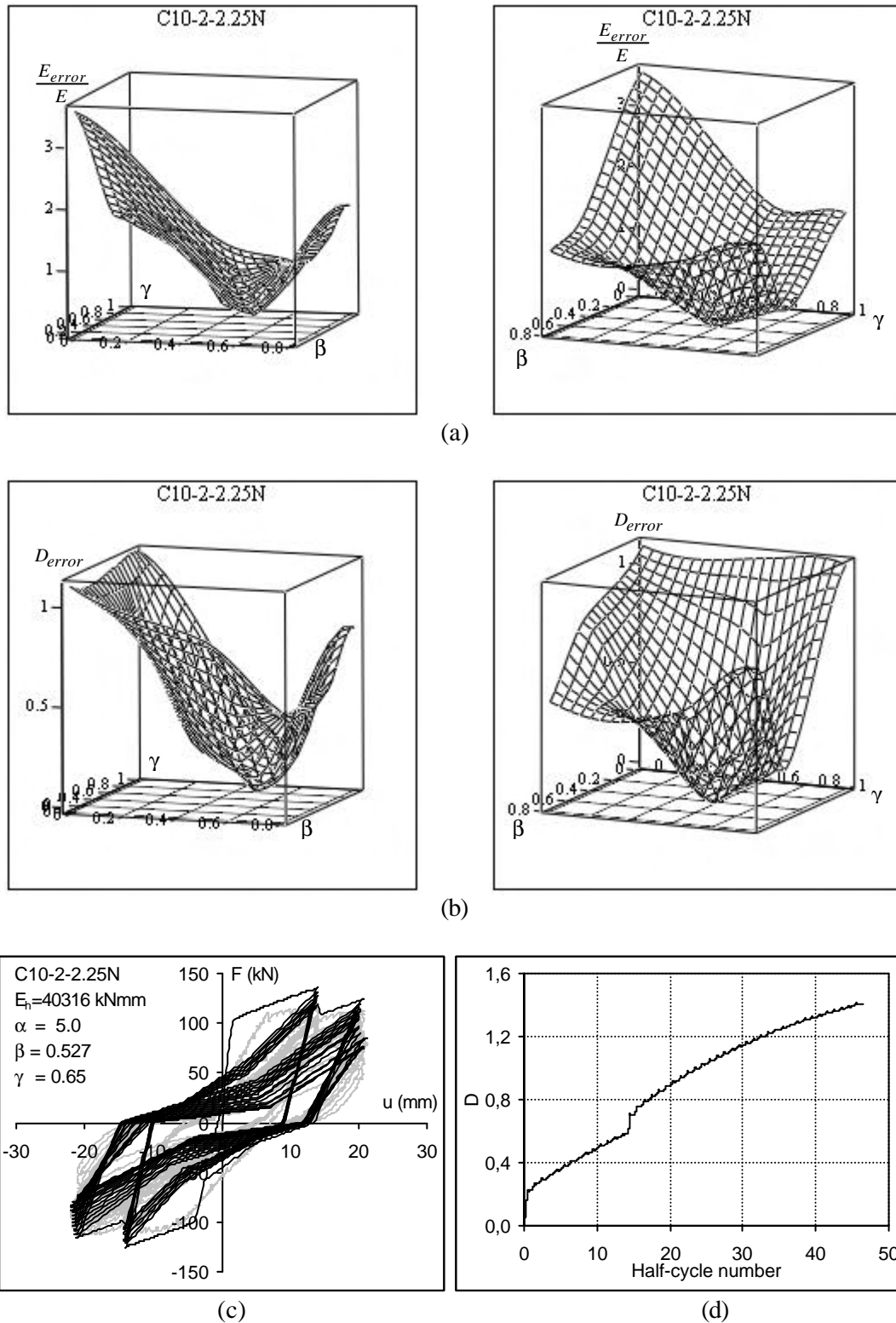


Figure 3.19 Pujol column test specimen C10-2-2.25 North: **a)** Surfaces of variation in the dissipated hysteretic energy error ratio for $\alpha=5.0$ and β and γ parameters, **b)** Surfaces of variation in the damage index error for $\alpha=5.0$ and β and γ parameters, **c)** Comparison of the experimental (gray curve) and analytical (black curve) force-deformation relationships, **d)** Analytical progressive damage curve

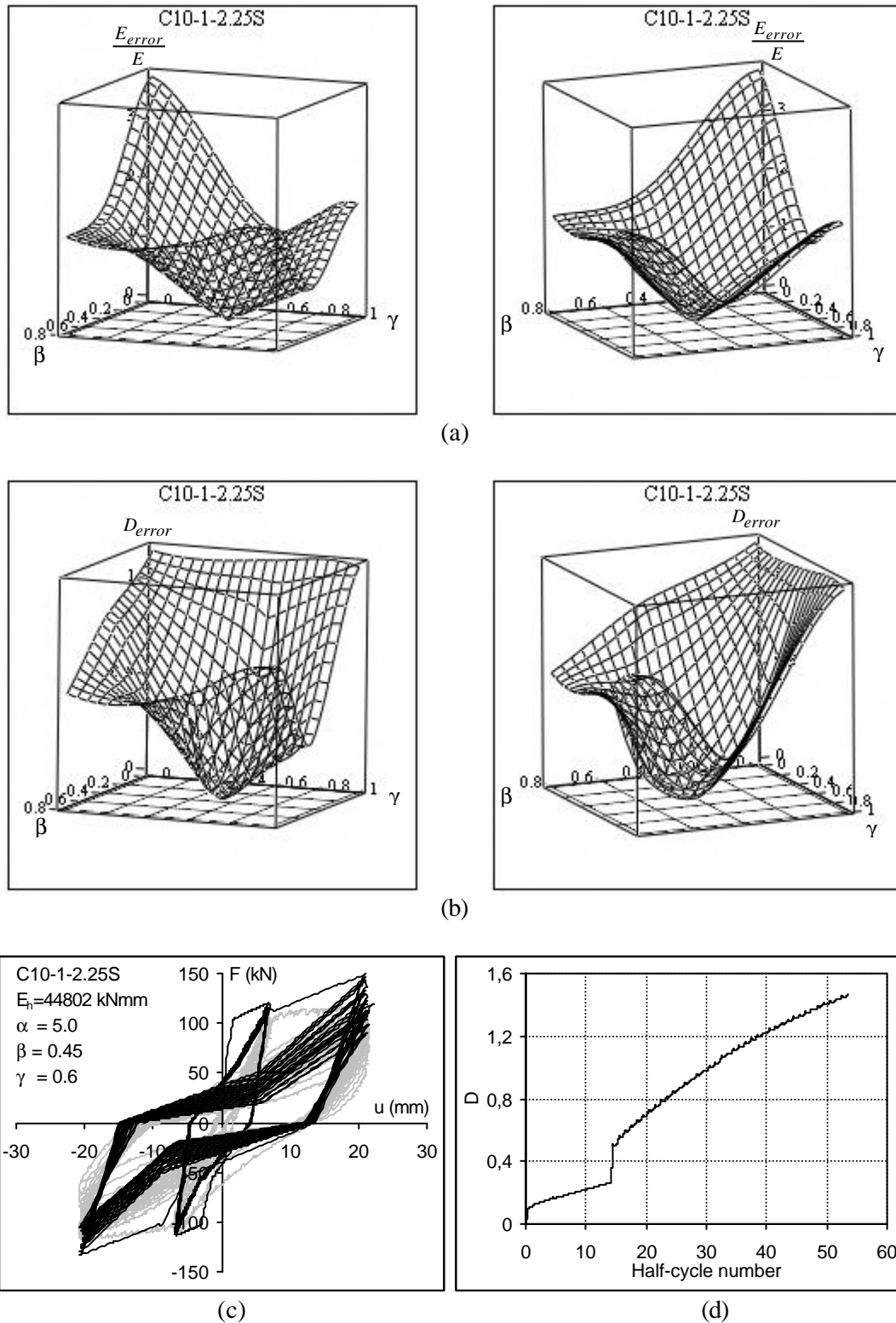


Figure 3.20 Pujol column test specimen C10-1-2.25 South: **a)** Surfaces of variation in the dissipated hysteretic energy error ratio for $\alpha=5.0$ and β and γ parameters, **b)** Surfaces of variation in the damage index error for $\alpha=5.0$ and β and γ parameters, **c)** Comparison of the experimental (gray curve) and analytical (black curve) force-deformation relationships, **d)** Analytical progressive damage curve

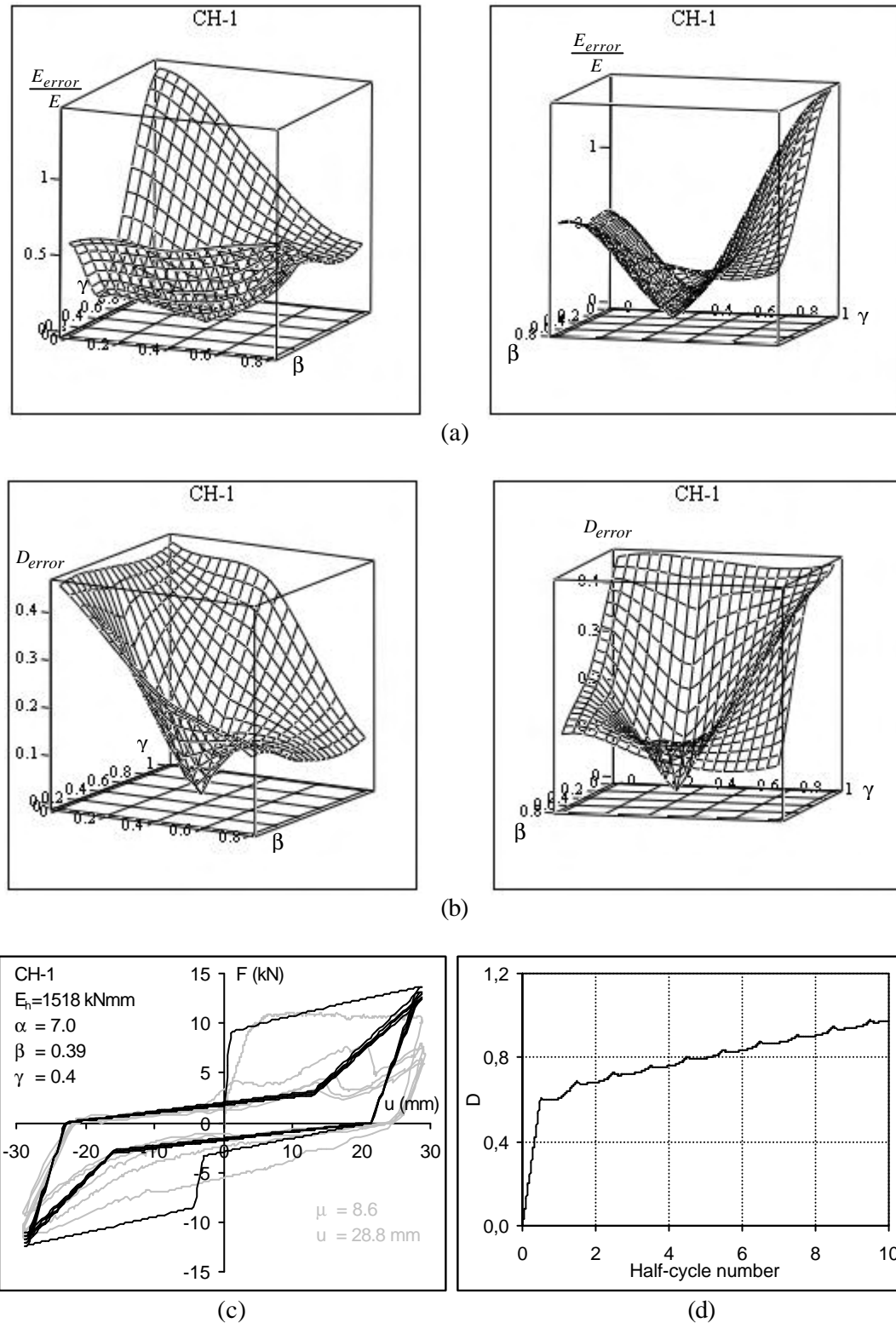


Figure 3.21 Erberik and Sucuođlu beam test specimen CH-1: **a)** Surfaces of variation in the dissipated hysteretic energy error ratio for $\alpha=7.0$ and β and γ parameters, **b)** Surfaces of variation in the damage index error for $\alpha=7.0$ and β and γ parameters, **c)** Comparison of the experimental (gray curve) and analytical (black curve) force-deformation relationships, **d)** Analytical progressive damage curve

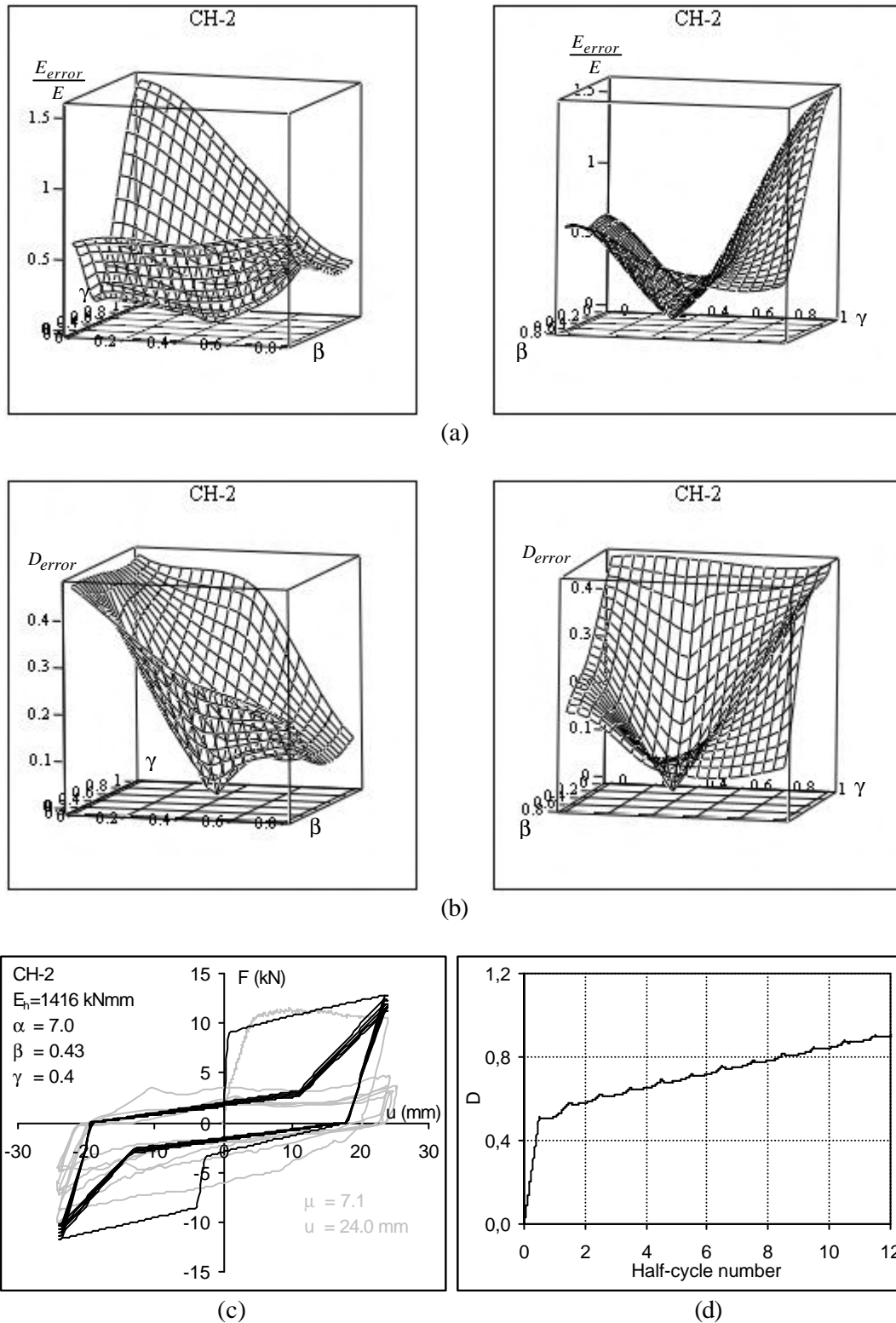


Figure 3.22 Erberik and Sucuođlu beam test specimen CH-2: **a)** Surfaces of variation in the dissipated hysteretic energy error ratio for $\alpha=7.0$ and β and γ parameters, **b)** Surfaces of variation in the damage index error for $\alpha=7.0$ and β and γ parameters, **c)** Comparison of the experimental (gray curve) and analytical (black curve) force-deformation relationships, **d)** Analytical progressive damage curve

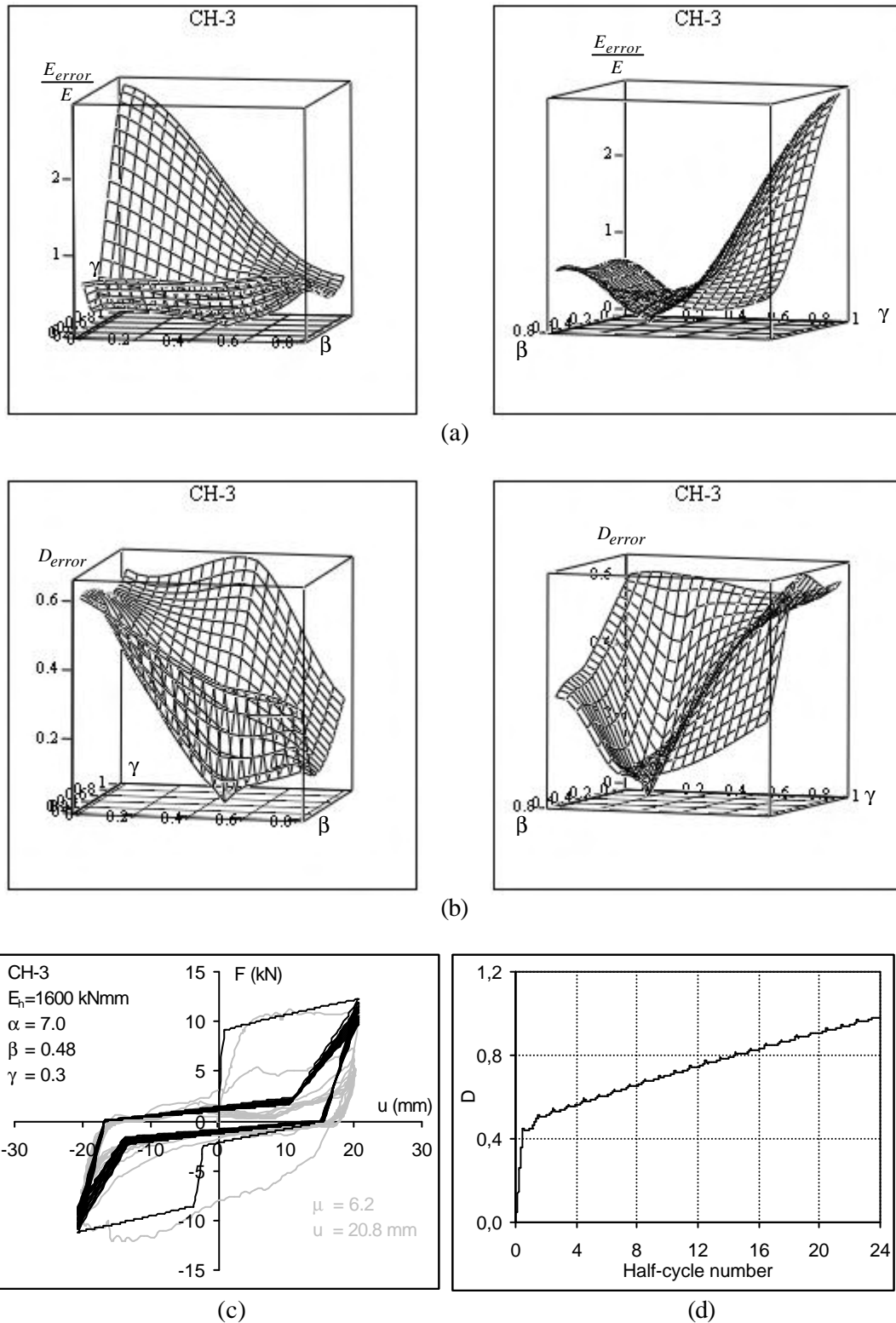


Figure 3.23 Erberik and Sucuođlu beam test specimen CH-3: **a)** Surfaces of variation in the dissipated hysteretic energy error ratio for $\alpha=7.0$ and β and γ parameters, **b)** Surfaces of variation in the damage index error for $\alpha=7.0$ and β and γ parameters, **c)** Comparison of the experimental (gray curve) and analytical (black curve) force-deformation relationships, **d)** Analytical progressive damage curve

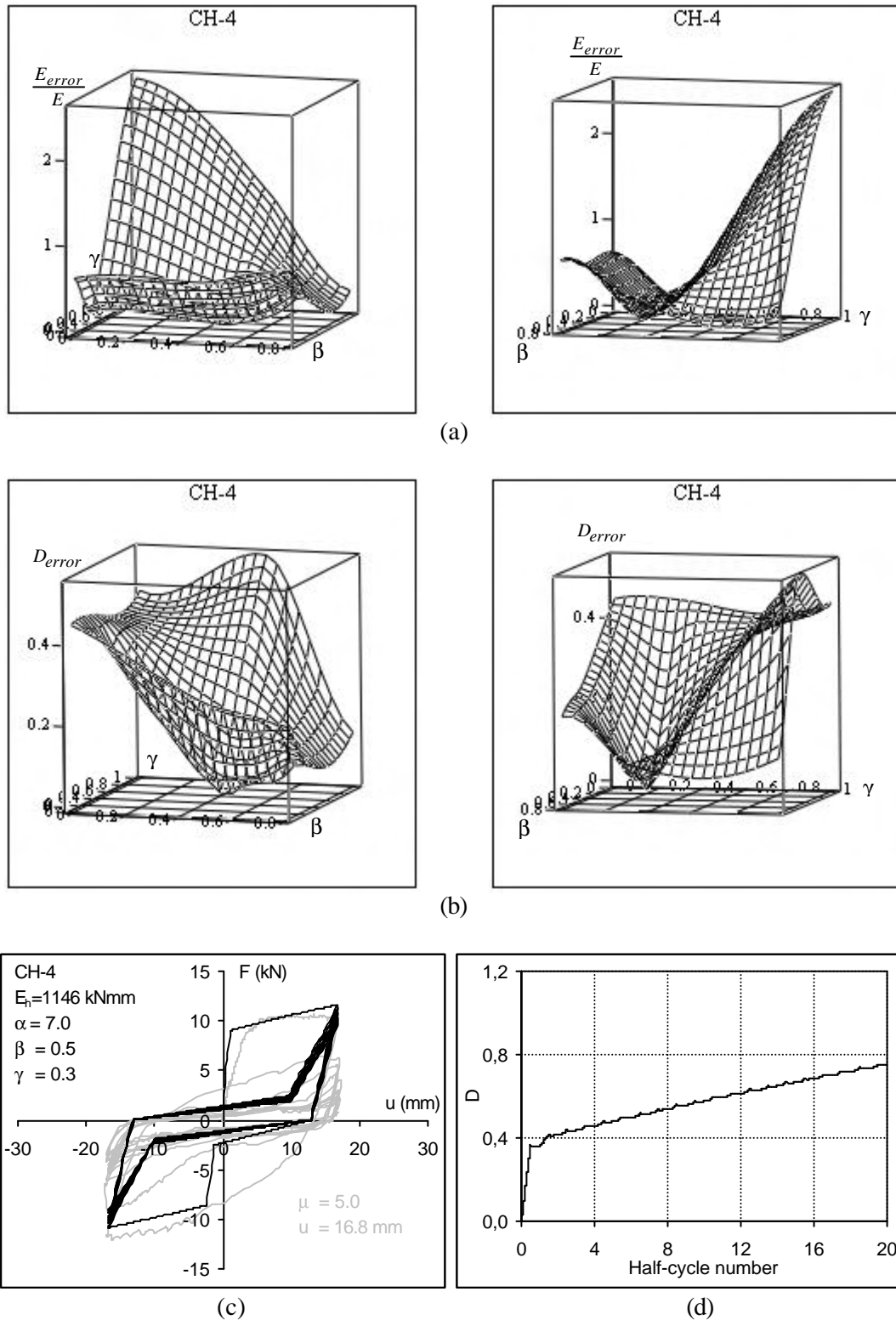


Figure 3.24 Erberik and Sucuođlu beam test specimen CH-4: **a)** Surfaces of variation in the dissipated hysteretic energy error ratio for $\alpha=7.0$ and β and γ parameters, **b)** Surfaces of variation in the damage index error for $\alpha=7.0$ and β and γ parameters, **c)** Comparison of the experimental (gray curve) and analytical (black curve) force-deformation relationships, **d)** Analytical progressive damage curve

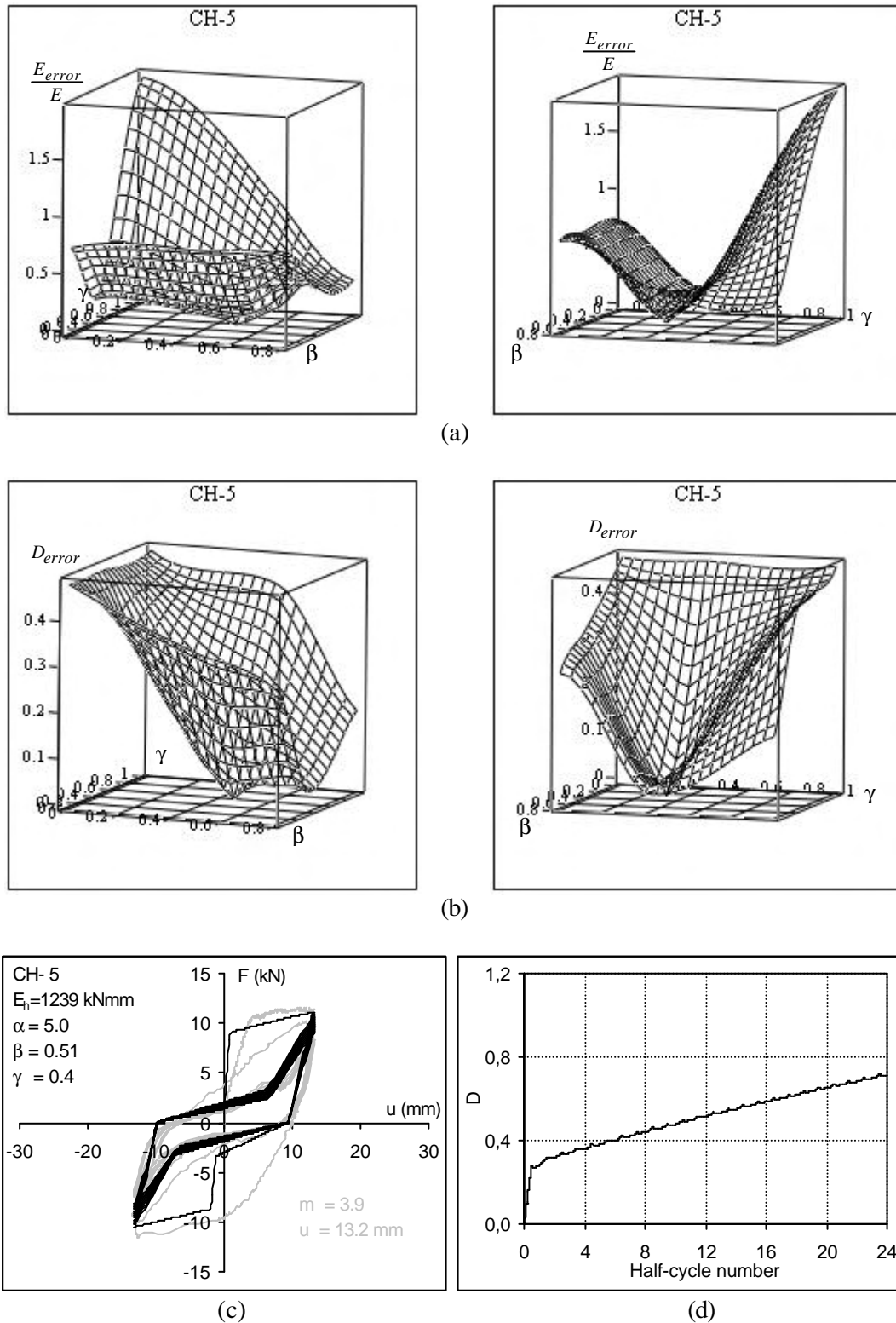
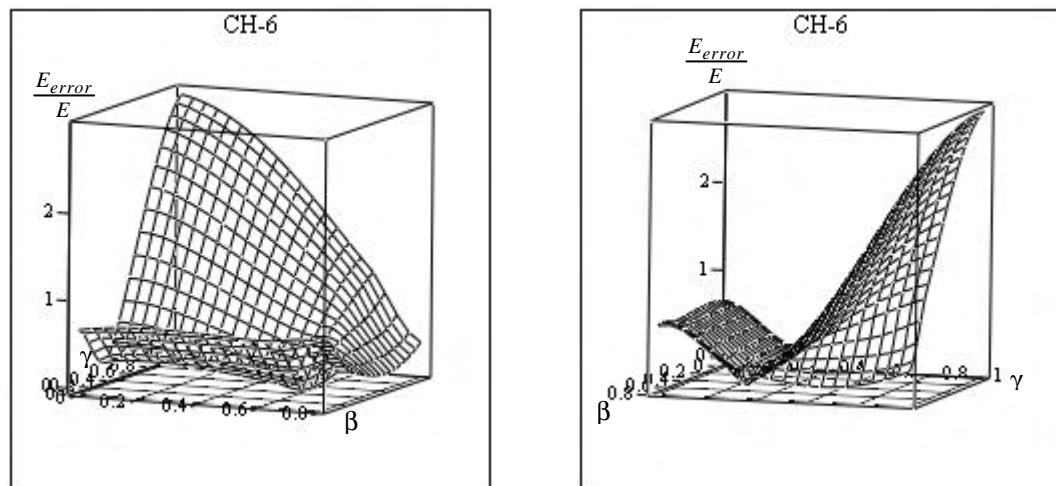
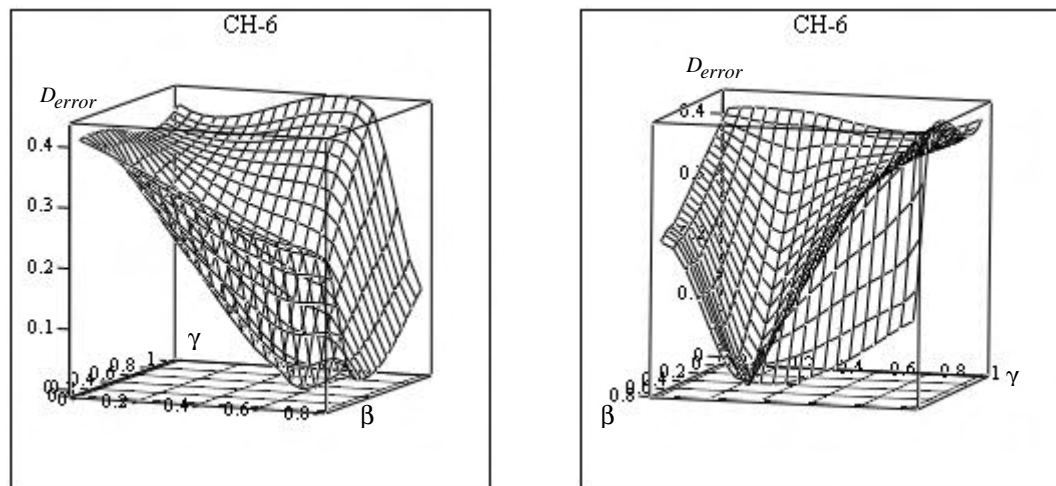


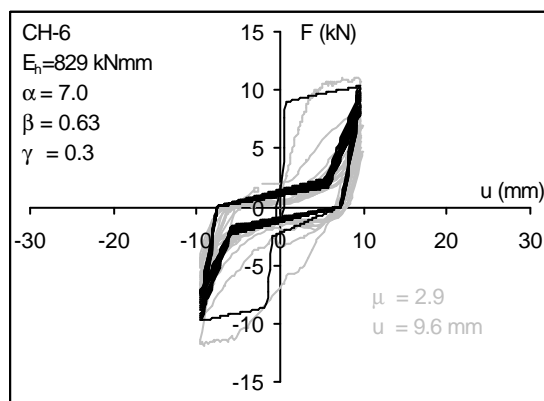
Figure 3.25 Erberik and Sucuođlu beam test specimen CH-5: **a)** Surfaces of variation in the dissipated hysteretic energy error ratio for $\alpha=5.0$ and β and γ parameters, **b)** Surfaces of variation in the damage index error for $\alpha=5.0$ and β and γ parameters, **c)** Comparison of the experimental (gray curve) and analytical (black curve) force-deformation relationships, **d)** Analytical progressive damage curve



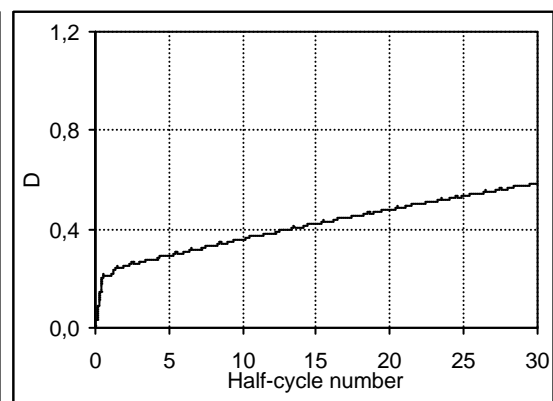
(a)



(b)



(c)



(d)

Figure 3.26 Erberik and Sucuođlu beam test specimen CH-6: **a)** Surfaces of variation in the dissipated hysteretic energy error ratio for $\alpha=7.0$ and β and γ parameters, **b)** Surfaces of variation in the damage index error for $\alpha=7.0$ and β and γ parameters, **c)** Comparison of the experimental (gray curve) and analytical (black curve) force-deformation relationships, **d)** Analytical progressive damage curve

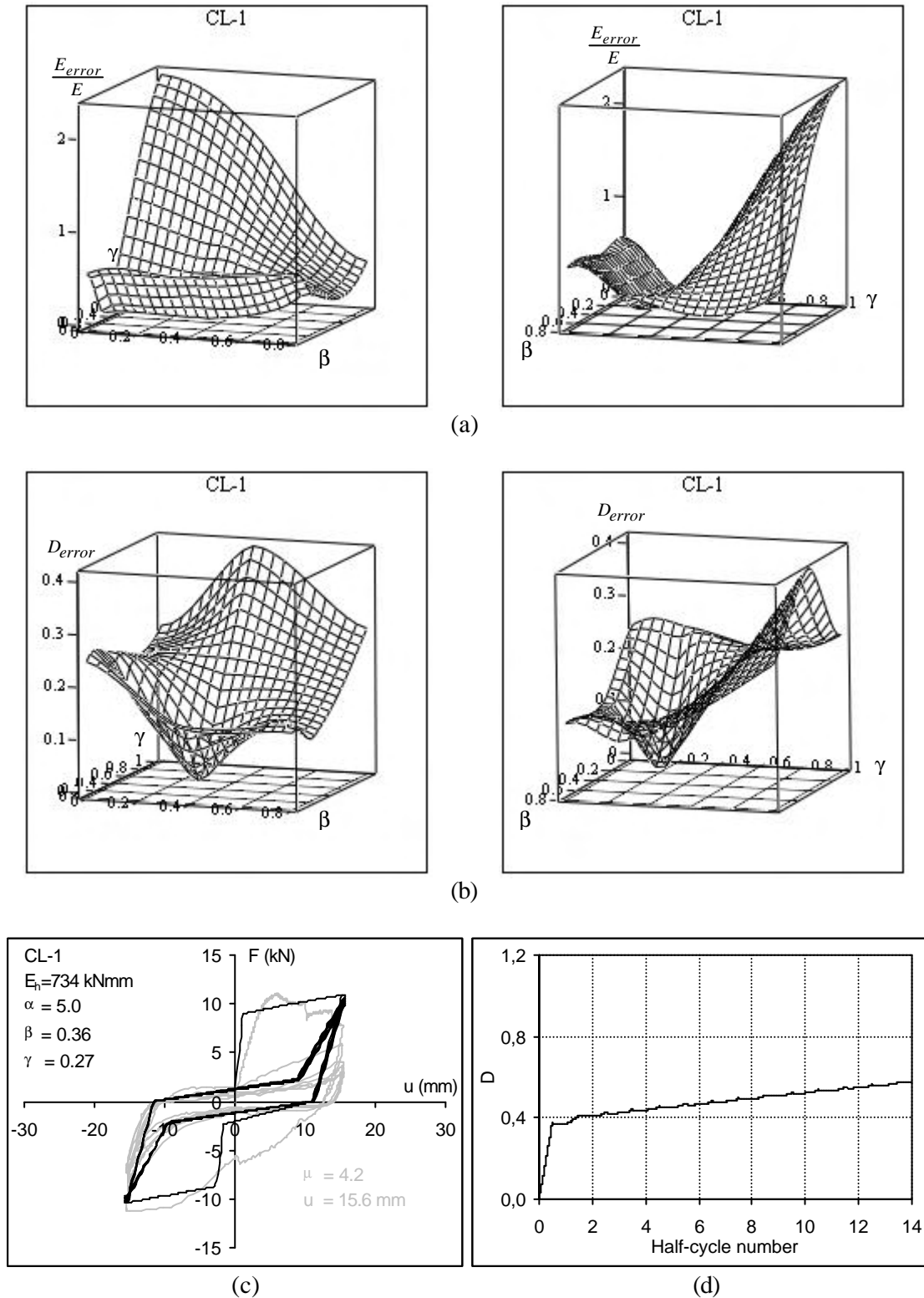


Figure 3.27 Erberik and Sucuođlu beam test specimen CL-1: **a)** Surfaces of variation in the dissipated hysteretic energy error ratio for $\alpha=5.0$ and β and γ parameters, **b)** Surfaces of variation in the damage index error for $\alpha=5.0$ and β and γ parameters, **c)** Comparison of the experimental (gray curve) and analytical (black curve) force-deformation relationships, **d)** Analytical progressive damage curve

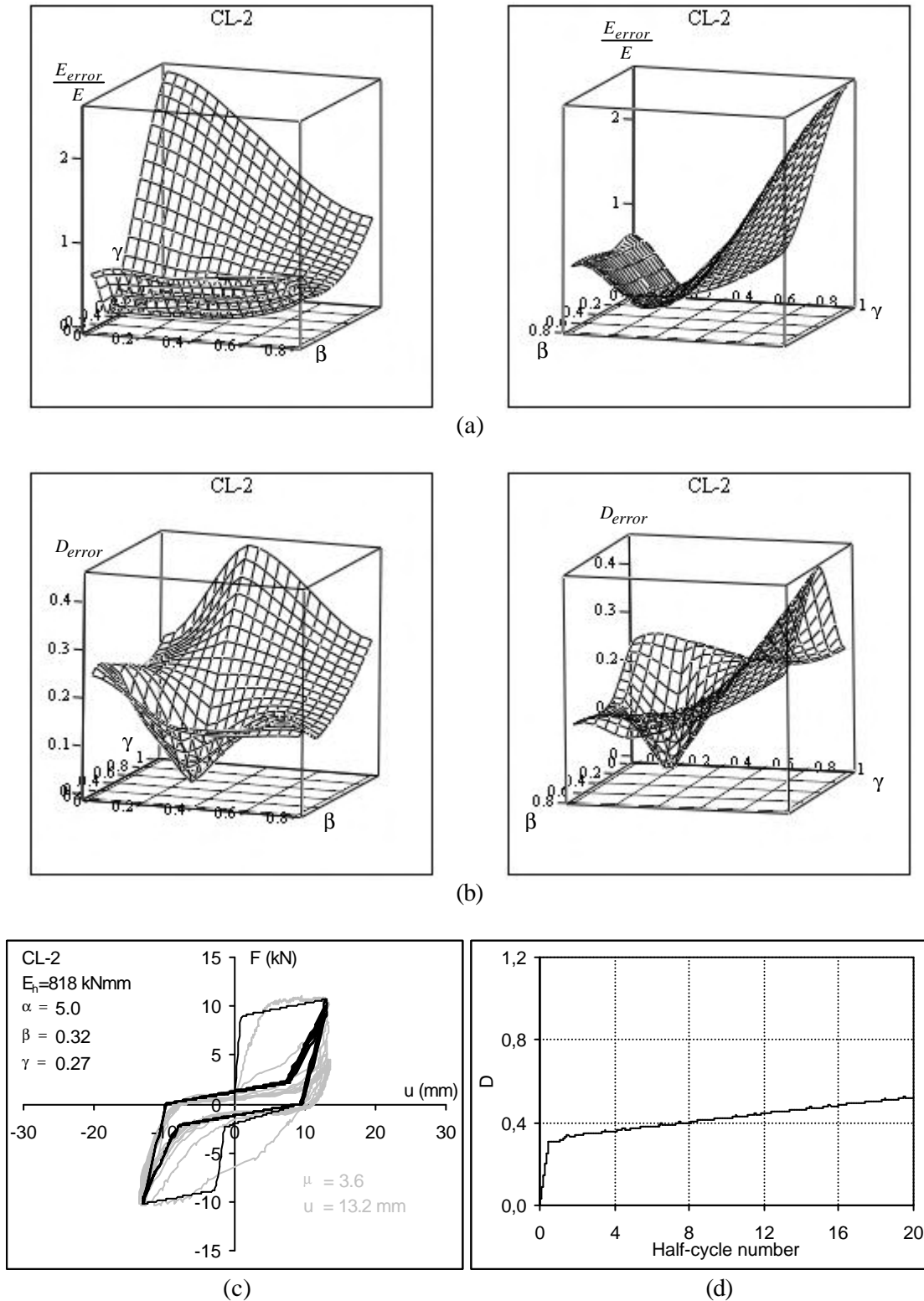


Figure 3.28 Erberik and Sucuođlu beam test specimen CL-2: **a)** Surfaces of variation in the dissipated hysteretic energy error ratio for $\alpha=5.0$ and β and γ parameters, **b)** Surfaces of variation in the damage index error for $\alpha=5.0$ and β and γ parameters, **c)** Comparison of the experimental (gray curve) and analytical (black curve) force-deformation relationships, **d)** Analytical progressive damage curve

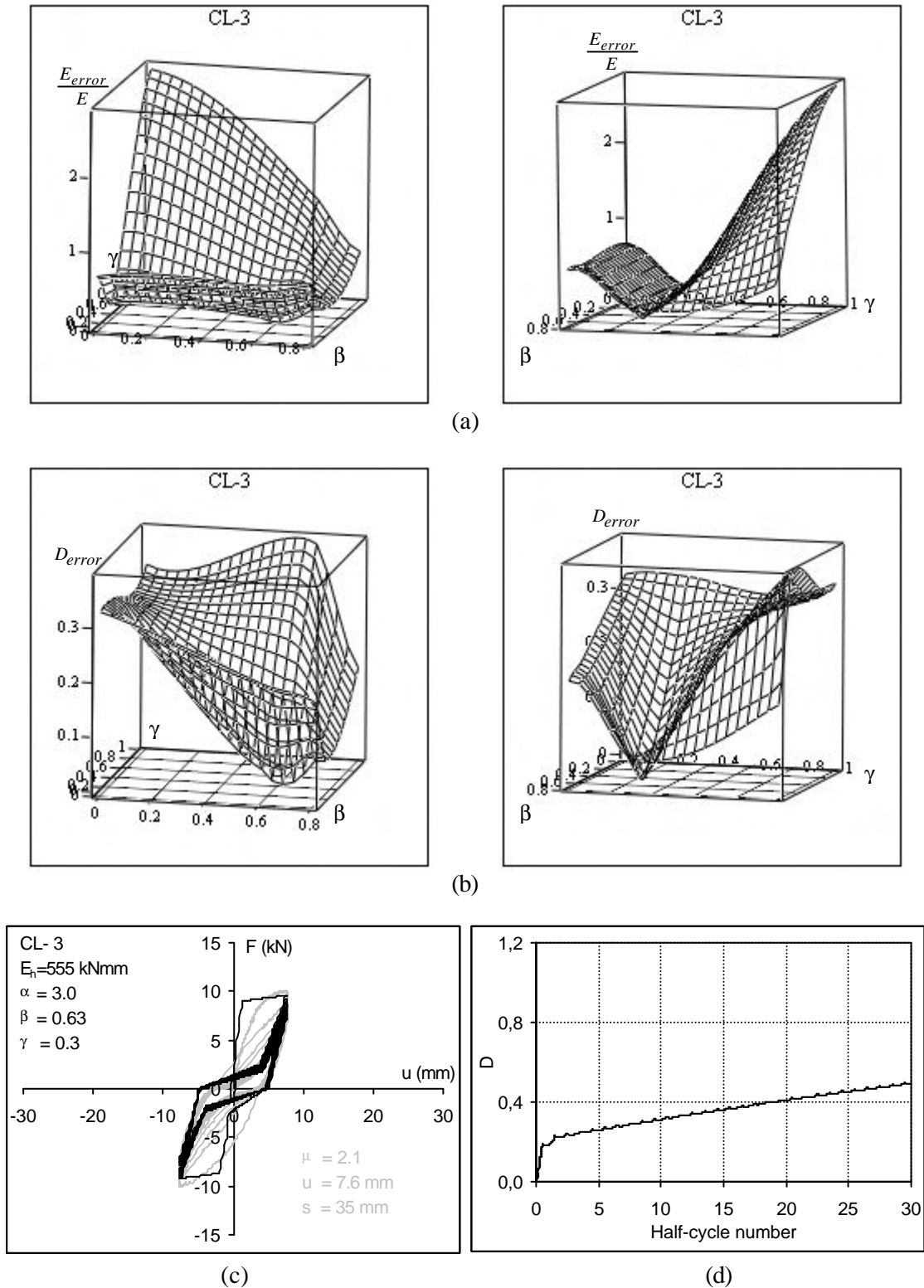


Figure 3.29 Erberik and Sucuođlu beam test specimen CL-3: **a)** Surfaces of variation in the dissipated hysteretic energy error ratio for $\alpha=3.0$ and β and γ parameters, **b)** Surfaces of variation in the damage index error for $\alpha=3.0$ and β and γ parameters, **c)** Comparison of the experimental (gray curve) and analytical (black curve) force-deformation relationships, **d)** Analytical progressive damage curve

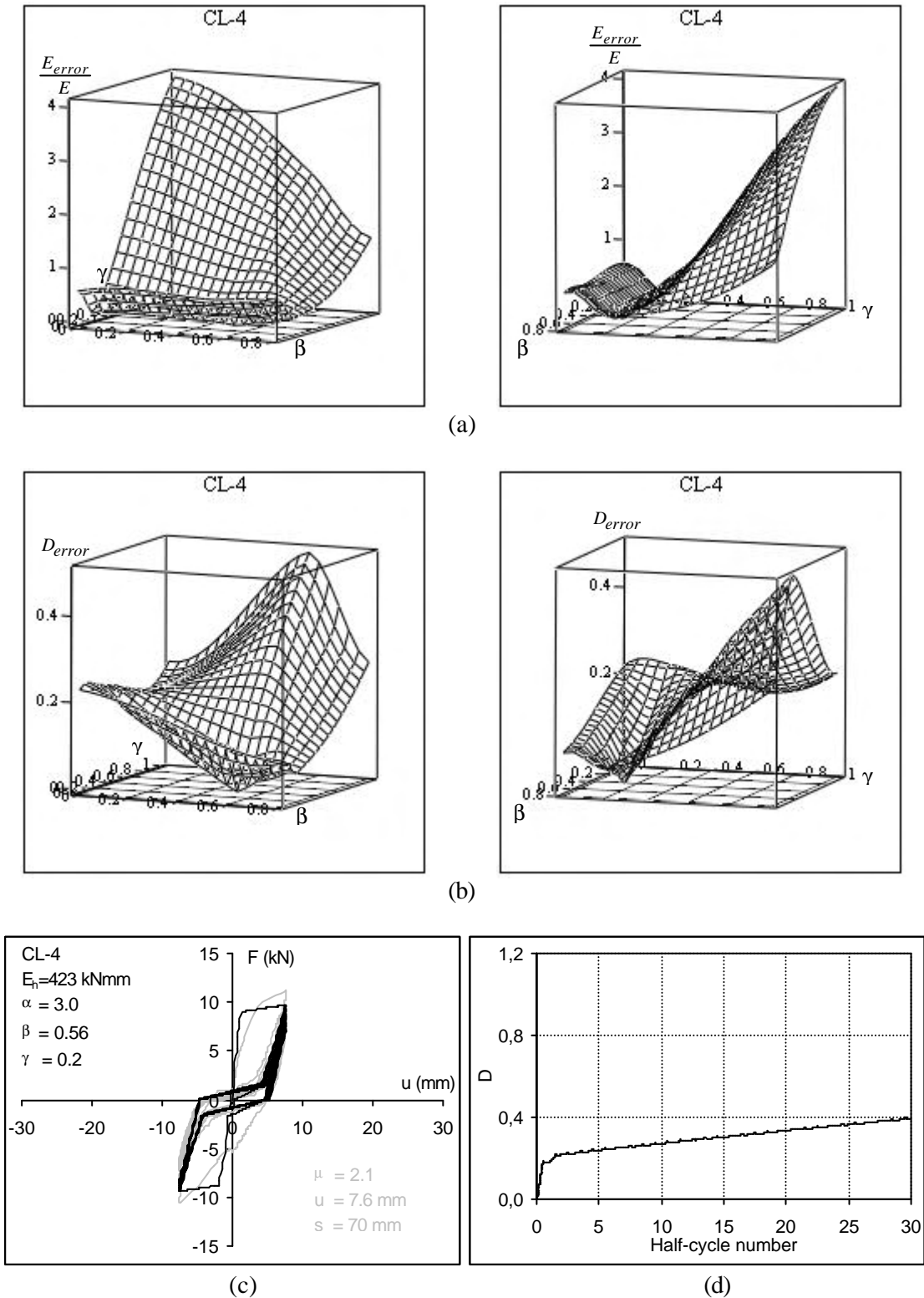
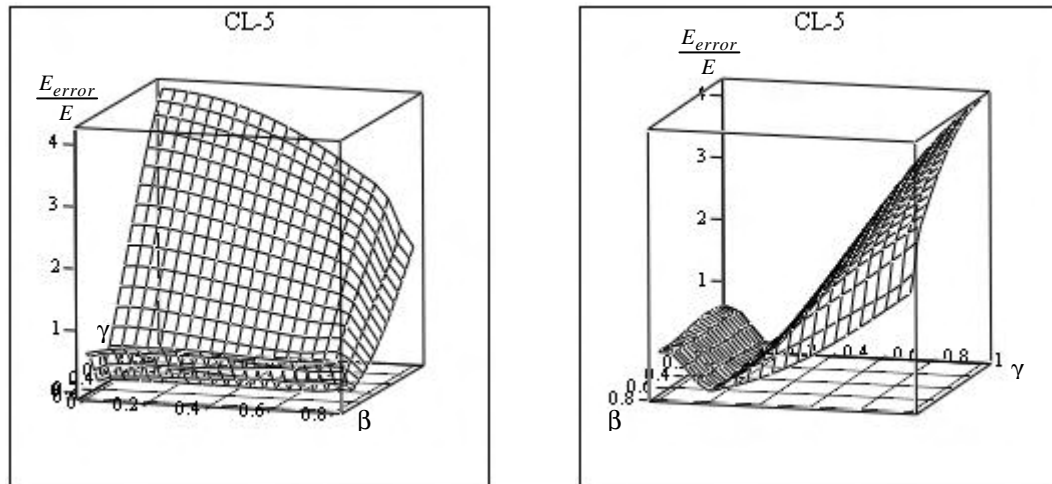
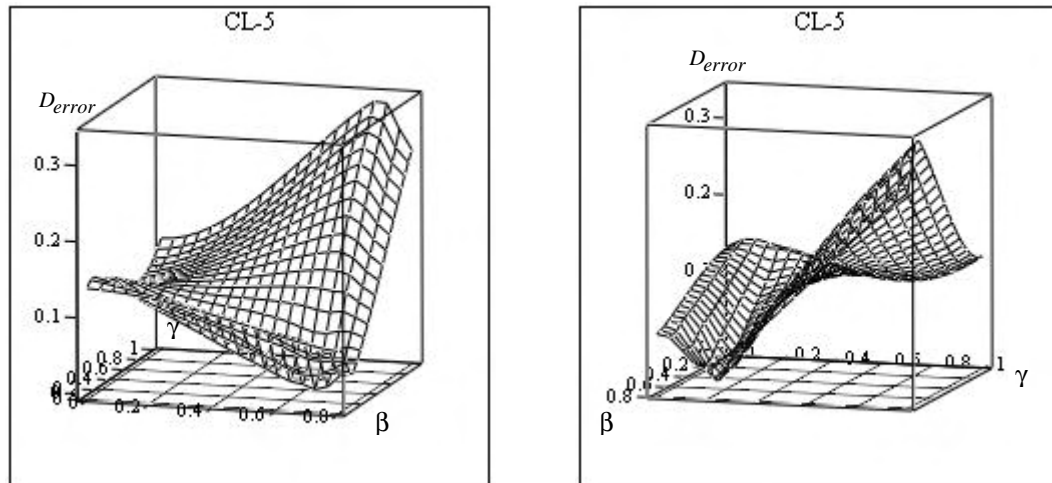


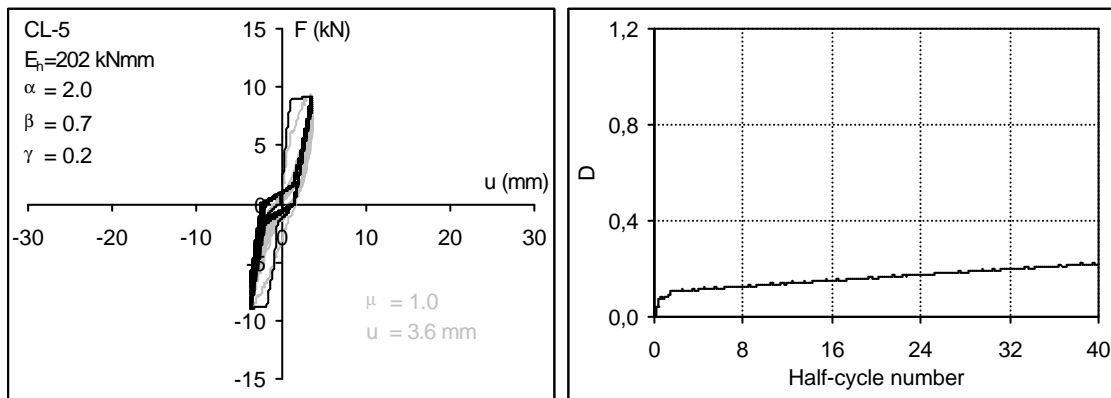
Figure 3.30 Erberik and Sucuođlu beam test specimen CL-4: **a)** Surfaces of variation in the dissipated hysteretic energy error ratio for $\alpha=3.0$ and β and γ parameters, **b)** Surfaces of variation in the damage index error for $\alpha=3.0$ and β and γ parameters, **c)** Comparison of the experimental (gray curve) and analytical (black curve) force-deformation relationships, **d)** Analytical progressive damage curve



(a)



(b)



(c)

(d)

Figure 3.31 Erberik and Sucuođlu beam test specimen CL-5: **a)** Surfaces of variation in the dissipated hysteretic energy error ratio for $\alpha=2.0$ and β and γ parameters, **b)** Surfaces of variation in the damage index error for $\alpha=2.0$ and β and γ parameters, **c)** Comparison of the experimental (gray curve) and analytical (black curve) force-deformation relationships, **d)** Analytical progressive damage curve

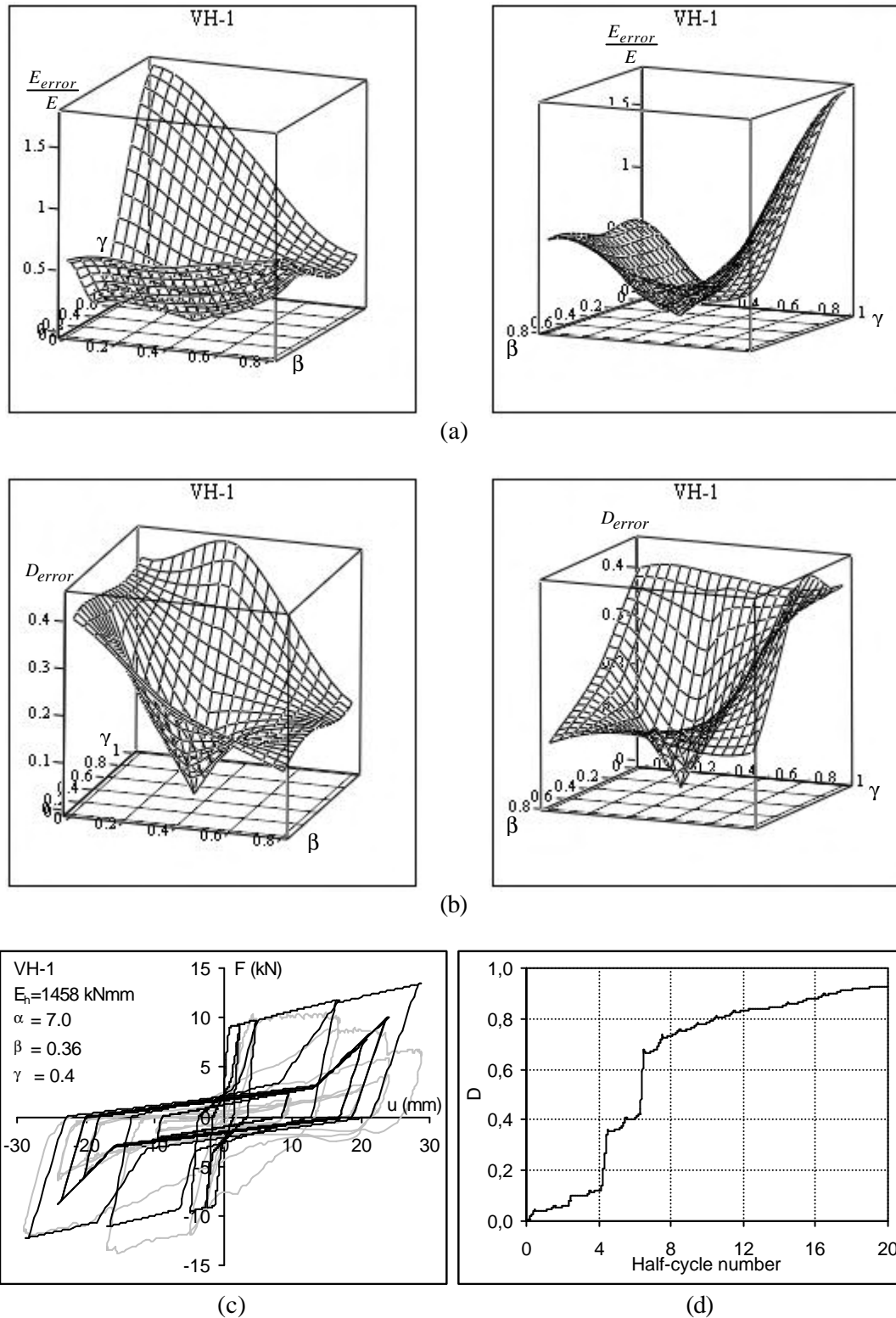


Figure 3.32 Erberik and Sucuođlu beam test specimen VH-1: **a)** Surfaces of variation in the dissipated hysteretic energy error ratio for $\alpha=7.0$ and β and γ parameters, **b)** Surfaces of variation in the damage index error for $\alpha=7.0$ and β and γ parameters, **c)** Comparison of the experimental (gray curve) and analytical (black curve) force-deformation relationships, **d)** Analytical progressive damage curve

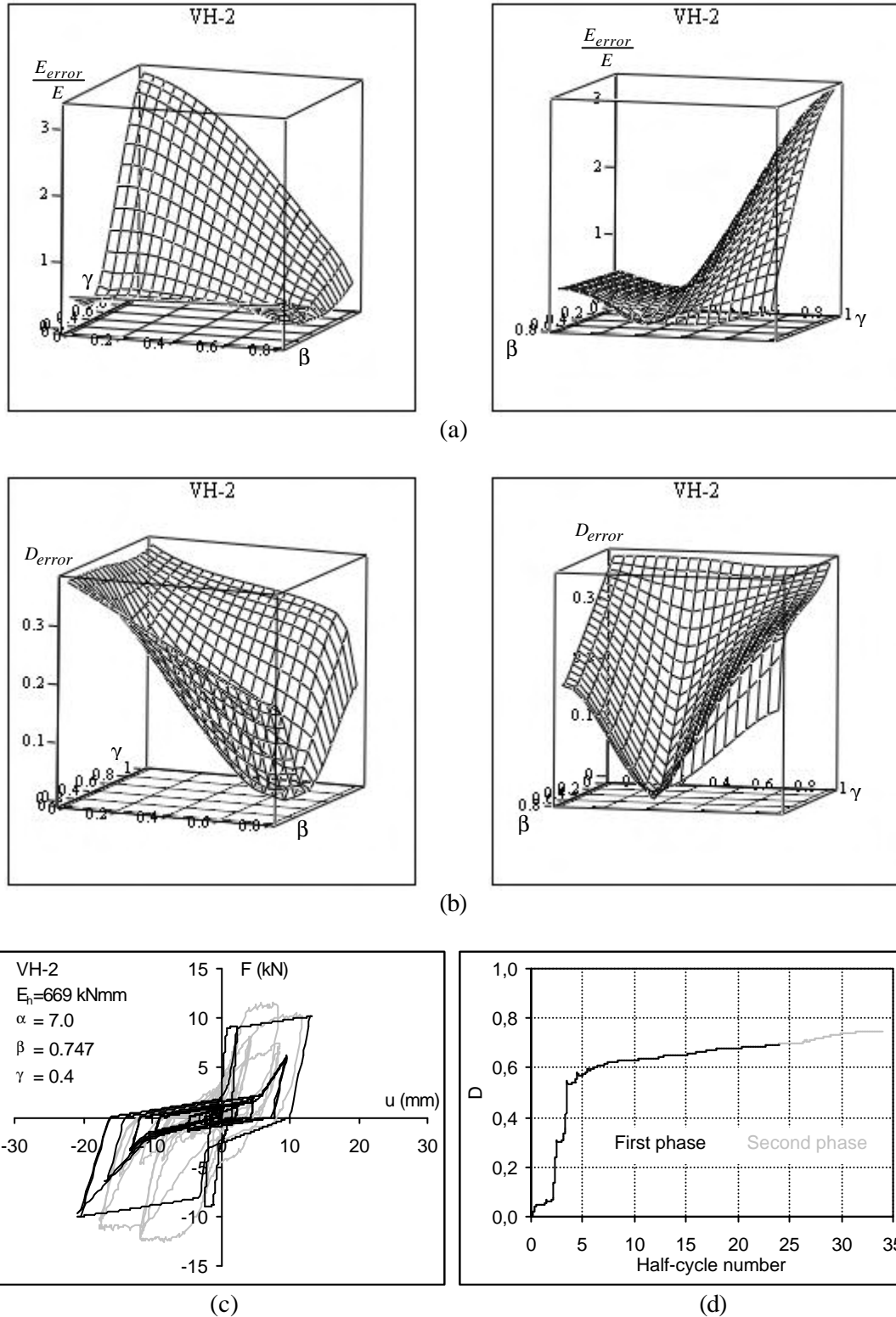


Figure 3.33 Erberik and Sucuođlu beam test specimen VH-2: **a)** Surfaces of variation in the dissipated hysteretic energy error ratio for $\alpha=7.0$ and β and γ parameters, **b)** Surfaces of variation in the damage index error for $\alpha=7.0$ and β and γ parameters, **c)** Comparison of the experimental (gray curve) and analytical (black curve) force-deformation relationships, **d)** Analytical progressive damage curve

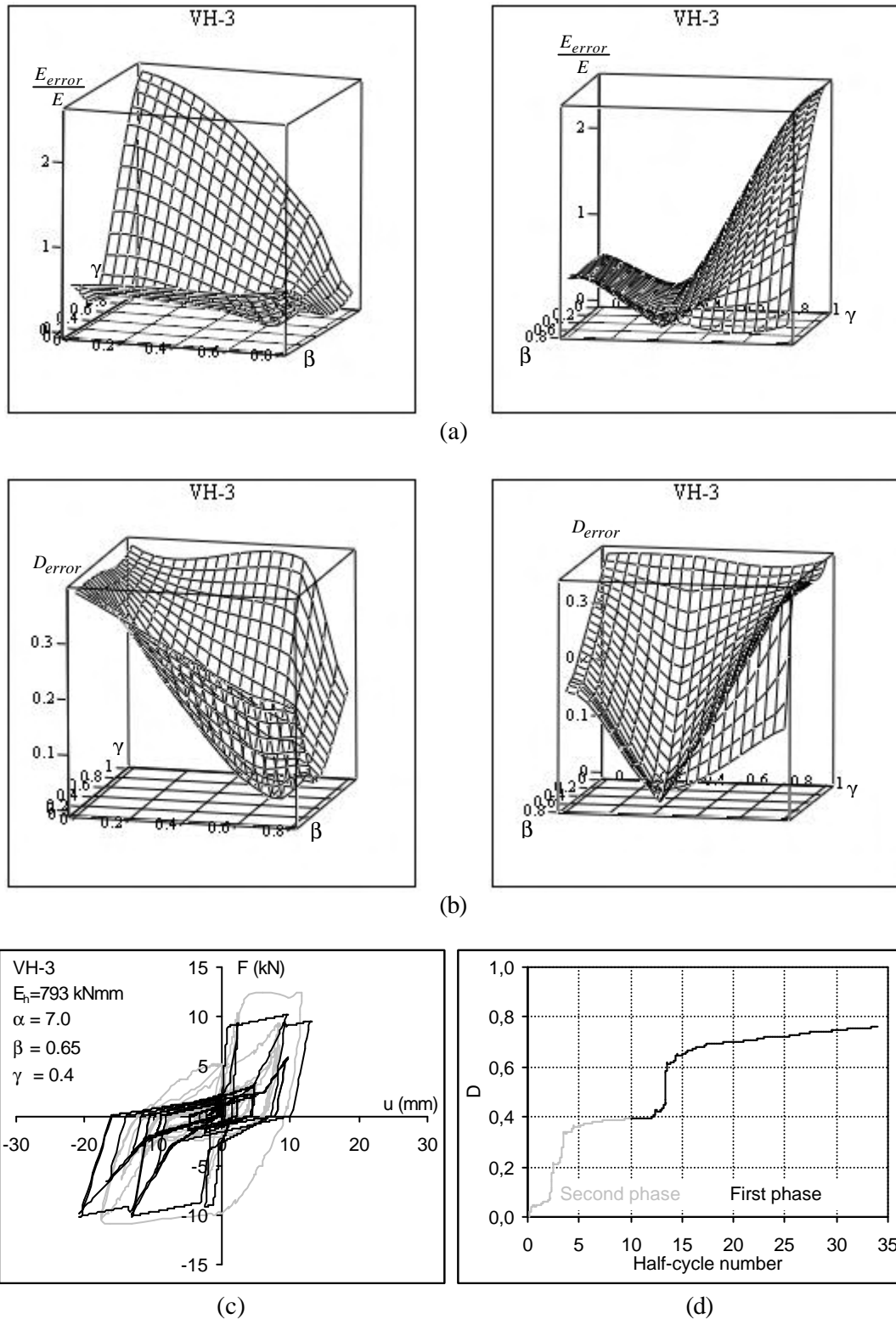


Figure 3.34 Erberik and Sucuođlu beam test specimen VH-3: **a)** Surfaces of variation in the dissipated hysteretic energy error ratio for $\alpha=7.0$ and β and γ parameters, **b)** Surfaces of variation in the damage index error for $\alpha=7.0$ and β and γ parameters, **c)** Comparison of the experimental (gray curve) and analytical (black curve) force-deformation relationships, **d)** Analytical progressive damage curve

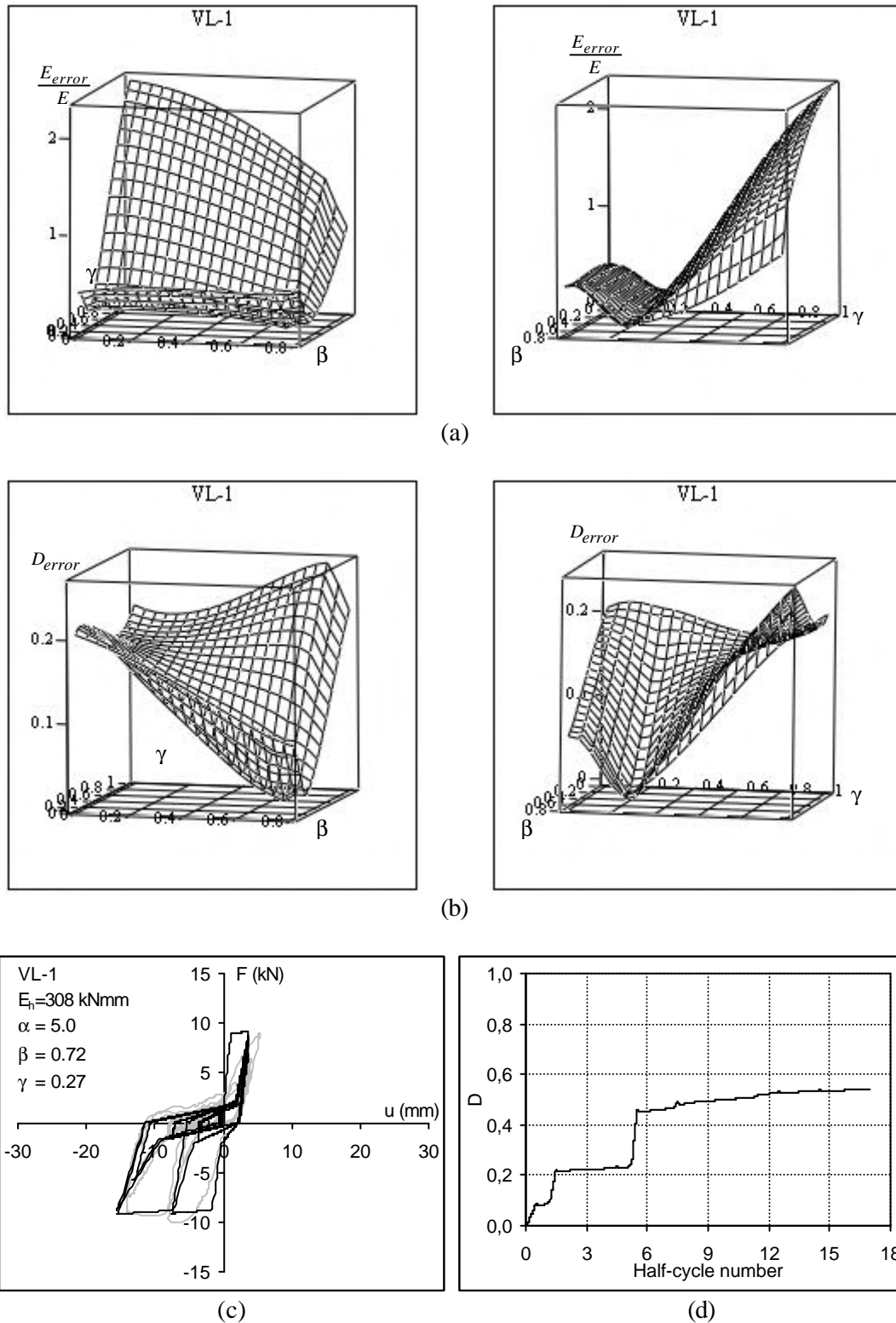


Figure 3.35 Erberik and Sucuođlu beam test specimen VL-1: **a)** Surfaces of variation in the dissipated hysteretic energy error ratio for $\alpha=5.0$ and β and γ parameters, **b)** Surfaces of variation in the damage index error for $\alpha=5.0$ and β and γ parameters, **c)** Comparison of the experimental (gray curve) and analytical (black curve) force-deformation relationships, **d)** Analytical progressive damage curve

In this study the stiffness degradation parameter, α , ranges between 1-100 represented in a logarithmic scale, the strength deterioration parameter, β , ranges between 0.0-0.8, and the pinching parameter ranges between 0.0-1.0.

In these error surface figures, in order to show error term (taking place in either damage index or energy dissipation) in the vertical axis of the cartesian coordinate system, only the relatively more sensitive strength deterioration and pinching parameters were displayed. The less sensitive stiffness degradation parameter, α , is kept constant at a reasonable value. The sensitivity of this parameter is also investigated and discussions on all the sensitivity of all parameters to structural characteristics will be presented later using two-dimensional plots. The contour plots are formatted in many ways to control their appearance and they are changed to observe what is occurring. For a good understanding of the effect of variation of strength deterioration and pinching parameters on energy dissipation capacity and damage index, two pairs of each specimen surface pictures are taken from the best viewpoints and presented in Figures 3.14a,b to 3.35a,b. In Appendix A, Tables A.1 lists the discrete values of each parameter used in the calibration process of the sample specimen. In this table, the solution points comprising the calibrated deterioration parameters values are given in the gray colored line cells.

As can be observed easily from the three-dimensional damage index and energy error surfaces shown in Figures 3.14a,b to 3.35a,b and the numerical values of the sample specimen presented in Appendix A, the error in the damage index and dissipated energy is either minimum or zero in the vicinity of the solution point. Inspection of the three-dimensional damage index and energy dissipation error surfaces revealed that at the solution point the error reached a slight or sharp dip close to zero error.

3.4.2.2.1 Error Variation in Hysteretic Energy Dissipation

Figures 3.14(a) to 3.35(a) each shows a pair of three-dimensional graphs representing variation surfaces of the dissipated hysteretic energy error ratio with

respect to the parameters β and γ , for each specimen presented in Table 3.1. The strength deterioration parameter, β , and pinching parameter, γ , are the two variables considered as the most sensitive parameters. The stiffness degradation parameter, α , is kept as constant because its value is selected considering the unloading stiffness of the force displacement curves.

By referring to these graphs it is possible to state that both parameters β and γ influence considerably the energy dissipation capacity of especially the columns (namely Pujol specimens) that are dissipated relatively large amount of energy. As an example, for the columns C10-2-2.25N and C10-1-2.25S, the error revealed in the dissipated hysteretic energy reached to 357.8 percent and 373.5 percent of the energy dissipation capacity of the specimens, respectively (Figures 3.19a and 3.20a). On the other hand, 3D gradient surfaces given in Figures 3.21a to 3.35a apparently show that, the parameter β has relatively small effect on the error ratio of the energy dissipation capacity for the beams (namely Erberik and Sucuođlu specimens). The more steep uphill and downhill gradients, away from the solution point, are in the direction of pinching parameter, γ . As an example, for the beam labeled as CH-3, with relatively high concrete compressive strength due to variation in γ , the error ratio of the energy dissipation capacity reached to level of 289.4 percent whereas the maximum value of this error ratio due to variation in β remained at level of 65.7 percent (Figure 3.23a). Similarly, for beams CL-4 and CL-5, with low concrete compressive strengths, due to variation in γ , the error ratio of the energy dissipation capacity exceeded 400 percent whereas the maximum values of this error ratio due to β are 57.8 percent and 65.6 percent, respectively (Figures 3.30a and 3.31a). The same variation is valid also for the beam specimens VH-1, VH-2, VH-3 and VL-1 tested under variable amplitude displacement reversals, in such a way that the parameter β has a small effect on the error variation revealed in the energy dissipation capacity, compared to pinching parameter, γ . Since variation of energy dissipation capacity was not very sensitive to small variations in parameter β , it makes the selection of this parameter easier.

3.4.2.2.2 Error Variation in Damage Index

Figures 3.14(b) to 3.35(b) present the pairs of the damage index error surfaces for all specimens under consideration. The numerical values of error obtained for damage index are presented in Table 3.2. For the sake of good sense of comparison, the variation surfaces were taken from the same viewpoints as of the dissipated hysteretic energy error ratio.

By referring to the graphs given in 3.14b to 3.35b, it can be stated that, both parameters β and γ affect significantly the damage index gathered for both the beam and column models analyzed. As an example, the error in the damage index for columns C10-2-2.25N and C10-1-2.25S reached 1.103 and 1.152, respectively (Figures 3.19b and 3.20b). Similarly, for the beam labeled as CH-3, with relatively high concrete compressive strength, due to variation in γ , the error of damage index reached to 0.642, whereas it is 0.606 due to variation in parameter β (Figure 3.23b). Similarly, for beams CL-4 and CL-5, with low concrete compressive strengths, due to variation in γ , the error values of damage index are 0.502 and 0.337, whereas the maximum values of this error due to variation in β are 0.228 and 0.137, respectively (Figures 3.30.b and 3.31.b). The same variation is valid also for the beam specimens VH-1, VH-2, VH-3 and VL-1 tested under variable amplitude displacement reversals.

Figures 3.14c to 3.35c present both experimental (gray curve) and analytical (black curve) force-deformation relationships for all specimens given in Table 3.1. The analytical force-displacement relationships are obtained by using the most suitable combination (calibrated values) of the parameters α , β and γ . It should be pointed out that the results obtained from analytical studies solutions were compared with the experimental results and good agreement was observed for not only the total amount of dissipated hysteretic energy (given numerically in the figures) but also in general shape of the curves. These figures contain also the total hysteretic energy dissipated by each specimen.

Finally, the progressive damage curves of the specimens obtained from the quasi-static analyses are presented in Figures 3.14d to 3.35d.

Table 3.2 Properties of R/C beam column test specimens and appropriate parameter values

Specimen	LP	f_c (MPa)	r_l (%)	r_s (%)	$N/f_c A_g$	$[N_{cycle}]$ A (mm)	$[N_{cycle}]$ δh (%)	α	β	γ	Class	
Pujol (2002)	C10-2-3N	VA	33.7	2.4	0.55	0.087	[7]14+[7]21	[7]2+[7]3	5.0	0.60	0.50	MOD
	C10-3-3N	CA	29.9	2.4	0.55	0.098	[9]21	[9]3	5.0	0.61	0.60	MOD
	C20-3-3S	CA	36.4	2.4	0.55	0.161	[9]21	[9]3	3.0	0.50	0.65	MOD
	C10-1-2.25S	VA	36.5	2.4	0.73	0.080	[7]7+[20]21	[7]1+[20]3	5.0	0.45	0.60	MOD
	C10-2-2.25N	VA	34.9	2.4	0.73	0.084	[7]14+[16]21	[7]2+[16]3	5.0	0.527	0.65	MOD
	C10-3-2.25N	CA	27.4	2.4	0.73	0.107	[19]21	[19]3	5.0	0.49	0.70	MOD
	C10-3-1.5S	VA	32.1	2.4	1.1	0.091	[7]21+[11]27	[7]3+[11]4	5.0	0.40	0.80	MLD
	C20-3-1.5*	VA	27.4	2.4	1.1	0.214	[7]21+[10]27	[7]3+[10]4	No experimental data			
Erberik and Sucuođlu (2004)	CH-1	CA	20.5	1.3	0.8	0	[5]28.8	[5]6.4	7.0	0.39	0.40	SVD
	CH-2	CA	20.6	1.3	0.8	0	[6]24.0	[6]5.3	7.0	0.43	0.40	SVD
	CH-3	CA	20.6	1.3	0.8	0	[12]20.8	[12]4.6	7.0	0.48	0.30	SVD
	CH-4	CA	20.6	1.3	0.8	0	[10]16.8	[10]3.7	7.0	.50	0.30	SVD
	CH-5	CA	21.2	1.3	0.8	0	[12]13.2	[12]2.9	5.0	0.51	0.40	SVD
	CH-6	CA	20.6	1.3	0.8	0	[15]9.6	[15]2.1	7.0	0.63	0.30	SVD
	CL-1	CA	13.0	1.3	0.8	0	[7]15.6	[7]3.5	5.0	0.36	0.27	SVD
	CL-2	CA	13.0	1.3	0.8	0	[10]13.2	[10]2.9	5.0	0.32	0.27	SVD
	CL-3	CA	13.0	1.3	0.8	0	[15]7.6	[15]1.7	3.0	0.63	0.30	SVD
	CL-4	CA	13.0	1.3	0.4	0	[15]7.6	[15]1.7	3.0	0.56	0.20	SVD
	CL-5	CA	13.0	1.3	0.8	0	[20]3.6	[20]1.0	2.0	0.70	0.20	SVD
	VH-1	VA	20.6	1.3	0.8	0	28.8(max)	6.4(max)	7.0	0.36	0.40	SVD
	VH-2	VA	21.2	1.3	0.8	0	20.8(max)	4.6(max)	7.0	0.747	0.40	SVD
	VH-3	VA	21.2	1.3	0.8	0	20.8(max)	4.6(max)	7.0	0.65	0.40	SVD
VL-1	VA	13.0	1.3	0.8	0	15.6(max)	3.5(max)	5.0	0.72	0.27	SVD	

*This test failed in an unexpected mode and the cycles applied were limited before buckling of the longitudinal reinforcement at the joint face (Pujol, 2002).

Experimental results obtained from the tests of different reinforced concrete beam column specimens are employed in order to calibrate the low-cycle fatigue based hysteretic model parameters and to relate them to the general behavior of structural systems under repeated loading. The experimental data used is listed in

Table 3.2 with the characteristic properties of each specimen. The last four columns of the table contain the most suitable combination of low-cycle fatigue parameters α , β and γ which give the reasonable accurate estimate of cyclic response and damage for the prescribed paths. Deterioration parameters have been obtained as a result of the calibration process using the search method. In the last column of Table 3.2, the specimens are classified according to their most suitable low cycle fatigue parameters.

The abbreviation “MLD” denotes mildly deteriorating system with parameter α larger than 7, β parameter closer to zero and γ parameter closer to unity. There is insufficient data representing this sort of behavior. For these specimens, parameter α ranges between 7-100, parameter β ranges between 0.1-0.2, and parameter γ ranges between 0.7-0.9. An example of mild deterioration (MLD) behavior is test specimen C10-3-1.5S. It represents a desired seismic behavior with stable loops and with little stiffness and strength deterioration. In such specimens the axial load level not exceeding $0.10f_cA_g$ is preferable. As it will be demonstrated also in the following chapter, whenever the design axial load is $1/6\sim 1/8$ of the axial load capacity or smaller than $0.10f_cA_g$, i.e., when the column is proportioned almost as a girder, the hysteretic action was greatly improved.

Examples of moderate deterioration (MOD) behavior belong to test specimens C10-2-3N, C10-3-3N, C20-3-3S, C10-1-2.25S, C10-2-2.25N and C10-3-2.25N, with parameter α ranging between 0.3-0.5, parameter β ranging between 0.45-0.6 and parameter γ ranging between 0.5-0.65. The observed behavior for “MOD” type of structural members is gradual deterioration in strength with increasing cycle number, and mild pinching. However the specimen can still dissipate a considerable amount of energy after a significant number of cycles. In these specimens axial load level is around $0.10f_cA_g$. Although the axial load did not affect significantly the number of constant-amplitude cycles that could be sustained, it influenced the rate of stiffness and strength deteriorations and pinching during the final displacement cycles. It can be stated that the higher levels of the axial load results in more abrupt failure of a structural component.

Severely deteriorating structural members include test specimens CH-1 to CH-6, CL-1 to CL-5, VH-1, VH-2, VH-3, VL-1 and C20-3-1.5. These specimens have low concrete compressive strength, plain longitudinal bars, low confinement ratio or axial load level exceeding $0.20f_cA_g$. When plain bars are used as longitudinal reinforcement, excessive bar slip occurs even in the early stages of displacement reversals leading to pinching and strength deterioration reduces the energy dissipation capacity significantly. Similarly when concrete with low compressive strength is used, a relatively limited number of cycles could be sustained. The extent to which such basic experimental deficiencies can be generalized is uncertain.

The purpose of this section of the dissertation was twofold: determining the most suitable combination of parameters α , β and γ in a given case to permit predictions rather than hindsight comments about inelastic behavior, and assessment of the relationships which exist between the deterioration parameters and structural characteristics, thus giving the material properties, axial load, and geometry, one should be able to make reasonably accurate estimates of cyclic response for a prescribed path.

3.4.2.3 Sensitivity of Deterioration Parameters to Structural Characteristics

Structural characteristics of the reinforced concrete members influence the stiffness degradation, strength deterioration and pinching parameters of the hysteretic behavior of the components. The purpose of this section is two fold: to determine the sensitivity of the deterioration parameters of concrete hysteresis to some of the principal structural characteristics; and to assess the effects of these characteristics on energy dissipation capacity and deterioration level of the structural component. To accomplish this purpose, the main variables controlled in the beam and column specimens, such as hoop spacing, axial load level and concrete strength, are taken into consideration. Moreover, effects of loading history on both energy dissipation capacity and damage index will be discussed in this section of the study. In this study the main tools will be variations in the dissipated hysteretic energy and damage index and variations in their errors obtained by the search method in the previous section.

The variations of the total dissipated hysteretic energy and damage index with respect to the three deterioration parameters, α , β and γ , are presented mutually in the Figures. In addition, the variations of the error in both dissipated hysteretic energy and damage index are displayed in these figures. The error variation curves dipped sharply or slightly at their optimal values corresponding to zero difference in the amounts of hysteretic energy obtained experimentally and analytically. It is estimated that the deterioration parameter values matching the dip points give the most reasonably accurate damage level for the prescribed loading path.

The main variables controlled in Pujol (2002) column specimens were the spacing of the hoops outside the center stub, axial load level and loading history. Figures 3.36 and 3.37 show the variations in the energy dissipation and damage index together with their error variation curves for Pujol specimens. The general shapes of the curves indicate the sensitiveness of the parameters to some of the principal structural characteristics. Inspections on these figures indicate that both energy dissipation and damage index are categorized into three groups in accordance with the hoop spacing: 38.1 mm, 57.1 mm and 76.2 mm.

Effect of all structural characteristics considered in the test programs will be discussed in detail in the following sections.

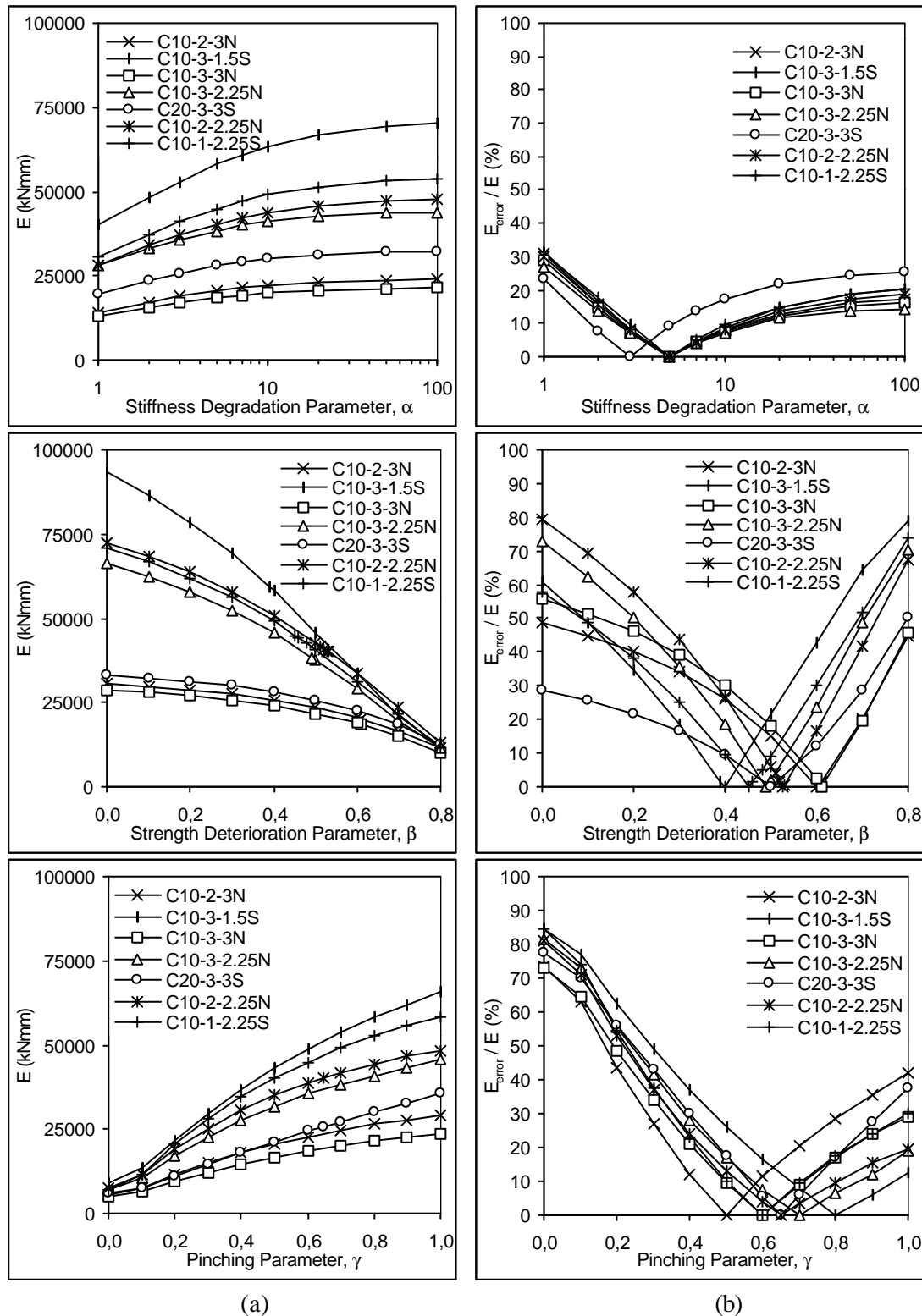


Figure 3.36 Effect of various characteristics (transverse reinforcement, axial load level and loading history) a) Dissipated hysteretic energy vs. deterioration parameters α , β and γ , b) Dissipated hysteretic energy error ratio vs. deterioration parameters α , β and γ

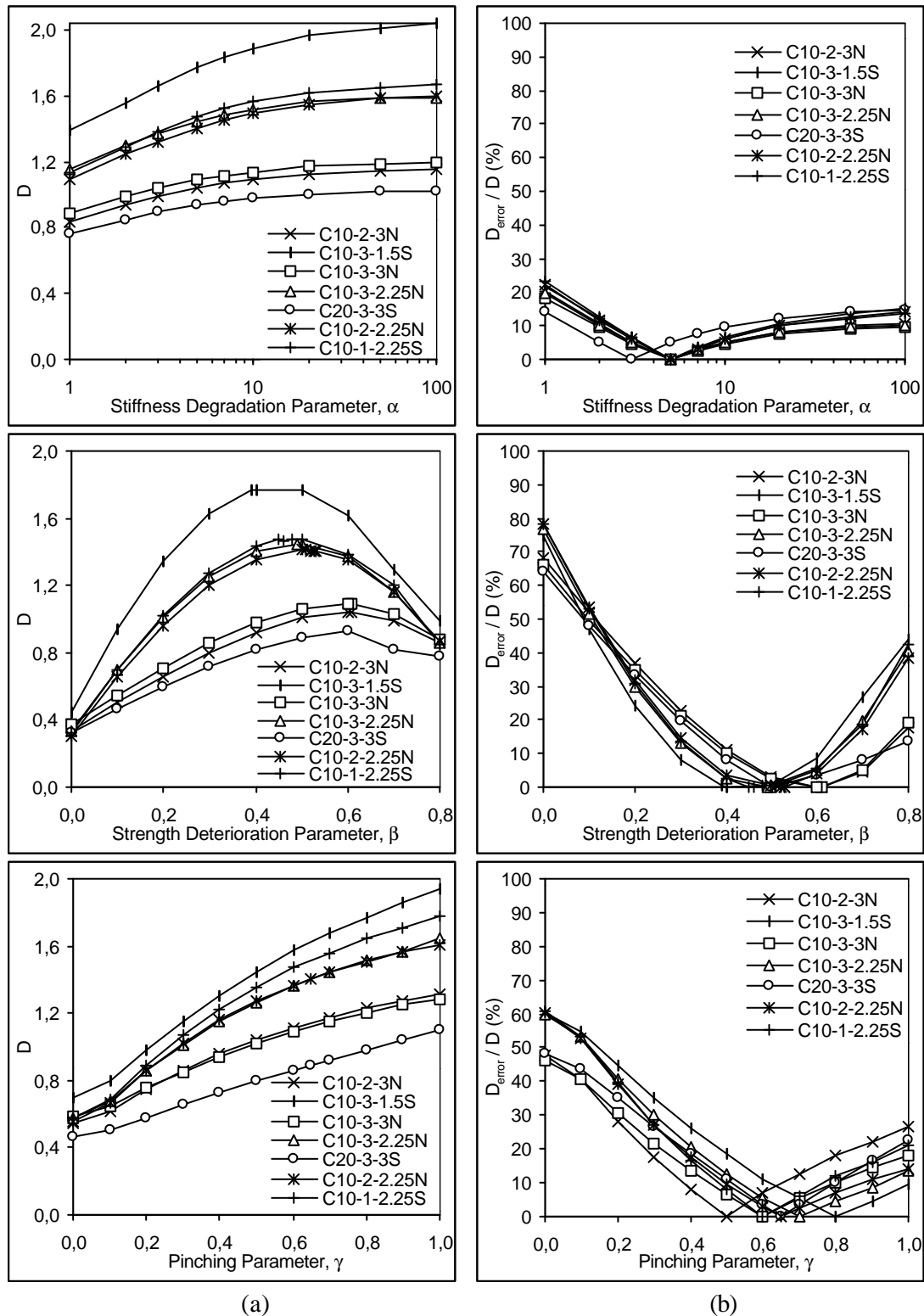


Figure 3.37 Effect of various characteristics (transverse reinforcement, axial load level and loading history) **a)** Damage index vs. deterioration parameters α , β and γ , **b)** Damage index error ratio vs. deterioration parameters α , β and γ

3.4.2.3.1 Amount of Transverse Reinforcement

The sensitivity of the deterioration parameters to the amount of transverse reinforcement during the loading histories of the specimens can be inferred from Figures 3.38 to 3.41. Figure 3.38 shows the variation of dissipated hysteretic energy and its error ratio with respect to the three deterioration parameters for specimens C10-3-1.5S, C10-3-2.25N and C10-3-3N. The variation of the damage index and its error with respect to the deterioration parameters for these specimens are shown in Figure 3.39. All specimens were tested under 136kN axial load and all were subjected to 7 displacement cycles at a maximum drift ratio of 2 percent before being displaced to a drift ratio of 3 percent. The hoops in specimens C10-3-1.5S, C10-3-2.25N and C10-3-3N were placed every 38.1 mm, 57.1 mm and 76.2 mm, respectively. Similarly the variation curves of the energy dissipation and damage index shown in Figures 3.40 and 3.41 are for the specimens C10-2-3N and C10-2-2.25N, tested under the same displacement schedule and axial load but with different amounts of transverse reinforcement. The hoops in specimen C10-2-3N were placed at 76.2 mm, and the hoops in specimen C10-3-2.25N were placed at 57.1 mm.

Inspections on the energy dissipation capacity curves presented in Figures 3.38 and 3.40 indicated that energy dissipation capacity and thus the deterioration level of the structural system are affected significantly by the ratio of transverse reinforcement. The specimens with transverse reinforcement ratios exceeding 1 percent (ρ_s for specimen C10-3-1.5S is 1.1 percent) exhibited considerably larger energy dissipation capacity with only slight deterioration of parameters. It should be stated that the smaller the hoop spacing the larger was the amount of hysteretic energy dissipated before failure.

As seen in Figures 3.38 - 3.41 the most sensitive parameters to the amount of transverse reinforcement are the strength deterioration and pinching parameters denoted by β and γ . The less sensitive parameter is the stiffness degradation parameter denoted by α ranging from 1 to 100 in a logarithmic scale.

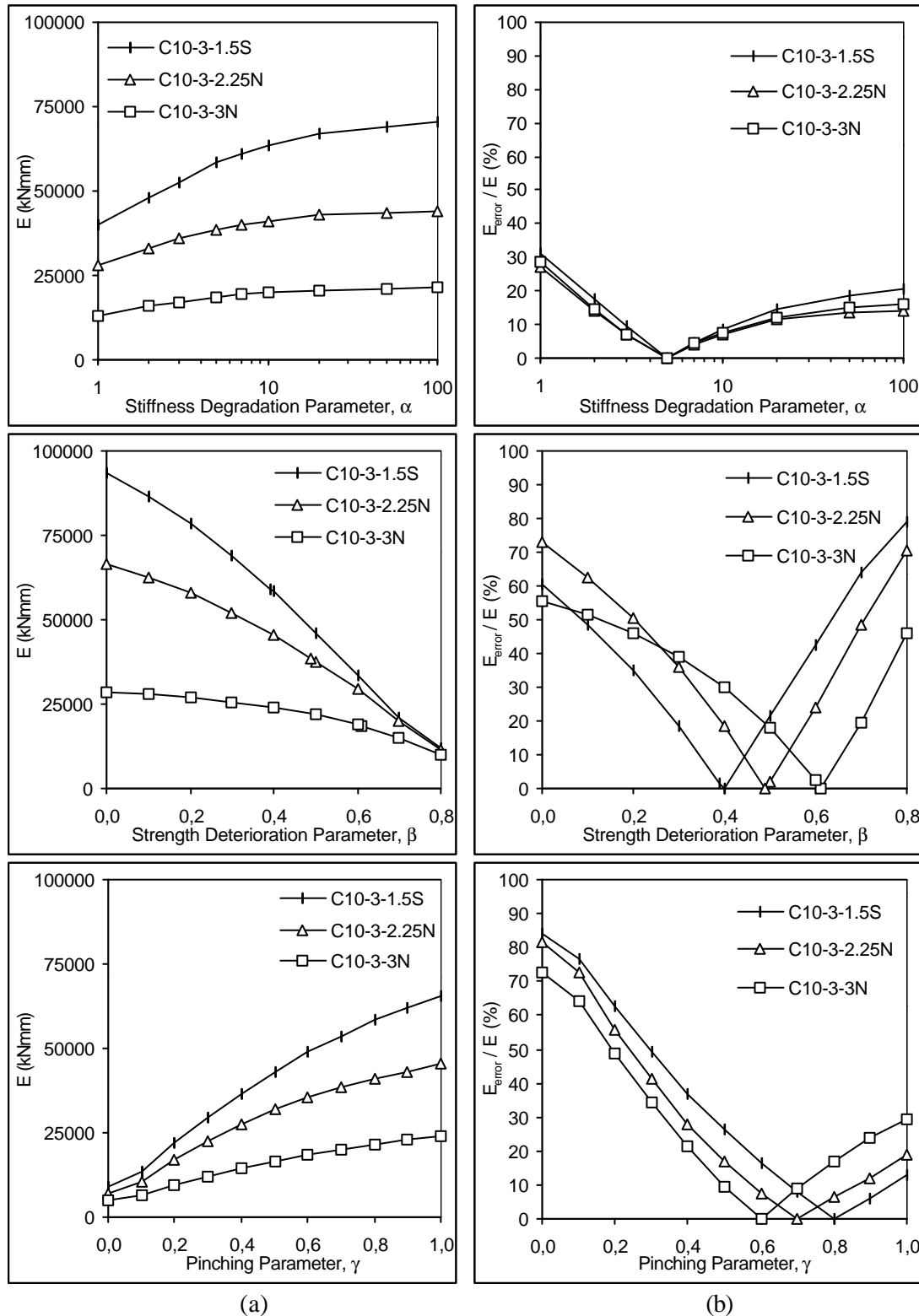


Figure 3.38 Effect of amount of transverse reinforcement-Set I **a)** Dissipated hysteretic energy vs. deterioration parameters α , β and γ , **b)** Dissipated hysteretic energy error ratio vs. deterioration parameters α , β and γ

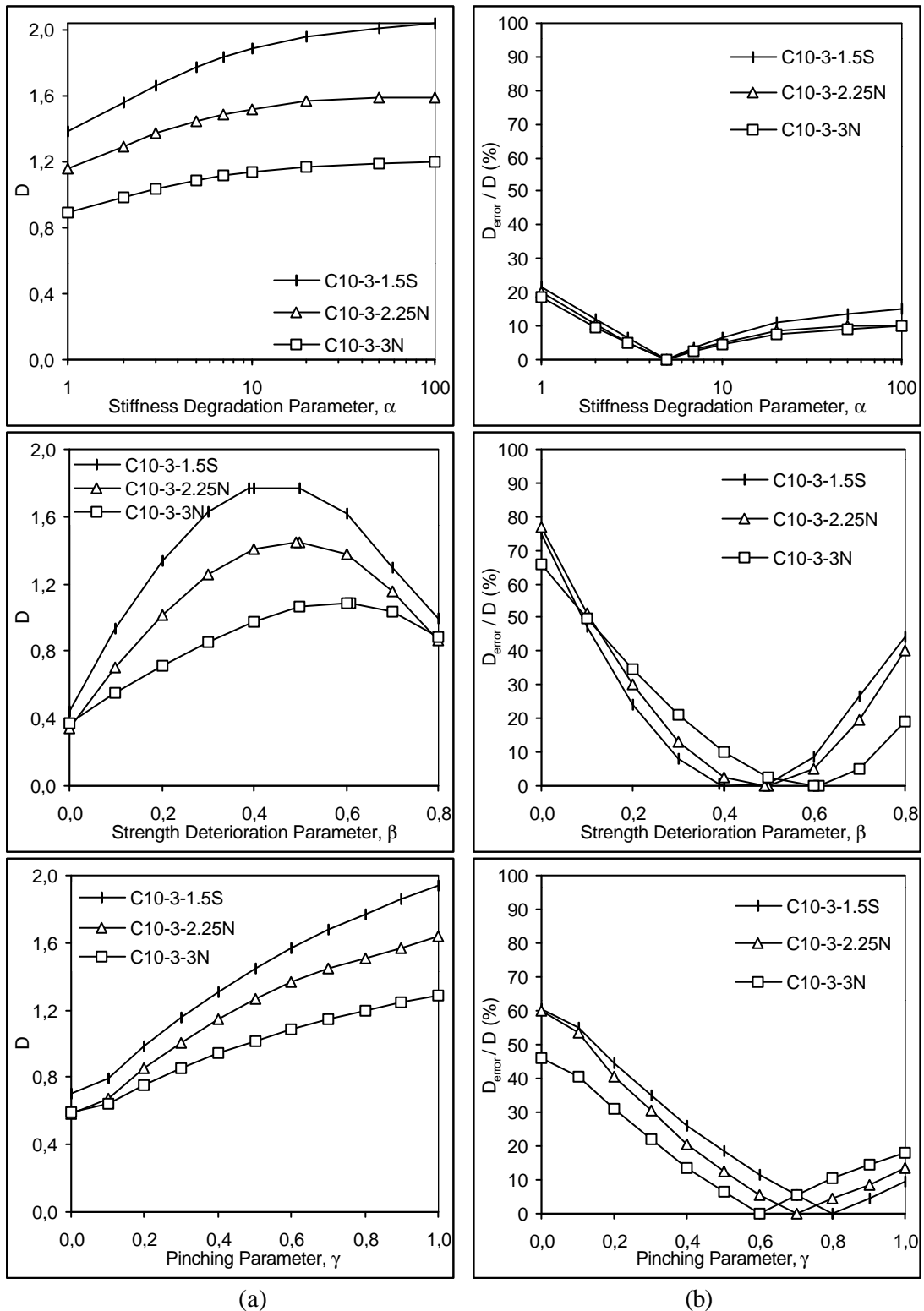


Figure 3.39 Effect of amount of transverse reinforcement-Set I **a)** Damage index vs. deterioration parameters α , β and γ , **b)** Damage index error ratio vs. deterioration parameters α , β and γ

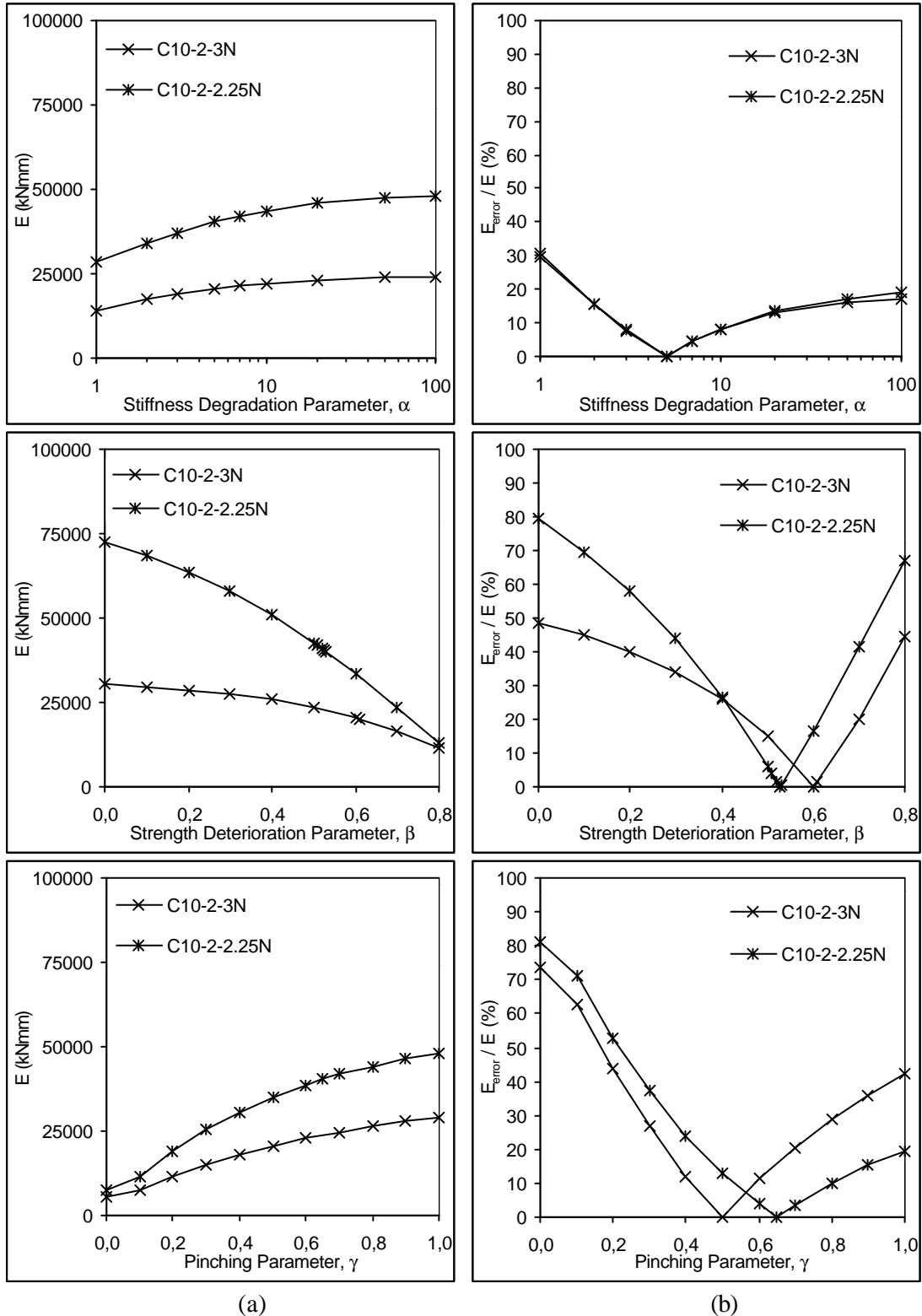
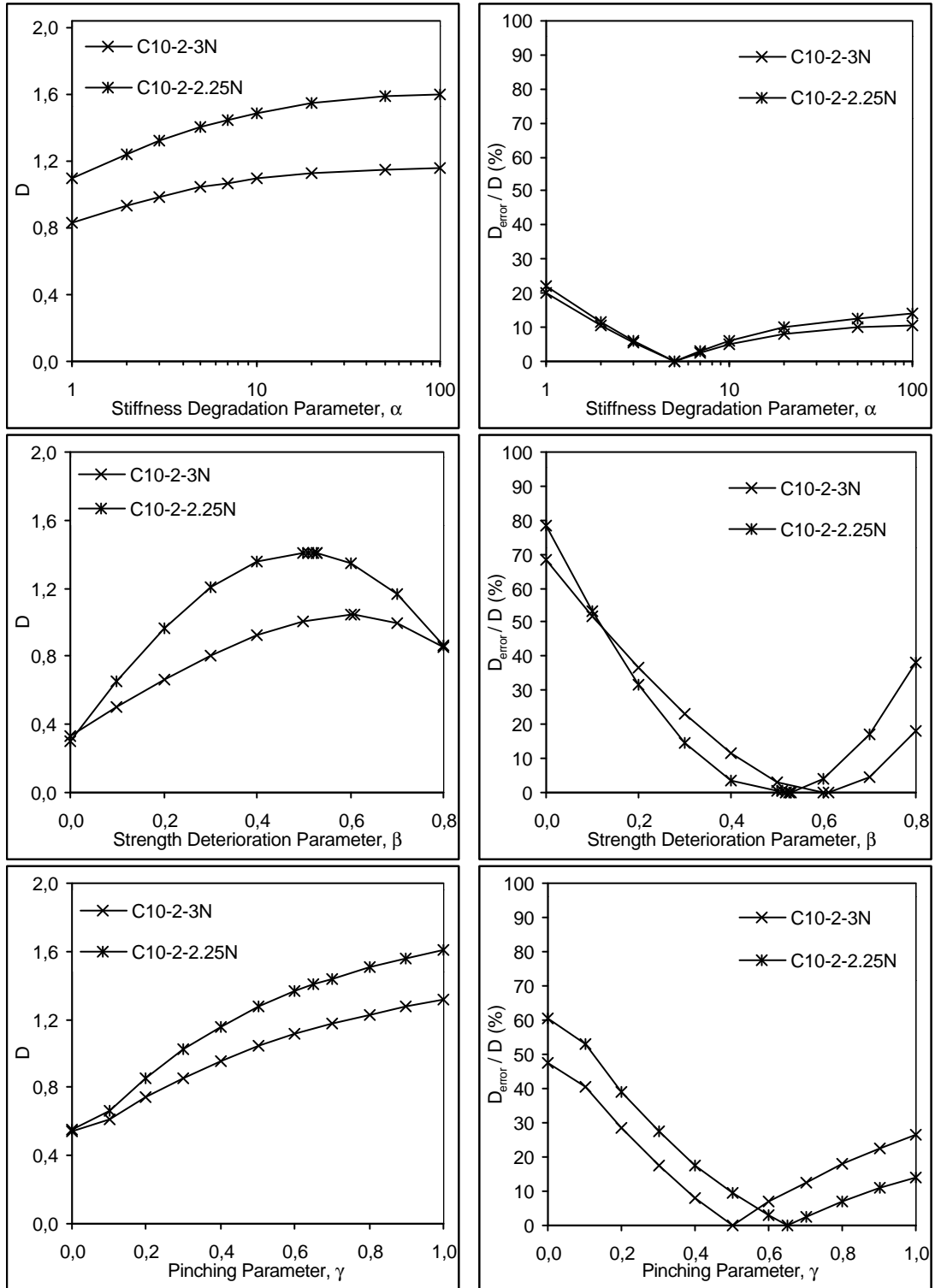


Figure 3.40 Effect of amount of transverse reinforcement-Set II **a)** Dissipated hysteretic energy vs. deterioration parameters α , β and γ , **b)** Dissipated hysteretic energy error ratio vs. deterioration parameters α , β and γ



(a) (b)
Figure 3.41 Effect of amount of transverse reinforcement-Set II **a)** Damage index vs. deterioration parameters α , β and γ , **b)** Damage index error ratio vs. deterioration parameters α , β and γ

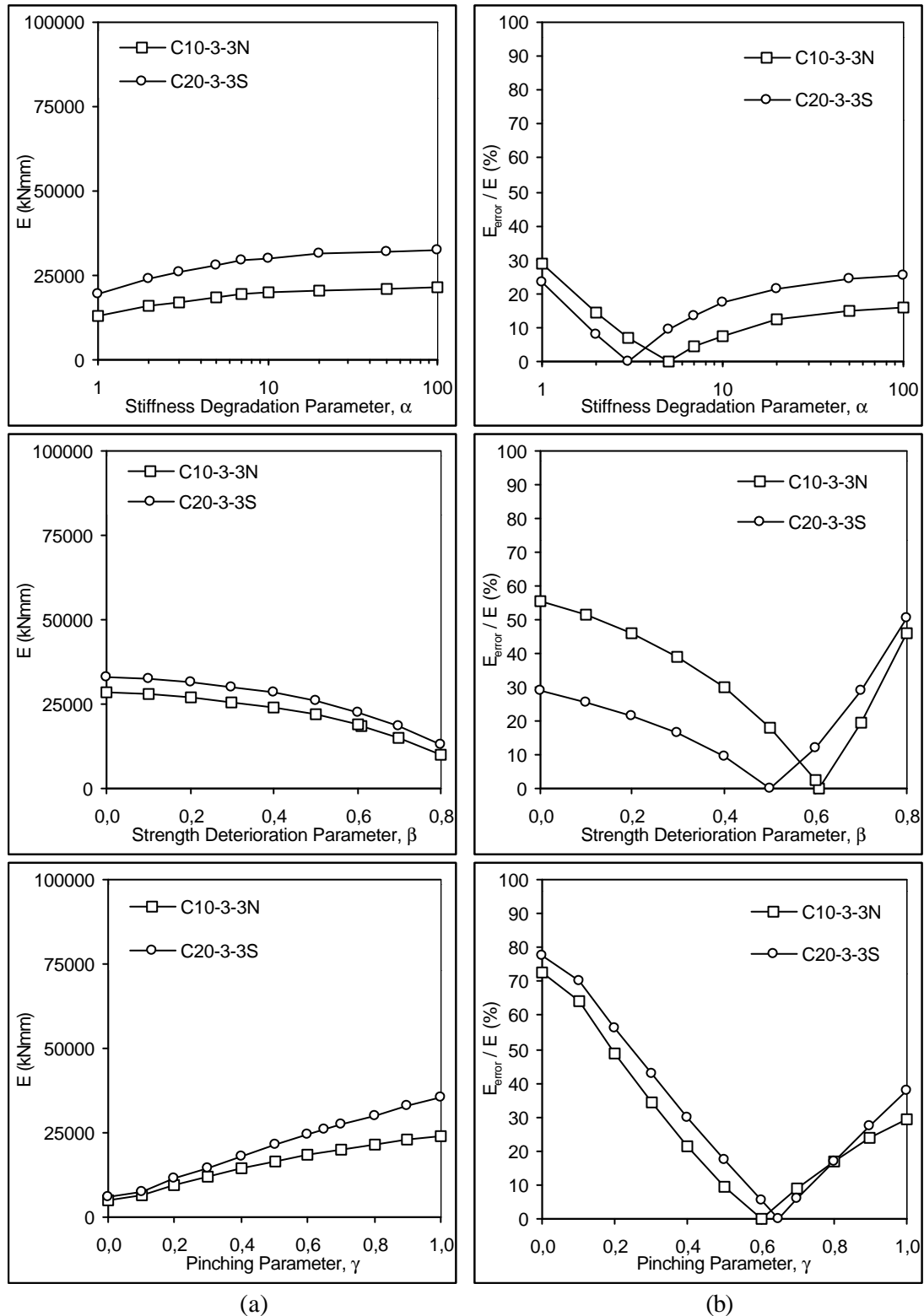


Figure 3.42 Effect of axial load level **a)** Dissipated hysteretic energy vs. deterioration parameters α , β and γ , **b)** Dissipated hysteretic energy error ratio vs. deterioration parameters α , β and γ

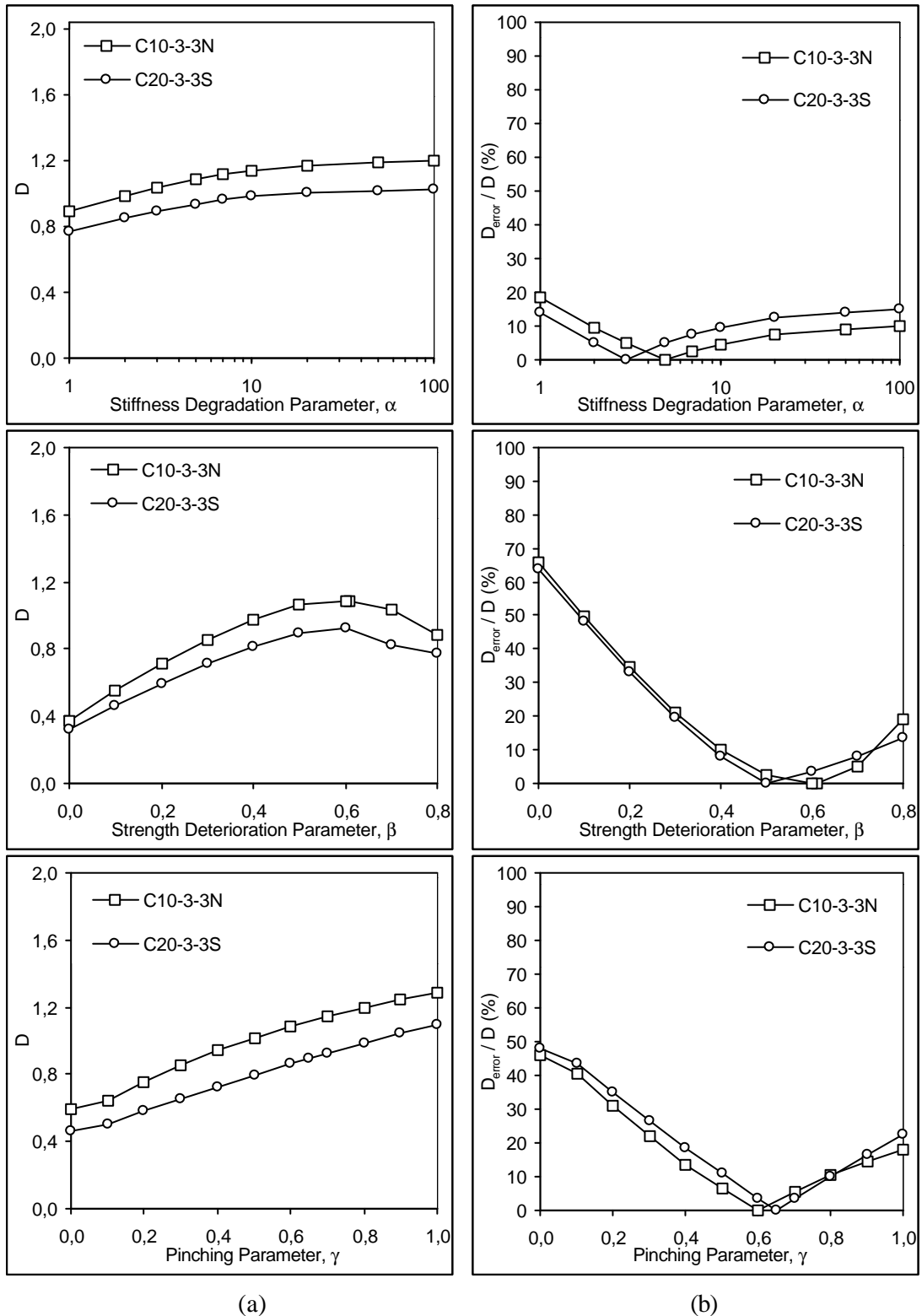


Figure 3.43 Effect of axial load level **a)** Damage index vs. deterioration parameters α , β and γ , **b)** Damage index error ratio vs. deterioration parameters α , β and γ

3.4.2.3.2 Axial Load Level

The sensitivity of the deterioration parameters to the axial load level during the loading histories of the specimens can be inferred from Figures 3.42 and 3.43. Figure 3.42 shows the variation of energy dissipation and its error ratio with respect to the three deterioration parameters for specimens C10-3-3N and C20-3-3S. The variation of the damage index and its error with respect to the deterioration parameters for these specimens are shown in Figure 3.43.

The specimens tested under the same displacement reversals and transverse reinforcements but with different axial load level. The specimens were tested under displacement cycles to a drift ratio of 3 percent. The spacing of the hoops in both specimens is 76.2 mm. But specimen C20-3-3 South was tested under a 272kN ($0.161f_cA_g$) while the axial load applied to specimen C10-3-3 North was 136kN ($0.098f_cA_g$). The axial load applied on the specimen C20-3-3S is two times of the specimen C10-3-3N. However the axial load level on specimen C20-3-3S load does not double that of specimen C10-3-3N, due to small differences in their concrete compressive strengths.

It is observed from the energy dissipation capacity curves presented in Figure 3.42 that the axial load level has an effect on the energy dissipation capacity and thus the deterioration level. Increase in the axial load level to a certain level leads to stiffening and strengthening of the cross section. Hence, the energy dissipation capacity was higher for the specimen with the higher axial load (C20-3-3 South). It should be stated that the smaller the axial load level the larger was the amount of hysteretic energy dissipated before failure.

However, it can be concluded that the axial load does not affect significantly the number of cycles that could be sustained at given drift ratio before failure. The axial load did affect the rate of deterioration. Inspection on damage curves in Figure 3.44 revealed that the higher the axial load, the more abrupt is the failure.

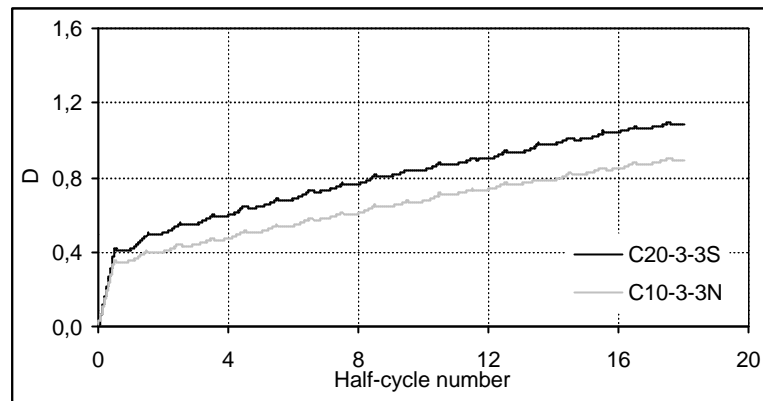


Figure 3.44 Effect of axial load level on damage

Similarly, specimens C10-3-1.5 and C20-3-1.5 were tested under the same displacement schedule and transverse reinforcement but with different axial load level. The spacing of the hoops in both specimens is 38.1 mm. But specimen C20-3-1.5 North was tested under a 272 kN ($0.214f_cA_g$) while the axial load applied to specimen C10-3-1.5 South was 136 kN ($0.091f_cA_g$). Both specimens were tested under displacement cycles at a drift ratio of 4 percent after 7 cycles at a drift ratio of 3 percent. Although the transverse reinforcement was designed to avoid buckling of longitudinal reinforcement during the tests, a limited number of cycles could be applied before buckling of longitudinal reinforcement at the joint face of specimen C20-3-1.5N (Pujol, 2002). Pujol (2002) stated that, the experimental results of specimen C20-3-1.5 had not been considered due to unexpected failure mode that was estimated to cause by the excessive axial load level of $0.214f_cA_g$.

Consequently, experimental and analytical evidence indicate that, under reversals of displacement into the nonlinear range, a factored axial compressive force exceeding $0.20f_cA_g$ acting on reinforced concrete column members causes an abrupt failure.

Figures 3.42 and 3.43 show that the most sensitive parameters to axial load level are the strength deterioration and pinching parameters denoted by β and γ . The stiffness degradation parameter, denoted by α ranging from 1 to 100 in a logarithmic scale, is the less sensitive.

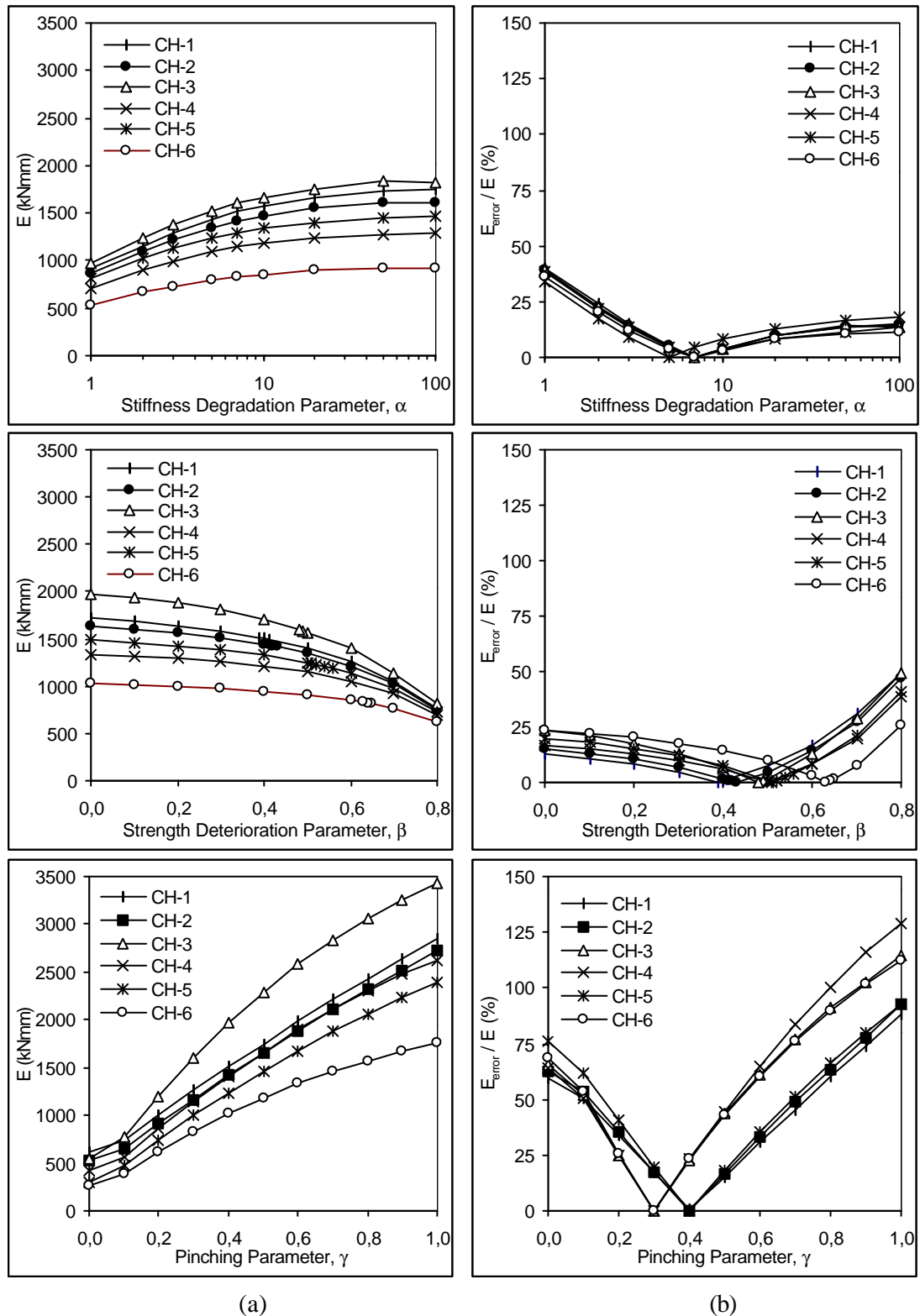


Figure 3.45 Effect of concrete strength and loading history-Set I **a)** Dissipated hysteretic energy vs. deterioration parameters α , β and γ , **b)** Dissipated hysteretic energy error ratio vs. deterioration parameters α , β and γ

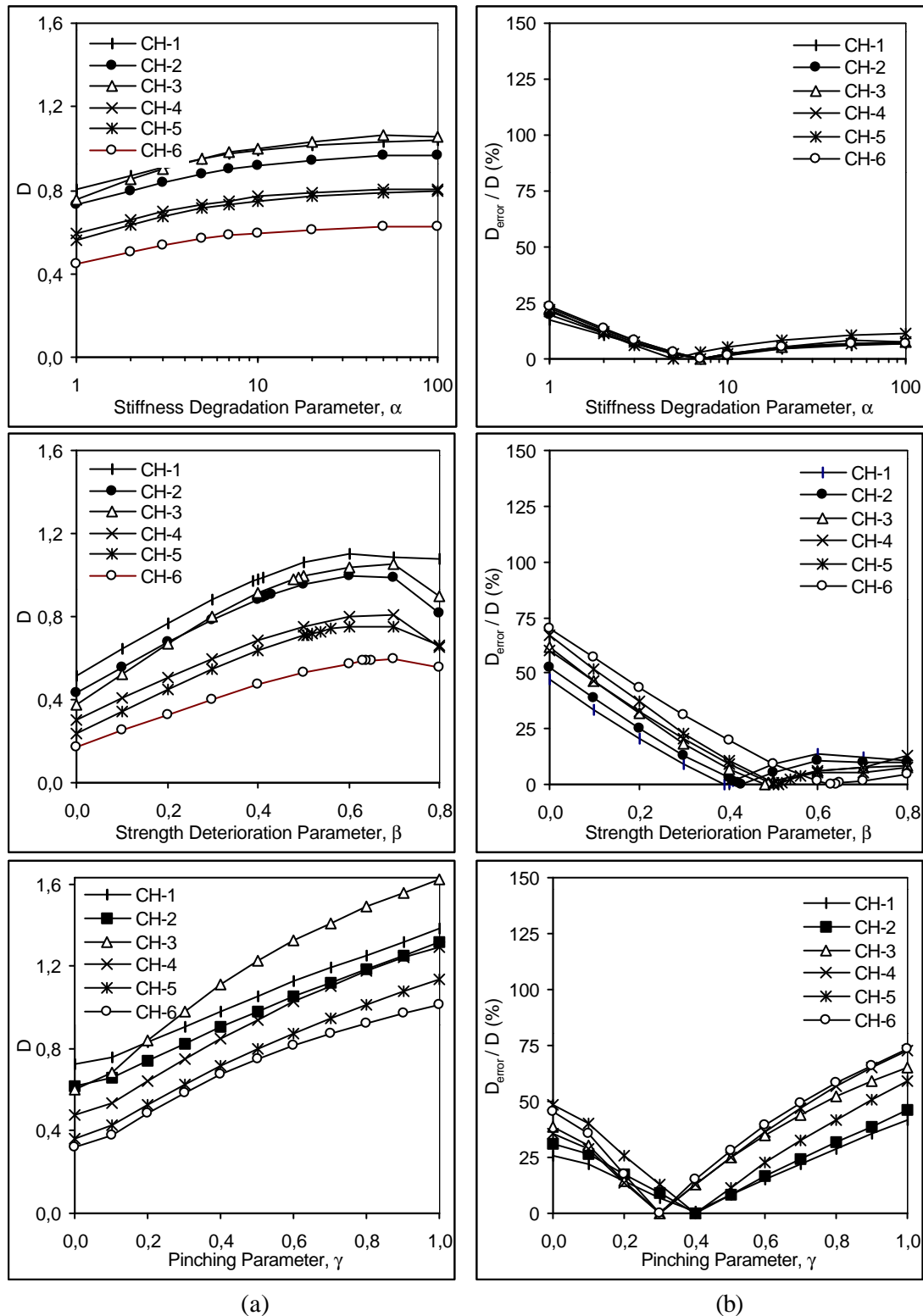


Figure 3.46 Effect of concrete strength and loading history-Set I **a)** Damage index vs. deterioration parameters α , β and γ , **b)** Damage index error ratio vs. deterioration parameters α , β and γ

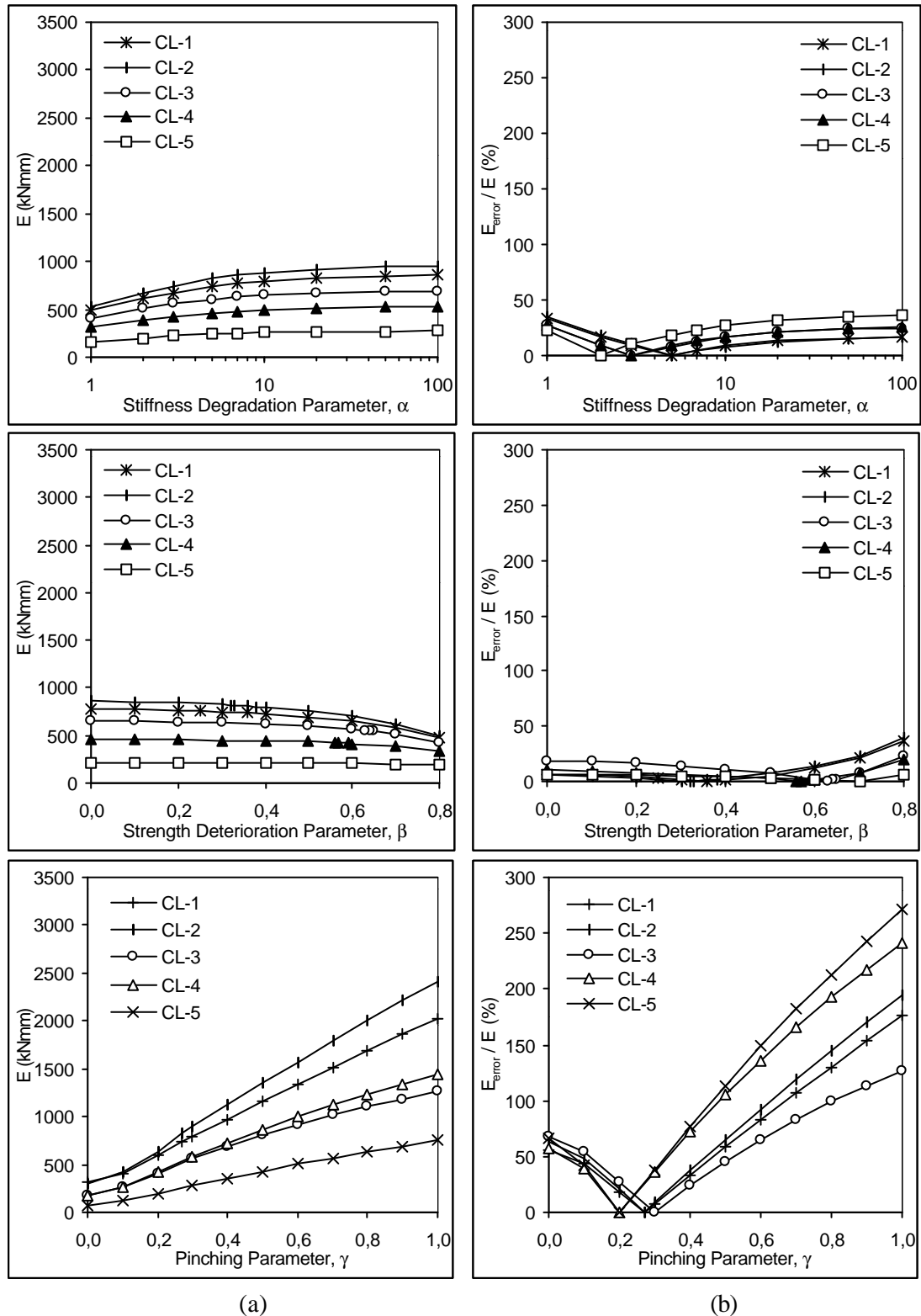


Figure 3.47 Effect of concrete strength and loading history-Set II **a)** Dissipated hysteretic energy vs. deterioration parameters α , β and γ , **b)** Dissipated hysteretic energy error ratio vs. deterioration parameters α , β and γ

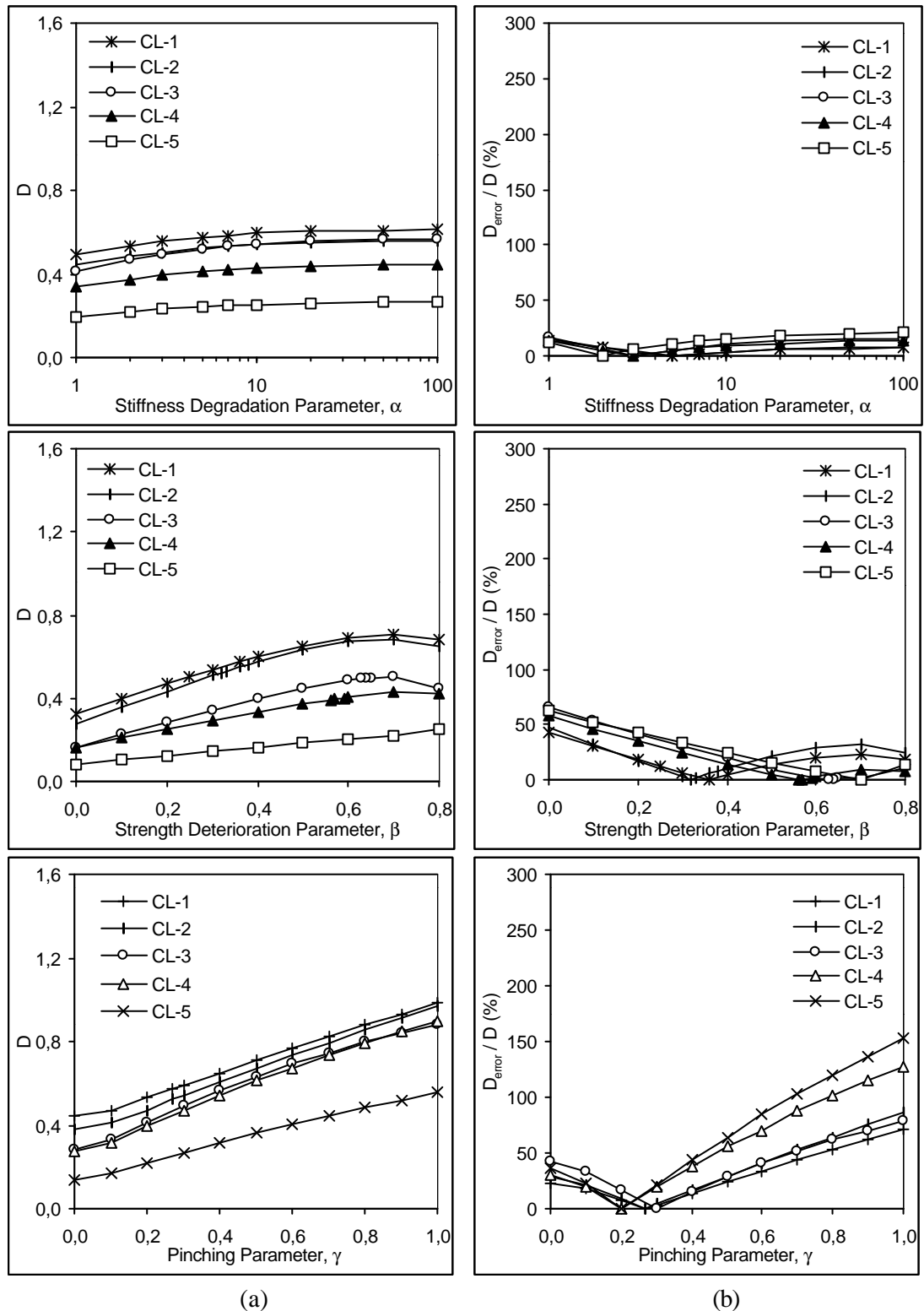


Figure 3.48 Effect of concrete strength and loading history-Set II **a)** Damage index vs. deterioration parameters α , β and γ , **b)** Damage index error ratio vs. deterioration parameters α , β and γ

3.4.2.3.3 Concrete Strength

The sensitivity of dissipated hysteretic energy and damage index to concrete strength can be inferred from Figures 3.45 and 3.47 for energy dissipation and Figures 3.46 and 3.48 for damage index. Inspections of energy dissipation and damage index and their mutually arranged error ratio curves for the specimens with 13MPa and 20MPa concrete strength, shown in Figures 3.45 to 3.48, reveal the effects of variations in deterioration parameters α , β and γ on dissipated hysteretic energy and damage index.

Figure 3.45 shows the variation of energy dissipation and its error ratio with respect to hysteretic model deterioration parameters for Erberik and Sucuođlu beam specimens (CH-1, CH-2, CH-3, CH-4, CH-5 and CH-6) with relatively high concrete strength of 20MPa. For these specimens the damage index and its error ratio with respect to the deterioration parameters are plotted in Figure 3.46. All specimens were tested without considering axial load. The specimens were subjected to various constant amplitude displacement histories, and they displaced to drift ratios ranging from 6.4 percent to 2.1 percent, as seen in the experimental program given in tabular form in the last columns of Tables 3.1 and 3.2. Similarly the variation curves of the energy dissipation and damage index for the specimens (CL-1, CL-2, CL-3, CL-4 and CL-5) with low concrete strength of 13MPa, are presented in Figures 3.47 and 3.48. The specimens were tested under constant amplitude displacement reversals with drift ratios ranging from 1 percent to 3.5 percent, without considering axial load.

Observation on energy dissipation variation curves in Figures 3.45a and 3.47a comparatively, indicates that the concrete strength has substantial effects on the energy dissipation capacity. It has been demonstrated that the specimens with low concrete strength do not have the ability to dissipate considerable amount of energy. The error ratio curves in Figures 3.45b and 3.47b indicate that the amount hysteretic energy dissipation is quite sensitive to variations in the deterioration parameters. It should be noted that the most sensitive parameter is the pinching parameter, γ .

As seen from the comparison of damage index variation curves in Figures 3.46a and 3.48a, concrete strength affect the structural damage significantly. It has been depicted that the deterioration level of the structural system affected significantly by the variations in concrete strength. The specimens with relatively high concrete strength exhibited considerably larger energy dissipation capacity with lower deterioration of the parameters. It should be stated that the higher the concrete strength the larger was the amount of hysteretic energy dissipated before failure This causes to relatively lower level of structural damage.

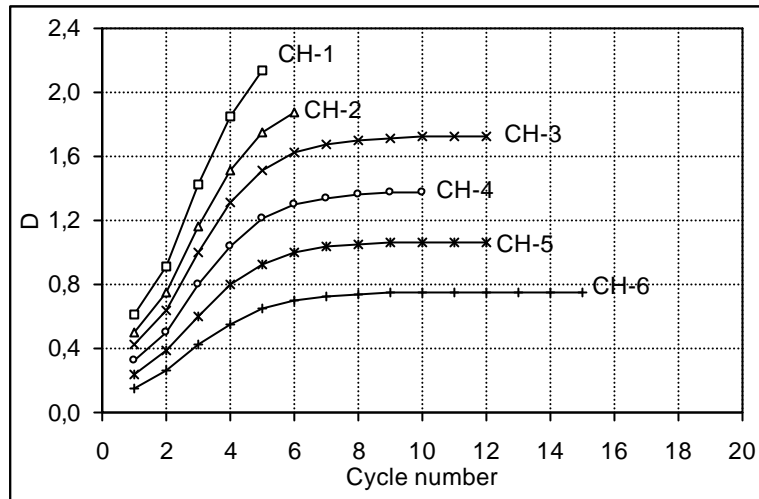
Figure 3.49 contains two plots. The first one shows the damage curves of the specimens tested by Erberik and Sucuođlu under constant amplitude displacement reversals. The damage model developed by the authors was employed for damage prediction of structural members (Erberik, 2001). The energy-based damage model is based on stiffness and strength degradation, but not pinching. This model was introduced in the first chapter of the dissertation. The model gives the total damage at the n^{th} full-cycle as follows;

$$D_{e,n} = \frac{\mathbf{m}_t - 1}{\mathbf{m}_t - 1} + \left(\frac{\mathbf{m}_t}{\mathbf{m}_t - 1} \right) \cdot \left(\frac{4}{5\overline{E}_{h,n}} - 1 \right) \quad (3.2)$$

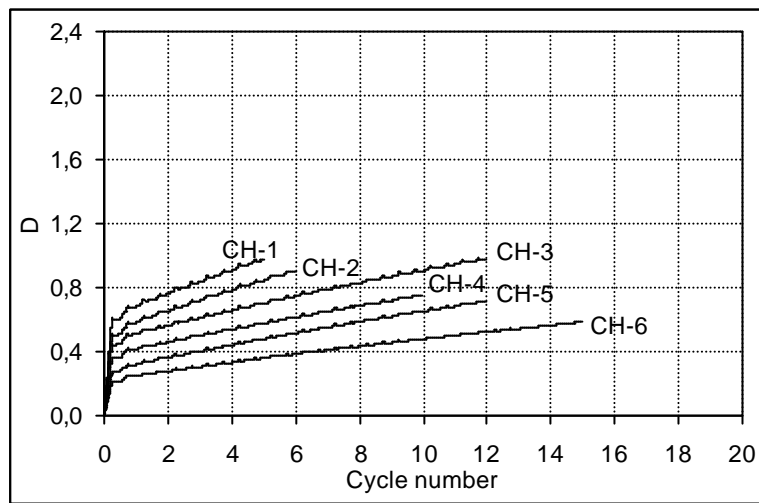
The first term represents damage due to maximum effective ductility, and the second term due to low cycle fatigue at $i_{eq,n}$ cycles. The second plot shows the damage curves of the same specimens obtained by using modified form of fatigue based modified Park and Ang damage model incorporated into IDARC. This model was also introduced in the first chapter. The formulation of the model is as follows:

$$D = \frac{\mathbf{f}_m - \mathbf{f}_y}{\mathbf{f}_u - \mathbf{f}_y} + \mathbf{b} \frac{\int dE}{M_y \mathbf{f}_u} \quad (3.3)$$

It should be noted that there is a similarity in between the first components of both models, but the second components are based on different concepts. Inspection on the damage curves obtained by using fatigue based two different damage models, which are shown in Figure 3.49, revealed that there is a large difference between the damage predictions from these two models. Effects of concrete strength on structural damage appear clearly from damage curves of the specimens with low (13MPa) and relatively high (20MPa) concrete strengths presented in Figures 3.49b and 3.50.



(a)



(b)

Figure 3.49 Damage curves for Erberik and Sucuođlu beam test specimens ($f_c=20\text{MPa}$) obtained by using damage model developed by **a)** Erberik and Sucuođlu and **b)** Park and Ang

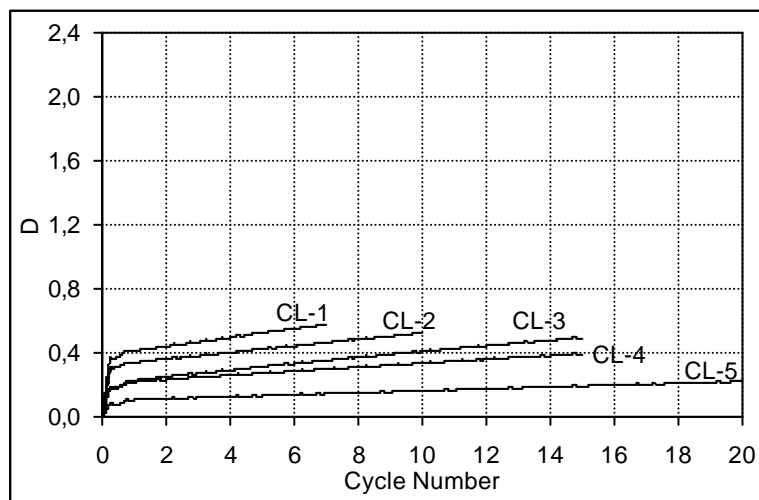


Figure 3.50 Damage curves for Erberik and Sucuođlu beam test specimens ($f_c=13\text{MPa}$) obtained by using Park and Ang damage model

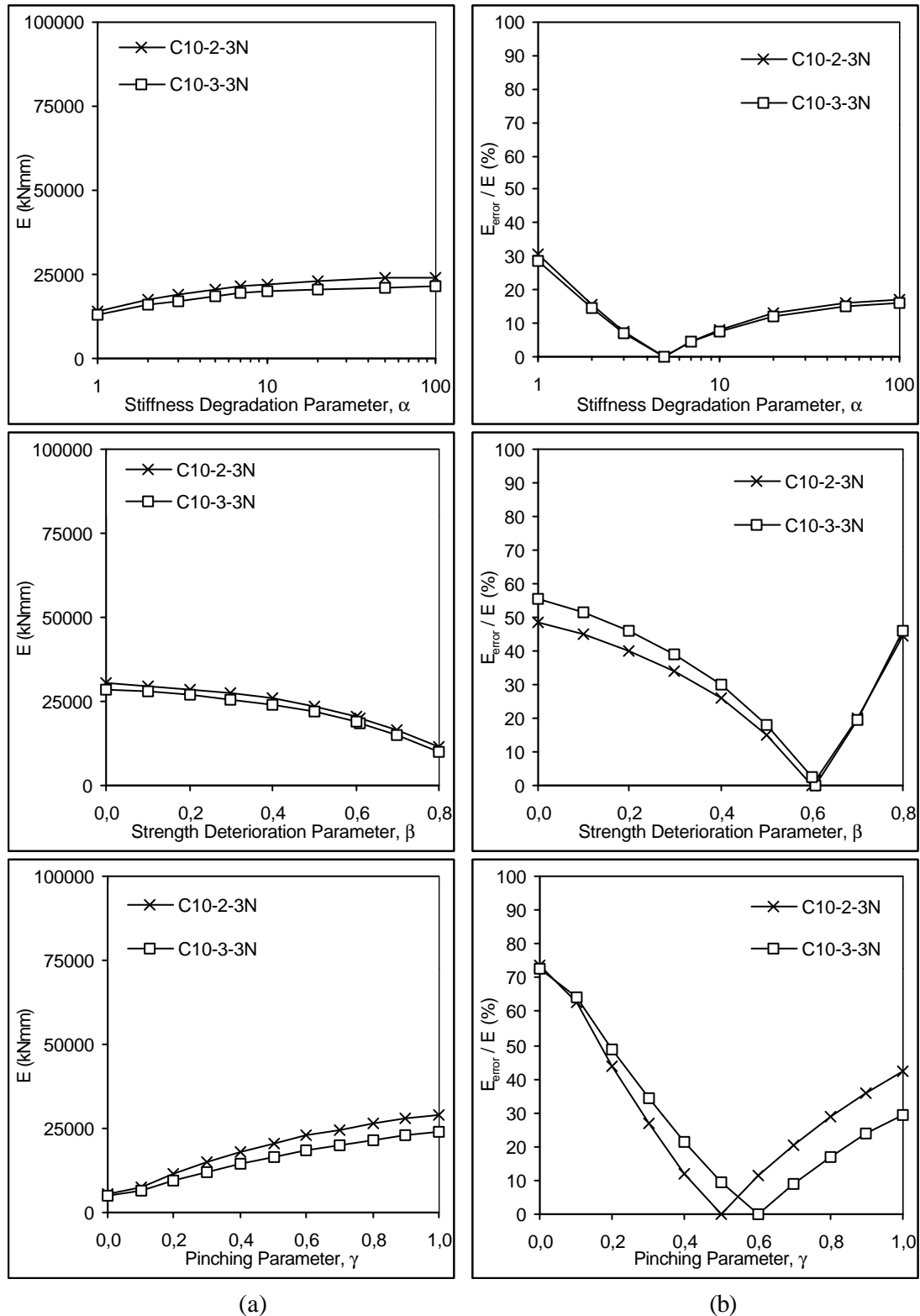


Figure 3.51 Effect of loading history-Set I **a)** Dissipated hysteretic energy vs. deterioration parameters α , β and γ , **b)** Dissipated hysteretic energy error ratio vs. deterioration parameters α , β and γ

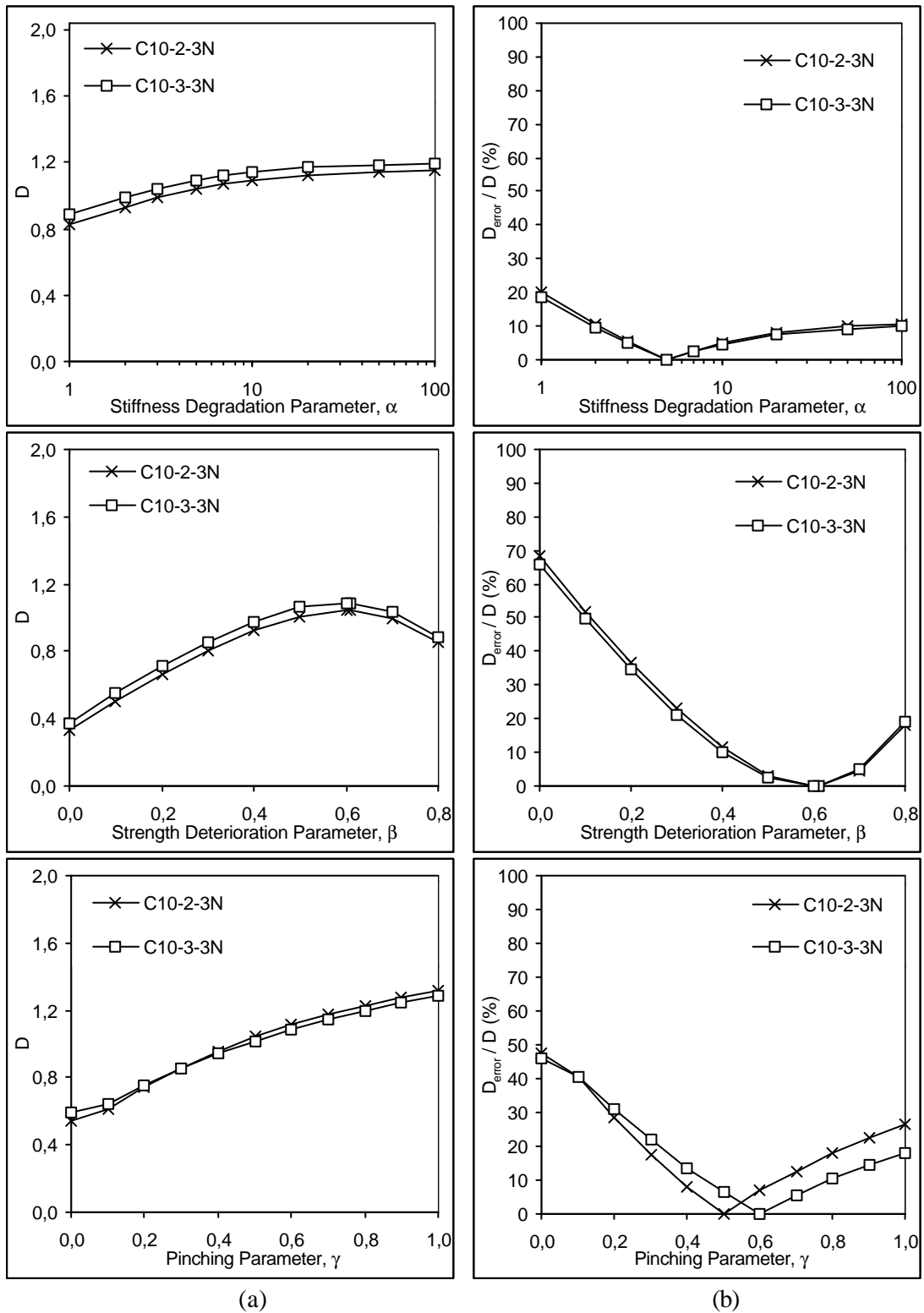


Figure 3.52 Effect of loading history-Set I **a)** Damage index vs. deterioration parameters α , β and γ , **b)** Damage index error ratio vs. deterioration parameters α , β and γ

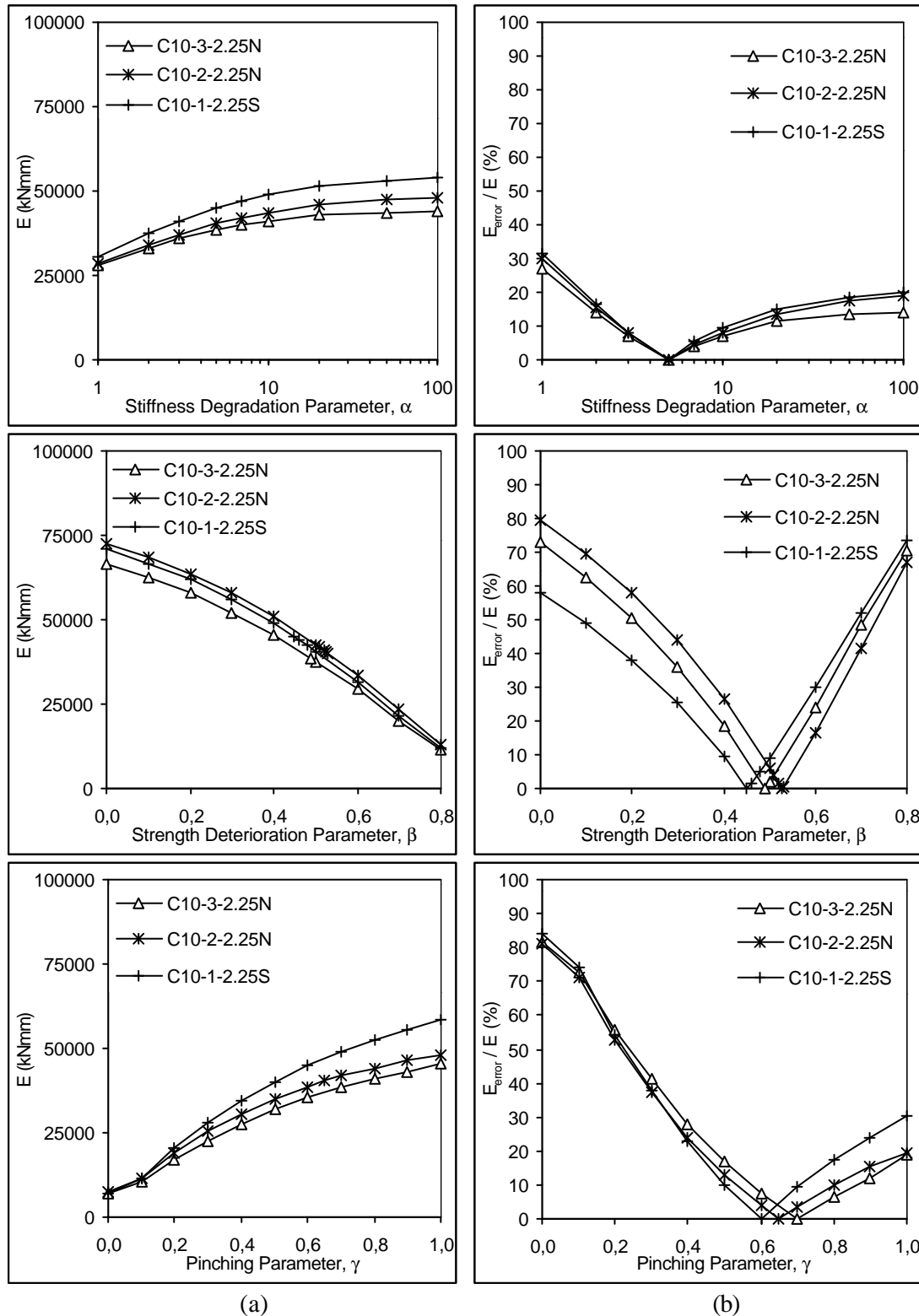


Figure 3.53 Effect of loading history-Set II **a)** Dissipated hysteretic energy vs. deterioration parameters α , β and γ , **b)** Dissipated hysteretic energy error ratio vs. deterioration parameters α , β and γ

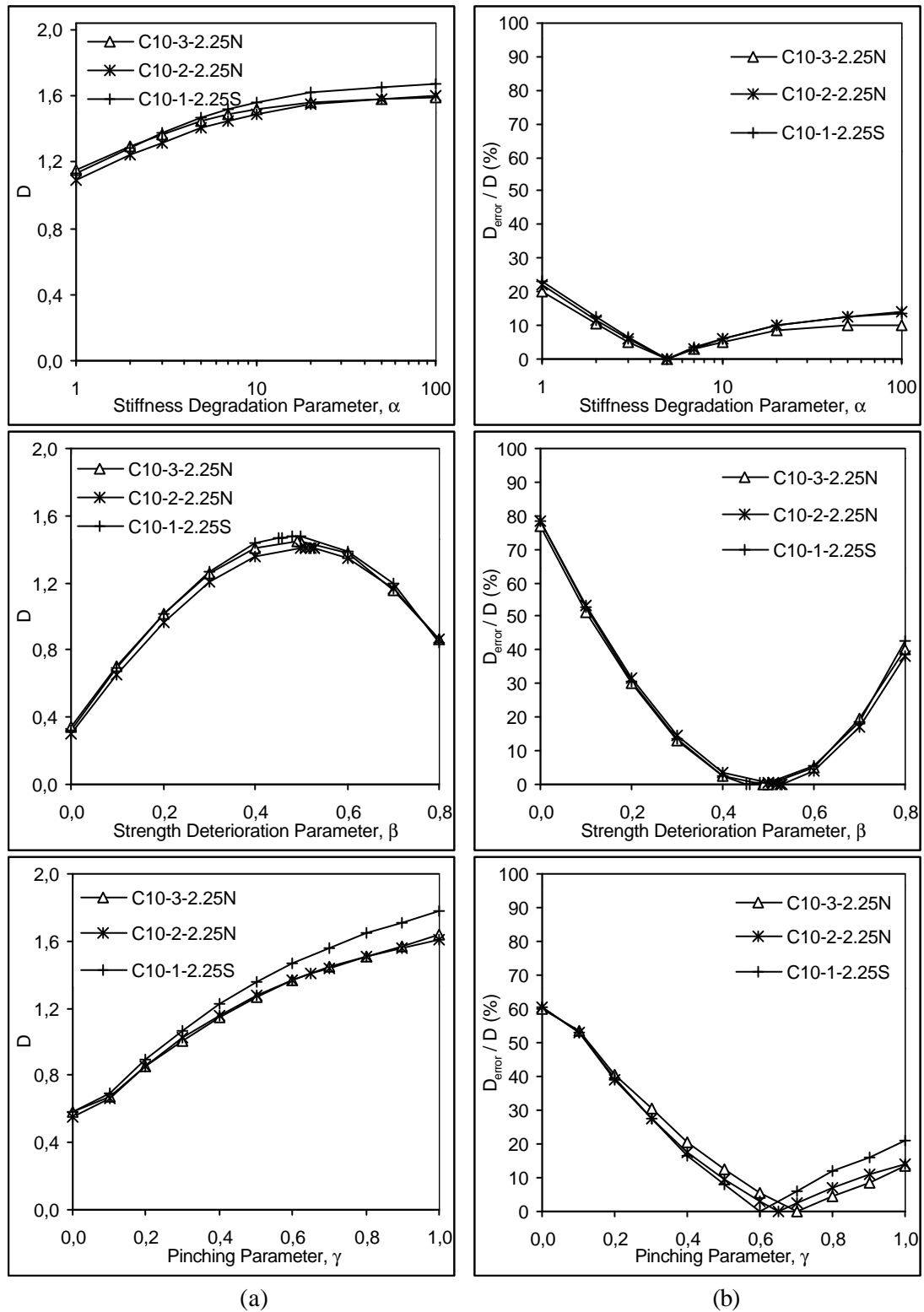


Figure 3.54 Effect of loading history-Set II **a)** Damage index vs. deterioration parameters α , β and γ , **b)** Damage index error ratio vs. deterioration parameters α , β and γ

3.4.2.3.4 Loading History

Two series of the specimens tested by Pujol (2002) under different displacement histories were for purposes of studying whether displacement history has an effect on energy dissipation capacity and damage. These two series of specimens are also used to assess the sensitivity of these characteristics to deterioration parameters α , β and γ .

Specimens C10-2-3 and C10-3-3 had the same axial load of 136 kN and the same amount of transverse reinforcement (76.2 mm of hoop spacing) but were tested under different displacement histories. Specimens C10-2-3 were subjected to seven cycles of a drift ratio of 2 percent before being tested at 3 percent. On the other hand C10-2-3 were tested directly at 3 percent.

Similarly, specimens C10-1-2.25, C10-2-2.25 and C10-3-2.25 were subjected to the same axial load of 136 kN. The spacing of the hoops in all specimens is 57.2 mm. All specimens were tested at a drift ratio of 3 percent. Specimens C10-3-2.25 were displaced directly to a drift ratio of 3 percent. Specimens C10-1-2.25 were subjected to seven cycles at a drift ratio of 1 percent (approximately the drift ratio at yield) and specimens C10-2-2.25 were subjected to seven cycles at a drift ratio of 2 percent before application of cycles at 3 percent.

The sensitivity of the deterioration parameters to loading history can be shown from Figures 3.51 to 3.54. Figure 3.51 shows the variation of energy dissipation and its error ratio with respect to the three deterioration parameters for specimens C10-2-3N and C10-3-3N. The variation of damage index and its error with respect to the deterioration parameters for these specimens are presented in Figure 3.52. Similarly Figures 3.53 and 3.54 show the same variations for the second series specimens C10-1-2.25, C10-2-2.25 and C10-3-2.25.

Inspection on the variation curves of damage index and energy dissipation, which are shown in Figures 3.51 to 3.54, indicate that the loading history has little effect on damage and amount of hysteretic energy dissipated in the end of the

histories (at failure stage). As seen in Figures 3.51 and 3.53 almost all curves are quite close to each other demonstrating the ineffectiveness of the loading history on the amount of energy to be dissipated at failure stage. The phenomenon can be observed from the damage curves presented in Figures 3.52 and 3.54. At failure, damage curves of two series of Pujol specimens each reached almost at the same level following different paths. Despite reaching the same damage level, the numbers of cycles sustained by each specimen of both series are different (Figure 3.55).

Inspection on the variation curves, which are shown in Figures 3.51 to 3.54, revealed that the most sensitive parameters to loading history are the strength deterioration and pinching parameters denoted by β and γ . Damage error ratio vs. parameter β curves form a trough and dip slowly through the solution points (Figure 3.52 and 3.54), whereas energy and damage error ratio vs. parameters α and γ curves dip sharply at that points (Figure 3.51 to 3.54). The less sensitive parameter is the stiffness degradation parameter denoted by α .

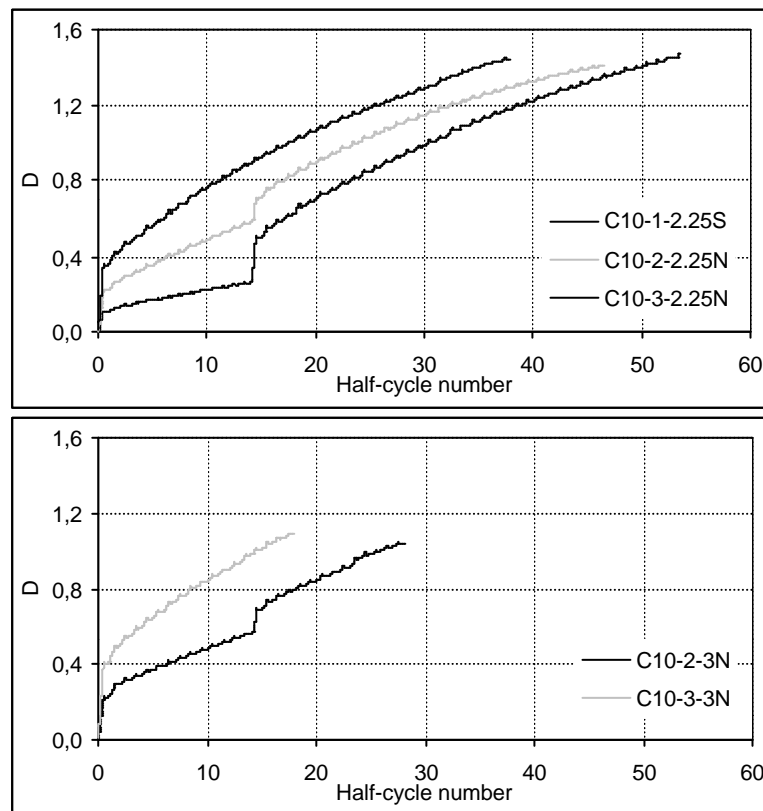


Figure 3.55 Progressive damage curves for the two sets of specimens subjected to variable-amplitude displacement histories (Pujol column specimens)

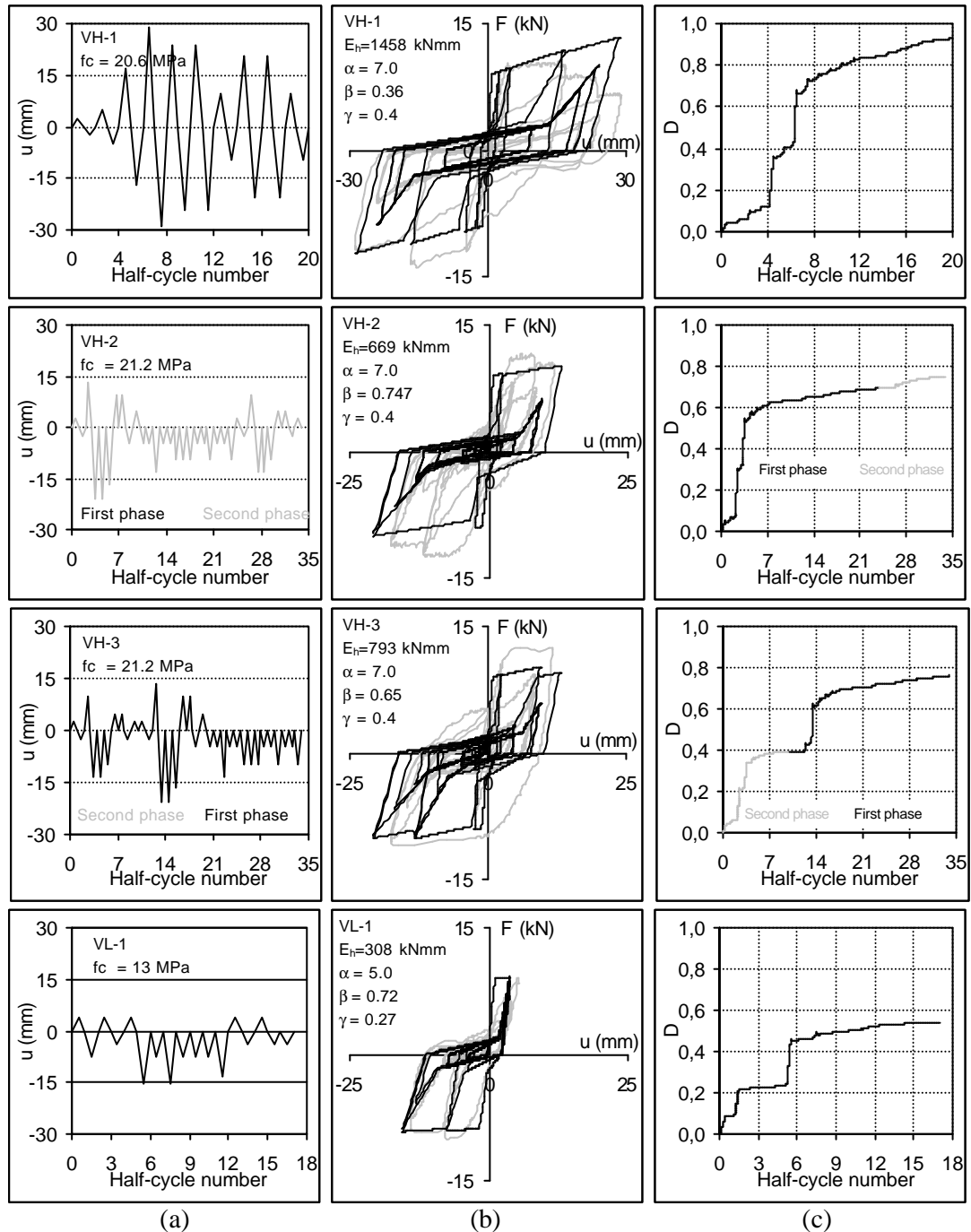


Figure 3.56 Effect of loading history (Erberik and Sucuođlu specimens) **a)** variable-amplitude displacement histories **b)** Experimental (gray) and analytical (black) force-displacement curves **c)** Damage curves

Figure 3.56 shows the variable-amplitude displacement histories imposed on the Erberik and Sucuođlu beam specimens, experimental (gray curves) and analytical (black curves) force-displacement relationships and damage curves. Discussion related to the effect of loading history on damage and energy dissipation mentioned above is not valid for these specimens except for specimens labeled as VH-2 and

VH-3. In case of specimens VH-2 and VH-3, energy dissipation and total damage are almost equal at the end of displacement patterns despite opposite ordering of cyclic amplitudes. This shows that cumulative energy dissipation and total damage are independent from the order of amplitudes along displacement paths consisting of the same number and amplitude of cycles. However, variable amplitude loading histories consisting of the different number and amplitude of cycles lead to considerably different level of damage and energy dissipated along the path.

3.4.3 Deterioration Parameters for Several Deterioration Levels

The sensitivity of parameters α , β and γ describing the level of deterioration in the stiffness, strength and pinching or slip, respectively, to several structural characteristics has been evaluated by employing the experimental database tabulated in Table 3.2. In this study the stiffness degradation parameter, α , ranges between 1-100, the strength deterioration parameter, β , ranges between 0.0-0.8, and the pinching parameter ranges between 0.0-1.0.

Material properties such as amount and grade of longitudinal and transverse reinforcements implemented in construction, concrete strength and axial load level excluding loading history are easily identifiable parameters for an existing building. It is demonstrated that the loading history has minor effect on the damage attained in the end and energy dissipated along the path.

A proposed range of deterioration parameters indicating the level of deterioration can be designed based on the range of values for these three parameters. For seismic performance evaluation of deteriorating structures, three different classes of structural systems are defined based on the evaluated experimental database. Table 3.3 contains the deterioration parameter values proposed for three different deteriorating reinforced concrete structural systems. These classes are defined as mildly deteriorating (MLD) systems, moderately deteriorating (MOD) systems and severely deteriorating (SVD) systems; a different combination of low cycle fatigue parameters (α , β , γ) is assigned to each class.

Table 3.3. Proposed range of parameters for deterioration levels of structural systems

Deterioration Level	Stiffness parameter (a)	Strength parameter (b)	Pinching parameter (g)	Structural Properties
Mild Deterioration	10	0.1	0.8	High strength concrete, Low axial load, $N \leq 0.10f_c A_g$, Confinement ratio, $\rho_s \geq 0.01$
Moderate Deterioration	6	0.3	0.5	Medium concrete strength, Axial load, $0.10f_c A_g \leq N \leq 0.20f_c A_g$, Confinement ratio, $0.005 \leq \rho_s \leq 0.007$
Severe Deterioration	3	0.6	0.3	Poor concrete strength, $f_c \leq 15$ MPa High axial load, $N \geq 0.20f_c A_g$, No confinement, Lack of anchorage, $\Sigma A_c / (n \times A_p) \leq 0.01$ (for low-rise bldg)

ΣA_c : the sum of the column areas at the base of a building

n : number of stories above the base

A_p : floor area of one story

ΣA_p : the sum of the floor area above the base ($n \times A_p$)

The general properties of the two of three level of deteriorating systems showing the superior and inferior structural performance can be summarized as follows.

Mildly deteriorating (MLD) systems contain well detailed reinforced concrete members with high concrete strength, transverse reinforcement ratios exceeding 1 percent and axial load level not exceeding $0.10f_c A_g$ for columns (Table 3.3). The specimens, such as Pujol column labeled as C10-3-1.5S, with transverse reinforcement ratios exceeding 1.0 percent and axial load level lower than $0.10f_c A_g$ exhibited only mild deterioration.

Severely deteriorating (SVD) systems are structural systems having the deficiencies commonly observed in damaged buildings after past earthquakes; such as low concrete strength, poor or no confinement of concrete, lack of anchorage of plain reinforcement, axial load level exceeding $0.20f_c A_g$, etc. Force-deformation relationships of the beam tests shown in Figures 3.11, 3.12 and 3.13 indicate that, plain bars placed in low to medium strength concrete leads to severe deterioration due to anchorage slip (Erberik and Sucuođlu (2004)). The SVD systems have concrete

strength lower than 15 MPa reflecting the strength of concrete in the existing concrete construction. It is known that majority of the existing concrete construction in Turkey fall into this range. The factored axial compressive force acting on column members of such systems exceeds the level of $0.20f_cA_g$. Low rise of such buildings have the *column ratio*, which is defined simply as *the ratio of the sum of the column areas at the base of a building to the floor area above the base*, lower than 1.0 percent.

The properties of the deterioration level in between the mildly deterioration (MLD) level and severely deterioration (SVD) level, namely moderately deterioration (MOD) level correspond to an ordinary properties of structural systems.

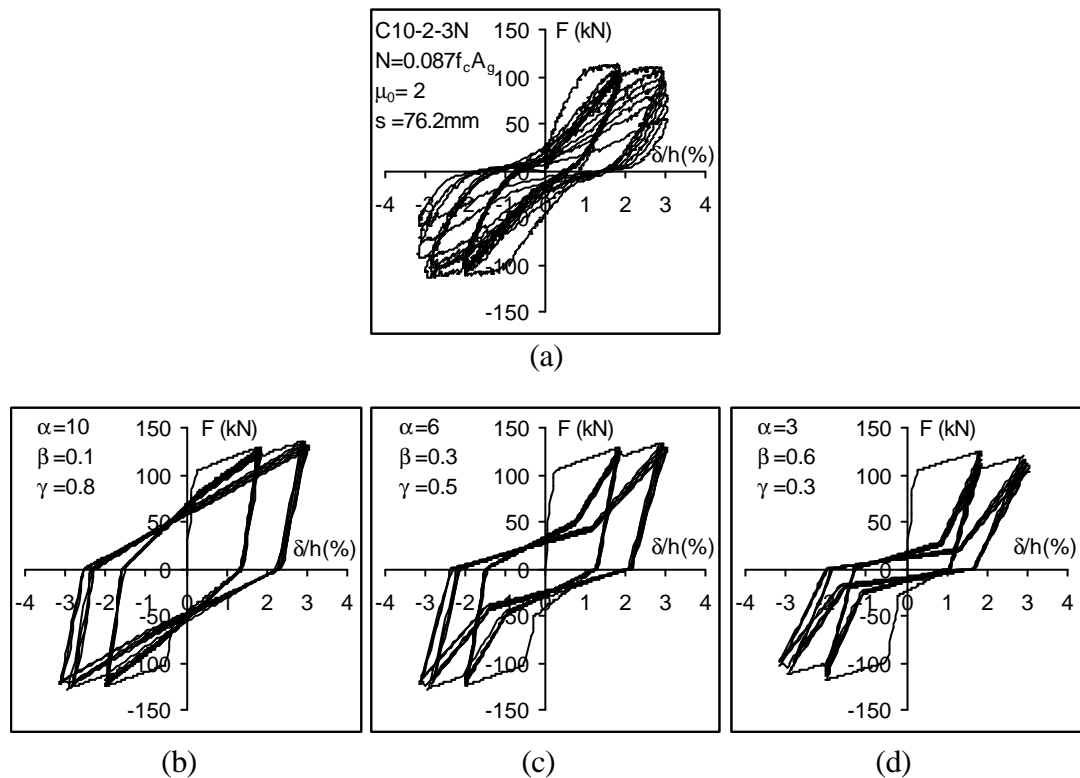


Figure 3.57 Sensitivity analysis of three-parameter model: **a)** Experiment, **b)** Simulation using $\alpha=10$, $\beta=0.1$ and $\gamma=0.8$, Mild deteriorating system (MLD), **c)** Simulation using $\alpha=6$, $\beta=0.3$ and $\gamma=0.5$, Moderate deteriorating system (MOD), **d)** Simulation using $\alpha=3$, $\beta=0.6$ and $\gamma=0.3$, Severe deteriorating system (SVD)

Examples of the typical analytical force-displacement relationships for these three different classes of structural systems, obtained by using the proposed α , β and γ parameters and loading history of specimen C10-2-3N, are shown in Figure 3.57.

3.5 Concluding Remarks

The discussion above underscores the fact that for the damage to be realistic, the model parameters should be selected such that the inelastic structural behavior in “reality” can be captured. Conducting a hysteretic energy error minimization exercise for each damage prediction attempt is clearly not a feasible option. However, the purpose in this section has not been the exact imitation of some beam and column laboratory tests, but to assess the effects of stiffness degradation, strength deterioration and pinching parameters on low cycle fatigue damage and energy dissipation.

It has been demonstrated that rational prediction of damage and damageability of reinforced concrete structures and their components strongly depends on the tuning of the stiffness degradation, strength deterioration and pinching parameter values. Selection of these parameter values plays a vital role in determination of damage index reflecting the level of damage sustained by a structural component. Arbitrary choices of the parameter values may result in a considerable deviation of the damage index used in damage-decision making.

It has also been demonstrated that selection of the parameter values plays a vital role in determination of damage index of the structural components reflecting the observed damage of reinforced concrete components, with a reasonable accuracy. An arbitrary choice of the parameter values results in a considerable deviation of the damage index and total amount of hysteretic energy to be dissipated.

Consequently, it should be stated that the dissipated hysteretic energy thus the damage index are significantly sensitive to hysteretic model parameters, and the calibration of these parameters is inevitable from standpoint of quantifying the damage state of a structural component reasonably well. In the light of the brief discussion mentioned above it can be stated that the parameters β and γ govern high damage whereas the parameter α governs small damage. Therefore for rational damage prediction, fine-tuning of the deterioration parameters, especially parameters β and γ , is essential. Table 3.3 is a useful guide for this purpose.

CHAPTER 4

ASSESSMENT OF CONTROLLING PARAMETERS ON DAMAGE

4.1 General

The state-of-the-art of seismic design of reinforced concrete structures widely requires and accepts that structures should be designed so that they will not collapse even during severe destructive earthquakes. Seismic provisions in the modern seismic codes prescribe minimum requirements that a structure must safely resist earthquake effects. Structures designed according to these requirements must have a certain level of stiffness, strength and ductility. The general design philosophy of the modern seismic codes is damage-control based. Damage control depends on satisfying the minimum design requirements provided by several structural parameters. If the structures are properly designed, they absorb energy of the earthquake so that little or tolerable damage occurs.

The majority of existing reinforced concrete construction in Turkey and in many other countries have common deficiencies. However, the structural damage caused by earthquakes can not only be attributed to defects in design or construction, but also to several structural parameters controlling damage during an earthquake. The main object of this chapter is systematic assessment of the principal structural damage control parameters. To accomplish this purpose, a large number of two-dimensional section analyses for reinforced concrete, inelastic time history and damage analyses of SDOF systems and seismic vulnerability assessment of several reinforced concrete buildings have been conducted.

4.2 Factors Governing Damage

One of the main purposes of this study is to shed light on design aspects and damage control parameters not commonly taken into consideration but applied in practice and cause structural damage and partially/totally collapse of buildings located in seismic areas. Structural damage caused by earthquake excitations is dependent on many factors. These factors can be enumerated as axial load level, concrete strength, longitudinal and transverse reinforcements ratios, ratio of total cross-sectional-area of an axial load carrying members to floor area, ductility ratio, loading history, prior earthquake damage, number of yield reversals, dissipated hysteretic energy. All these factors must be considered interactively for a rational prediction of damage and damageability of structures. Effects of these variables on the structural behavior, damage and damageability of structural components will be widely examined using moment-curvature and axial force-curvature relationships, interaction diagrams and damage progression curves.

4.2.1 Effect of Axial Load Level

Many of the design codes limit the axial load on the column. Limitation on the axial load level specified in several building and seismic codes are summarized as follows:

$$\text{TS 500 (2000)} \quad : \frac{N_d}{f_c A_c} \leq 0.6 \quad (4.1)$$

$$\text{TEC (1998)} \quad : \frac{N_d}{f_c A_c} \leq 0.5 \quad (4.2)$$

ACI 318 (1971) : Columns subjected to factored axial compressive forces less than 40 percent of that corresponding to balanced load level behave essentially as flexural members and may be designed in accordance with the provisions governing beams. When the axial load on a column exceeds 40 percent of the balanced load level, the columns requires special transverse reinforcement and should be confined by closely spaced transverse reinforcement near the ends (Park and Paulay, 1975).

ACI 318 (2002) : Columns subjected to factored axial compressive forces less than axial load level of $f_c A_g/10$ behave essentially as flexural members and may be designed in accordance with the provisions governing beams. However, in case of axial load level exceeding the level of $f_c A_g/10$, the column should satisfy a large number of strict requirements relating to the cross-sectional dimensioning, the ratio of both longitudinal and transverse reinforcements, concrete contribution in shear design, development length, detailing of the connection joints, etc.

The axial load affects the curvature; therefore there is no unique moment-curvature curve for a given column section subjected to axial load in addition to bending moment (Pfrang et al., 1964). Such curves are shown in Figure 4.1, for several levels of constant axial load ranging from simple bending (no axial load) to ultimate strength, including balanced case. Both axes of the figure have been normalized. These curves belong to column sections with 2 percent of longitudinal reinforcement ratio.

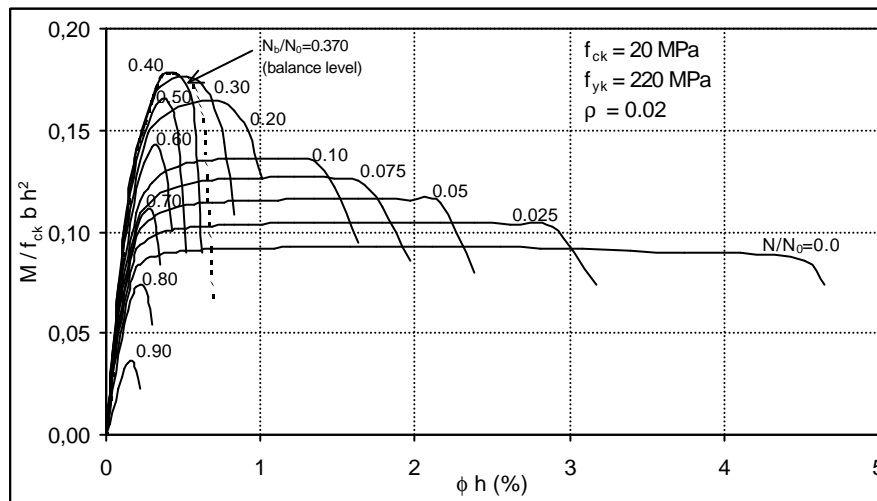


Figure 4.1 Effects of axial load level on moment curvature relationships

Figure 4.1 illustrates that axial load level substantially affects the moment-curvature relationships. By referring to these curves it is possible to state that sections have large amount of ductility at low load levels. As the load level increases, ductility decreases considerably. In case of axial load levels equal or greater than the balanced failure load, the amount of ductility remains for sections is almost

negligible. For the axial load level decreasing from balanced case towards simple bending case the ductility rapidly increases.

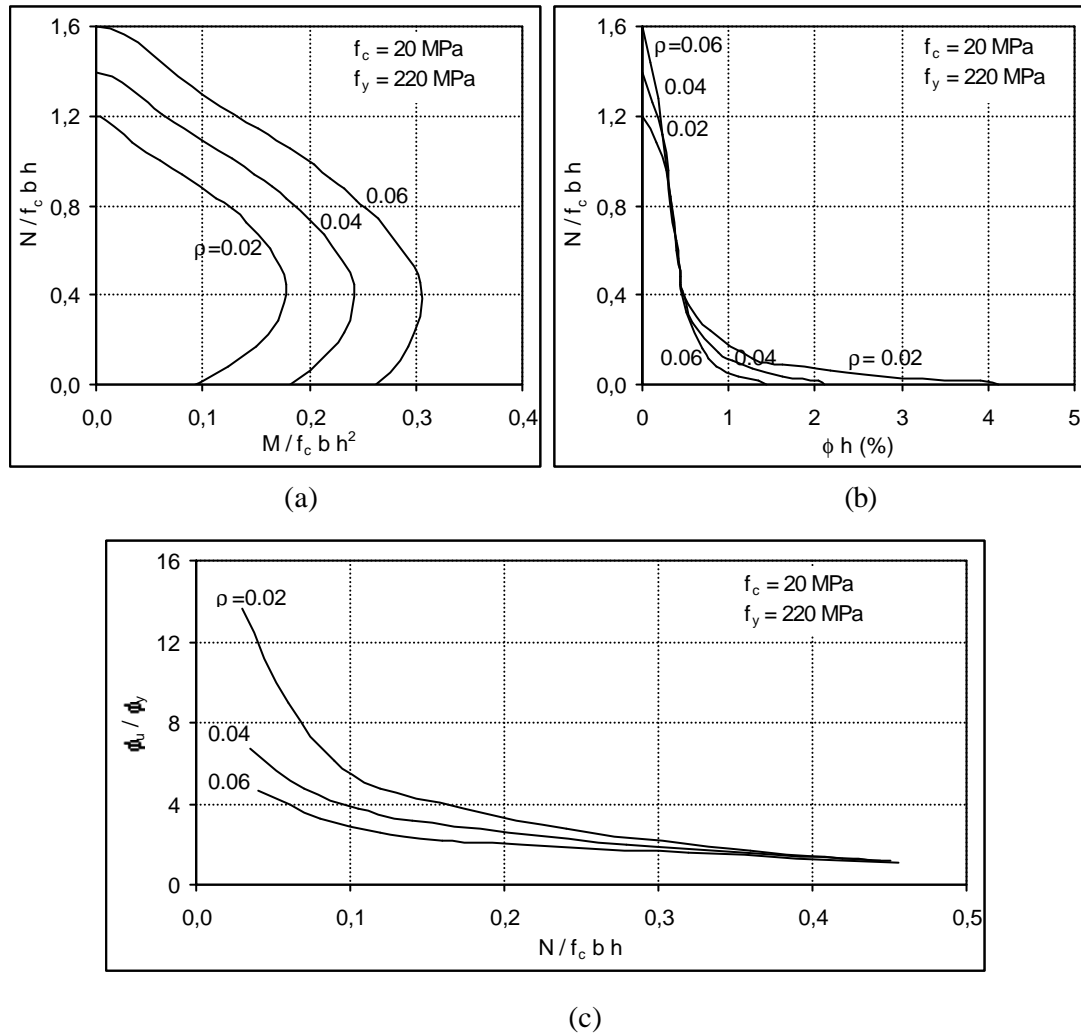


Figure 4.2 Strength and ductility of column sections with different values of reinforcement ratio **a)** Interaction diagrams **b)** Axial load level versus curvature **c)** Curvature ductility versus axial load level

It is possible to plot the combinations of axial load N and moment M which cause the section to reach the ultimate capacity and the curvature f corresponding to those combinations. The effect of both axial load and reinforcement ratio on the relationships between moment and curvature can be shown in Figure 4.2. N - f curve shows the curvature corresponding to the combinations of N and M when useful limit of concrete strain of 0.003 or ultimate condition is reached. The ratios f_u/f_y obtained from the curves given in Figure 4.1, and they are plotted against the axial load levels, $N/f_c A_g$, in Figure 4.2b. For the sake of comparison, the vertical scale

for N is kept the same in the two plots arranged mutually in Figure 4.2a and 4.2b. For a good sense of evaluation, the axial load is plotted in units of $f_c b h$, the moment in units of $f_c b h^2$ and the curvature in units of $1/h$.

Axial load levels corresponding to that of balanced conditions, N_b/N_0 , are 0.370, 0.322 and 0.285 for reinforcement ratios of 0.02, 0.04 and 0.06, respectively. Evidence show that, increasing axial load, the section ductility significantly decreases. This effect is most striking for the sections containing low ratio of longitudinal reinforcement. For example, if the column load is 20 percent of the axial load capacity (N_0), the f_u/f_y value is reduced to about 1.95, 2.60 and 3.25 for 2, 4 and 6 percent of reinforcement ratio, respectively. Curvature ductility ratios are smaller for higher axial load levels.

4.2.2 Effect of Longitudinal Reinforcement Ratio

Effects of reinforcement ratio on ductility can be seen from the curves given in Figures 4.2. General shape of the curves is remarkably influenced by the ratio of reinforcement. The cross section shows negligibly small ductility for load levels above balanced case, while a certain degree of ductility always exists at load levels below balance. Increase of the longitudinal reinforcement ratio results in reduction in ductility. However, strength and stiffness of the section increase as the ratio of reinforcement increases.

A study of Figure 4.2a shows the effects of reinforcement ratio on the interaction relationship. In addition to that the cross section is stiffened and strengthened by the addition of reinforcement, there are several other features. The magnitude of the balanced load level, as defined herein, is independent of the amount of reinforcement. The moment corresponding to the balanced failure is increased considerably by the addition of reinforcement. It is thus apparent that at the balanced load level, addition of equal amounts of reinforcement in tension and compression increases the cross-sectional stiffness but does not affect ductility. Increase in moment is directly proportional to the increase in the ratio of reinforcement. Similarly, increase in the axial load capacity of the cross section is proportional to

the increase in the longitudinal reinforcement ratio. Since the portion of the N - M interaction between the balance load level and the N axis can be satisfactorily approximated by a straight line, it can be said that the increase in moment for all load levels above balance is proportional to the increase in the ratio of reinforcement.

4.2.3 Effect of Concrete Strength

In general, due to lack of good care and supervision significant variations in concrete strength are observed during the construction, and the concrete strength in the structural components is found to be much lower than the strength of the selected concrete grade. Experience gained from earthquakes and observations made on reinforced concrete structures after the destructive earthquakes that occurred in Turkey in the last decade reveal that the great majority of existing reinforced concrete buildings do not have adequate concrete strength. For instance, after the two major earthquakes experienced in 1999, investigations made on 100 reinforced concrete buildings located in Düzce revealed that compressive strength of concrete used ranged from 7 MPa to 15 MPa (Sözen, 2001).

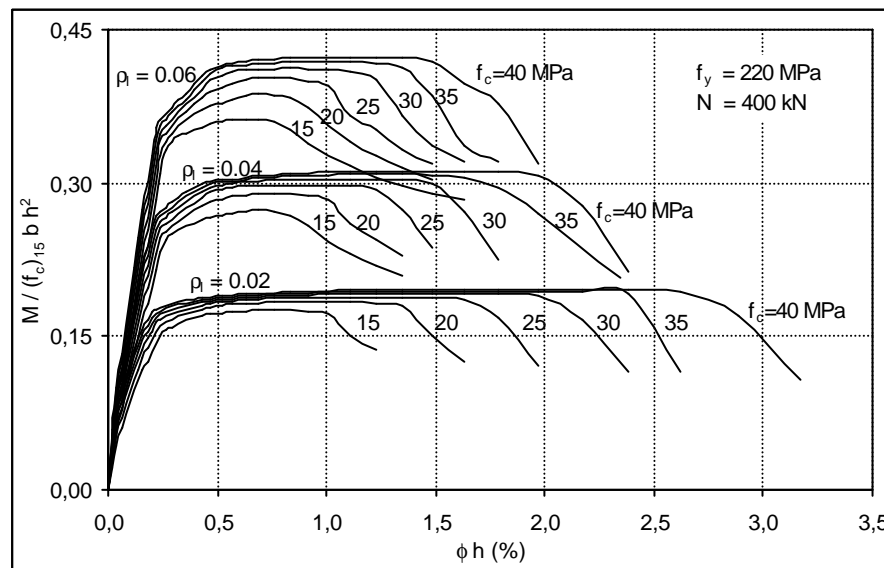


Figure 4.3 Effect of concrete strength and longitudinal reinforcement ratio on moment curvature relationships

In this section, effects of concrete compressive strength on both the lateral strength and deformation capacity and seismic performance and damageability of

reinforced concrete systems will be evaluated via section analyses and inelastic time history and damage analyses. Exemplifying the concrete strength of the existing buildings in Turkey, very low concrete strengths, such as 10MPa and 15MPa, have been taken into consideration.

The moment-curvature curves presented in Figure 4.3 are obtained for a trio of longitudinal reinforcement ratio. The main variable considered in these analyses is the concrete strength ranging from 15 to 40 MPa. The axial load considered in all section analyses is kept constant as 400 kN corresponding to $0.167f_cA_g$, $0.125f_cA_g$, $0.100f_cA_g$, $0.083f_cA_g$, $0.071f_cA_g$ and $0.063f_cA_g$ for sections with concrete strengths of 15MPa, 20MPa, 25MPa, 30MPa, 35MPa and 40MPa, respectively.

Figure 4.3 indicates that concrete strength has substantial effect on section ductility. Cross-sections with lower reinforcement ratio exhibit relatively larger ratio of ductility. By referring to these graphs, it can be stated that concrete strength does not have a substantial effect on the moment capacity of the section. These curves reveal that increase in concrete compressive strength, f_c , result in stiffening and strengthening of the cross section.

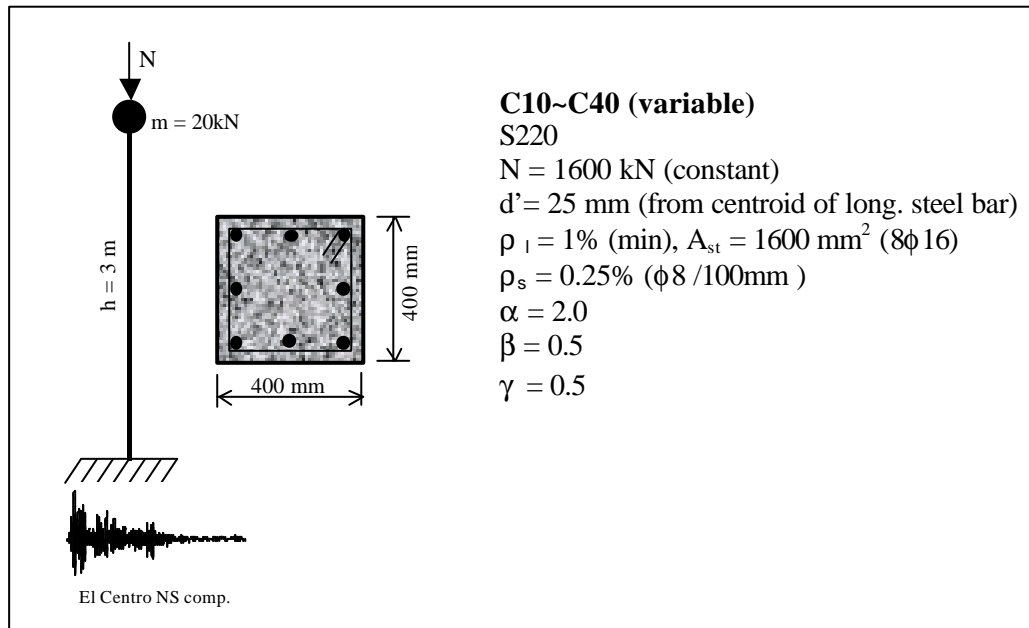


Figure 4.4 Cantilever column model properties

Explicitly, the actual seismic response of a structure can be obtained by non-linear time history analysis. A series of inelastic time history and damage analyses of SDOF systems with concrete strengths ranging from 10MPa to 40MPa have been conducted using El Centro earthquake, NS record. Details and properties of the column model used in the analyses are shown in Figure 4.4. Hysteretic model deterioration (stiffness degradation, strength deterioration and pinching) parameter values considered are 2.0, 0.5 and 0.5, respectively.

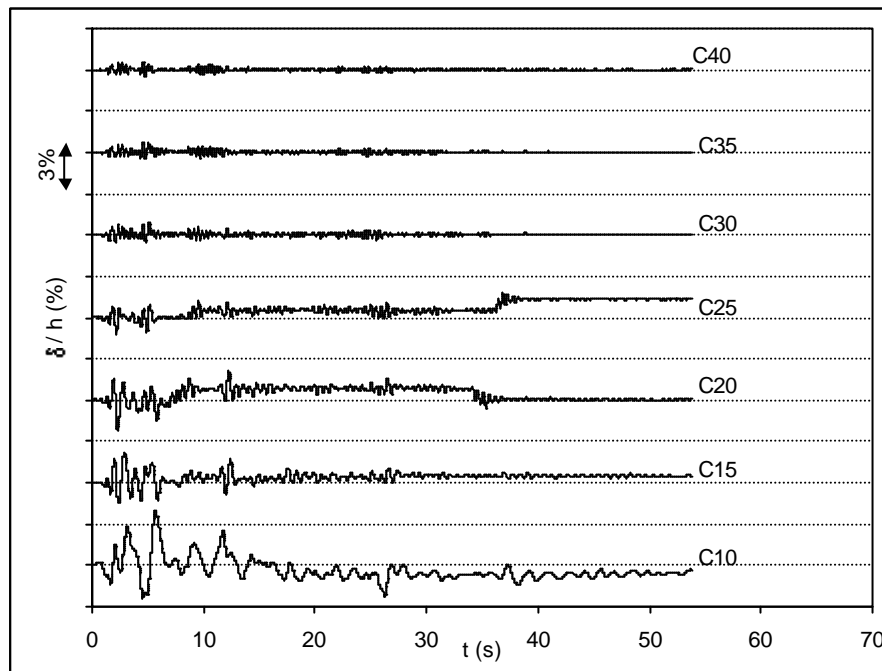


Figure 4.5 Effect of concrete strength on drift ratio histories in time domain,

Table 4.1 Effect of concrete strength on seismic performance and damage

f_c (MPa)	$(d/h)_{max}$ (%)	V_{max} / W (%)	T (s)	E_{hyst} (kNmm)	D_{def} (1)	D_{str} (2)	D_{total} (1+2)
10	4,00	5,08	1,06	4095	0,294	0,188	0,482
15	2,19	19,67	0,59	11540	0,107	0,107	0,215
20	2,18	33,04	0,50	14120	0,107	0,072	0,179
25	1,78	38,35	0,43	10970	0,107	0,046	0,153
30	0,93	41,44	0,39	7046	0,054	0,025	0,079
35	0,76	42,92	0,36	6648	0,042	0,028	0,071
40	0,60	44,81	0,34	5097	0,032	0,014	0,046

Figure 4.5 shows the drift ratio histories in time domain for the SDOF systems with various concrete strengths ranging from 10MPa to 40MPa. The numerical values of their maxima are presented in Table 4.1. Inspection on the drift ratio histories, shown in Figure 4.5, revealed that the concrete strength has substantial effect on the deformation capacity of the structural systems. Increase in the concrete strength decreases the general amplitude of the drift ratio histories in time domain and thus the maximum drift ratio. The system with concrete strength between 10MPa and 25MPa drifted beyond the elastic limit. The maximum drift ratio for the system with 10MPa concrete strength was determined as 4 percent, exceeding the *life safety* limit of 2 percent, specified in ATC 40 (1996). Increasing the concrete strength from 10MPa to 15 MPa, the maximum drift ratio decreases to 2 percent corresponding to the upper limit of *damage control* performance level. Increase in the concrete strength brings about further steady decrease in the maximum drift ratio. However, for the systems with concrete strengths of 30MPa, 35MPa and 40MPa, the values of the maximum drift ratio obtained as 0.93 percent, 0.76 percent and 0.60 percent, respectively. They are less than 1 percent, which is commonly accepted as upper limit for damage in non-structural components only.

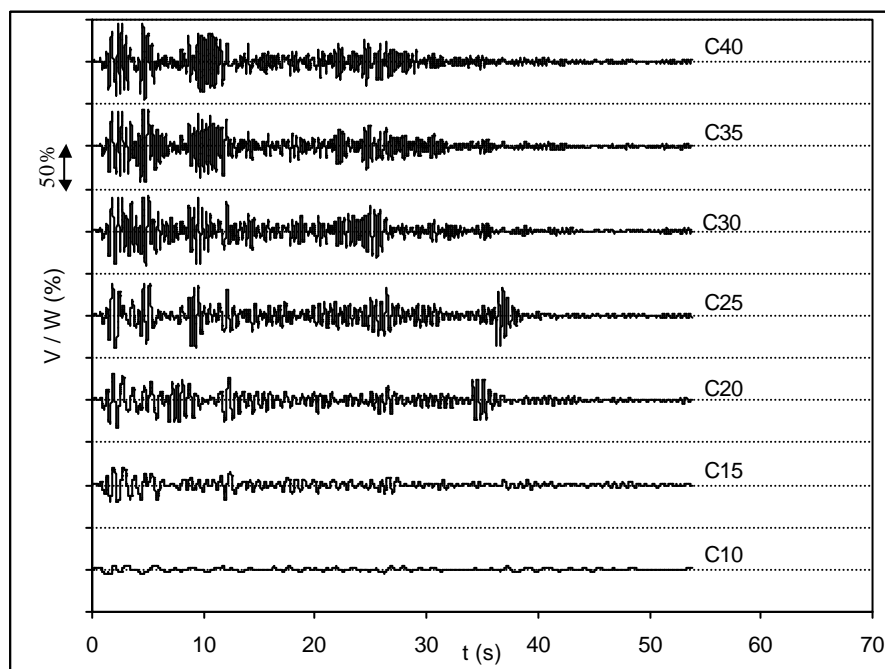


Figure 4.6 Effect of concrete strength on base shear ratio histories in time domain

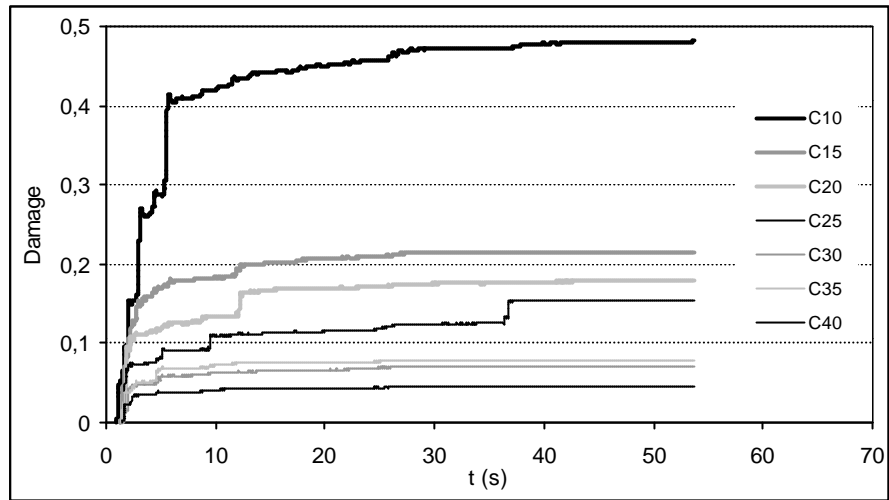
Figure 4.6 shows the base shear ratio variations in time domain for various concrete strengths ranging from 10MPa to 40MPa, the numerical values of their maxima are presented in Table 4.1. As can be seen from the normalized base shear histories and variation of their maxima, increase in the concrete strength leads to increase in the lateral load resistance. Inspection on the variation in maximum base shear ratio given in Table 4.1, reveals that the lateral load capacity of the system influenced significantly in case of concrete strengths between 10MPa and 20MPa. Since this portion of the variation can be satisfactorily approximated by a straight line, it can be stated that increase in the lateral load capacity is proportional to increase in the concrete strength in this interval. Then, there is a steady increase in lateral load capacity with increasing concrete strength.

The numerical values of the accumulated hysteretic energy and period are presented in Table 4.1. The variation of the dissipated hysteretic energy reached the peak for the system with 20MPa concrete strength. Inspection on the base shear histories indicate that the cross section is strengthened by increase in the concrete strength. The strengthening and stiffening of the structural member diminishes the oscillation period of the system as shown in Table 4.1. The data presented provides evidence that the period values determined for low concrete strength, such as 10MPa, is considerably longer than those observed for systems with relatively higher concrete strengths. This phenomenon can be observed from the oscillation traces of drift ratio histories presented in Figure 4.5.

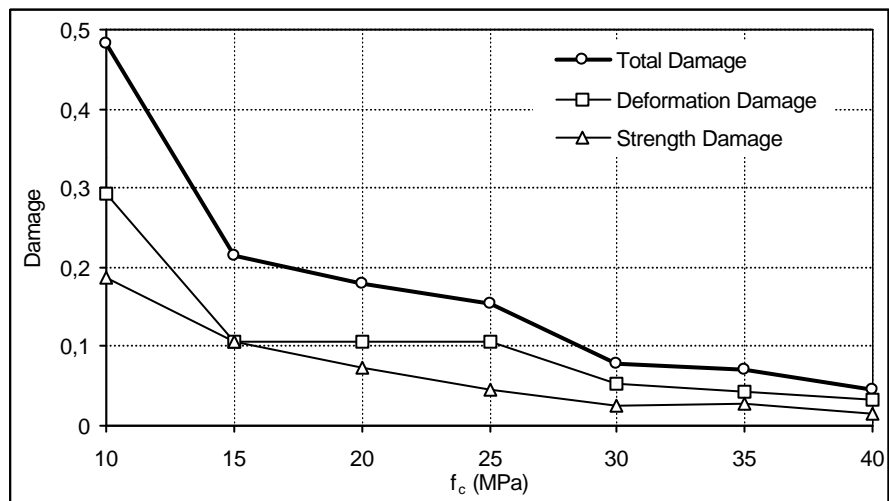
Figure 4.7 indicates the effects of concrete strength on damage. This figure contains damage variation curves in time domain and the total damage (deformation and strength components) attained at the end. Table 4.1 presents the final damage and its deformation and strength parts originating from the deformation and energy terms of the combined type Park and Ang damage model.

A study of Figure 4.7 indicates that the concrete strength has a substantial effect on damage and damageability of structural systems. As seen in Figure 4.7a, sudden impacts of the strong parts of the ground motion cause rapid increases in

damage. The first jump in damage corresponds to the initial strong pulse of the ground motion. Afterwards, there are steady increases in damage.



(a)



(b)

Figure 4.7 Effect of concrete strength on damage; **a)** progressive damage variation curves **b)**total damage and their components

By referring to Figures 4.5, 4.6 and 4.7, it can be definitely stated that the system with low concrete strength seems to undergo relatively more damage, due to excessive drifts and low lateral load capacity. As seen in Figure 4.7 the system with concrete strength of 10MPa was observed to undergo significant damage.

4.2.4 Effect of Cross-Sectional Area of Load Carrying Members

Figure 4.8 shows moment-curvature curves for various sections identical in all respects except for dimensions of the cross sections. The unique variable considered is the cross-sectional area of the sections. The cross-sectional dimensions considered range from 250 mm to 600 mm. The other variables such as axial load, concrete strength and amount and yield strength of the reinforcement have been kept constant. For the sake of a good sense of comparison, bending moment and curvature values are normalized. For this purpose, the curvature plotted in units of $1/h$ and the moment capacity in units of $f_c(bh^2)_{25}$. The normalization process of the bending moment is performed considering the smallest cross-sectional dimension, 250mm.

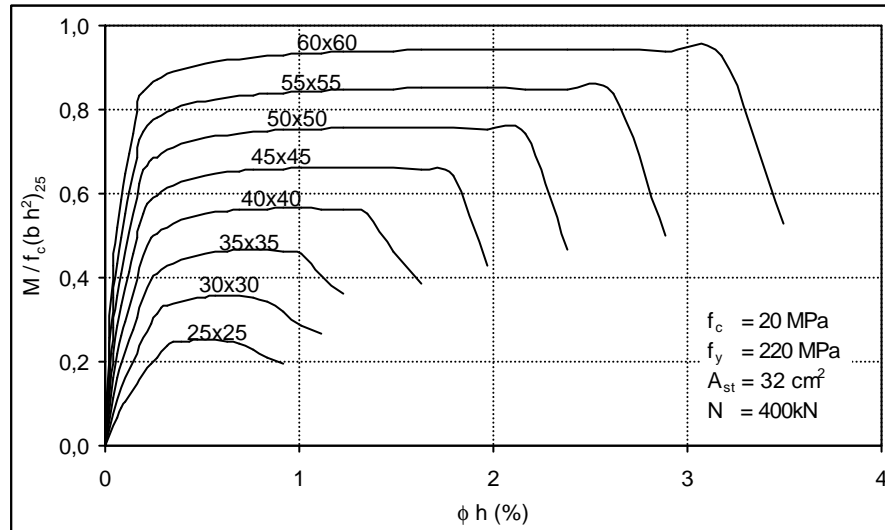


Figure 4.8 Moment curvature relationships for various cross-sectional areas

Since a load carrying structural member resists nearly constant axial force from factored loads on all floors or roof, the axial load has been kept constant in the section analyses performed in this study. Under constant axial load, increase in the cross-sectional area indirectly causes reduction in the axial load level. The resulted axial load levels for the chosen symmetrically reinforced square-cross-sections are $0.320f_cA_g$, $0.222f_cA_g$, $0.163f_cA_g$, $0.125f_cA_g$, $0.099f_cA_g$, $0.080f_cA_g$, $0.066f_cA_g$ and $0.055f_cA_g$ for the cross-sections with dimensions of 250, 300, 350, 400, 450, 500, 550 and 600 mm, respectively.

A comparison of the curves plotted in Figure 4.8 indicates the effects of the cross-sectional area, A_g , on the relationship between moment and curvature. An

increase the cross-sectional area decidedly stiffens and strengthens the section. It can be shown that under a constant axial load, increase in ductility accompanies an increase in cross-sectional area of a load-carrying member.

Investigations made in seismic areas and experience gained from past earthquakes have shown that the average ratio of the *total cross-sectional area of vertical load carrying members to the total floor area* is less than 1 percent in the majority of the reinforced concrete buildings. However, analytical and experimental research conducted by earthquake engineering community indicates that this criterion plays a role in seismic resistance of reinforced concrete members (Sözen, 1981; Gülkan and Sözen, 1999).

Numerical Example: Çeltiksuyu Regional Primary Education School Buildings

In this section of the study, effects of this criterion on the seismic performance and damageability of reinforced concrete structures will be examined using the procedure proposed by Gülkan and Sözen (1999) for the seismic structural vulnerability assessment of reinforced concrete frame buildings.

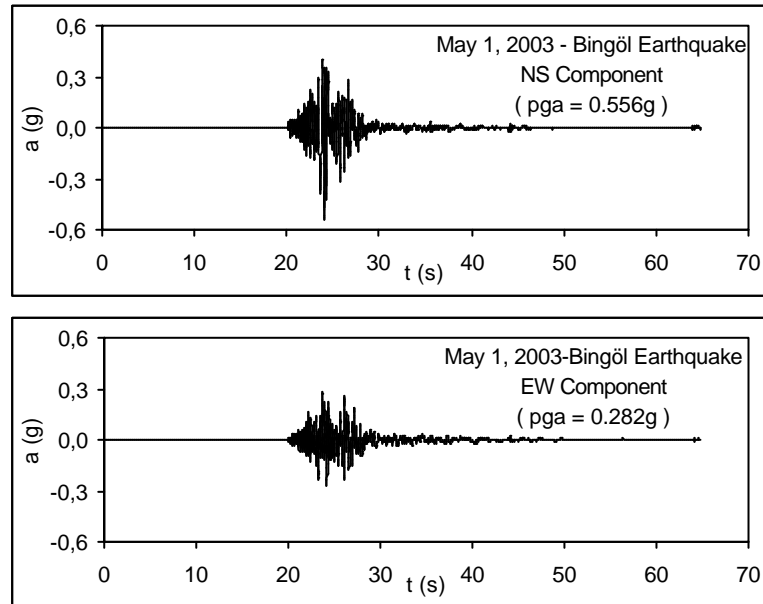


Figure 4.9 The ground acceleration histories of May 1, 2003 Bingöl earthquake, Bingöl Ministry of Public Work and Settlement Office Station records

For this purpose three case study buildings, located at Çeltiksuyu village of Bingöl and subjected to the 1 May 2003 Bingöl earthquake having a magnitude of 6.4, will be evaluated. The primary use has been the Regional Primary Education School. The ground acceleration histories recorded at Bingöl Ministry of Public Work and Settlement Office Station are given in Figure 4.9.

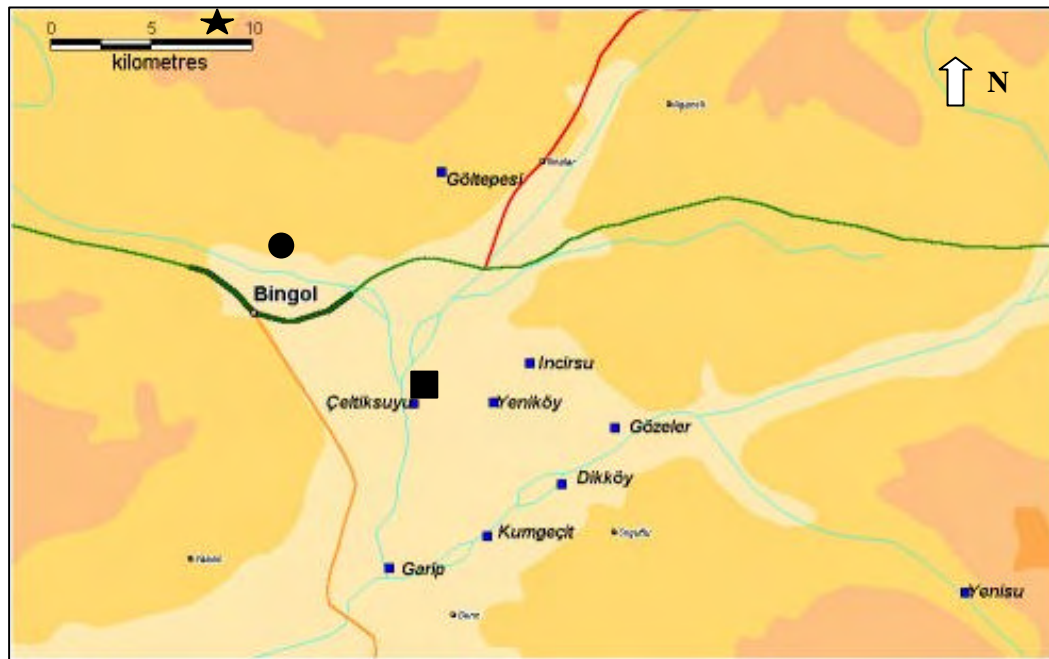


Figure 4.10 Location of the epicenter (star), the strong motion record station (circle) and the investigated buildings (square)

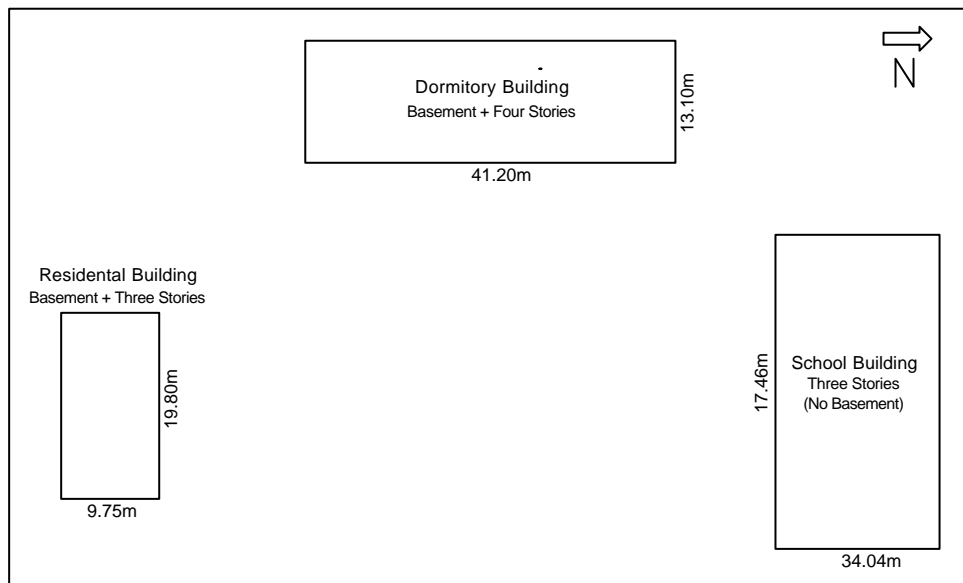


Figure 4.11 Key plan showing locations of buildings

Locations of the epicenter, the strong motion record station and the investigated buildings are marked on a map presented in Figure 4.10. Figure 4.11 shows the site plan showing locations of the buildings. General properties, engineering drawings and damage state pictures of the Çeltiksuyu Regional Primary Education School buildings can be inspected in Appendix B. Three dimensional views of these buildings and engineering showing ground stories giving column, beam and slab dimensions are presented in Figures B.1 to B.5. Finally to give an opinion about the damaged state of the buildings, the photos of the buildings taken right after the earthquake are put together in Figure B.6.

The Çeltiksuyu Regional Primary Education School complex was comprised of three reinforced concrete buildings: five-story *dormitory building* which had basement story of 4.05 meters height, three-story *school building* without basement story and four-story *residential building* with basement. They have plan areas of 540, 594 and 193 square meters, respectively. There was a shelter at the basement of the residential building surrounded by 60 cm thick shear walls. The stories above ground had a total cross-sectional area of 0.95 m^2 shear walls. On the other hand, the load carrying system of the five-story *dormitory building* and three-story *school building* comprised slender column elements and they did not contain any shear wall components as seen from the scaled engineering drawings given in Appendix B.

The three buildings were located in Çeltiksuyu village on top of an alluvial deposit, approximately 10 km away from the strong motion record station and Bingöl city, and 25 km away from the epicenter of the earthquake, as shown in Figure 4.10. These buildings were designed and constructed during 1995 to 2000. The same builder built all buildings. Field surveys made in construction site and examinations on the design documents of these buildings after the earthquake have shown that, in all three buildings there were almost the same deficiencies, construction mistakes, inadequate detailing and proportioning. In other words they came from the same spectrum workmanship quality, materials and designs. Lack of longitudinal and transverse reinforcements was one of the major deficiencies. There were differences in the amount of reinforcement of the as-built and the required according to design project. It was observed that the deficiency in the longitudinal reinforcement

exceeded 70 percent of the required amount of reinforcement in the ground floor column members. It is estimated that, the other reason of the observed failures was the poor quality of concrete. There was only one ready-mixed concrete plant in the vicinity. The contractor produced concrete by using the un-washed material from the Murat River as aggregate for all three buildings to minimize cost.

Of particular interest were the damage state levels of the three buildings. Although the residential building did not suffer any structural damage, brittle failure of the other two buildings' columns resulted in their total collapse during the earthquake. As a result of the story mechanisms that occurred, the children's five-story *dormitory building* failed killing more eighty students. The three-story *school building* also collapsed due to the story mechanism at the ground story. However, it is highly attractive that four-story *residential building* did not suffer any structural damage.

Table 4.2 Comparison of the sum of the cross-sectional areas of vertical load carrying members to the floor area in both directions of the buildings

Building	ΣA_c (m ²) [1]	ΣA_w (m ²) [2]	n [3]	A_p (m ²) [4]	ΣA_p nx A_p (m ²) [5]	ρ_c (%) [1/5]	ρ_w (%) [2/5]	Comments
Dormitory	12.216	10.112 (12.930)	4 (+1)	540	2160	0.566	0.468 (0.599)	Not safe
School	6.450	12.373 (14.150)	3	594	1782	0.362	0.694 (0.794)	Not safe
Residential	7.910	2.849 (2.608)	3 (+1)	193	579	1.366	0.492 (0.450)	Safe

ΣA_c : the sum of the column areas at the base of a building

ΣA_w : the sum of the column areas at the base of a building

(the values in parentheses are for transverse direction of the buildings)

n : number of stories above the base

A_p : floor area of one story

ΣA_p : the sum of the floor area above the base

ρ_c : column ratio

ρ_w : wall ratio (the values in parentheses are for transverse direction of the buildings)

For principal directions of the three buildings, the values of *the ratio of the sum of the column areas at the base to the floor area above the base and the ratio of the sum of the wall areas at the base of a building to the floor area above the base* are calculated using the aforementioned method and tabulated in Table 4.2.

The damage data gathered from the architectural and engineering drawings of the longitudinal and transverse directions of three buildings are presented in Figure 4.12. As seen in this figure, in all buildings *the ratio of the sum of the wall areas at the base of a building to the floor area above the base* is considerably small and it is about 0.5 percent. In this figure the solid symbols are for longitudinal direction of the buildings while the hollow symbols are given for transverse direction of the buildings.

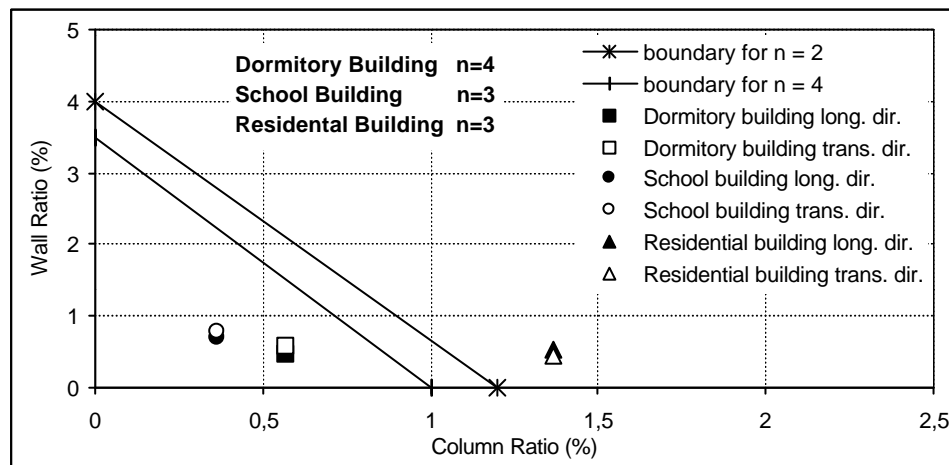


Figure 4.12 Damage data for the principal directions of three buildings

Gülkan and Sözen (1999) state that if the two indexes (the column and wall ratios) define a point inside a triangular region, drawn considering the effect of number of stories, a particular building is judged to have heavy damage. The seismic vulnerability of the three buildings had quite different levels of damage as assessed using this procedure. As a result, it was established that for principal directions of both school building of three story and dormitory building of four stories above ground the column and wall ratio indexes, ρ_c and ρ_w display (circle and square) points inside the triangles, means they are judged to be candidates for heavy damage. For

the principal directions the residential building which did not sustain any structural damage, as shown in Figure B.6, these indexes define points outside the triangles (Figure 4.12).

The data presented put to evidence that *the ratio of the sum of the column areas at the base of a building to the sum of the floor area above the base* has a substantial impact on the seismic performance and damageability of reinforced concrete structures. Consequently the accuracy of the seismic vulnerability assessment procedure, proposed by Güllkan and Sözen (1999) and based on limitation of maximum drift ratio, has been validated via evaluation of three buildings data.

All infill walls contribute to framing systems in resisting the lateral force induced by earthquake forces in some degree. It is obvious that infill walls without openings are much more efficient in carrying lateral loads. In general these walls have windows or doors, openings, decreasing their efficiency considerably. Additionally, especially in framing systems the amount of the efficient infill walls is not enough to take into consideration in resistance of the earthquake induced lateral forces. As mentioned earlier, for the buildings examined in this study *the ratio of the sum of the wall areas at the base of a building to the floor area above the base* is around 0.5 percent. By referring to Figure 4.12, it is recommended that, without taking into account the contribution of the infill walls to framing system in the resistance of the seismic lateral load, *the ratio of the sum of the column areas at the base of a building to the sum of the floor area above the base* should be taken at least 1.0 percent in low-rise buildings. The walls will then provide additional protection.

4.3 Concluding Remarks

Seismic structural damage and energy dissipation capacity of reinforced concrete members depend on structural properties such as the axial load level, concrete strength, cross-sectional area, amount of longitudinal and transverse reinforcements.

Reinforced concrete members subject to both axial load and flexure do not have the ability to dissipate hysteretic energy as much as members subjected to only flexure. However, large deformations could not be attained safely because of the lack of ductility causes brittle failures. It is depicted that when the design axial load is 1/6~1/8 of the axial load capacity, the member action is greatly improved. Actually, the revision of the building and seismic codes should be based on firm bases of the effective parameters resulting from evidences of both extensive experimental and analytical researches and observations on the structural behavior after actual earthquakes. But, site observations after major earthquakes have shown that the great majority of buildings do not have adequate concrete strength, confinement, etc., and could not possess adequate ductility. Inadequate concrete strength indirectly causes to increase in the axial load level. Commonly observed damages have shown that the plastic hinges formed at the ends of the columns result in brittle failure at even moderate levels of axial compression load. It should be emphasized that structural member design closing to the limits of the code provisions is a poor tradition in Turkey. Therefore, in order to make the deficiencies commonly observed in reinforced concrete buildings ineffective, the limitation related to axial load level specified in the national building and earthquake codes, TS 500 (2000) and TEC (1998), should be revised in such that the limits specified in these codes should be reduced to one-fourth or one-fifth of the limits in force (Acar and Gülkan, 2004).

Concrete strength has a substantial effect on damage and damageability of structural systems. Specimens with relatively high concrete strength exhibited considerably larger energy dissipation capacity with lower deterioration of parameters. The higher the concrete strength the larger was the amount of hysteretic energy dissipated before failure. The system with low concrete strength seems to undergo relatively more damage, due to excessive drifts and low lateral load capacity. According to Turkish Earthquake Code (1998), the concrete strength less than 16MPa should not be used in all buildings to be built in seismic zones. Additionally, in the first and second seismic zones it is mandatory to use 20MPa or higher strength concrete in (i) the buildings with structural systems comprised only of frames of *high ductility level*, and (ii) all buildings with Building Importance Factor of $I=1.5$ and $I=1.4$, without considering the structural system. The system

with 15 MPa or lower concrete strength is a candidate to undergo significant damage. Due to lack of good care and supervision significant variations in concrete strength are observed during the construction, and the concrete strength in the structural components is found to be much lower than the strength of the selected concrete grade. Observations made after past earthquakes have shown that in the majority of existing concrete construction in Turkey and in many other countries do not have adequate concrete strength and could not possess adequate ductility. If there is a doubt in providing the required sufficient concrete strength, the cross-sectional dimensions should be kept larger deliberately.

It is revealed that *the ratio of the sum of the column areas at the base of a building to the sum of the floor area above the base* has a substantial impact on the seismic performance and damage of reinforced concrete structures. It is recommended that without taking into account the contribution of the infill walls to framing system in the resistance of the seismic lateral load, *the ratio of the sum of the column areas at the base of a building to the sum of the floor area above the base* should be taken at least 1.0 percent in low-rise buildings. The walls will then provide additional protection.

CHAPTER 5

PRIOR AND SUCCESSIVE EARTHQUAKES DAMAGE

5.1 General

Damage accumulated during severe, long duration ground motions associated with a major earthquake as well as during several severe earthquake sequences that may occur during the service life of a reinforced concrete structure. Field surveys and observations made on reinforced concrete structures following recent major successive earthquakes in Turkey indicate that successive earthquakes can substantially increase structural damage. It is not unusual for this accumulation of damage to lead to collapse during the later events. But how can the damage from these events be predicted and what intensity of these excitations may cause to noteworthy progress in the major (or design) earthquake damage? What is the contribution of the aftershocks to structural damage caused by the main shocks, and does the damage stemming from the aftershocks lead to collapse or not? The prior earthquake or foreshock of what intensity may affect substantially the damage to be sustained during the major earthquake ground motions is another question. Since cumulative damage resulted from such seismic events may exceed that predicted using ground motion records commonly employed in seismic response analyses, more stringent design criteria may be necessitated where long duration and successive motions can occur.

It can be estimated that, the loading history may play vital role in the assessment of seismic performance and damage. Researchers have investigated the issue of cyclic loading histories to be used in the tests of structural components (Krawinkler, 1996), and the following questions have been raised;

- How many cycles, what deformation amplitudes, and what sequence of cycles should be employed to evaluate seismic performance?
- How can the results of one experiment under a predetermined loading history be generalized so that conclusions can be drawn on the response of the same component under different loading histories?

One of the primary purposes of this study is to investigate effects of loading history on structural damage and total energy dissipation capacity of reinforced concrete members. This purpose has been accomplished through the use of (i) inelastic displacement reversals of various constant amplitudes, (ii) variable amplitude inelastic displacement reversals with increasing and decreasing order in the inelastic time history and damage analyses of SDOF systems. In these analyses, the test model of a typical beam specimen tested by Erberik will be subjected to the same total displacement histories in which the sequence of the applied displacement altered without introducing additional cycles or altering amplitudes. For all loading patterns the force-displacement relationships and damage progression curves have been obtained.

Explicitly, the actual response of structural systems can be obtained by inelastic time history analysis. Hence, to assess the effects of load paths on damage of structural systems subjected to successive earthquakes, an inelastic time history and damage analyses of SDOF systems will be carried out using a total of four real earthquake records. Each synthetic ground motions comprises one of the ground motion acceleration records and preceded or followed by its various times amplitude-compressed record acting as a foreshock and aftershock. The sequence of the records constituting the path will be altered so as to force the structural system to follow a different loading history. These analyses will be performed using a cantilever column specimen tested by Pujol (2002). For all loading histories the damage progression curves will be presented.

In these analyses, the test model of a typical beam specimen, tested by Erberik under displacement patterns of constant amplitudes, has been used. The

models are designated using two letters and several numerals: the letter ‘CH’ or ‘VH’ is the abbreviation of the imposed loading histories of ‘Constant amplitude’ or ‘Variable amplitude’. The numerals 1, 2 and 3 indicate the cycles of 10mm, 20mm and 30mm amplitudes, respectively. The beam specimens suffered severe damages during the tests (Erberik and Sucuođlu, 2004). Therefore, the stiffness degradation, strength deterioration and pinching parameter values considered are 7.0, 0.7 and 5.0, respectively.

5.2 Constant Amplitude Loading

The main variable in the quasistatic analyses was the amplitude of the displacement reversals. Each loading pattern contained three subsequent cycles with 10mm, 20mm and 30mm amplitudes. These models were labelled as CH-111, CH-222 and CH-333. For each constant amplitude, corresponding damages (deformation, strength components), and final energy dissipation capacity are obtained. The deformation damage is comprised of the first term, whereas the strength damage stems from the energy term of the damage model. These are tabulated in Table 5.1. The loading histories, hysteretic relationships and progression of the total damage are plotted in Figure 5.1.

Table 5.1 Damage variation and dissipated energy for VH-111, VH-222 and VH-333

Loading Pattern	Damage Index			E_{hyst} (kNmm)
	D_{def}	D_{str}	D_{total}	
VH-111	0.181	0.195	0.376	372
VH-222	0.363	0.367	0.730	701
VH-333	0.544	0.502	1.046	959

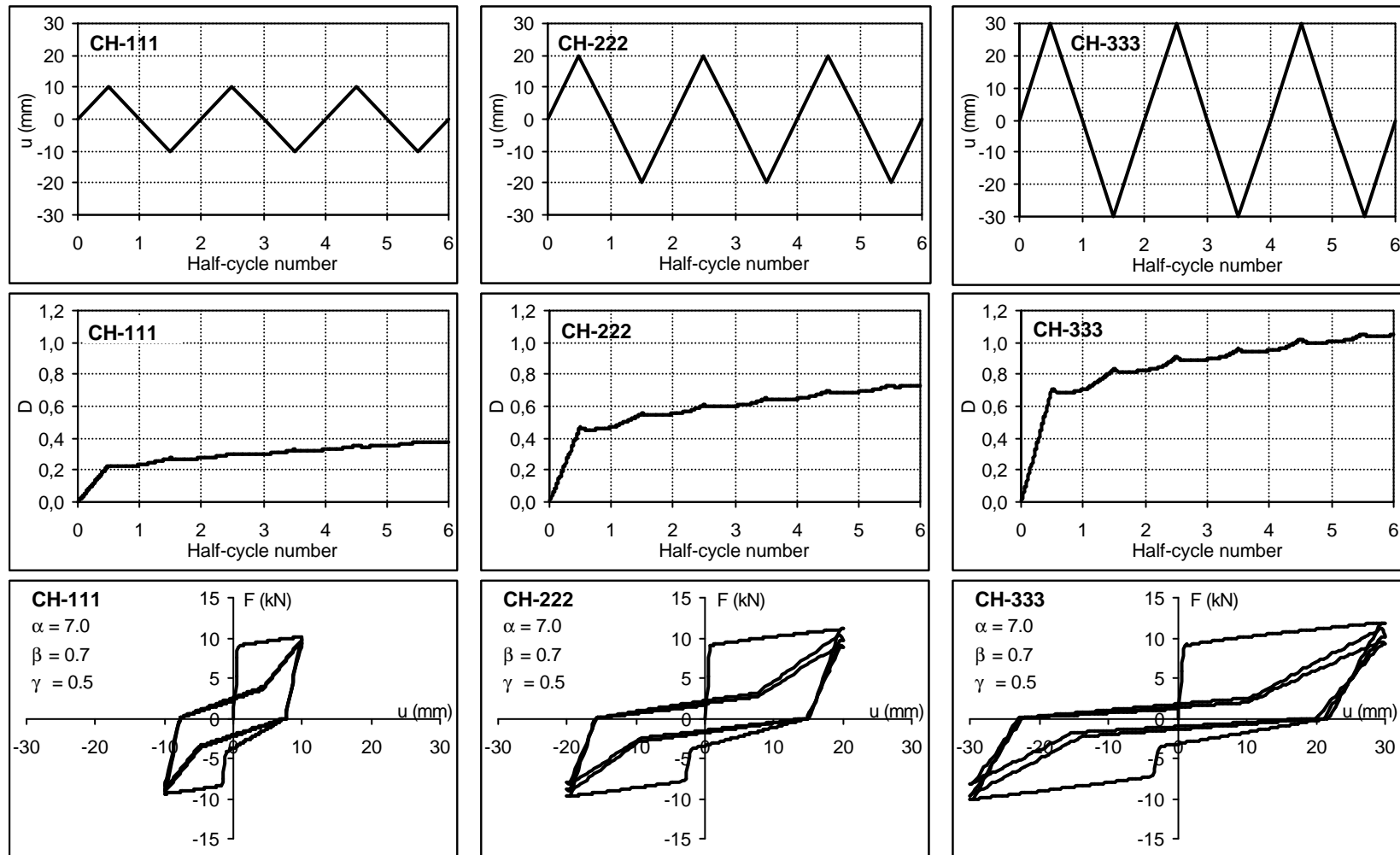


Figure 5.1 Constant amplitude loading histories, damage progression curves and force-displacement relationships

Figure 5.1 shows that, the total damage increases linearly in the ascending portion of the first half-cycle. The damage that occurred in this stage, regardless of the amplitude of the imposed loading patterns, constitutes the major part of the total damages. Later, the structural damage progression seems to be in an almost linear path and relatively very low rate. Comparison of the the calculated damage values at the end of the analyses, given in both the table and the figure, indicates that the total damage is increased in proportion to increase in the cycle amplitudes. However, there is no similar variation between the cycle-amplitude and dissipated hysteretic energy. Increase in the amplitude of the cycles caused relatively smaller amount of dissipated energy. For example 100 percent and 200 percent increase in the amplitude result in 88 percent and 158 percent increase in the energy dissipated.

In the preceding discussion it is established that different structural damage levels are attained under effects of constant amplitude cycles of different ductility levels. But how many cycles and what deformation amplitudes should be employed to evaluate seismic performance and to predict damageability of the structural systems? To accomplish this purpose the quasistatic analyses of the structural model of a beam test specimen, ($N=0.0$, $\alpha=7.0$, $\beta=0.7$ and $\gamma=0.5$) subjected to constant amplitude displacement cycles with different ductility ratios of $\mu=3, 4, 5, 6, 8$ and 10 , have been performed. In accordance with the damage classification of the model, the damage index value of 0.25 corresponds to the upper limit of the light damage level as well as the lower limit of moderate damage level. Similarly, the damage level of 0.45 corresponds to the upper limit and lower limit of the moderate and severe damage levels, respectively. A damage level of 1.0 represents the totally or partially collapse of a structural system. Therefore, the damage level to be attained for all ductilities was decided as 1.0 , while the upper limits of the light and moderate damage levels are 0.25 and 0.4 , respectively. However, three concrete grades are taken into account to evaluate whether the concrete compressive strength influences the number of cycles to failure. The number of cycles to failure, estimated to occur at the target damage index equal to unity, are obtained for each ductility. These are tabulated in Table 5.2.

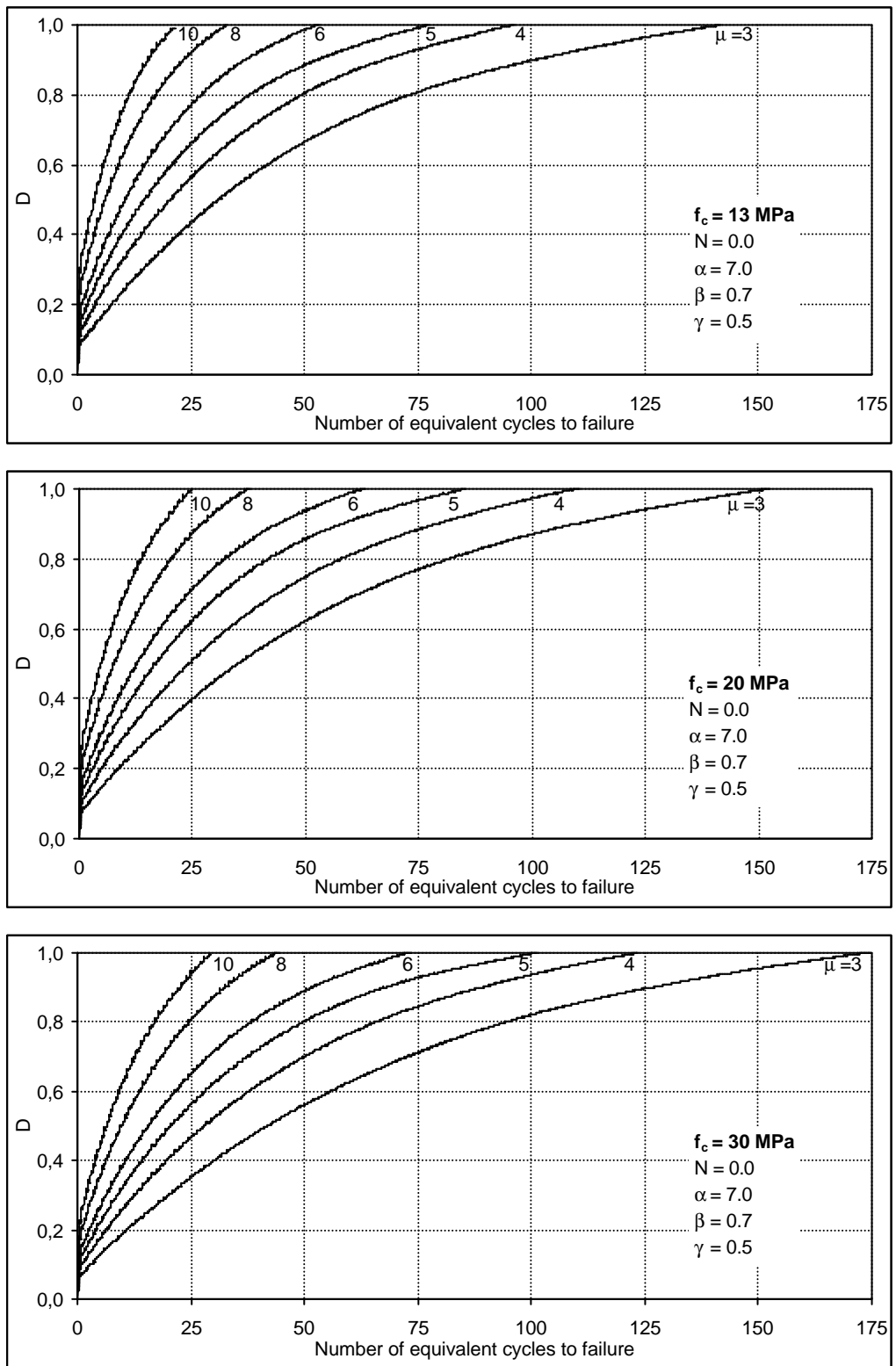


Figure 5.2 Damage progression curves for constant amplitude displacement cycles of various ductilities and concrete grades

Table 5.2 Ductility and equivalent number of cycles to failure (N_{eq}) for various concrete strength

Ductility	$f_c = 13 \text{ MPa}$	$f_c = 20 \text{ MPa}$	$f_c = 30 \text{ MPa}$
3	141	152	174
4	96	110	123
5	77	85	101
6	53	63	73
8	33	37	44
10	21	25	29

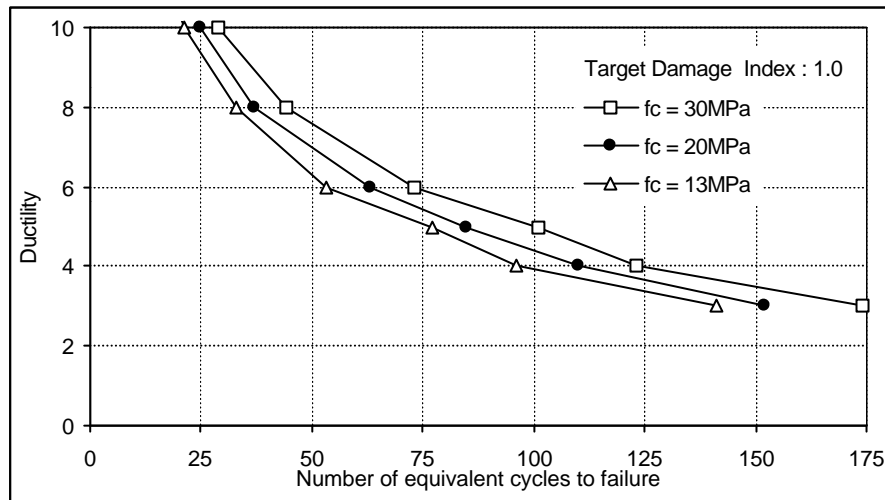


Figure 5.3 Failure lines under constant amplitude displacement reversals

Figure 5.2 shows the variation of damage with increasing number of cycles at each constant amplitude displacement history. The number of cycles at the topmost points of the curves, corresponding to damage value of 1.0, is the cycle number at failure, N_{eq} . In this figure total damage eventually increases parabolically with increasing displacement amplitude, thus the total damage is dependent on the ductility level. In this respect, for reinforced concrete members the damage rule developed by Miner (1945) fails, because it assumes that the accumulation of damage is linear and independent of load path. Figure 5.3 presented the failure lines for the considered three concrete grades. A comparison of the damage variation and ductility vs. N_{eq} curves presented in Figures 5.2 and 5.3 indicate that the number of cycles to failure affected by variation in concrete strength. By use of higher strength concrete, for the same ductility level, a relatively greater number of cycles to failure, N_{eq} , is achieved as indicated in these figures.

5.3 Variable Amplitude Loading

Seismic loads induce several inelastic displacement reversals at relatively large ductility levels combined with many smaller cycles. So the fatigue behavior of the structural components should be assessed under variable-amplitude loading histories, that may differ from the monotonous constant-amplitude loading. In this section, the nonlinear quasi-static and damage analyses of the same beam specimen have been performed to evaluate whether the load path has an effect on the resultant energy dissipation capacity and total damage.

The loading histories considered in these analyses contain variably sequenced cycles of the same number and amplitude. The loading paths are consisting of two and three cycles sequenced in increasing, decreasing or mixed order.

To simulate the actual seismic behavior imposed by successive ground motions, the quasi-static analyses have been performed using the generated SDOF displacement response of the El Centro 1940 record including of its smaller-scale amplitude history as the pre and post-events.

5.3.1 Displacement Path Consisting of Two Cycles

Two inverse order of variable amplitude two-cycle-displacement-patterns are used in the quasistatic analyses of this section. The main variable is the ordering of cycles along the displacement path. The loading histories imposed on specimen models are exactly the same except for the sequence of loading. The displacement amplitude of the cycles is 10mm and 20mm. The models labeled in accordance with the order of cycles: VH-12 and VH-21.

Figure 5.4 shows these loading patterns and corresponding damage curves and force-displacement relationships. The numerical damage (deformation and strength components) values and hysteretic energy dissipated in the end are presented in Table 5.3.

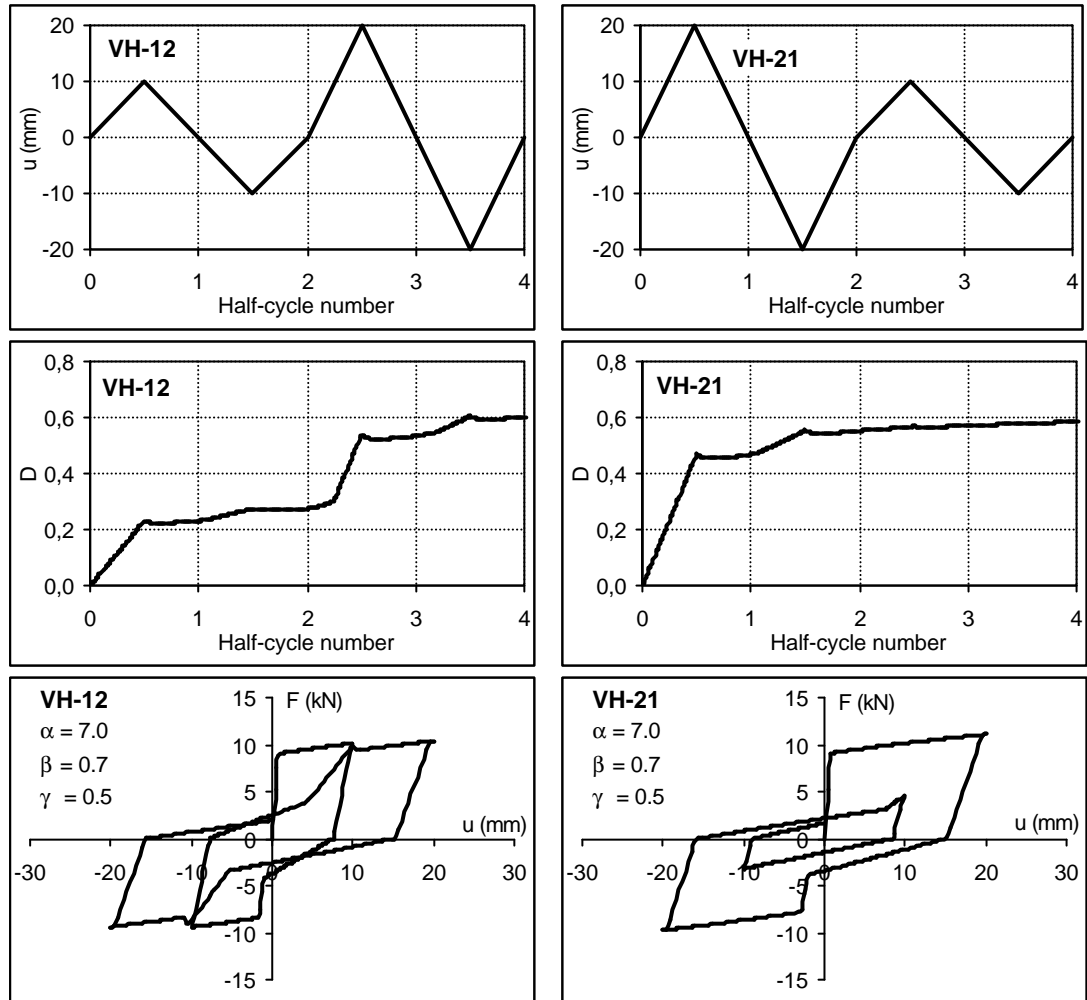


Figure 5.4 Variable amplitude loading histories, damage progression curves and force-displacement relationships

Table 5.3 Damage variation and dissipated energy for VH-12 and VH-21

Loading Pattern	Damage Index			E_{hyst} (kNmm)
	D_{def}	D_{str}	D_{total}	
VH-12	0.363	0.239	0.602	457
VH-21	0.363	0.222	0.585	425

Figure 5.4 and Table 5.3 show that, energy dissipation and total damage are almost equal at the end of displacement patterns in spite of opposite ordering of cyclic amplitudes. This shows that cumulative energy dissipation and total damage are relatively independent from the order of amplitudes along displacement paths consisting of the same number and amplitude of cycles.

5.3.2 Displacement Path Consisting of Three Cycles

The quasistatic analyses of the same system have been performed under the effects of the three-cycle displacement paths. The cycles of the histories are in increasing order, decreasing order or mixed order. All displacement histories are the same with exception of cycle orders. The displacement amplitude of the cycles is 10mm, 20mm and 30mm. The models labeled in accordance with order of cycles as VH-123, VH-132 and VH-321 for which the numerals referring to the size of the cycle amplitudes.

The loading histories and corresponding damage curves and force-displacement relationships are presented in Figure 5.5. For each loading case, the numerical damage (deformation and strength components) values and hysteretic energy dissipated in the end are tabulated in Table 5.4.

Table 5.4 Damage variation and dissipated energy for VH-123, VH-132 and VH-321

Loading Pattern	Damage Index			E_{hyst} (kNmm)
	D_{def}	D_{str}	D_{total}	
VH-123	0.544	0.403	0.947	770
VH-132	0.544	0.381	0.925	727
VH-321	0.544	0.365	0.909	697

The comparison of the damage curves shown Figure 5.5 and the numerical values given in Table 5.4 indicate that, despite variably ordering of the cycles in the histories, the discrepancies revealed between the energy dissipation and total damage level achieved at the end of the analyses are negligibly small. The analytical evidence indicates the independency of the cumulative energy dissipation and total damage from the order of amplitudes along displacement paths consisting of the same number and amplitude of cycles.

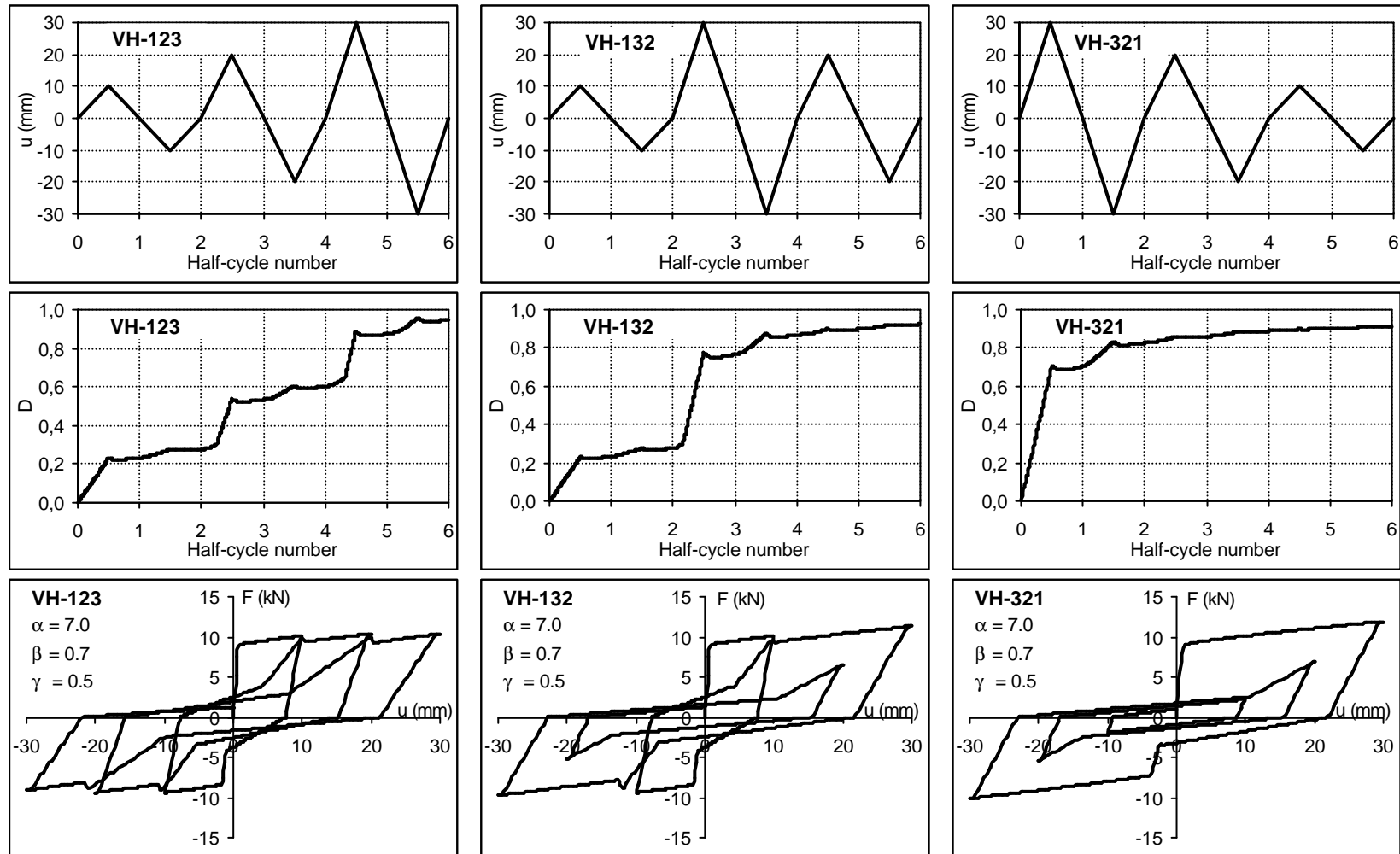


Figure 5.5 Variable amplitude loading histories, damage progression curves and force-displacement relationships

5.3.3 Variable Amplitude Cyclic Loading Generated from Earthquake Response

Structures are subjected to variable-amplitude cyclic loading, and the response varied from cycle to cycle throughout the earthquake. The fatigue behavior of the structural components should be assessed under variable-amplitude loading histories, that may be differ from the monotonous constant-amplitude loading. To imitate the actual seismic behavior of the structural components imposed by successive ground motions, the quasi-static analyses of the specimen are performed under the simulated displacement response of ground motions with the foreshock (or prior earthquake) and aftershock (or successive earthquake).

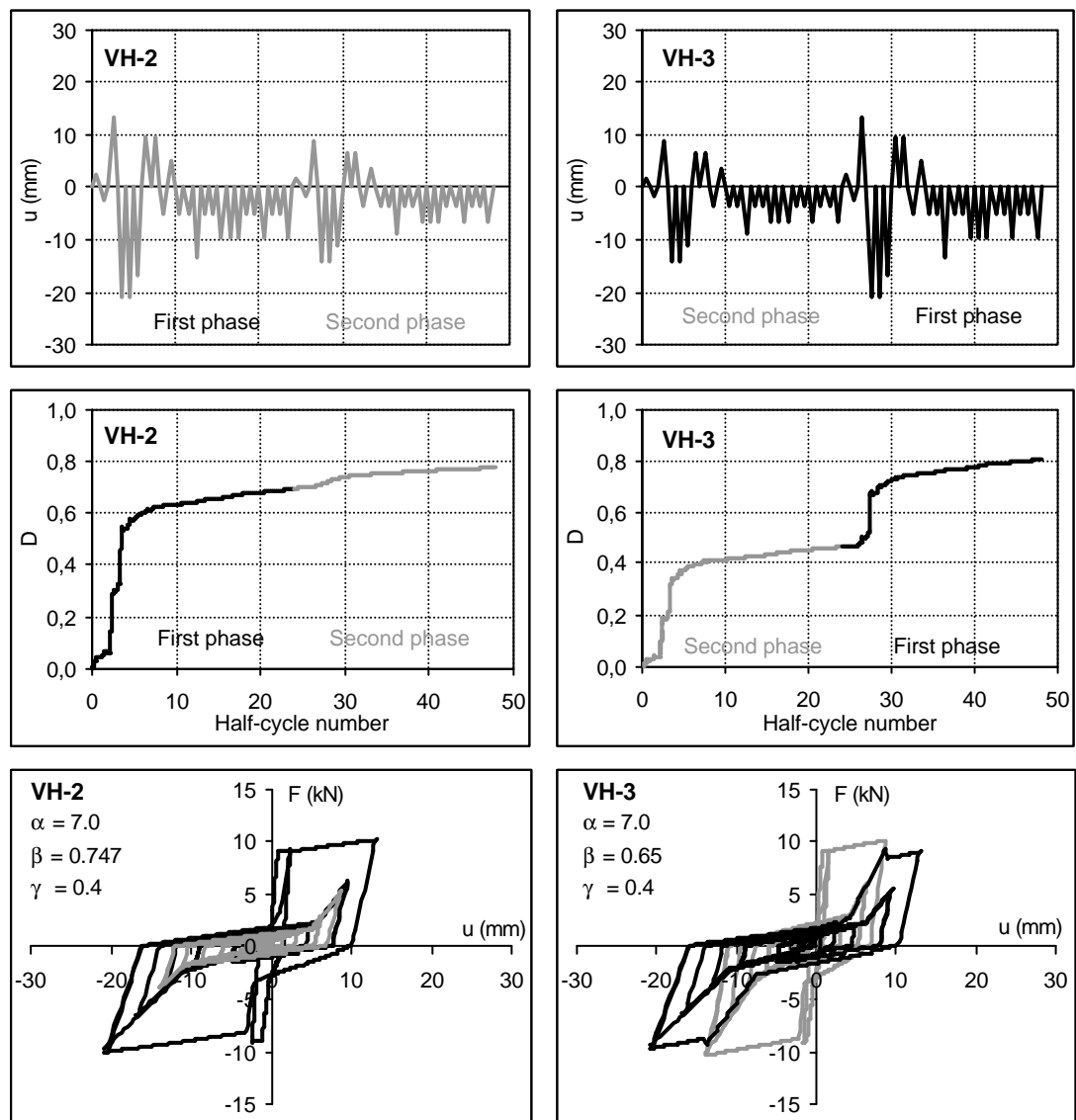


Figure 5.6 Force-displacement relationships, imposed loading histories and damage curves of the specimens VH-2 and VH-3

Table 5.5 Total damage and total damage values for the specimens VH-2 and VH-3

Loading Pattern	Damage Index							E_{hyst} (kNmm)
	$(D_T)_{def}$ (1)	$(D_T)_{str}$ (2)	D_1 (3)	D_2 (4)	D_T (1+2) or (3+4)	D_2 / D_1 (%)	D_2 / D_T (%)	
VH-2	0.372	0.405	0.696	0.081	0.777	11.6	10.4	750
VH-3	0.372	0.437	0.344	0.465	0.809	74.0	57.5	929

Two specimens (VH-2 and VH-3) were subjected to variable-amplitude displacement histories, which were generated from the displacement responses of nonlinear, stiffness degrading SDOF systems under recorded ground motions. VH-2 and VH-3 loading patterns were obtained from the SDOF displacement response to 12 November 1999 Düzce earthquake, Bolu-L component (Erberik, 2001). Figure 5.6 shows the variation in displacement given by dark trace and labeled as ‘first phase’. In the displacement histories, the gray part labeled as ‘second phase’, was obtained by scaling the strong part of the displacement amplitude by two-thirds. The gray part is considered to act as a foreshock and aftershock to the original response to determine the path dependency of both damage progression and cumulative hysteretic energy dissipation. It is estimated that considering two inversely ordered displacement reversals, similar to the histories shown in Figure 5.6, is a reasonable way for assessment of the path dependency of the damage progression and cumulative energy dissipation response.

The imposed loading histories and analytical damage curves and force-displacement relationships of the specimen models are shown in Figure 5.6. The gray colored parts shown in these curves correspond to the foreshock and aftershock, which constitutes the ‘second phase’ of the loading path. Table 5.5 presents the numerical values of the dissipated hysteretic energy and sustained damage level and their components. The second and third columns show the numerical values of deformation, $(D_T)_{def}$, and strength, $(D_T)_{str}$, components of the total damage level. The damage levels attained at the end of each phase alone for the both composite displacement histories, VH-2 and VH-3, are presented in the fourth and fifth columns of the table, respectively. The following columns of the table contain the

proportional values reflecting the effect of the second phase damage to the first phase damage and total damage. In the last column of the table, the cumulative hysteretic energy dissipation values attained in the end of the two inversely ordered loading sequences are given. The contribution of each of these two phases to total damage obtained at the end can be observed from the same table.

A comparison of the loading history and damage progression curves given in Figure 5.6 indicate that in spite of the inverse ordering of the strong (first phase) and relatively weaker stage (second phase) of the displacement history, the total damage level and the cumulative dissipated hysteretic energy attained in the end are almost equal and they do not differ much. The progressive damage reached to the nearly same level following completely different paths along the inversely-ordered displacement histories consisting of the same number and amplitude of cycles.

Graphical representation of the damage progression, plotted in Figure 5.6 indicate that the damage sustained by the aftershock (i.e., second) part of the loading history, VH-2, is considerably small compared to the damage stemming from the strong (i.e., first) part of the history. The numerical values of the first phase damage, second phase damage and total damage are shown in Table 5.5. The ratios of the post event (labeled as *second phase*) damage (D_2) to the preceding main part (labeled as *first phase*) damage (D_1) and total damage (D_T) are 11.6 percent and 10.4 percent, respectively. In other words the contribution of the damage raised from the aftershock (obtained by scaling the displacement amplitude of the main part by *two-thirds*) to the total damage is considerably small, and remain around one-tenth of the total.

The study presented in this section reveals that the progression of the structural damage and cumulative hysteretic energy dissipation for simple systems are path dependent and not linear. The resultant structural damage and accumulated hysteretic energy dissipated along a path seem apparently to depend on the number and amplitude of cycles constituting the path. However, the resultant of the cumulative hysteretic energy dissipation and the total damage sustained along a

loading path are independent from the ordering of the same number and amplitude cycles along the path.

5.4 Successive Earthquake Ground Motions

Field surveys and observations made on reinforced concrete structures following recent major successive earthquakes in Turkey in the past decade indicate that successive earthquakes (or aftershocks) can substantially increase structural damage. It is not unusual for this accumulation of damage to lead to collapse during the later events. But how can the damage from these events be predicted and what intensity of these excitations may cause to noteworthy progress in the major (or design) earthquake damage? The prior earthquake or foreshock of what intensity may affect substantially the damage to be sustained during the major earthquake ground motions is another question. To accomplish this purpose, an inelastic time history and damage analyses of SDOF systems subjected to two successive earthquakes sequenced in increasing and decreasing order have been performed.

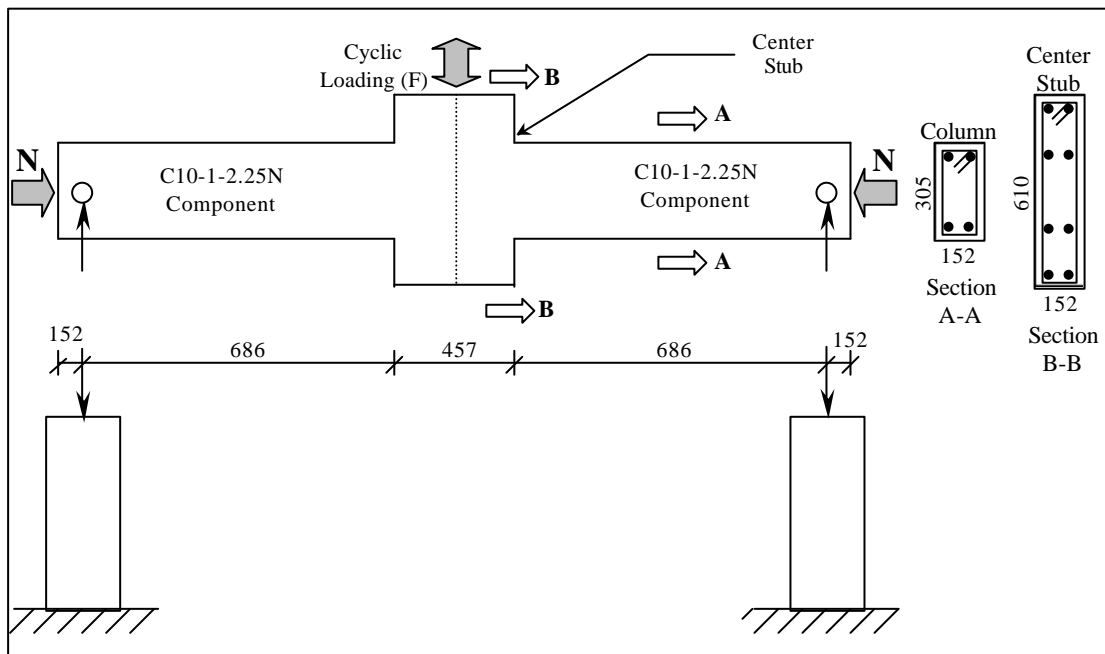


Figure 5.7 Description of test assembly (dimensions in mm)

The inelastic time history and damage analyses are performed using the cantilever column test specimen, labelled as C10-1-2.25N, tested by Pujol (2002).

The properties of the column test specimen are given in Figure 5.7. The column properties can be summarized as follows. The cross section of the specimen was 152 mm wide and 305 mm deep and the shear span was 686 mm. The effective depth (d) was 254 mm, for a shear span to effective depth ratio (a/d) of 2.7. The longitudinal reinforcement consisted of four continuous 19 mm ($\frac{3}{4}$ in) diameter deformed bars with average yield strength of 453 MPa and an average ultimate strength of 642.6 MPa. Transverse reinforcement outside the center stub consisted of 57.2mm spacing hoops made from plain 6.35 mm ($\frac{1}{4}$ in) diameter bars with average yield strength of 411 MPa and an average ultimate strength of 526.8 MPa. Average concrete strength of 150x300 mm cylinder samples of the specimen was 36.48 MPa. The axial load applied to the specimen was 136 kN ($0.08f_cA_g$). The stiffness degradation, strength deterioration and pinching parameter values used are 5.0, 0.2 and 0.448, respectively.

The ground motions used in this study are described first. Then the inelastic time history and damage analyses of inelastic SDOF systems are performed using synthetic ground motion histories. Finally, the effects of prior earthquake and aftershock on the damage stemming from the main earthquake are demonstrated.

5.4.1 Selected Ground Motions

An inelastic time history and damage analyses of SDOF systems subjected to generated synthetic accelerograms, with durations ranging up to 130 sec., were performed to assess whether the prior earthquake and aftershock damage has an effect on the major or design earthquake damage. To accomplish this purpose, four different ground motions are employed. The first one is the north-south component of the ground motion recorded at El Centro, California, in 1940 (Figure 5.8). The reason for using this record is that it is a benchmark in earthquake engineering since it has been used and referred by many researchers in the past. The second and third records are the original records of the 17 August 1999 Marmara Earthquake, Sakarya

Station east-west component and Yarýmca Petrochemical Complex (YPT) Station, north-south component, respectively. The second record is a long (65 sec.) duration record with the main shock and relatively small shock. The fourth record is the transverse component of the ground motion recorded at the Düzce Station during the 12 November 1999 earthquake (Figure 5.8). For the sake of simplicity these ground motions are referred as ELC, SKR, YPT and DZC, respectively. Table 5.6 shows the characteristics of ground acceleration data of these records. The intensity parameters are described below.

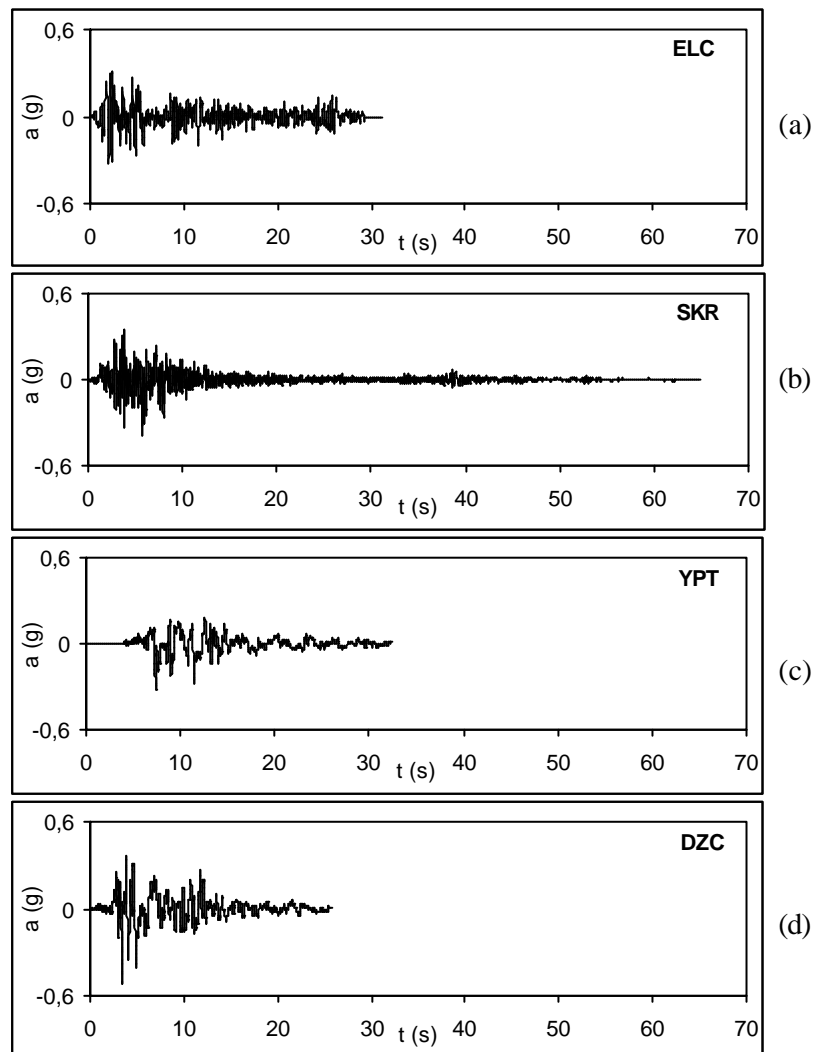


Figure 5.8 The ground motions used in this study. **a)** El Centro 1940, NS component, **b)** 17 August 1999 Marmara Earthquake, Sakarya Station, EW component, **c)** 17 August 1999 Marmara Earthquake, Yarýmca Petrochemical Complex (YPT) Station, NS component, **d)** 12 November 1999 Düzce Earthquake, Düzce Station, NS component

Table 5.6 Ground motion intensity parameters

Ground Motion	PGA (cm/s²)	EPA (cm/s²)	PGV (cm/s)	V/A (s)	T_{eff} (s)
ELC	340.3	278.7	34.67	0.1019	24.43
SKR	396.03	286.86	57.27	0.145	44.41
YPT	313.5	222.8	73.20	0.2335	31.85
DZC	399.61	427.20	69.48	0.174	11.14

PGA : Peak ground acceleration

EPA : Effective peak acceleration

PGV : Peak ground velocity

V/A Ratio : Ratio of PGV to PGA

T_{eff} : Effective duration

5.4.2 Prior and Successive Earthquakes

A number of synthetic accelerograms have been taken into consideration to assess the effect of damage from prior earthquake (foreshock) and successive earthquake (aftershock) on the structural performance of reinforced concrete structures, via accumulation of damage during successive ground motions. Inelastic time history and damage analyses of SDOF systems subjected to synthetic accelerograms, with durations ranging up to 130 s, have been performed. In order to simulate the successive earthquake excitations, these records have been preceded or followed by an equal or smaller amplitude artificial-records without quiescent period. The various amplitude artificial records acting as prior or successive earthquakes have been generated from the original main records. The synthetic accelerograms have been constituted from two phases: an original ground motion record and a foreshock or aftershock obtained by scaling the amplitude of the original ground motion record by one, three-fourth, a half, one-third or one-fourth, successively. Table 5.7 presents a complete summary of the synthetic ground motions that were applied.

Table 5.7 Synthetic ground motions generated from selected earthquake records

Record	Synthetic Ground Motion	Event	Increasing Order Records			Decreasing Order Records		
			Purpose	Scale*	PGA (g)	Purpose	Scale*	PGA (g)
El Centro, 1940	1	1	Prior	1.00	0.35	Main	1.00	0.35
		2	Main	1.00	0.35	Successive	1.00	0.35
	2	1	Prior	0.75	0.26	Main	1.00	0.35
		2	Main	1.00	0.35	Successive	0.75	0.26
	3	1	Foreshock	0.50	0.17	Main	1.00	0.35
		2	Main	1.00	0.35	Aftershock	0.50	0.17
	4	1	Foreshock	0.33	0.12	Main	1.00	0.35
		2	Main	1.00	0.35	Aftershock	0.33	0.12
	5	1	Foreshock	0.25	0.09	Main	1.00	0.35
		2	Main	1.00	0.35	Aftershock	0.25	0.09
Sakarya, 17.08.1999	1	1	Prior	1.00	0.40	Main	1.00	0.40
		2	Main	1.00	0.40	Successive	1.00	0.40
	2	1	Prior	0.75	0.30	Main	1.00	0.40
		2	Main	1.00	0.40	Successive	0.75	0.30
	3	1	Foreshock	0.50	0.20	Main	1.00	0.40
		2	Main	1.00	0.40	Aftershock	0.50	0.20
	4	1	Foreshock	0.33	0.13	Main	1.00	0.40
		2	Main	1.00	0.40	Aftershock	0.33	0.13
	5	1	Foreshock	0.25	0.10	Main	1.00	0.40
		2	Main	1.00	0.40	Aftershock	0.25	0.10
Yarýmca, 17.08.1999	1	1	Prior	1.00	0.32	Main	1.00	0.32
		2	Main	1.00	0.32	Successive	1.00	0.32
	2	1	Prior	0.75	0.24	Main	1.00	0.32
		2	Main	1.00	0.32	Successive	0.75	0.24
	3	1	Foreshock	0.50	0.16	Main	1.00	0.32
		2	Main	1.00	0.32	Aftershock	0.50	0.16
	4	1	Foreshock	0.33	0.11	Main	1.00	0.32
		2	Main	1.00	0.32	Aftershock	0.33	0.11
	5	1	Foreshock	0.25	0.08	Main	1.00	0.32
		2	Main	1.00	0.32	Aftershock	0.25	0.08
Düzce, 12.11.1999	1	1	Prior	1.00	0.41	Main	1.00	0.41
		2	Main	1.00	0.41	Successive	1.00	0.41
	2	1	Prior	0.75	0.31	Main	1.00	0.41
		2	Main	1.00	0.41	Successive	0.75	0.31
	3	1	Foreshock	0.50	0.21	Main	1.00	0.41
		2	Main	1.00	0.41	Aftershock	0.50	0.21
	4	1	Foreshock	0.33	0.14	Main	1.00	0.41
		2	Main	1.00	0.41	Aftershock	0.33	0.14
	5	1	Foreshock	0.25	0.10	Main	1.00	0.41
		2	Main	1.00	0.41	Aftershock	0.25	0.10

* Multiplying factor on acceleration amplitude

In general, the intensity of the aftershock is either one-fourth, one-third or at most a half of the main shock intensity. However, the amplitude of the foreshocks and aftershocks considered in this study is equal or lower than that of the main event. The amplitude of the seismic events preceding or following the main ground motion is equal or lower than the amplitude of main history acting. However, the objective of this study covers the assessment of not only the foreshock and aftershock damage effects but also the prior earthquake and successive earthquake damage effects. Hence, the foreshocks or aftershocks with intensity of the same and three-fourth scaled of the ground motions have been taken into account.

The following sections contain plots of several composite ground motion histories and corresponding damage progression curves. The plots were arranged mutually for the sake of simple comparison. The same comparison can be made by means of numerical damage values given in tabular form.

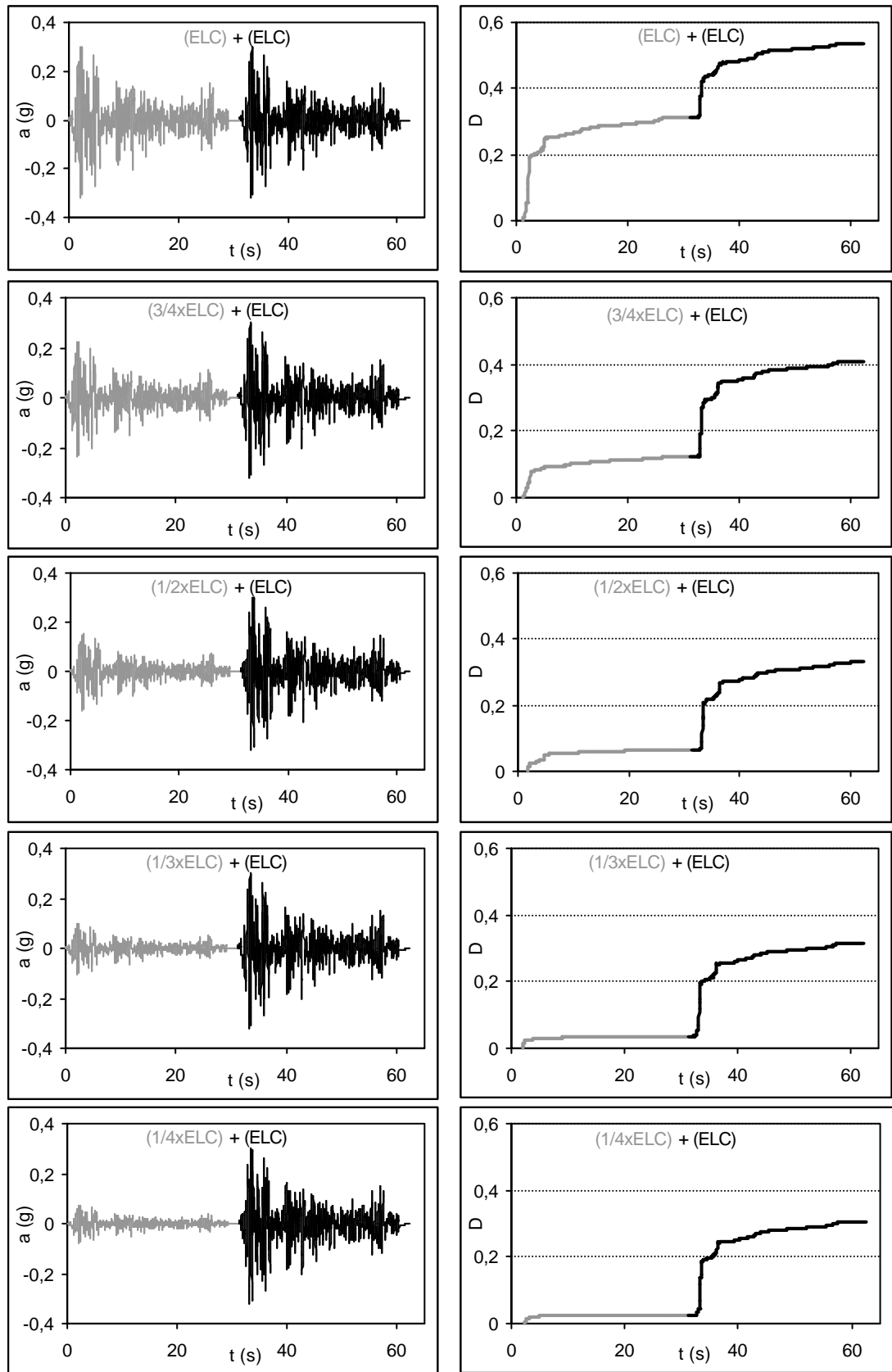


Figure 5.9 Synthetic ground acceleration histories (El Centro 1940, NS component preceded by various amplitude foreshocks) and damage variation curves for Pujol column

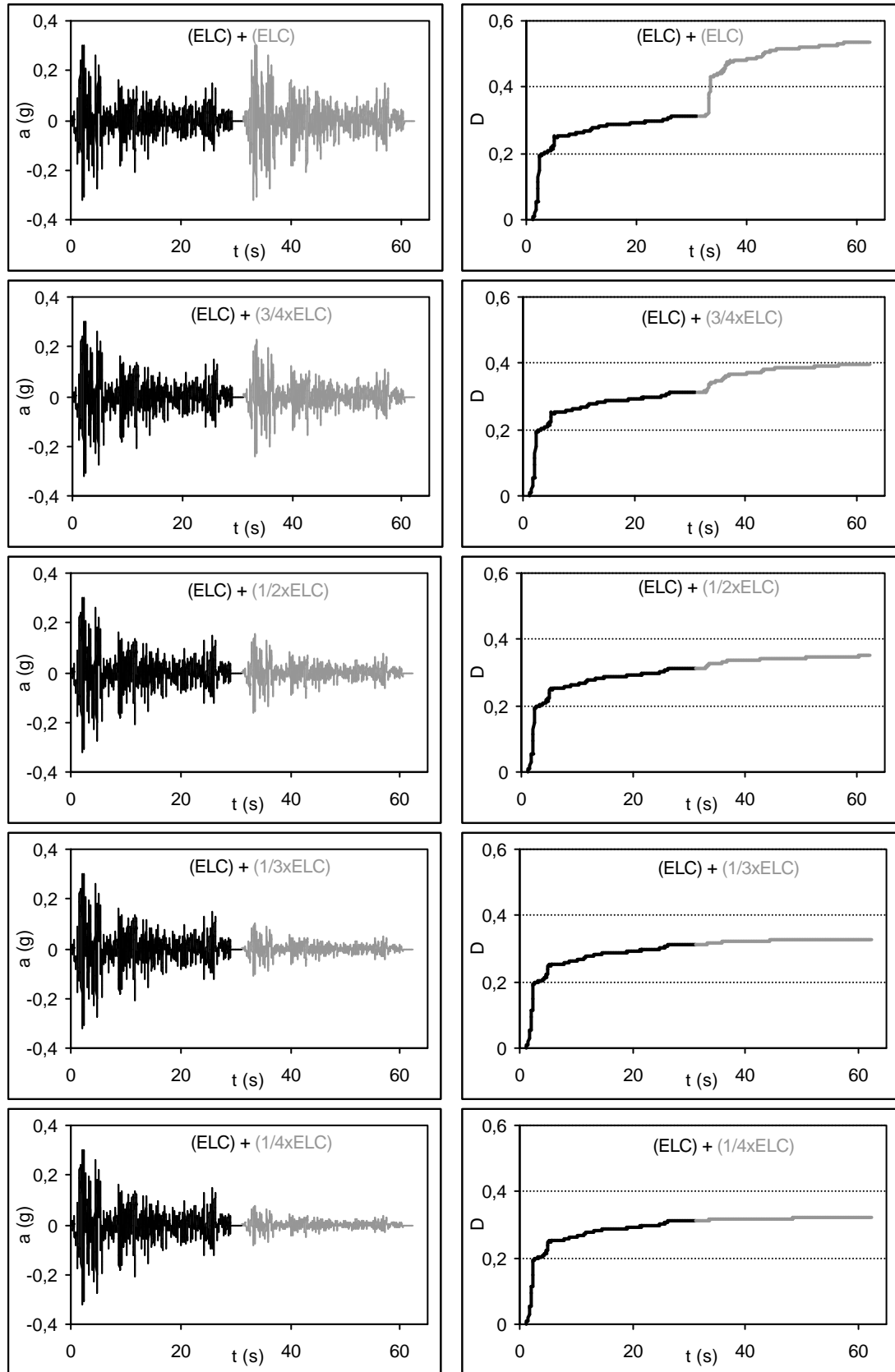


Figure 5.10 Synthetic ground acceleration histories (El Centro 1940, NS component followed by various amplitude aftershocks) and damage variation curves for Pujol column

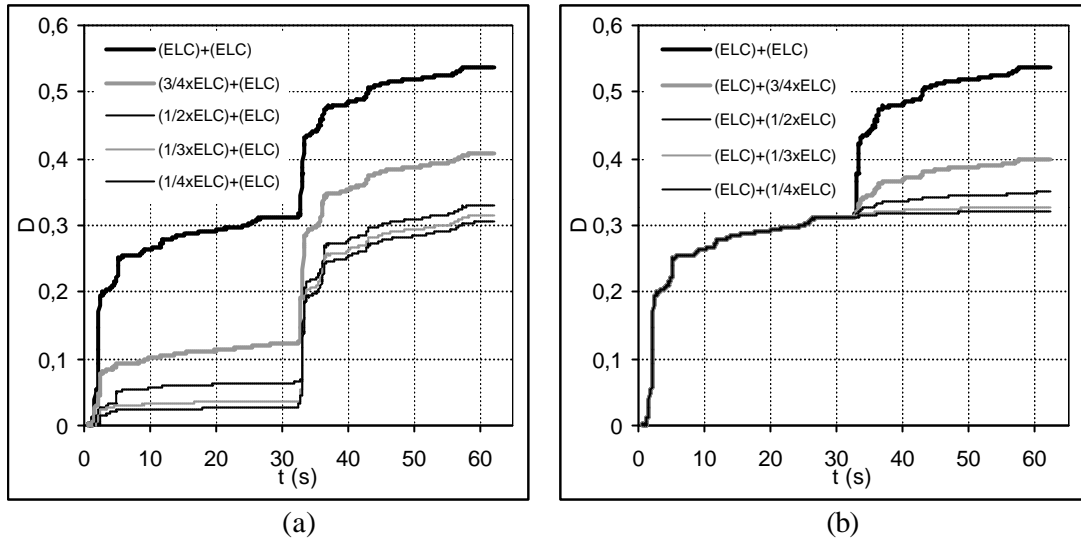


Figure 5.11 Comparison of damage curves for Pujol column subjected to the synthetic ground acceleration histories comprising El Centro 1940, NS component and its various amplitude **a)** foreshocks and **b)** aftershocks

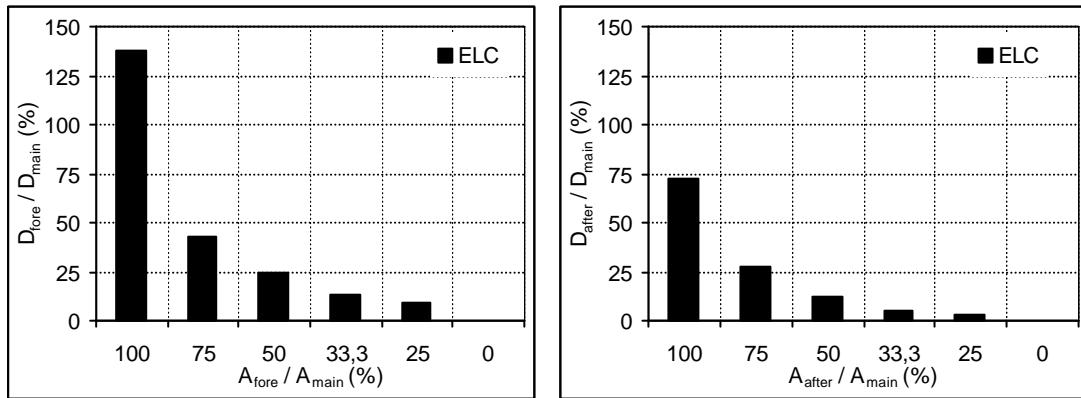


Figure 5.12 Effect of foreshock and aftershock damage on the damage sustained by the main ground motion, El Centro 1940, NS component

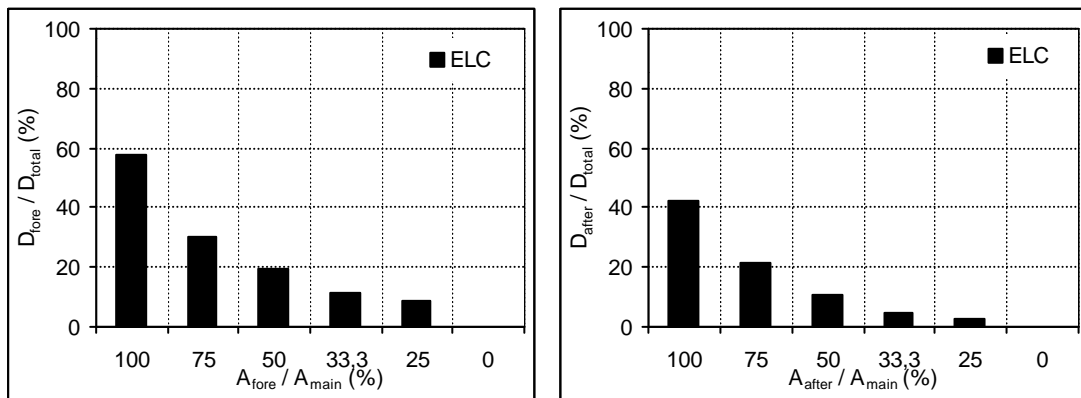


Figure 5.13 Effect of foreshock and aftershock damage on the total damage sustained by the synthetic ground acceleration histories originated from El Centro 1940, NS component

Table 5.8 Damage values for Pujol column subjected to synthetic ground acceleration histories (El Centro 1940, NS component and its various amplitude foreshocks)

Synthetic Ground Motion	D_{fore} (1)	D_{main} (2)	D_{total} (1+2)	D_{fore}/D_{main} (%)	D_{fore}/D_{total} (%)
ELC+ELC	0,312	0,226	0,538	138,05	57,99
3/4ELC+ELC	0,122	0,285	0,407	42,81	29,98
1/2ELC+ELC	0,065	0,265	0,330	24,53	19,70
1/3ELC+ELC	0,036	0,279	0,315	12,90	11,43
1/4ELC+ELC	0,026	0,279	0,305	9,32	8,52
ELC	0,000	0,312	0,312	0,00	0,00

Table 5.9 Damage values for Pujol column subjected to synthetic ground acceleration histories (El Centro 1940, NS component and its various amplitude aftershocks)

Synthetic Ground Motion	D_{main} (1)	D_{after} (2)	D_{total} (1+2)	D_{after}/D_{main} (%)	D_{after}/D_{total} (%)
ELC+ELC	0,312	0,226	0,538	72,44	42,01
ELC+3/4ELC	0,312	0,087	0,399	27,88	21,80
ELC+1/2ELC	0,312	0,038	0,350	12,18	10,86
ELC+1/3ELC	0,312	0,016	0,328	5,13	4,88
ELC+1/4ELC	0,312	0,009	0,321	2,88	2,80
ELC	0,312	0,000	0,312	0,00	0,00

Figures 5.9 and 5.10 show the synthetic ground acceleration histories comprising El Centro 1940, NS component and its various amplitude foreshocks and aftershocks and the corresponding time variation damage curves for Pujol Column Specimen C10-1-2.25N. The gray parts of these curves correspond to the foreshock/aftershock phases. For the sake of comparison, these curves are plotted all together in Figure 5.11a and b. The numerical values obtained in the end of both foreshock/aftershock and main shock phases alone and the overall histories, labeled as D_{fore} , D_{after} , D_{main} and D_{total} are tabulated in the first three columns of Tables 5.8 and 5.9. The ratio values denoted by D_{fore}/D_{main} , D_{fore}/D_{total} , D_{after}/D_{main} and D_{after}/D_{total} are given in the last two columns to reveal the effects of foreshock and aftershock damage on both main shock and overall damage.

Figures 5.9 and 5.11a reveal that the damage increases rapidly at the time values corresponding to sudden increases in the reversal. A comparison of the damage curves plotted in Figure 5.11a reveals the influence of the foreshock damage, on the main shock and overall damage of the SDOF system. Note here that damage inflicted on the SDOF system by the foreshock is not proportional to its intensity. There is a nonlinear relationship between the earthquake excitation intensity and the damage attained in the end. In addition, it should be noted that increase in the foreshock amplitude results in decrease in the damage inflicted by the main shock as can be seen from the third column of Table 5.8.

A comparison of the damage curves plotted in Figure 5.11b illustrates the effect of the aftershock damage, D_{after} , on both the main shock and total damage. Increase in the aftershock amplitude does not lead to proportional increase in the damage attained in the end. Increase in the aftershock amplitude results in the relatively greater rate of damage progression. Damage curves given in Figures 5.10 and 5.11b show that the damage resulted by the aftershocks with one-fourth, one-third and even a half of the main shock amplitude are negligibly small and they do not lead to substantial damage. The graphical representation of this evidence can be seen also in Figure 5.12 and 5.13.

A comparison of the damage progression curves and numerical data presented shown above in demonstrate that the same intensity of loading history acting as foreshock (or prior earthquake) and aftershock (or succeeding earthquake) does not lead to the same amount of damage. As an example the $1/2\text{ELC}$ history acting as foreshock and aftershock caused to damage values of 0.065 and 0.038, respectively. Comparison of the damage curves shown in Figure 5.11a and 5.11b indicates that the total damage level attained in the end is almost equal. The data show the path independency of the total damage from the order of amplitudes along loading paths consisting of the same number and amplitude of cycles.

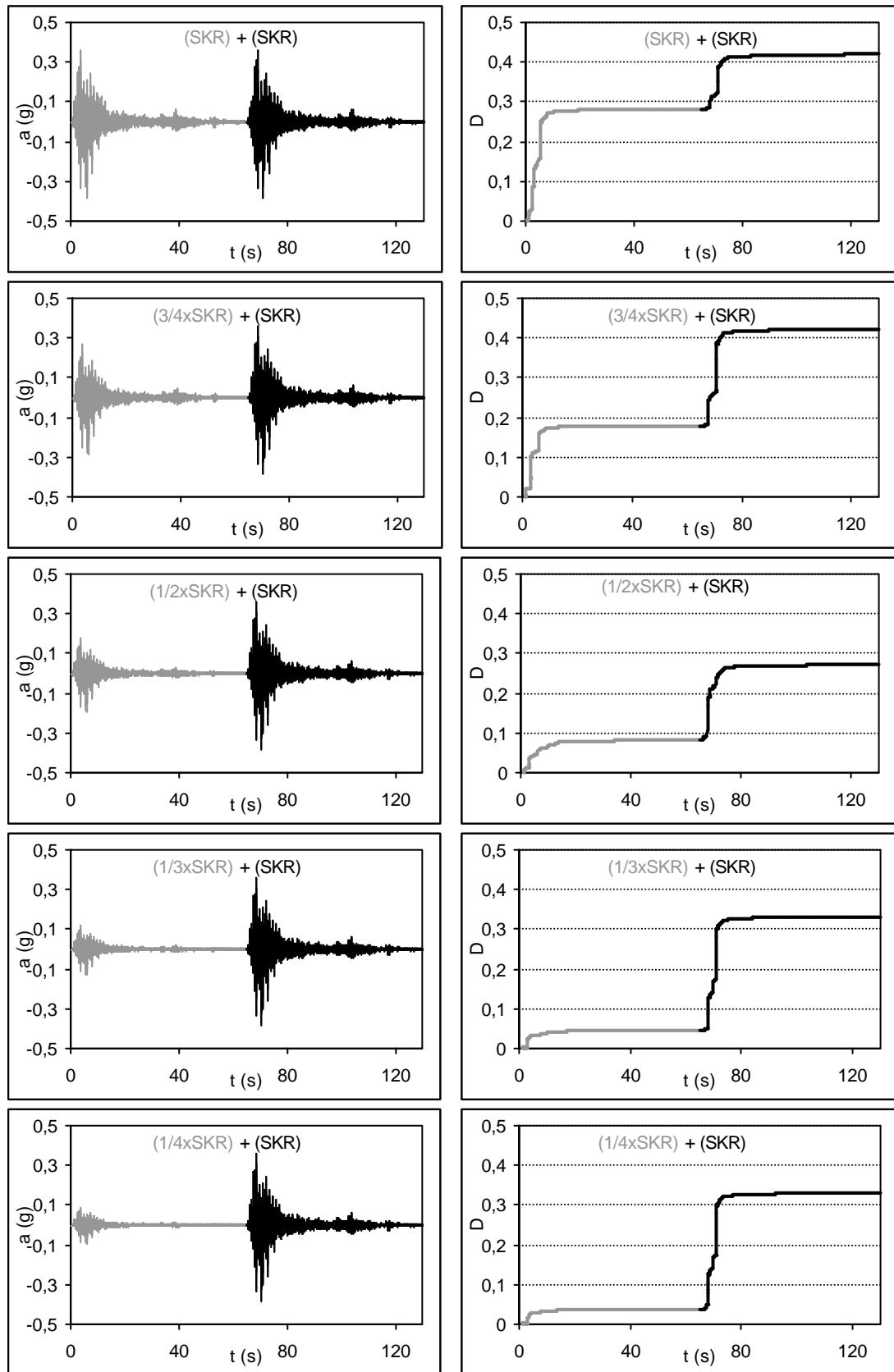


Figure 5.14 Synthetic ground acceleration histories (17 August 1999 Marmara Earthquake Sakarya-EW component preceded by various amplitude foreshocks) and damage variation curves for Pujol column

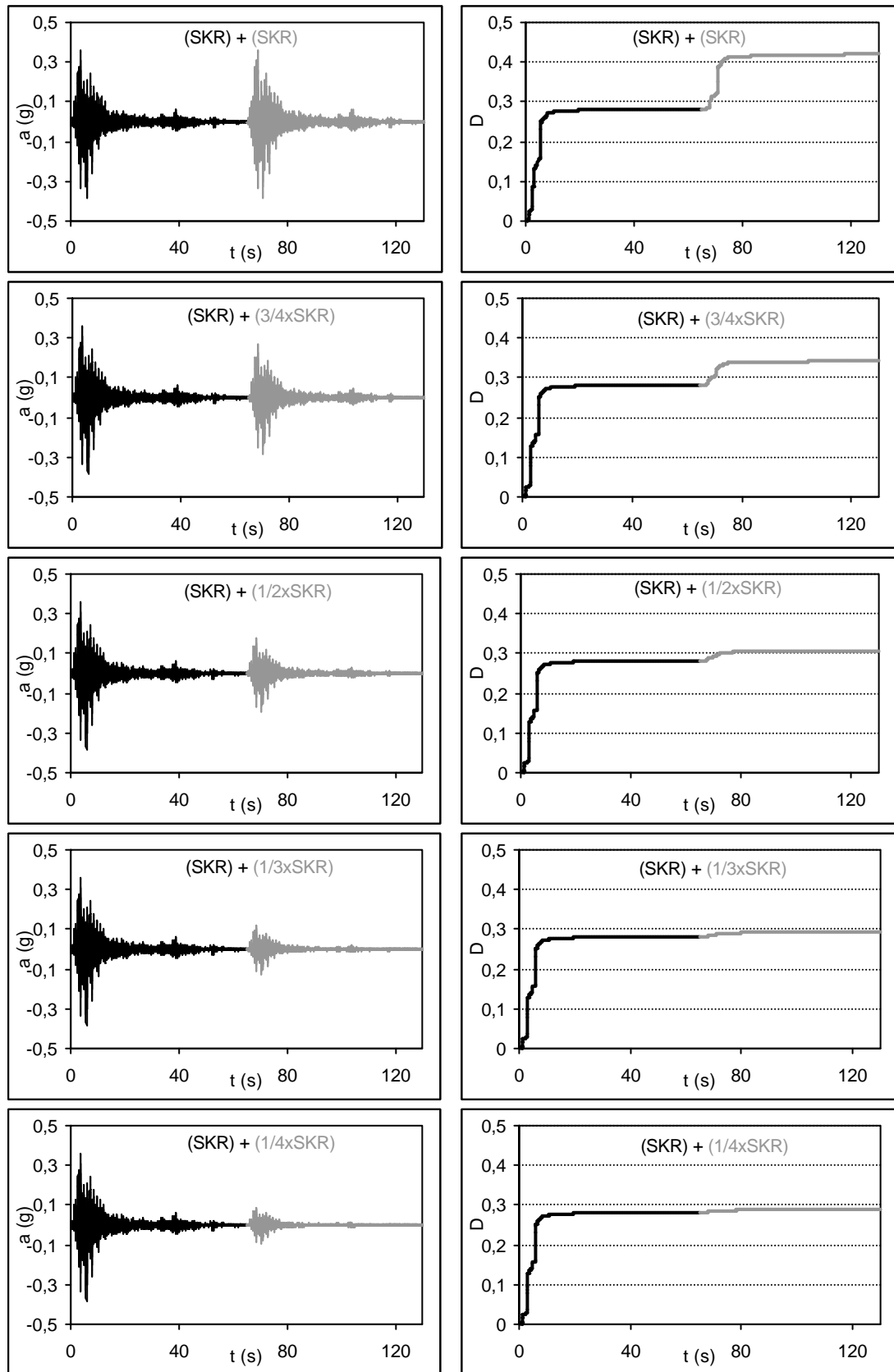


Figure 5.15 Synthetic ground acceleration histories (17 August 1999 Marmara Earthquake Sakarya-EW component followed by various amplitude aftershocks) and damage variation curves for Pujol column

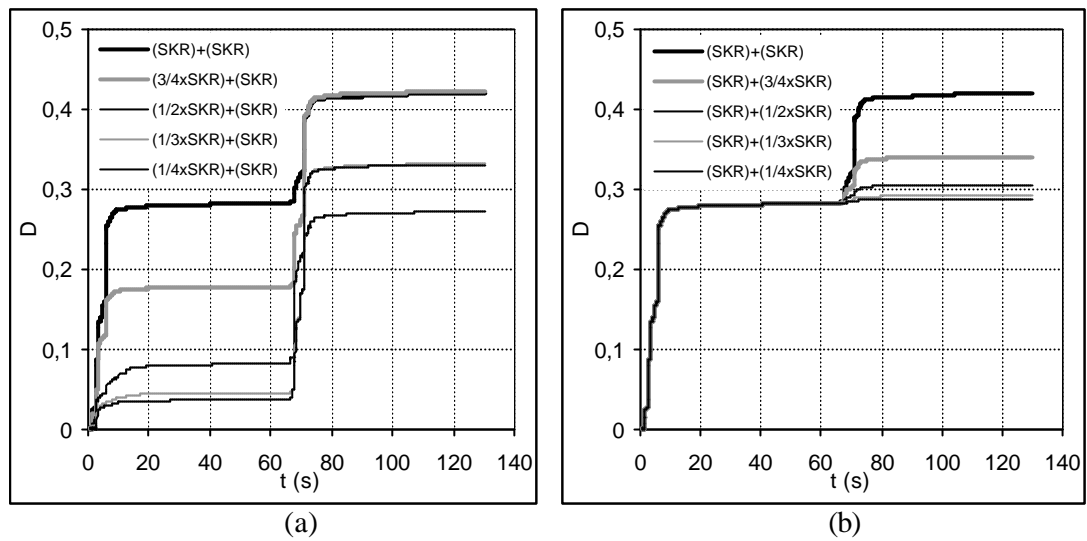


Figure 5.16 Comparison of damage curves for Pujol column subjected to the synthetic ground acceleration histories comprising 17 August 1999 Marmara Earthquake, Sakarya station, EW component and its various amplitude **a)** foreshocks and **b)** aftershocks

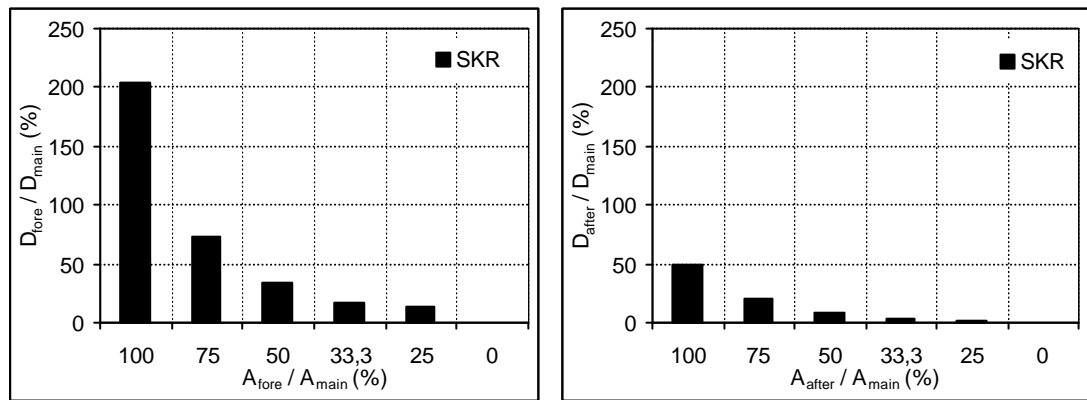


Figure 5.17 Effect of foreshock and aftershock damage on the damage sustained by the main ground motion, 17 August 1999 Marmara Earthquake, Sakarya station, EW component

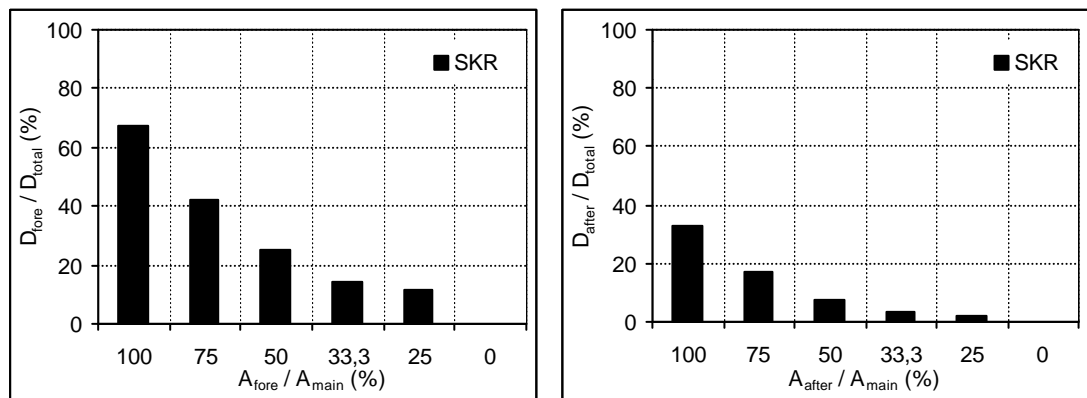


Figure 5.18 Effect of foreshock and aftershock damage on the total damage sustained by the synthetic ground acceleration histories originated from 17 August 1999 Marmara Earthquake, Sakarya station, EW component

Table 5.10 Damage values for Pujol column subjected to synthetic ground acceleration histories (17 August 1999 Marmara Earthquake, Sakarya-EW component and its various amplitude foreshocks)

Synthetic Ground Motion	D_{fore} (1)	D_{main} (2)	D_{total} (1+2)	D_{fore}/D_{main} (%)	D_{fore}/D_{total} (%)
SKR+SKR	0,282	0,138	0,420	204,35	67,14
3/4SKR+SKR	0,178	0,245	0,423	72,65	42,08
1/2SKR+SKR	0,088	0,265	0,353	33,21	24,93
1/3SKR+SKR	0,047	0,285	0,332	16,49	14,16
1/4SKR+SKR	0,039	0,292	0,331	13,36	11,78
SKR	0,000	0,282	0,282	0,00	0,00

Table 5.11 Damage values for Pujol column subjected to synthetic ground acceleration histories (17 August 1999 Marmara Earthquake, Sakarya-EW component and its various amplitude aftershocks)

Synthetic Ground Motion	D_{main} (1)	D_{after} (2)	D_{total} (1+2)	D_{after}/D_{main} (%)	D_{after}/D_{total} (%)
SKR+SKR	0,282	0,138	0,420	48,94	32,86
SKR+3/4SKR	0,282	0,059	0,341	20,92	17,30
SKR+1/2SKR	0,282	0,023	0,305	8,16	7,54
SKR+1/3SKR	0,282	0,010	0,292	3,55	3,42
SKR+1/4SKR	0,282	0,006	0,288	2,13	2,08
SKR	0,282	0,000	0,282	0,00	0,00

The composite ground acceleration histories comprising 17 August 1999 Marmara Earthquake, Sakarya-EW component and its various amplitude foreshocks and aftershocks and the corresponding time variation damage curves, obtained for the SDOF systems, are given in Figures 5.14 and 5.15. The gray colored parts of the curves denote the foreshock and aftershock phases. For comparison, damage curves were introduced together in Figures 5.16a and b. The numerical values obtained in the end of both foreshock/aftershock and main shock phases alone and the overall history, are tabulated in the first three columns of Tables 5.10 and 5.11. The ratios denoted by D_{fore}/D_{main} , D_{fore}/D_{total} , D_{after}/D_{main} and D_{after}/D_{total} are given in the last two columns showing the foreshock and aftershock damage effects on both main shock and overall damage.

It is observed from the damage curves in Figures 5.14 and 5.16a that the damage increased rapidly due to the strong pulses at the beginning of the ground motions. Comparison of the damage curves plotted in Figure 5.16a indicates the effects of foreshock damage on the main shock and overall damage. The variation of the damage sustained due to foreshock is not proportional to its intensity. The damage caused by the foreshocks with one-fourth, one-third and even half amplitude is relatively small remaining below 25 percent of the total damage. Increasing the amplitude of the foreshocks result in comparably larger damage in the end. In addition, it should be noted that increase in the foreshock amplitude results in decrease in the damage inflicted by the main shock as can be seen from the third column of Table 5.10.

A comparison of the damage curves plotted in Figures 5.15 and 5.16b illustrates the effect of the aftershock damage, D_{after} , on both the main shock and total damage. Increase in the aftershock amplitude results in the relatively greater rate of damage progression. The damage caused by the aftershocks with one-fourth, one-third and even a half of the main shock amplitude are negligibly small compared to total damage, and even the aftershock with three-fourth amplitude does not lead to substantial damage. These evidences can be inspected in Figures 5.17 and 5.18.

It was demonstrated that the same intensity of loading history acting as foreshock(or prior earthquake) and aftershock(successive earthquake) does not lead to the same amount of damage. Comparison of the damage curves shown in Figure 5.16a and 5.16b indicates that there is no much difference between the damage caused by synthetic ground motion histories containing the same intensity foreshock and aftershock. The data presented underscores the fact that the total damage seem to be independent from the order of amplitudes along loading paths consisting of the same number and amplitude of cycles.

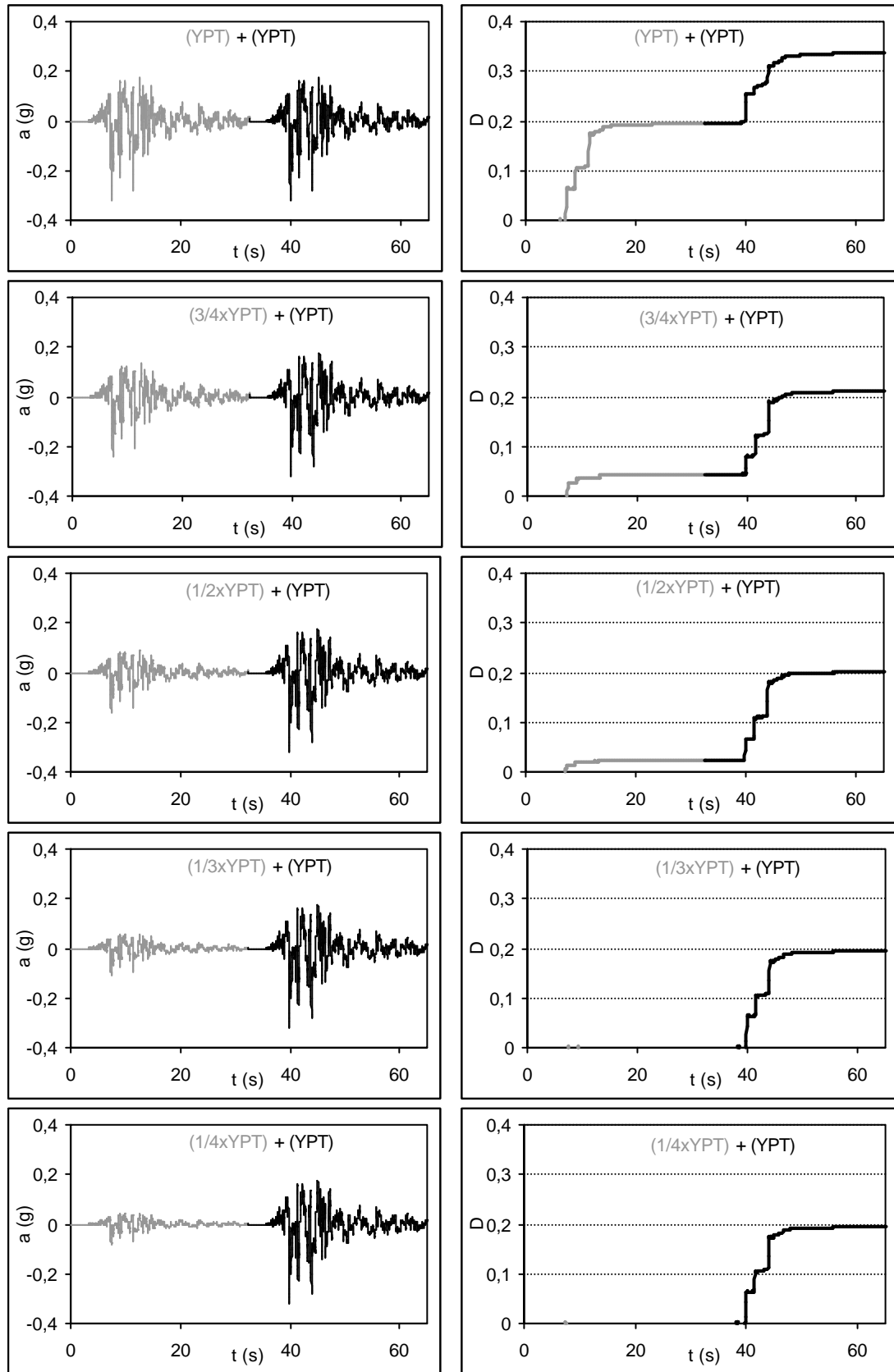


Figure 5.19 Synthetic ground acceleration histories (17 August 1999 Marmara Earthquake YPT (Yarýmca Petrochemical Complex) Station, NS component preceded by various amplitude foreshocks) and damage variation curves for Pujol column

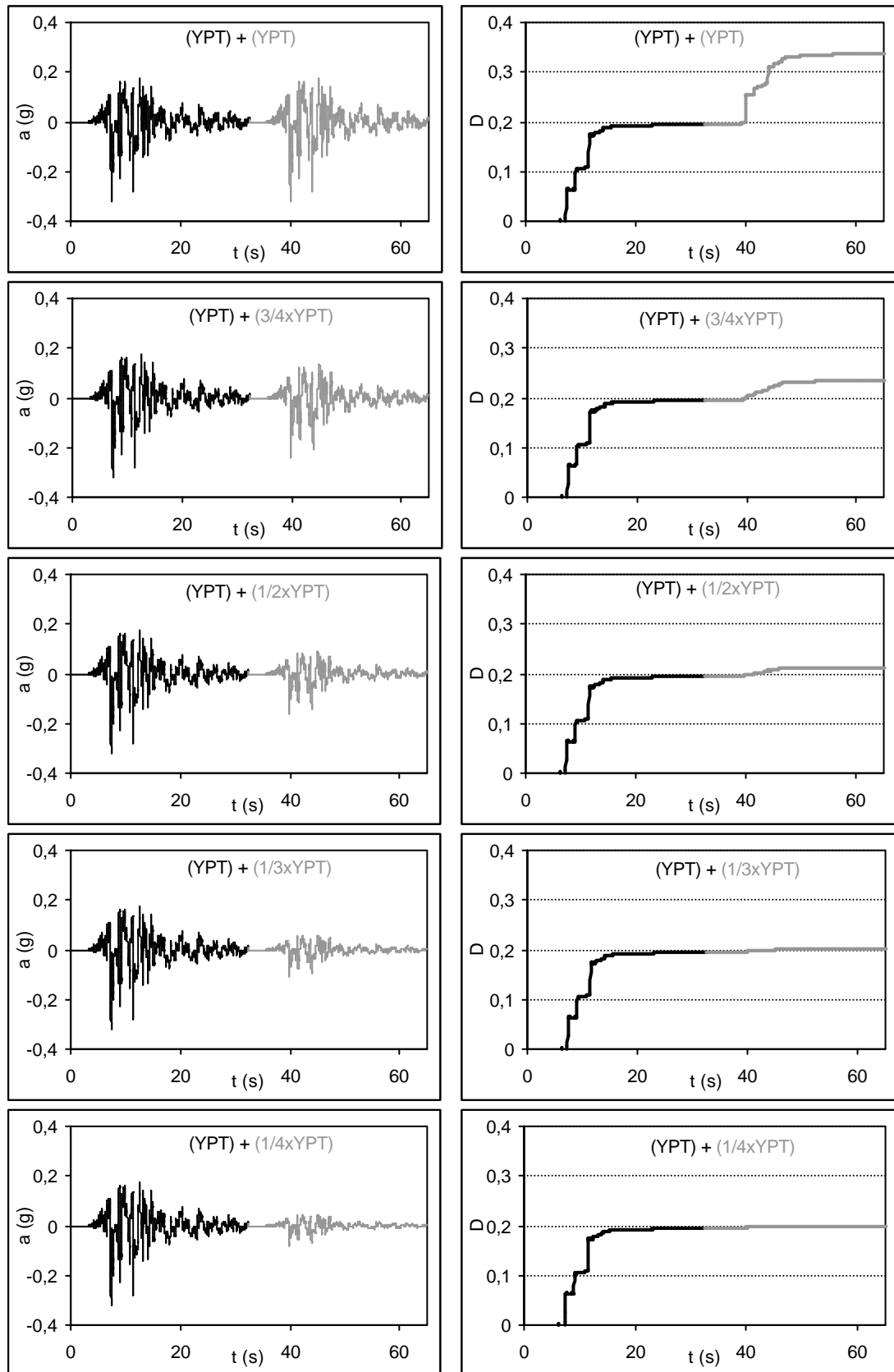


Figure 5.20 Synthetic ground acceleration histories (17 August 1999 Marmara Earthquake, YPT (Yarýmca Petrochemical Complex) Station, NS component followed by various amplitude aftershocks) and damage variation curves for Pujol column

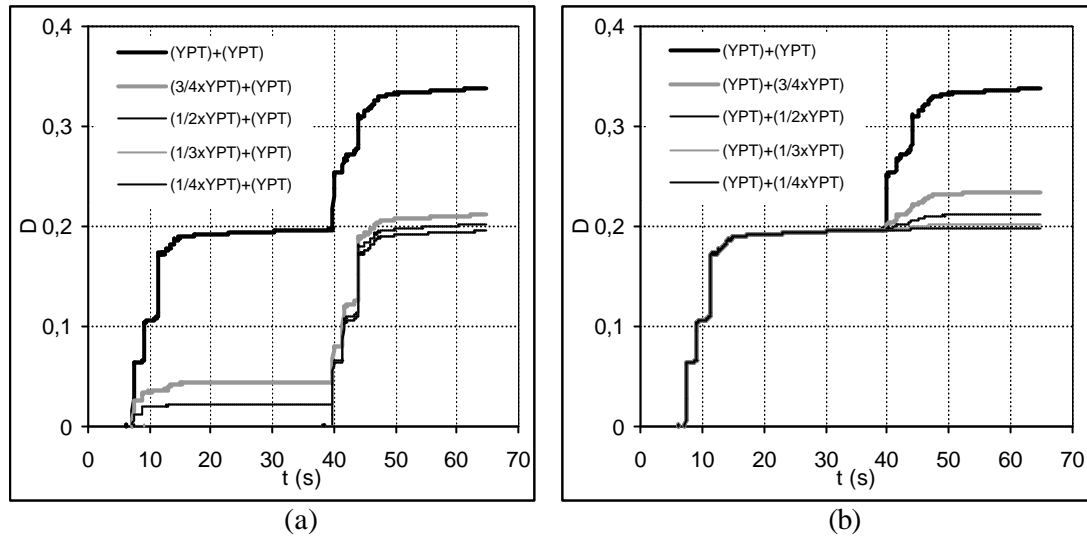


Figure 5.21 Comparison of damage curves for Pujol column subjected to the synthetic ground acceleration histories comprising 17 August 1999 Marmara Earthquake, YPT (Yarýmca Petrochemical Complex) Station, NS component and its various amplitude a)foreshocks and b)aftershocks

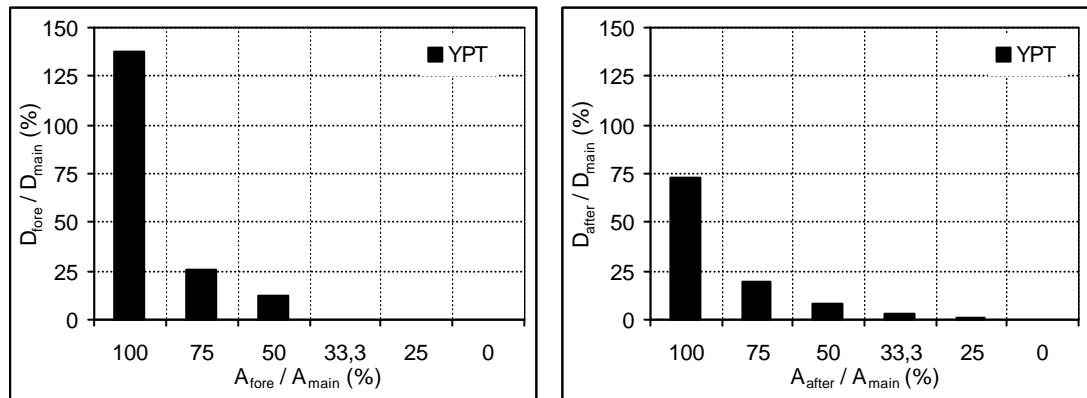


Figure 5.22 Effect of foreshock and aftershock damage on the damage sustained by the main ground motion, 17 August 1999 Marmara Earthquake, YPT (Yarýmca Petrochemical Complex) Station, NS component

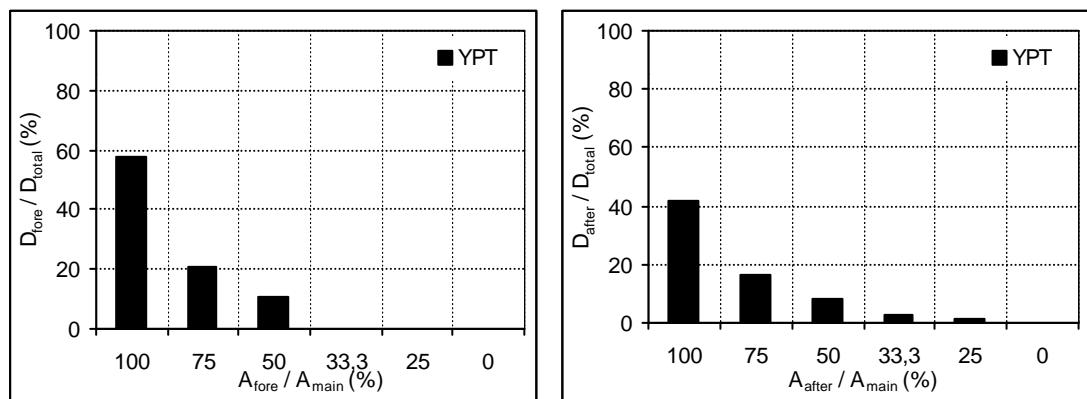


Figure 5.23 Effect of foreshock and aftershock damage on the total damage sustained by the synthetic ground acceleration histories originated from 17 August 1999 Marmara Earthquake, YPT (Yarýmca Petrochemical Complex) Station, NS component

Table 5.12 Damage values for Pujol column subjected to synthetic ground acceleration histories (17 August 1999 Marmara Earthquake, YPT (Yarýmca Petrochemical Complex) Station, NS component and its various amplitude foreshocks)

Synthetic Ground Motion	D_{fore} (1)	D_{main} (2)	D_{total} (1+2)	D_{fore}/D_{main} (%)	D_{fore}/D_{total} (%)
YPT+YPT	0,196	0,142	0,338	138,03	57,99
3/4YPT+YPT	0,044	0,168	0,212	26,19	20,75
1/2YPT+YPT	0,022	0,180	0,202	12,22	10,89
1/3YPT+YPT	0,000	0,196	0,196	0,00	0,00
1/4YPT+YPT	0,000	0,196	0,196	0,00	0,00
YPT	0,000	0,196	0,196	0,00	0,00

Table 5.13 Damage values for Pujol column subjected to synthetic ground acceleration histories (17 August 1999 Marmara Earthquake, YPT (Yarýmca Petrochemical Complex) Station, NS component and its various amplitude aftershocks)

Synthetic Ground Motion	D_{main} (1)	D_{after} (2)	D_{total} (1+2)	D_{after}/D_{main} (%)	D_{after}/D_{total} (%)
YPT+YPT	0,196	0,142	0,338	72,45	42,01
YPT+3/4YPT	0,196	0,039	0,235	19,90	16,60
YPT+1/2YPT	0,196	0,017	0,213	8,67	7,98
YPT+1/3YPT	0,196	0,006	0,202	3,06	2,97
YPT+1/4YPT	0,196	0,003	0,199	1,53	1,51
YPT	0,196	0,000	0,196	0,00	0,00

A combined representation of the synthetic ground acceleration histories comprising 17 August 1999 Marmara Earthquake, YPT Station, NS component and its various amplitude foreshocks and aftershocks and the corresponding damage variation curves are given in Figures 5.19 and 5.20. The damage caused by the foreshock/aftershock indicated by the gray colored parts of the curves. Damage variation curves are given together, in Figure 5.21a and b, to permit simple comparison. The numerical values obtained in the end of both foreshock/aftershock and main shock phases alone and the overall histories, labeled as D_{fore} , D_{after} , D_{main} and D_{total} are tabulated in the first three columns of Tables 5.12 and 5.13. These tables comprise the values denoted by D_{fore}/D_{main} , D_{fore}/D_{total} , D_{after}/D_{main} and D_{after}/D_{total} showing the foreshock and aftershock damage effects on both main shock and overall damage.

The damage progressed rapidly during the sudden increases in the loading history (see Figures 5.19, 5.20 and 5.21). The effects of the foreshock damage on the

main shock and overall damage can be seen from the damage curves shown in Figure 5.21a. There is no linear variation between the foreshock damage and its amplitude. There is no damage from the foreshocks with one-fourth and one-third of the main shock amplitude. It is interesting that the damage caused by the foreshock of half amplitude is nearly zero. An increase in the amplitude of the foreshock leads to relatively higher damage levels in the end. The graphical representation of this evidence appears in Figures 5.22 and 5.23. Increases in the foreshock amplitude result in increase in total damage but decrease in the main shock damage, as can be observed from the curves as well as damage data given the third column of Table 5.12.

The damage curves presented in Figures 5.20 and 5.21b illustrate the effect of the aftershock damage on both the main shock and total damage. Increase in the aftershock amplitude results in the relatively greater rate of damage progression. A comparison study of damage curves illustrated the non-linear relationship between the earthquake excitation intensity and the damage values obtained in the end. The damages caused by the aftershocks having 25 percent, 50 percent and 100 percent amplitude of the main shock constitute the 1.51 percent, 7.98 percent and 42.01 percent of the total damage (Table 5.13). Damage curves given in Figures 5.20 and 5.21b show that the damage caused by the aftershocks with one-fourth, one-third and even a half of the main shock amplitude are negligibly small and they do not lead to substantial damage. The graphical representation of this evidence can be seen also in Figure 5.22 and 5.23.

The numerical data presented above illustrates that the same intensity of loading history acting as foreshock and aftershock does not lead to the same amount of damage. Comparison of the damage curves shown in Figures 5.21a and b indicates that the total damage level attained in the end are almost equal and they do not differ much for all synthetic ground motion histories containing the same intensity foreshock and aftershock. Furthermore, the damage data, presented in Tables 5.12 and 5.13, shows the path independency of the total damage from the order of amplitudes along loading paths consisting of the same number and amplitude of cycles.

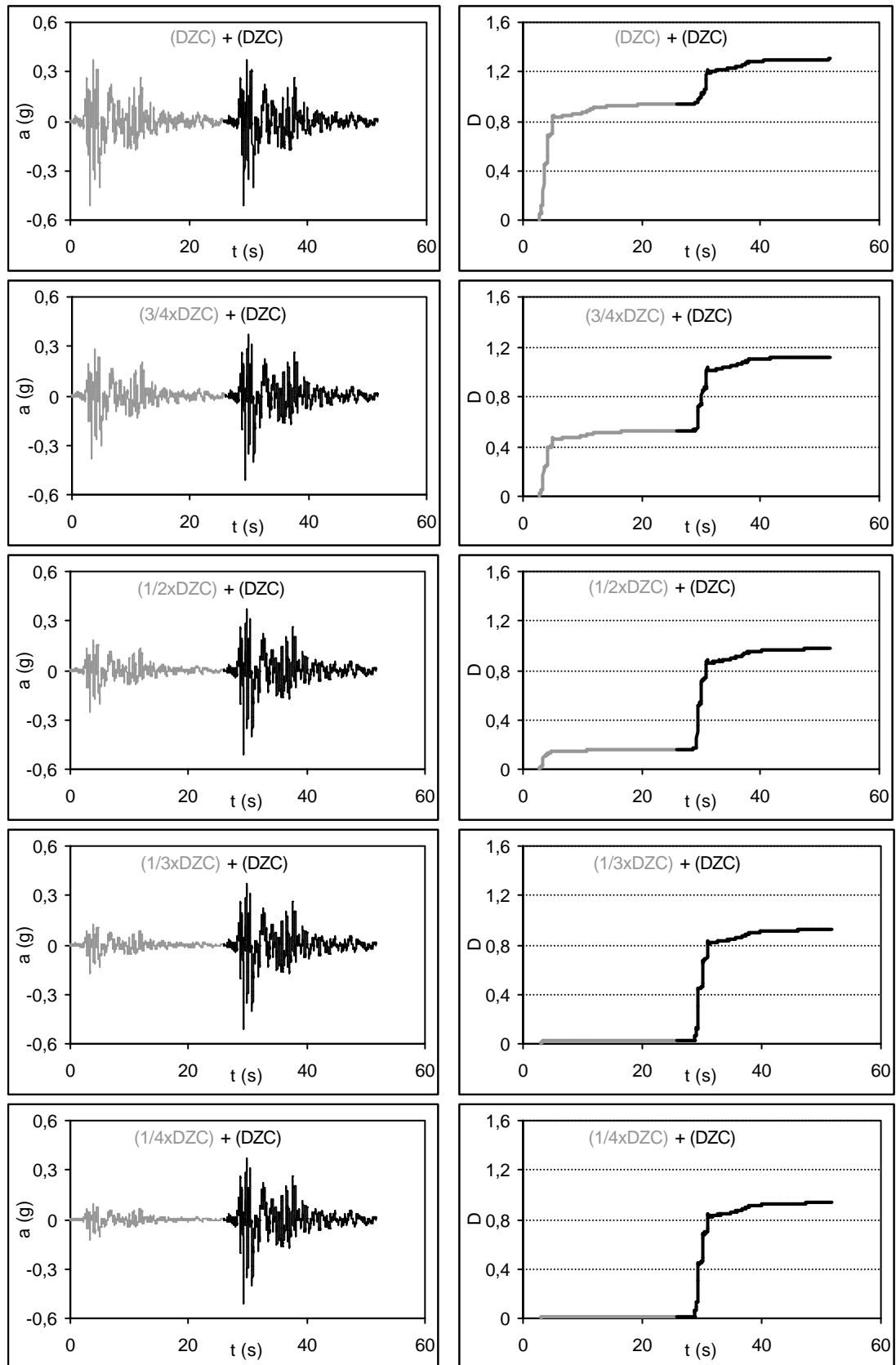


Figure 5.24 Synthetic ground acceleration histories (12 November 1999 Düzce Earthquake, Düzce Station, NS component preceded by various amplitude foreshocks) and damage variation curves for Pujol column

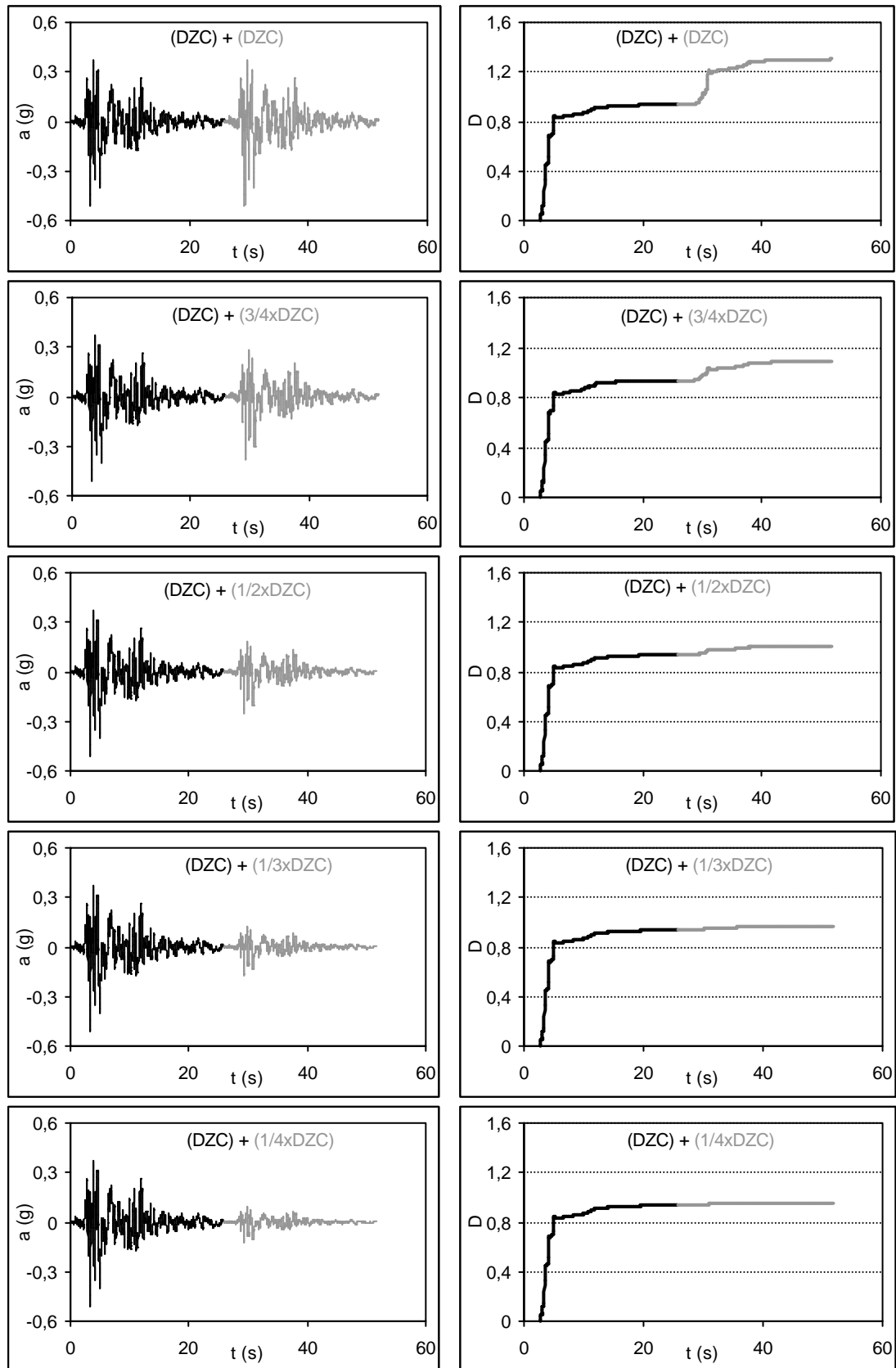


Figure 5.25 Synthetic ground acceleration histories (12 November 1999 Düzce Earthquake, Düzce Station, NS component followed by various amplitude aftershocks) and damage variation curves for Pujol column

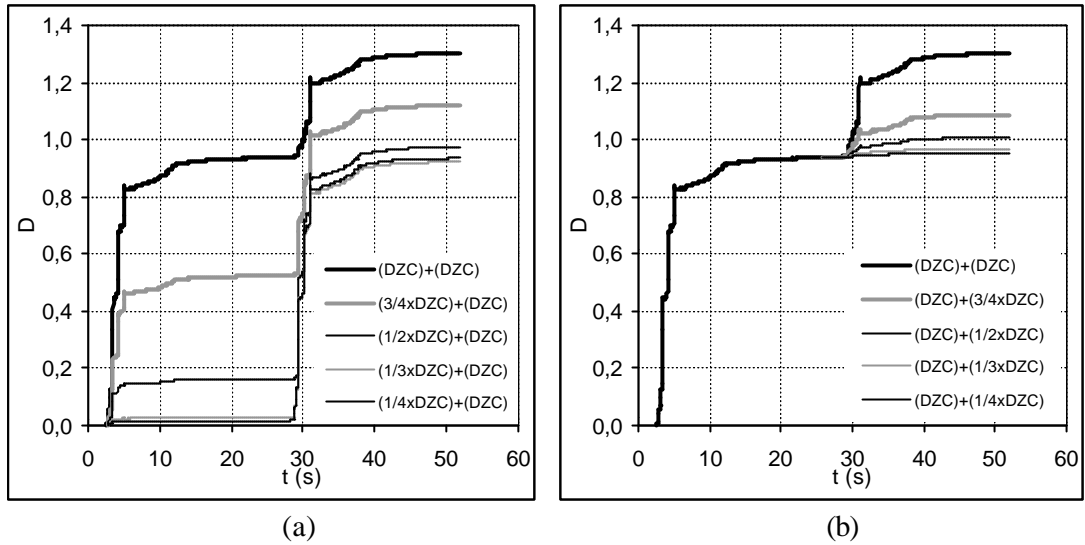


Figure 5.26 Comparison of damage curves for Pujol column subjected to the synthetic ground acceleration histories comprising 12 November 1999 Düzce Earthquake, Düzce Station, NS component and its various amplitude a) foreshocks and b) aftershocks

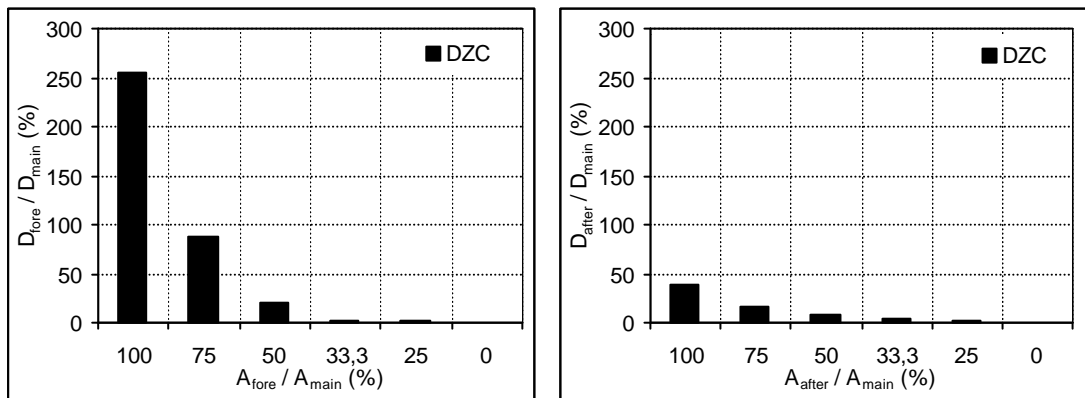


Figure 5.27 Effect of foreshock and aftershock damage on the damage sustained by the main ground motion, 12 November 1999 Düzce Earthquake, Düzce Station, NS component

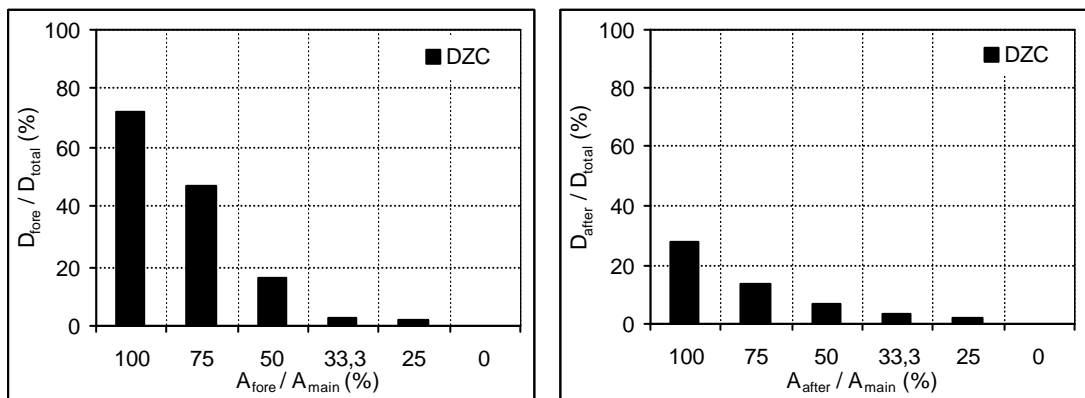


Figure 5.28 Effect of foreshock and aftershock damage on the total damage sustained by the synthetic ground acceleration histories originated from 12 November 1999 Düzce Earthquake, Düzce Station, NS component

Table 5.14 Damage values for Pujol column subjected to synthetic ground acceleration histories (12 November 1999 Düzce Earthquake, Düzce Station, NS component and its various amplitude foreshocks)

Synthetic Ground Motion	D_{fore} (1)	D_{main} (2)	D_{total} (1+2)	D_{fore}/D_{main} (%)	D_{fore}/D_{total} (%)
DZC+DZC	0,936	0,367	1,303	255,04	71,83
3/4DZC+DZC	0,523	0,597	1,120	87,60	46,70
1/2DZC+DZC	0,161	0,813	0,974	19,80	16,53
1/3DZC+DZC	0,026	0,897	0,923	2,90	2,82
1/4DZC+DZC	0,017	0,918	0,935	1,85	1,82
DZC	0,000	0,936	0,936	0,00	0,00

Table 5.15 Damage values for Pujol column subjected to synthetic ground acceleration histories (12 November 1999 Düzce Earthquake, Düzce Station, NS component and its various amplitude aftershocks)

Synthetic Ground Motion	D_{main} (1)	D_{after} (2)	D_{total} (1+2)	D_{after}/D_{main} (%)	D_{after}/D_{total} (%)
DZC+DZC	0,936	0,367	1,303	39,21	28,17
DZC+3/4DZC	0,936	0,151	1,087	16,13	13,89
DZC+1/2DZC	0,936	0,070	1,006	7,48	6,96
DZC+1/3DZC	0,936	0,031	0,967	3,31	3,21
DZC+1/4DZC	0,936	0,018	0,954	1,92	1,89
DZC	0,936	0,000	0,936	0,00	0,00

The composite ground acceleration histories and the corresponding time variation damage curves for Pujol Column Specimen C10-1-2.25N are represented mutually in the Figures 5.24 and 5.25. The gray parts of these curves correspond to the foreshock/aftershock phases. The damage progression curves are comparable in form and characterized with loading history curves. The numerical values obtained in the end of each shock phase solely and the overall history are given in tabular form in the first three columns of Tables 5.14 and 5.15. In the last two columns of the table the ratios denoted by D_{fore}/D_{main} , D_{fore}/D_{total} , D_{after}/D_{main} and D_{after}/D_{total} are given illustrating the foreshock and aftershock damage effects on both main shock and overall damage.

The structural damage increases instantaneously whenever the reversal increases suddenly (Figure 5.24 and 5.26a). A comparison of the damage curves

plotted in Figure 5.26a reveals the influence of the foreshock damage, on the main shock and overall damage during their complete histories. Note here that damage inflicted to the SDOF system by the foreshock is not proportional to its intensity. It was demonstrated that the damage caused by foreshocks of one-fourth, one-third and even half amplitude do not lead to substantial damage. Increase in the foreshock amplitude result in relatively larger damage levels in the end. It refers to the nonlinear relationship between the event's intensity and damage attained in the end. The graphical representation of this evidence appears clearly in Figure 5.27 and 5.28. It should be noted that increase in the foreshock amplitude leads to decrease in the main shock damage, as can be seen from the third column of Table 5.14.

Damage curves plotted together in Figure 5.26b show the aftershock damage effect on both main shock and total damage. Increase in the aftershock amplitude does not lead to a proportional but relatively more rapidly increase in the damage attained in the end. The comparison of the analytical damage results put forward by this non-linear relationship between the earthquake excitation intensity and the damage values obtained in the end. Damage curves given in Figures 5.24 and 5.26b show that the damage from the aftershocks with one-fourth, one-third and even a half of the main shock amplitude are negligibly small and they do not lead to substantial damage. The graphical representation of this evidence can be seen also in Figure 5.27 and 5.28.

The discussions mentioned above are related to the prior earthquake and aftershock damage effects on the major or design earthquake damage, considering each of the selected ground motions separately. These randomly selected ground motions have different forms, characteristics, durations and intensities. It should be emphasized that, in many cases a structure will not be subjected to an earthquake with magnitude equivalent to the design earthquake during its lifetime. However, the probability is very high that it may be subjected to several smaller past earthquakes. Because of the series of various smaller-magnitude earthquake, no visible damage may occur and the structure will retain its integrity after it is subjected to these successive earthquakes. However, this does not mean that no damage occurs in the structure. Furthermore, there is no realistic quantification of the magnitudes of these

smaller-amplitude successive earthquakes that the structure may experience during its life time, or of the structural or nonstructural damage likely to occur. Because of these uncertainties, the damage variations obtained as a result of the inelastic time history and damage analyses of the SDOF systems subjected to various composite ground motions generated from four randomly selected ground motions should be compared to expose common sense on the foreshock and aftershock damage effects.

5.4.2.1 Effects of Foreshock and Aftershock Damage on Main Shock Damage

The effects of foreshock and aftershock damage on the main earthquake damage can be inferred from Figure 5.29 and Tables 5.16 and 5.17. Figure 5.29 contains two plots. One shows the relationships between A_{fore}/A_{main} and D_{fore}/D_{main} and the other relationships between A_{after}/A_{main} and D_{after}/D_{main} , where A and D denotes the acceleration amplitude and damage, respectively. The resultant damage values attained in the end of the foreshock and aftershock have been normalized with the damage values obtained in the end of main shocks. D_{fore}/D_{main} and D_{after}/D_{main} values are plotted all together using bar column representation, for the four different considered composite ground motions. The variation of D_{fore}/D_{main} and D_{after}/D_{main} values are comparable in form and characteristics with each other and the foreshock or aftershock intensity. The ratios of the foreshock and aftershock damage values to the main damage values attained in the end are tabulated in Tables 5.16 and 5.17. The average of these ratios are given in the last rows of the tables.

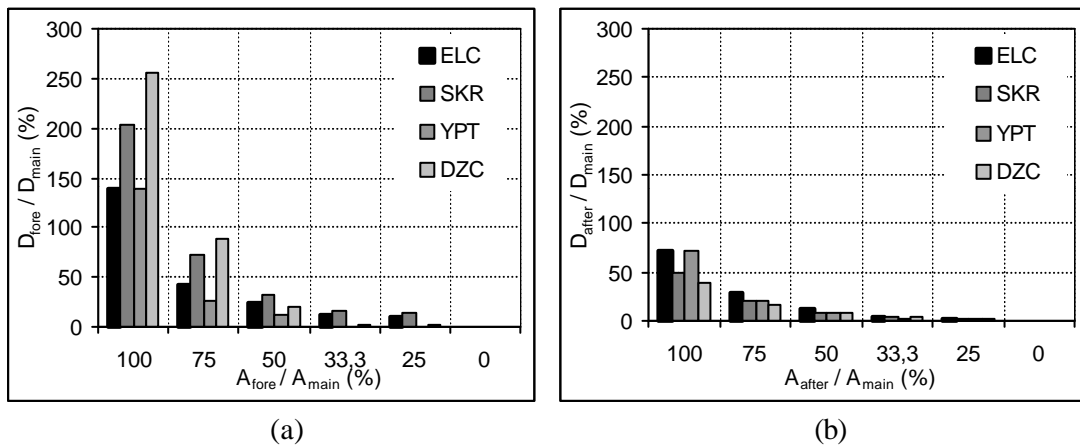


Figure 5.29 Effect of foreshock and aftershock damage on the main ground motion damage

Table 5.16 Contribution of foreshock damage to main ground motion damage

Ground Motion	$D_{\text{fore}} / D_{\text{main}} (\%)$				
	(1)+(1)	(3/4)+(1)	(1/2)+(1)	(1/3)+(1)	(1/4)+(1)
ELC	138,05	42,81	24,53	12,90	9,32
SKR	204,35	72,65	33,21	16,49	13,36
YPT	138,03	26,19	12,22	0,00	0,00
DZC	255,04	87,60	19,80	2,90	1,85
Average	183,87	57,31	22,44	8,07	6,13

Table 5.17 Contribution of aftershock damage to main ground motion damage

Ground Motion	$D_{\text{after}} / D_{\text{main}} (\%)$				
	(1)+(1)	(1)+(3/4)	(1)+(1/2)	(1)+(1/3)	(1)+(1/4)
ELC	72,44	27,88	12,18	5,13	2,88
SKR	48,94	20,92	8,16	3,55	2,13
YPT	72,45	19,90	8,67	3,06	1,53
DZC	39,21	16,13	7,48	3,31	1,92
Average	58,26	21,21	9,12	3,76	2,12

By referring to Figure 5.29 and Tables 5.16 and 5.17 the following conclusions can be drawn;

1. The resultant damage caused by the foreshocks and aftershocks is not proportional to their intensity in terms of cycle-amplitude. Increase in the aftershock amplitude leads to more damage attained in the end.
2. A history with a definite intensity acting as a foreshock and aftershock leads to substantially different amounts of damage. Damage effects of a definite intensity loading history as a foreshock (prior earthquake) and aftershock (succeeding earthquake) can be inferred by comparing both plots given in Figure 5.29, and damage variations presented in Tables 5.16 and 5.17. In respect of the main shock damage, the damage caused by a loading history acting as an aftershock is approximately one-third of the damage resulted by the same history acting as a foreshock. The histories with a quarter of the main shock amplitude acting as foreshock and aftershock, for instance, caused to average damage of 6.13 percent and 2.12 percent of the main shock damage, respectively.

5.4.2.2 Effects of Foreshock and Aftershock Damage on Total Damage

The effects of foreshock and aftershock damage on the total damage caused by the composite ground motions can be inferred from Figure 5.30 and Tables 5.18 and 5.19. Figure 5.30 illustrates the relationships between A_{fore}/A_{main} and D_{fore}/D_{main} and the relationships between A_{after}/A_{main} and D_{after}/D_{main} . In this figure the resultant damage values attained in the end of the foreshock and aftershock have been normalized with respect to the damage values obtained in the end of the composite ground motion. For the sake of simple comparison, the variations in D_{fore}/D_{total} and D_{after}/D_{total} values are plotted together. These values are comparable in form and characteristics. The ratios of the foreshock and aftershock damage values to the total damage values attained in the end are presented in Tables 5.18 and 5.19. The average of these ratios are given in the last rows of the tables.

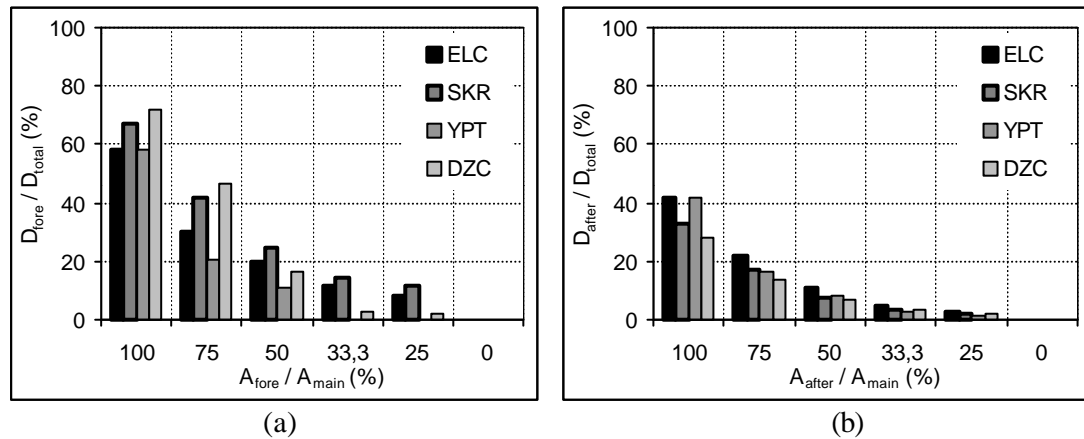


Figure 5.30 Effect of foreshock and aftershock damage on the total damage

Table 5.18 Contribution of foreshock damage to total damage

Ground Motion	$D_{fore} / D_{total} (\%)$				
	(1)+(1)	(3/4)+(1)	(1/2)+(1)	(1/3)+(1)	(1/4)+(1)
ELC	57,99	29,98	19,70	11,43	8,52
SKR	67,14	42,08	24,93	14,16	11,78
YPT	57,99	20,75	10,89	0,00	0,00
DZC	71,83	46,70	16,53	2,82	1,82
Average	63,74	34,88	18,01	7,10	5,53

Table 5.19 Contribution of aftershock damage to total damage

Ground Motion	$D_{\text{after}} / D_{\text{total}} (\%)$				
	(1)+(1)	(1)+(3/4)	(1)+(1/2)	(1)+(1/3)	(1)+(1/4)
ELC	42,01	21,80	10,86	4,88	2,80
SKR	32,86	17,30	7,54	3,42	2,08
YPT	42,01	16,60	7,98	2,97	1,51
DZC	28,17	13,89	6,96	3,21	1,89
Average	36,26	17,40	8,34	3,62	2,07

The following conclusions can be made based on the damage variations presented in Figure 5.30 and Tables 5.18 and 5.19;

1. The final damage from foreshocks and aftershocks is not proportional to their intensity in terms of the amplitude of the ground acceleration. Increase in the aftershock amplitude leads to more damage attained in the end. As can be seen from Table 5.18, as an average of the four different composite ground motions, the foreshocks with 25 percent, 50 percent, 75 percent and 100 percent amplitude of the main shock caused to average damage of 5.53 percent, 18.01 percent, 34.88 percent and 63.74 percent of the damage resulted by the main shock phase of the histories.
2. The amounts of damage by the foreshocks and aftershocks with the intensity (in terms of acceleration amplitude) up to one-third of the main shock are negligibly small.
3. The damage caused by the foreshocks with intensity ranging from 25 to 50 percent of the main shock intensity does not exceed about 18 percent of the total damage in average. The same histories acting as aftershocks that follow the main shock lead to approximately 8 percent of the total damage.

5.5 Concluding Remarks

On the basis of inelastic time history and damage analyses of SDOF systems under constant and variable amplitude inelastic displacement reversals and synthetic

ground motions, carried out to assess the effects of prior damage on structural response to subsequent earthquakes, the following conclusions are made:

1. The number of load cycles has an effect on the level of damage sustained by a reinforced concrete component. Increase in the amplitude of the constant amplitude cycles diminishes the number of cycles to failure.
2. Structural damage progression and accumulated dissipated energy follow different paths in variable amplitude loading histories. Hence, damage and cumulative hysteretic energy dissipated along a path seem to depend on the number and amplitude of cycles constituting the path. However, the resultant damage attained in the end of the loading history and accumulated hysteretic energy dissipated along the loading path are independent of the ordering of the same number and amplitude cycles along the path. The damage levels attained in the end of the different paths with the same number and amplitude cycles are almost equal. The same interpretation is valid for dissipated energy.
3. Structural damage is dependent on the ductility level for constant amplitude reversals. Damage increases rapidly during the first pulse of the constant amplitude loading history. Regardless of ductility, this damage constitutes the major part of the total damage. Later, damage progression seems to be in an almost linear path and relatively very low rate. Damage increases almost in proportion to increase in the cycle amplitudes. In this respect, the damage rule developed by Miner (1945) fails for reinforced concrete members, because it assumes that the accumulation of damage is linear and independent of load path.
4. The relationship between the earthquake excitation intensity and the resultant damage attained in the end is not linear. Increase in the amplitude leads to asymptotical increase in damage.

5. The prior earthquake damage has substantial effect on the SDOF system response to subsequent future earthquakes. Increase of the prior earthquake intensity causes reduction in the damage from the succeeding main earthquake. Damage from prior earthquakes of one-fourth and one-third amplitude of the main earthquake record is negligibly small compared to the damage caused by the main earthquake.

6. A ground motion record acting as prior earthquake and successive earthquake leads to substantially different amounts of damage. In comparison with the total damage, damage caused by such ground motion acting as prior earthquake is two-times of the damage resulted by the same ground motion acting as subsequent earthquake.

7. The same or smaller amplitude intensity succeeding earthquakes cause damage ranging up to about 60 percent of the main earthquake damage. Successive earthquake with intensity ranging from one to one-fourth of the main earthquake intensity cause to damage ranging from about 58 percent to 2 percent of the main earthquake damage, respectively.

CHAPTER 6

DAMAGE EVOLUTION FOR SELECTED BUILDINGS SUBJECTED TO REPEATED EARTHQUAKES

6.1 General

Engineering structures built in an area where earthquakes occur quite often may be subjected to earthquake excitations of smaller magnitude prior to being shaken by severe destructive earthquake excitations. The damage inflicted to structures by prior milder intensity earthquake excitations may have substantial effects on the response of structures to subsequent earthquakes. Structural damage caused by successive earthquakes can not only be attributed to defects in design or construction, but also to low cycle fatigue effects due to accumulation of damage.

In the last decade, two destructive successive ground shakings, with magnitudes exceeding 7.0, have been experienced nearly 3 months apart in the north-western region of Turkey. The distance between the epicenters of these successive ground motions was about 110 km. The two major successive earthquakes, that occurred on 17 August and 12 November 1999 in Marmara region, provide a unique possibility to verify the effect of prior earthquake damage on the structural damage and performance to future earthquakes. It is the first time that such strong successive earthquakes hit structures producing either accumulated extensive damage or collapse. It is worthwhile to note that these events constitute benchmarks to shed light on effects of low cycle fatigue on successive damage.

In this chapter it is aimed to assess the effects of prior damage on response of damaged reinforced concrete structures to subsequent future earthquakes. The motivation has arisen from the collapse or heavy damage suffered in many reinforced

concrete structures subjected to the major earthquakes occurred in 1999, in Marmara region, Turkey. These unusual building failures observed after the two major successive earthquakes in Marmara region, especially surroundings of Düzce and Bolu cities, attracted special attention of the earthquake engineering community (Sözen, 2000; Sucuoğlu and Yılmaz, 2001). Sözen stated that there may be no linear relation between the earthquake intensity and damage. Basically it was estimated that collapses probably resulted from damage accumulation that had been caused by the first (Marmara) long duration earthquake and increased by the following (Düzce) motion. It is believed that the reasons behind the seismic performance observed of the structures may be expressed via bases of low cycle fatigue phenomenon.

To assess the low cycle fatigue effects in the damage caused by the prior earthquake, two five-story reinforced concrete buildings were selected. The buildings have experienced the two destructive earthquakes. For this purpose, an inelastic time history and damage analyses of these two five-story case study buildings have been carried out using composite ground motion accelerograms composed of base input provided by these two recorded successive ground motions.

6.2 Strong Ground Motions in 1999 Marmara and Düzce Earthquakes

The Marmara earthquake strongly affected the north-western part of Turkey, especially İzmit, Sakarya, Bolu, Bursa, Düzce, Yalova, İstanbul, Zonguldak and Eskişehir. According to official records about 20 thousand people died, over 25 thousand people were injured. The number of residential houses that suffered light-to-heavy damage during this earthquake was about 214000 (USGS, 1999).

During this earthquake, ground motion was recorded totally at 34 stations, 24 of Ministry of Public Works and Settlement and 10 operated by Boğaziçi University Kandilli Observatory and Earthquake Research Institute (KOERI). The ground acceleration trace recorded in Düzce is shown in Figure 6.1. Ground acceleration during the Marmara earthquake could not be recorded at Bolu because the instrument at the branch office of Ministry of Public Works and Settlement in this site was placed immediately after the Marmara earthquake.

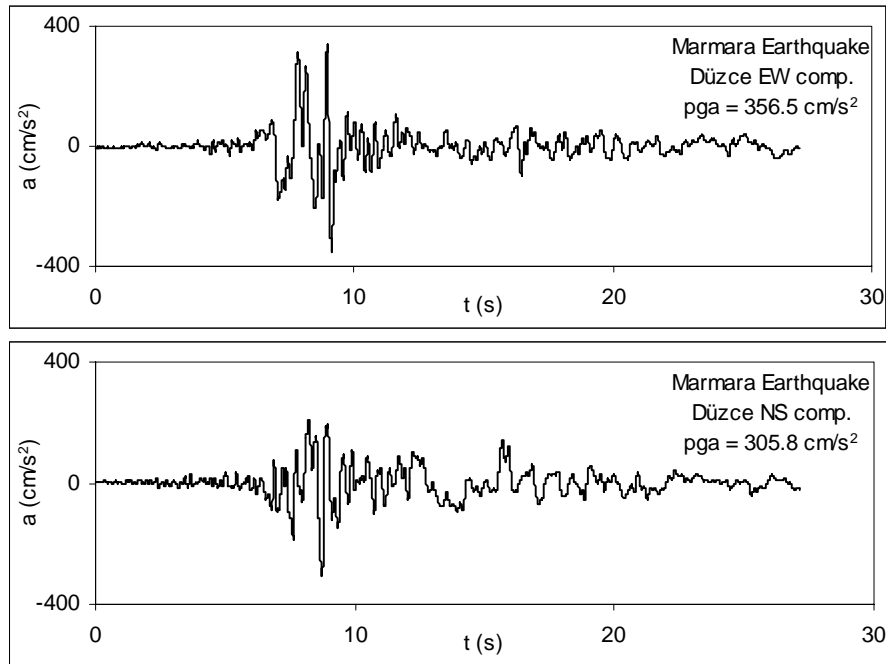


Figure 6.1 The ground motion acceleration histories of 17 August 1999 Marmara earthquake, Düzce records

The second one of the two destructive strong earthquakes shaken the west region of the North Anatolian Fault is Düzce earthquake occurred about three months after the Marmara earthquake. Officially, more than 760 people died and about 5000 people were injured during this earthquake. Loss of life was rather limited since buildings that had been damaged by the previous Marmara earthquake had already been vacated. The buildings, sustained heavy damage or collapsed during the succeeding Düzce earthquake, were generally suffered damage ranging from light-to-moderate during the earlier Marmara earthquake.

Severe effects of the 12 November 1999 Düzce earthquake were mainly concentrated in the cities of Düzce and Bolu. The buildings that sustained heavy damage in Düzce were evenly distributed over the city. Severely damaged buildings in Bolu were situated at the north of the city where one of the case study buildings is located. The high-rise buildings (5-6 story buildings) sustained more damage compared to low-rise buildings (1-2 story buildings) in both Düzce and Bolu. The 40 km long surface trace of the strike-slip fault rupture was well exposed and could be traced between Düzce and Bolu. Fault movements caused collapse of many low-rise

masonry buildings located near the line of fault rupture. Nevertheless, many other buildings that were close to the rupture surprisingly did not sustain severe damage. Occurrence of strong horizontal and vertical ground motions in Düzce resulted in overturning of parked trucks and busses.

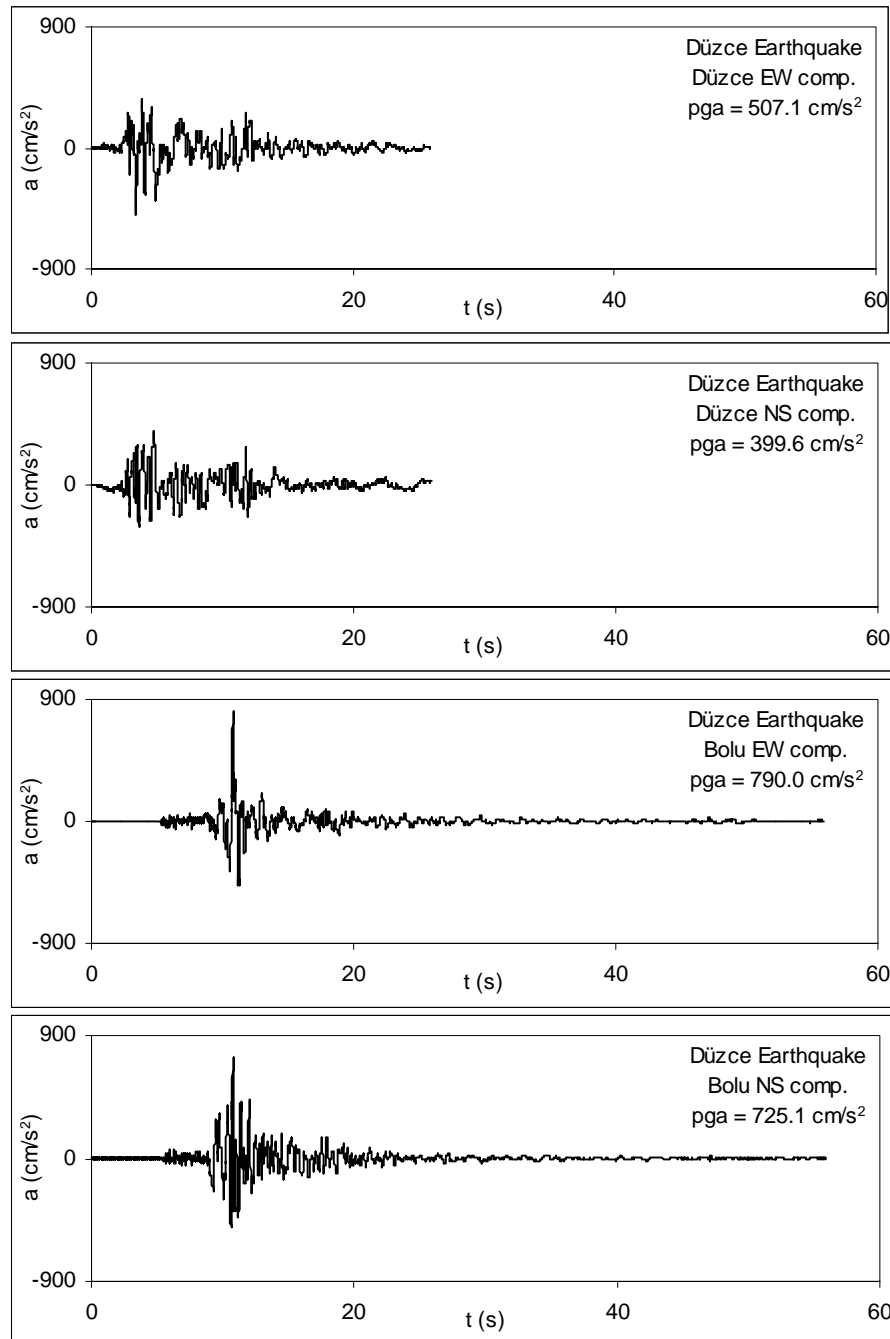


Figure 6.2 The ground motion acceleration histories of the 12 November 1999 Düzce earthquake, Düzce and Bolu records

During the Düzce earthquake, ground motion was recorded at 20 different stations of Ministry of Public Works and Settlement. The horizontal components of the ground acceleration trace recorded by the instruments at the branch office of Ministry of Public Works and Settlement in Düzce and Bolu are shown in Figure 6.2. Both East-West and North-South records of Bolu station have peak acceleration values over 0.7g, which are the highest maximum ground acceleration values ever recorded in Turkey.

Table 6.1 Ground Motion Intensity Parameters

Earthquake	Station	Dir.	Soil	ED (km)	FD (km)	PGA (cm/s ²)	EPA (cm/s ²)	PGV (cm/s)	T _{eff} (s)
Marmara	Düzce	EW	S	107.0	11.0	356.52	349.16	58.56	11.93
	Düzce	NS	S	107.0	11.0	305.82	271.47	56.49	11.89
Düzce	Düzce	EW	S	9.3	7.0	507.03	391.36	88.01	8.55
	Düzce	NS	S	9.3	7.0	399.61	427.20	69.48	9.03
	Bolu	EW	S	39.0	5.5	790.09	473.11	65.15	11.14
	Bolu	NS	S	39.0	5.5	725.13	624.40	54.91	10.89

Table 6.1 shows the characteristics of ground acceleration data of the two earthquakes recorded at Düzce and Bolu (Sucuoğlu et al. 2000). PGA values of Düzce earthquake-Bolu station records are relatively high compared to Düzce station components recorded during both Marmara and Düzce earthquakes. High PGA values were recorded at the Düzce station due its being near the epicenter and at the Bolu station due possibly to directivity effect.

6.3 Synthetic Ground Motions

Inelastic time history and damage analyses of two five-story case study buildings have been conducted, to assess the effects of prior earthquake damage on the response of MDOF frame type reinforced concrete structures to future earthquakes. In these analyses two families of synthetic accelerograms, created by superposing strong parts of the base input data provided by these two major recorded successive ground motions, have been used.

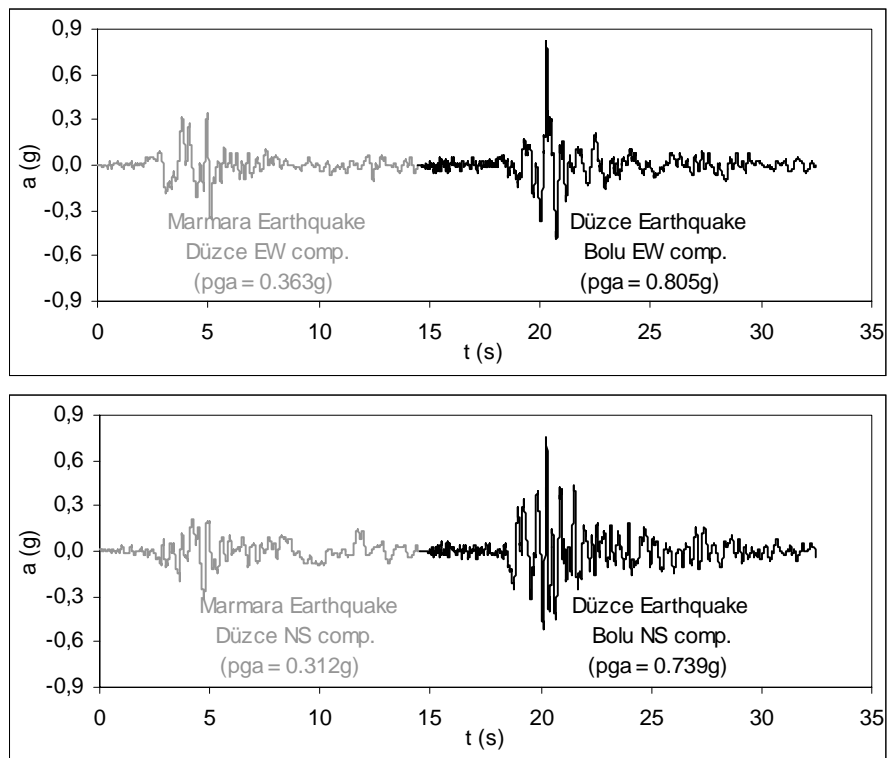


Figure 6.3 Synthetic ground acceleration histories used in the analyses of the building located at Bolu

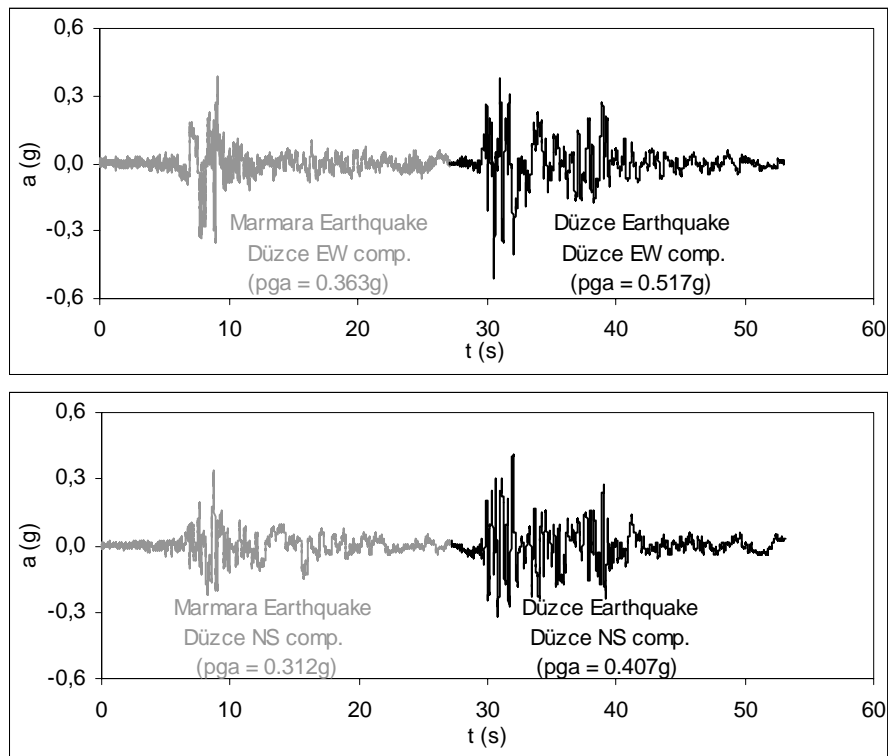


Figure 6.4 Synthetic ground acceleration histories used in the analyses of the building located at Düzce

The seismic inputs are provided successively as a continuous ground motion without a quiescent period during which the structure comes to rest. Hence the effect of first event will be carried forth to the following without returning the system to undamaged conditions. All records were scaled to ground acceleration of g . The synthetic acceleration histories used in the analyses are shown in Figures 6.3 and 6.4. In these figures, the gray colored parts of the histories denote the first event (Marmara), while the dark parts belong to the following event (Düzce) records. As far as the intensity in terms of the ground acceleration amplitude is concerned, the first earthquake excitation is relatively milder compared to the second one in both Düzce and Bolu.

The recording instrument at the branch office of Ministry of Public Works and Settlement in Bolu was placed shortly after the Marmara earthquake, hence ground acceleration during the Marmara earthquake could not be recorded at this site. The synthetic ground motion, used in the analyses of the first case study building located at Bolu, has been constituted by using the base input recorded in the nearest station placed in Düzce. Düzce is about 40 kilometers away from the location of the case study building at Bolu.

6.4 Structural Damage

In general, traditional building codes have used strength as the main parameter to judge the seismic performance problem, relegating limitation of the inter-story drift ratio in the design process. However, experience gained from past earthquakes and seismic design knowledge developed as a result of analytical and experimental research has revealed that there is a good correlation between damage and the drift ratio: the low drift ratio reflects low damage level. The importance of drift control is established when it is accepted that the earthquake induced displacements are the main causes and measure of seismic structural distortion and damage. Seismic drift calculation is required by the several seismic codes such as TEC (1998), UBC, ACI. Seismic drift control procedure is based on imposing limits on maximum seismic drift or its relative values (Sözen, 1981; Gülkan and Sözen, 1999; ATC 40, 1996).

The interstory drift ratio, defined as the difference in maximum drift response between two consecutive stories divided by the story height, was used by Sözen (1981) as a measure of damage at the story level. A drift ratio equal or smaller than 1 percent corresponds to damage in non-structural components while drift ratio greater than 4 percent may lead to irreparable structural damage or collapse. Failure is considered to occur when the drift ratio exceeds 6 percent.

Performance levels based on limitation of inter-story drift ratio are prescribed in ATC 40 (1996). In accordance with the judgmental performance limits specified in ATC 40, maximum drift ratio of 1 percent is the upper limit of the *immediate occupancy* performance level, while maximum drift ratio ranging from 1 percent to 2 percent corresponds to *damage control* level. The requirement of *life safety* performance level can be satisfied whenever the drift ratio does not exceed 2 percent (Table 6.2). According to the Turkish Earthquake Code (1998), residential buildings should be designed for *life safety* performance level under the extreme loading.

Table 6.2 Deformation limits (ATC 40, 1996)

Inter-story Drift Limit	Performance Level			
	Immediate Occupancy	Damage Control	Life Safety	Structural Stability ⁽³⁾
Maximum total drift ⁽¹⁾ (%)	1	1-2	2	$0.33 \frac{V_i}{P_i}$
Maximum inelastic drift ⁽²⁾ (%)	0.5	0.5-1.5	No limit	No limit

⁽¹⁾ Maximum total drift is defined as the inter-story drift at the performance point displacement.

⁽²⁾ Maximum inelastic drift is defined as the portion of the maximum total drift beyond the effective yield point.

⁽³⁾ V_i is the total calculated lateral shear force in story i , P_i is the total gravity load (i.e. dead plus likely live load) at story i .

Two-dimensional models of the buildings were used in these analyses. The program includes the option to determine the response of the structure at instants during the analyses. Several types of response snapshots are displacement profile, element stress ratios, dynamic characteristics, structural collapse state and element, story and overall damage indices. The program keeps track if a structural element has cracked, yielded or failed. This information is automatically reported graphically at the end of the analyses. Additional information about the damage state of the

structure can be recovered at any step of the damage analysis using the response snapshot option that can be requested by the user during pushover, quasi-static or time history analyses. This feature makes it easy to monitor the damage state of the system at stages in between the successive ground motions. The structural damage state is reported for each frame in the structure following a simple graphical convention to identify cracked or yielded elements. The symbol used for cracking is 'x', while 'o' identifies the yielding state. The symbol '*' used to denote component failure.

6.5 Case Study Buildings

Effects of the prior earthquake/s damage on the structural response of damaged buildings have been investigated using selected two five-story reinforced concrete buildings. This purpose is accomplished by performing inelastic time history and damage analyses of these two case study buildings. These analyses have been carried out using the artificial ground motion accelerograms comprised of base input provided by these two recorded ground motions. One of these buildings was located in Bolu and, the other was in Düzce city. They were designed considering the Seismic Code. The first case study building was a public building and used as the branch office of the Ministry of Public Works and Settlement at Bolu. The second one was a private building located in Düzce. Analytical damage analyses results are interpreted considering the observed damage state of the structures. To determine the prior earthquake damage effects, the overall structural damages caused by the following 12 November Düzce earthquake has been quantified using the overall structural damage index of the previous (Marmara) destructive ground motion.

6.5.1 The Ministry of Public Works and Settlement Building at Bolu

The building was a five-story reinforced concrete building located in Bolu, approximately 39 km away from the epicenter of the 12 November 1999 Düzce earthquake. This building was designed and constructed in the 1980s. The photographs of the exterior perspective and backside of the building taken after the earthquake are shown in Figure 6.5. In the same site, there are four buildings other

than this building. Their primary use has been as the branch office of Ministry of Public Works and Settlement. A simple key plan showing locations of these buildings is given in Figure 6.6.



Figure 6.5 Damage state of the case study building

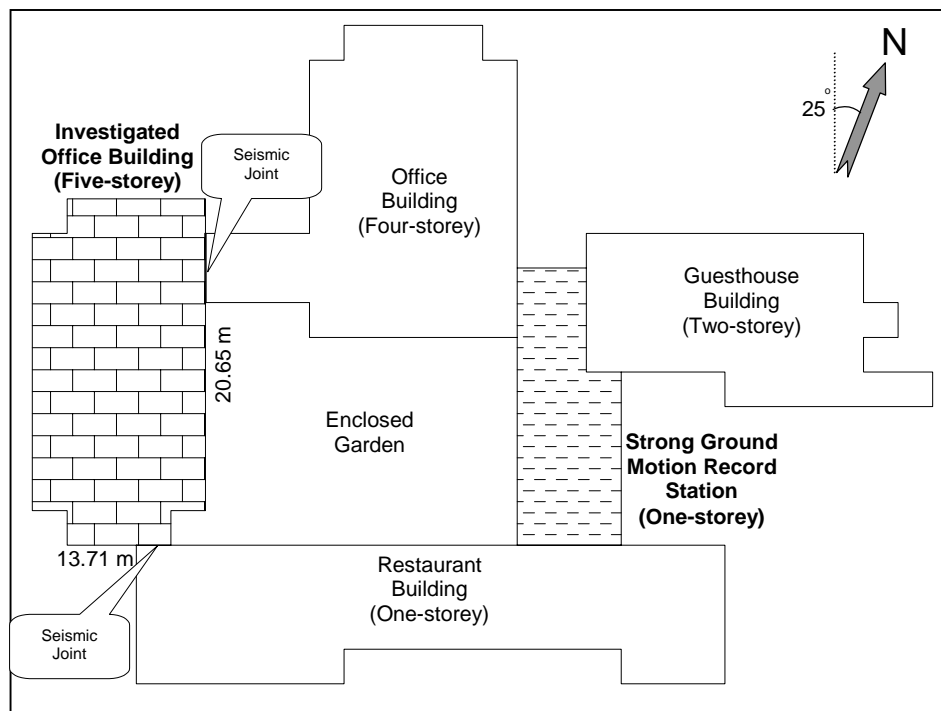


Figure 6.6 Key plan showing locations of buildings

The building was rectangular in plan and the dimensions measured from out to out are 20.65 by 13.71 meters. A story plan area is 230 m². It has three bays both in the longitudinal (north-south) and transverse (east-west) directions of the building. The exterior frames of the building were perimeter beams with depths of 1.2 m. Seven columns of this structure can be classified as ‘shear walls’ according to the Turkish Earthquake Code (TEC), 1975 that was applicable when the building was designed. Four of these are oriented in the North-South direction and the other three are L-shaped columns. Except for L-shaped columns at corners and three shear walls oriented in the longitudinal direction of the building, dimensions of the columns in addition to amount of longitudinal reinforcement in these members decrease progressively from the lower to the upper stories. However, dimensions of beams and amount of longitudinal reinforcement in them do not vary from story to story. The longitudinal direction of the building is about 25° counterclockwise from the north-south direction. Effect of this deviation is ignored in the analyses.

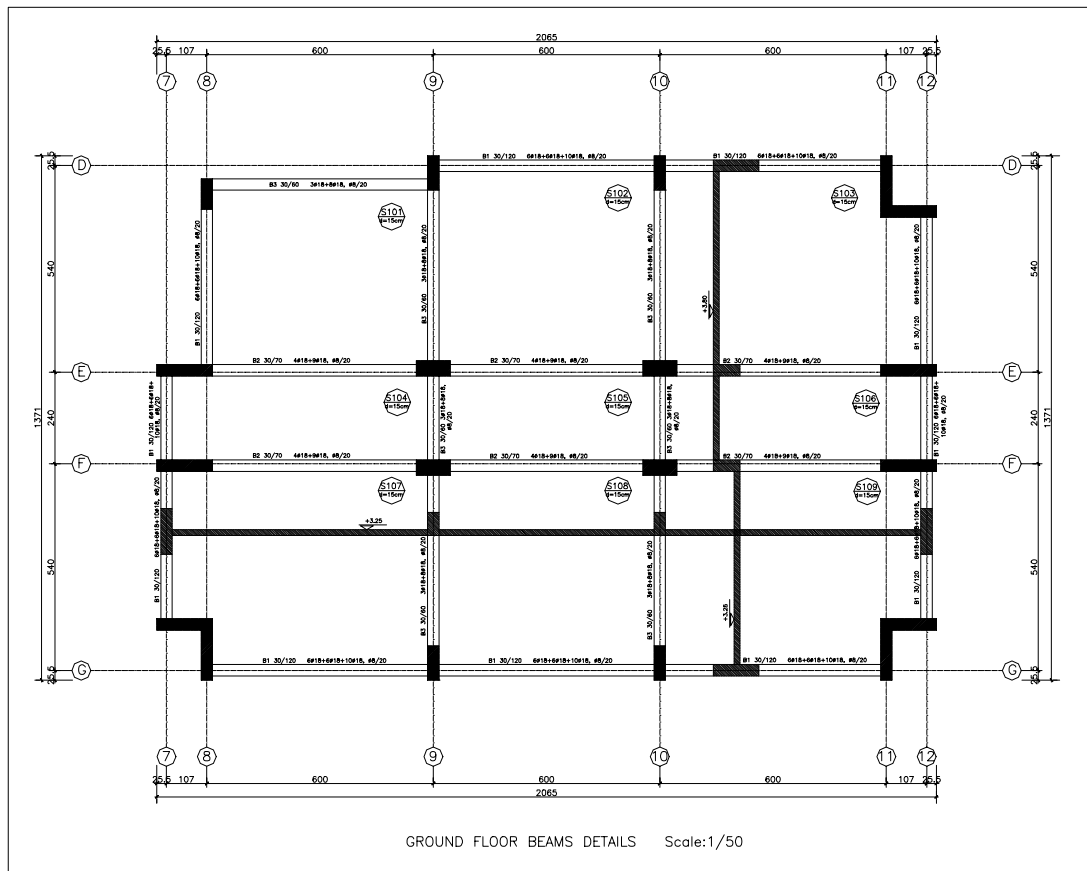


Figure 6.7 Ground floor plan

The snapshot of three-dimensional elevation of the building model is presented in Figure C.1 of Appendix C. The ground floor plan is presented in Figure 6.7. Samples of floor and column application plans indicating the dimensions and reinforcements of beams and columns can be seen in Figures C.2 and C.3. The ground story height was 3.8 m, while the height of the upper stories was 3.2 m. Slab thickness was 15 cm unchanging throughout the building. At the ground floor and the fourth floor, the number of masonry infill walls is less than that at other floor levels. Therefore the infill walls will not be taken into consideration in the analytical models. Seismic performance of the building was evaluated by Çağnan (2001) via performing its three dimensional nonlinear dynamic analyses.

In the design calculations, the following characteristic material properties had been specified for the building. Normal weight concrete having a characteristic strength of 16 MPa was required for the beams, columns and slabs. Grade-220 (St-I) reinforcement was required as longitudinal and transverse reinforcement in all-structural members. After the 12 November 1999 Düzce earthquake, engineers of the Ministry of Public Works and Settlement took several concrete samples for testing. The average compressive strength was found to be 20 MPa. They also checked the amount of longitudinal reinforcement in some of the columns. It is seen that the required area of reinforcement was provided in almost all columns. Although some design and construction mistakes such as short columns, deep beams and inadequate confinement at joints had been made, the building is a well designed and built structure. It was well maintained before the 12 November 1999 Düzce earthquake and might have sustained light or non-damage during the 17 August 1999 Marmara earthquake that occurred approximately three months before the Düzce earthquake.

Note here that damage in this building by the successive earthquake of 12 November 1999 was rather heavy. The damage consisted primarily of shear failures at the top of columns. The major limitation of the existing damage indices is that they are formulated and validated almost exclusively on the basis of flexural response, neglecting the effect of shear as a cause of seismic damage (Williams et al, 1997). However, experience in recent earthquakes suggests that structures often fail in shear or in combined shear and flexure. On the basis of comparisons against

one set of shear-dominated tests, Williams et al (1997) maintained that the relatively simple, deformation-based damage indices such as modified Park and Ang damage model provide a more reliable indication of the various damage levels than many of the apparently more sophisticated models. Since the case study buildings damage is shear-dominated, it is believed that use of the IDARC incorporating general features of modified Park and Ang damage model is an appropriate choice.

6.5.1.1 Observed Damage

Damage state of the building after the Marmara earthquake of August 17, 1999 was not recorded. However, after the Düzce earthquake of 12 November 1999, the sustained damage distribution was recorded carefully throughout the building. It was determined that during the Düzce earthquake, the case study building sustained severe damage that included column shear failures at various locations of the lowest three stories. All structural failures occurred as a result of inadequate shear capacity of columns. The short column effect due to masonry infill walls with opening and peripheral beams with unusual depths (1.2 m) and inadequate confinement in columns were the main causes of these failures. Flexural cracks were visible in almost all beams. Some of the ground story beams had diagonal shear cracks. The recorded damage distribution after the Düzce earthquake is presented in the following photographs in Figures 6.8 to 6.38.



Figure 6.8 Front and rear elevations of the building after Düzce earthquake



Figure 6.9 Diagonal crack in column D8 at the ground story



Figure 6.10 Diagonal crack in column D9 at the ground story



Figure 6.11 Failed D10 columns at the ground and first stories



Figure 6.12 Failed column D10 at the ground story



Figure 6.13 Column D12 at the ground story



Figure 6.14 Shear cracks in column E8 at the ground story



Figure 6.15 Diagonal crack in column E9 at the ground story



Figure 6.16 Diagonal cracks in column E10 at the ground story



Figure 6.17 Diagonal cracks in column E12 at the ground story



Figure 6.18 Cracked masonry infill walls between D9 and D12 columns at the ground and first story levels (rear elevation)



Figure 6.19 Diagonal crack in column F8 at the ground story

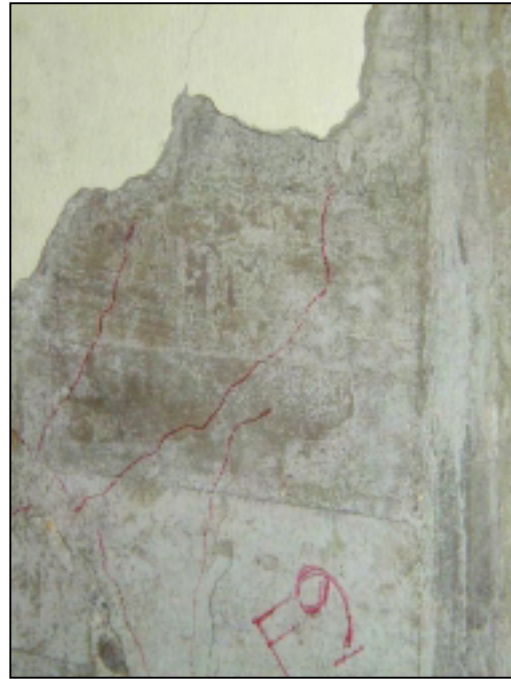


Figure 6.20 Diagonal crack in column F9 at the ground story



Figure 6.21 Crack observed in column F10 at the ground story



Figure 6.22 Diagonal crack in column F12 at the ground story

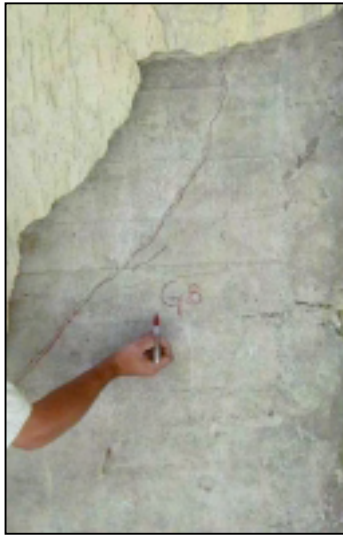


Figure 6.23 Diagonal crack in column G8 at the ground story



Figure 6.24 Diagonal crack in column G9 at the ground story



Figure 6.25 Column G10 at the ground story



Figure 6.26 Flexural cracks in the beam spanning between D10 and D12 at the ground story



Figure 6.27 Severely damaged column D10 at the first story



Figure 6.28 Column G12 at the first story



Figure 6.29 Diagonal cracks in column E9 at the first story



Figure 6.30 D9 columns at the first and second stories



Figure 6.31 G12 and F12 columns at the first story



Figure 6.32 Collapsed infill wall between columns D10 and E10 at the first story



Figure 6.33 Severely damaged infill wall between columns F9 and F7 at the first story



Figure 6.34 Severely damaged infill wall between columns D12 and F12 at the first story



Figure 6.35 Severely damaged infill wall between columns G12 and F12 at the first story

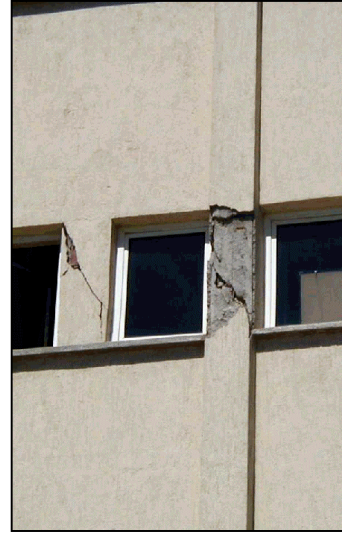


Figure 6.36 Column G9 at the second story



Figure 6.37 Diagonal crack in column F9 at the second story

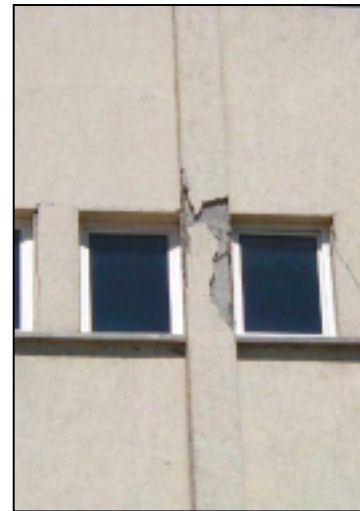


Figure 6.38 Diagonal crack in column G10 at the second story

6.5.1.2 2D Modeling and Inelastic Time History and Damage Analyses

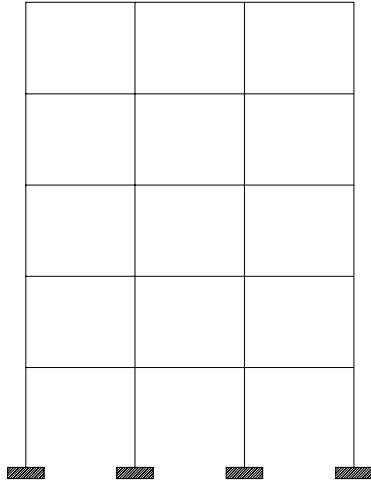
At this stage of the research, the inelastic time history and damage analyses of this building were performed under artificial composite ground motions comprising the damageable strong parts of the experienced ground motions. Figure 6.3 shows the synthetic ground motion acceleration traces.

The building is modeled as a series of plane frames linked by rigid horizontal elements. Setting the hinge moment to zero and condensing out the corresponding degree of freedom model the rigid link member hinges. Each frame is in the same vertical plane, and no torsional effects are considered. Since the floors are considered infinitely rigid, identical frames are simply lumped together. Input data is only prepared for each of the typical frames. Two-dimensional frame models of the building were prepared in both longitudinal and transverse directions for the inelastic time history and damage analyses. The structural system has three bays in both principal directions. As indicated in Figure 6.6, the east-west and north-south directions are slightly deviated from the longitudinal and transverse directions of the building. Except for one rectangular column located in the corner, the system is symmetric in plan in both directions as shown in Figure 6.7. The structural system having ordinary properties is evaluated as moderately deteriorating system (MOD). Hence the hysteretic model deterioration parameter values proposed in the third chapter for such systems have been used in the analyses.

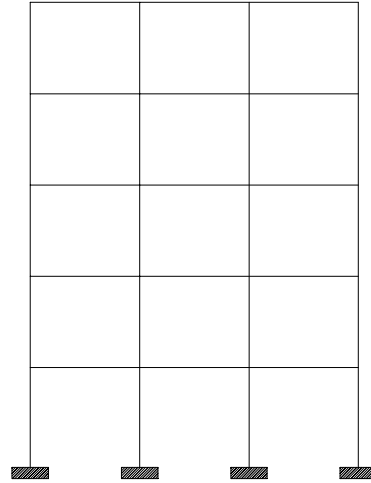
6.5.1.2.1 Transverse (East-West) Direction of Building

Figure 6.39 shows the 2D models composed of frames in transverse (east-west) direction of the building. Damage states of the corresponding frames computed after the Marmara and Düzce earthquakes are given mutually in Figures 6.40 and 6.41, respectively.

The roof drift ratio and base shear ratio variations and overall damage progression curve, which were computed by applying only the transverse component of the synthetic ground acceleration, are presented in Figure 6.42.

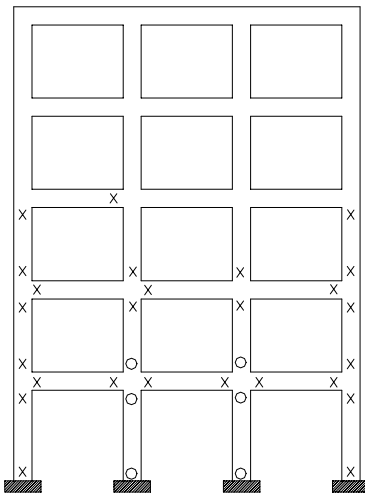


Frame 9

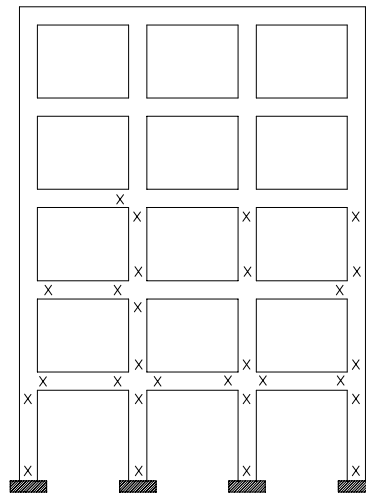


Frame 8

Figure 6.39 2D Frame model used in the inelastic analyses in transverse (EW) direction

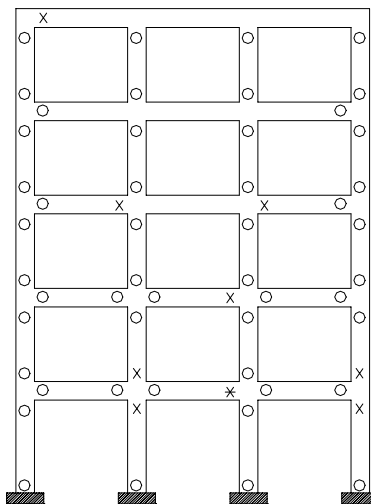


Frame 9

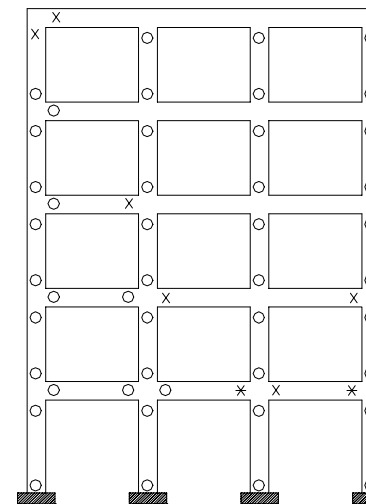


Frame 8

Figure 6.40 Damaged state of 2D Frame model used in the inelastic analyses in transverse (EW) direction after Marmara earthquake (x : crack , o : yield , * : failure)



Frame 9



Frame 8

Figure 6.41 Damaged state of 2D frame model used in the inelastic analyses in transverse (EW) direction after Düzce earthquake (x : crack, o : yield, * : failure)

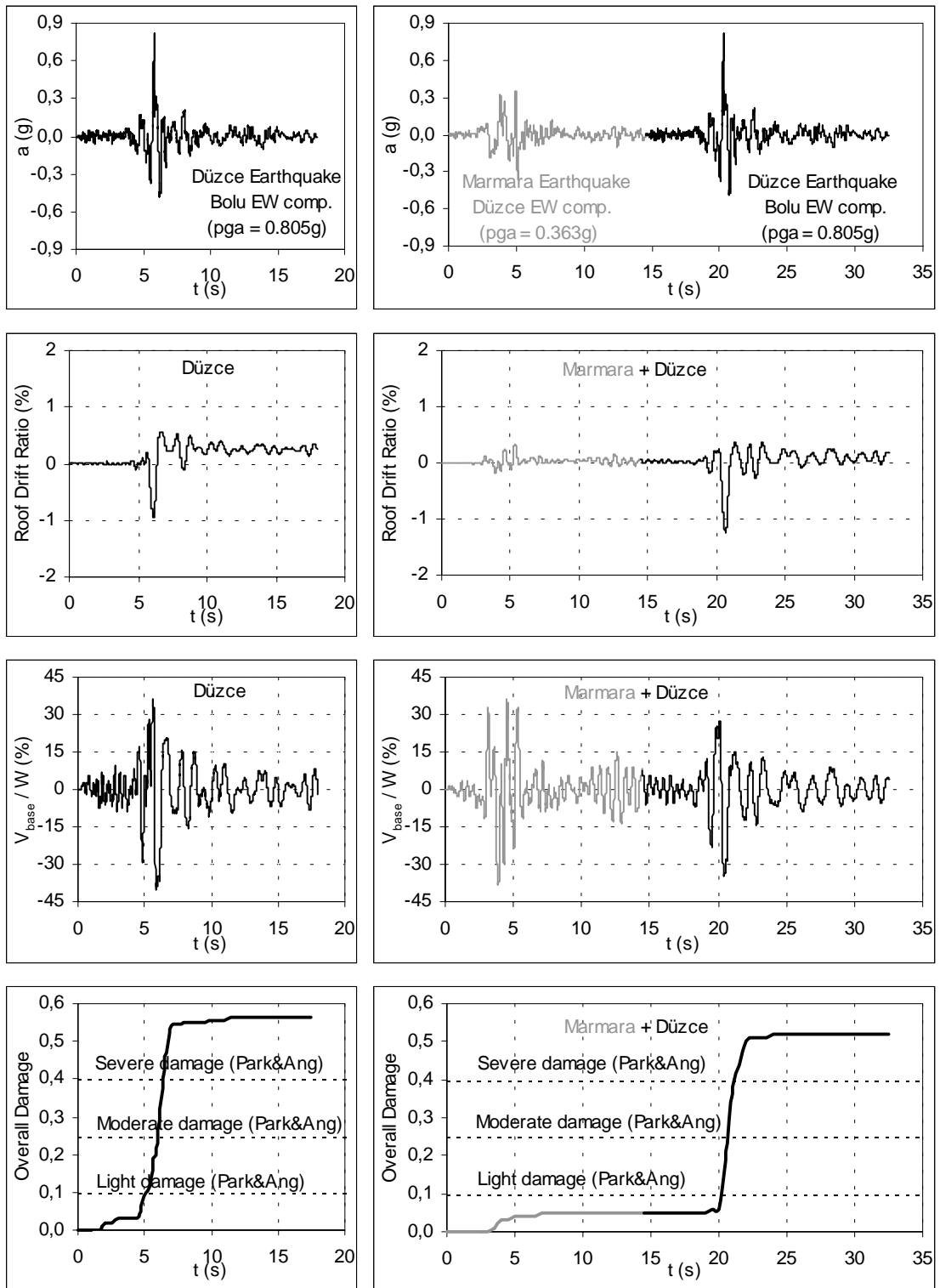


Figure 6.42 Ground acceleration histories, roof drift ratio variations, base shear ratio variations and damage curves for transverse (east-west) direction model of the building located at Bolu

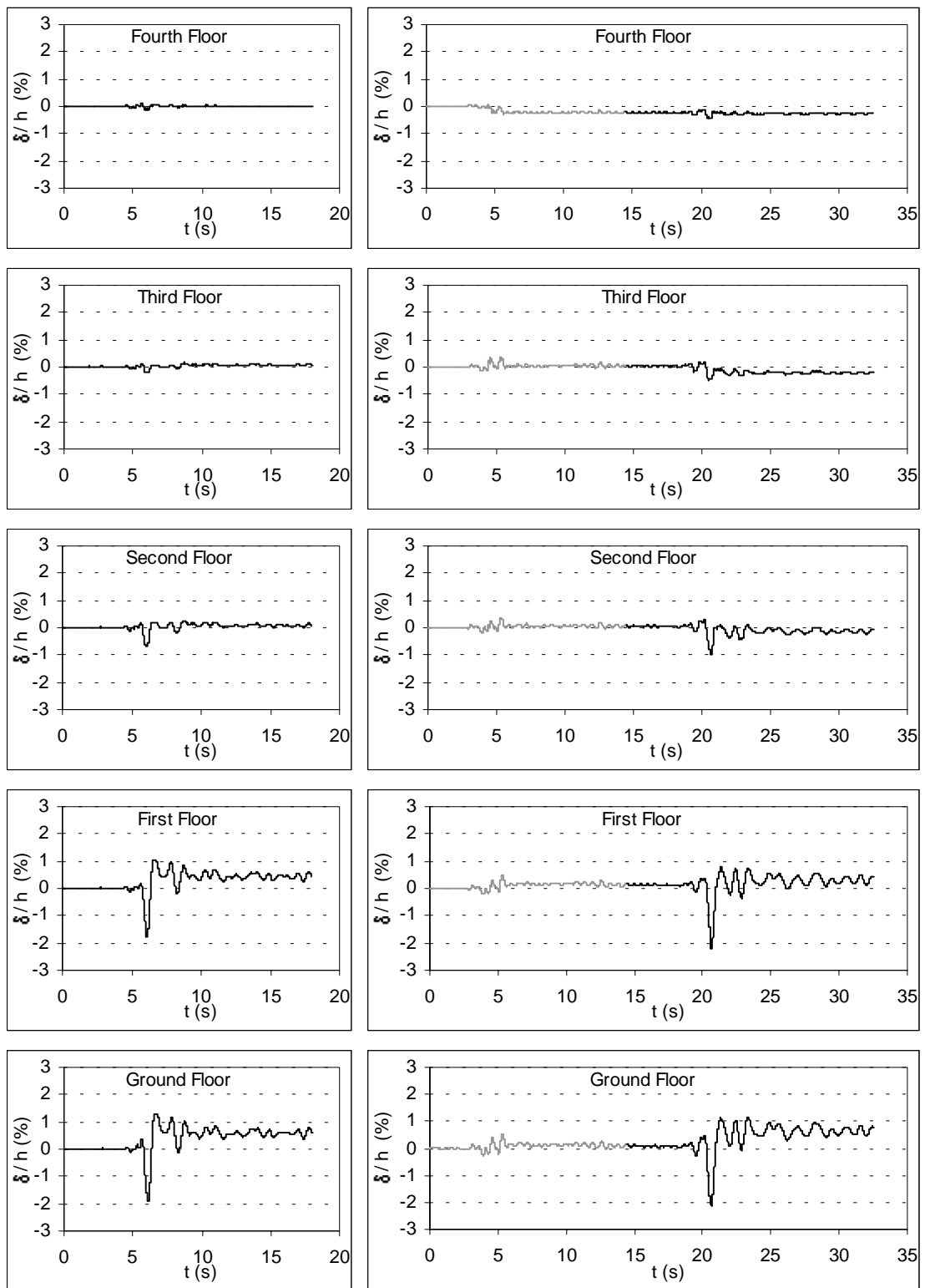


Figure 6.43 Interstory drift ratio histories for transverse (east-west) direction model of the building located at Bolu

The curves placed at the topmost of Figure 6.42 are the single (Düzce) and synthetic (Marmara + Düzce) ground acceleration histories used in the analysis. The story drift histories in the transverse direction of the building are shown in Figure 6.43. The gray parts of the relationships in Figures 6.42 and 6.43 are belonging to the Marmara earthquake.

Table 6.3 Maximum response values for the transverse (EW) direction of the building

Ground Motion	PGA (g)	Roof Drift Ratio (%)	V_{base} / W (%)	Overall Damage
Düzce	0.805	0.94	39.9	0.57
Marmara+Düzce [1] [2]	0.363[1], 0.805[2]	0.31[1], 1.23[2]	37.5[1], 33.8[2]	0.52 (0.05+0.47)

Maximum response values obtained for the transverse (east-west) direction of the building, subjected to both single and synthetic ground motion, are presented in Table 6.3. Peak values of the inter-story drifts and drift ratios resulted by both single and synthetic ground motion are summarized in Table 6.4.

Table 6.4 Maximum drift response in the transverse (EW) direction of the building

Story	Düzce Earthquake		Marmara + Düzce Earthquakes	
	Interstorey Drift (mm)	Drift Ratio (%)	Interstorey Drift (mm)	Drift Ratio (%)
5	3	0.11	13	0.44
4	7	0.21	14	0.47
3	22	0.67	29	0.97
2	57	1.77	71	2.20
1	72	1.90	80	2.12

Inspection on the roof drift ratio, base shear ratio and damage curves in Figure 6.42 and inter-story drift ratios in Figure 6.43 revealed that there is rapid increases at time values corresponding to the sudden increases in both single and synthetic ground motions. The overall damage inflicted to the system by the Marmara earthquake remains below the light damage level, meaning non-damage would occur at the first event of the synthetic ground motion.

Maximum roof drift ratio of 1.23 percent is obtained during the synthetic ground motion whereas it is found as 0.94 percent during the single (Düzce) ground motion. As seen in Figure 6.43 the structure was observed to undergo significant permanent sway in the transverse direction. At the ground floor the permanent drift was about 0.7 percent, and it was less than 1 percent, which is commonly accepted as the permanent drift ratio about which significant structural strength deterioration and stiffness degradation occurs and second order effects become significant.

It is observed from the inter-story drift ratio histories resulted by the synthetic ground motion that peak story drift ratios obtained for the lowest two floor levels are significantly higher than those obtained for the other three floor levels. Peak story drift ratios obtained for the ground and first floor levels exceed drift limit of 2 percent given by ATC 40 (1996) for *life safety* performance level. Peak story drift ratios obtained for the other floor levels did not reach the drift limit of 1 percent given by ATC 40 (1996) for *immediate occupancy* performance level (Figure 6.43). It should be noted that peak drift response at each floor and at the top of the model exposed to synthetic ground motion is slightly larger than that for the same system subjected to single (Düzce) ground motion. It is shown that prior damage does not have substantial effect on maximum drift response in future larger earthquakes.

Similarly, base shear attains peak values of 37.5 percent and 33.8 percent of the total building weight for the first and second events of the synthetic ground motion, whereas it reaches 39.9 percent whenever the same system is exposed to single ground motion (Figure 6.42 and Table 6.3). Reduction in the lateral load carrying capacity strongly indicates the softening and deterioration of the system during the prior earthquake.

It has been demonstrated that although the prior earthquake damage does not substantially affect the maximum drift response in future larger earthquakes, it has significant effects on the damage due to succeeding earthquake. It can be stated that a structural system with a prior damage suffers less damage in an earthquake in comparison with the one without a prior damage (Figure 6.42).

IDARC2D v5.0 provisions were made so that the user can request printing of the variation of the fundamental period of the structure as the analysis progresses (Valles et al, 1996). The user can request response snapshots during the analysis. To monitor the softening of the system the variation of the fundamental period, at the ends of both the single and each of the two successive ground motions and undamaged state of the building, is determined via requested snapshots.

Table 6.5 Modal Period variations in the transverse (EW) direction of the building

Mode	Undamaged State	Düzce Earthquake	Marmara + Düzce Earthquakes	
			End of first event (Marmara Earth.)	End of second event (Düzce Earth.)
1	0.37	0.81	0.54	0.94
2	0.12	0.18	0.18	0.22
3	0.06	0.09	0.10	0.12
4	0.03	0.06	0.06	0.07
5	0.02	0.04	0.04	0.05

The first five vibration modes, for the case study building states at the end of each event in addition to its undamaged state, were computed by carrying out an eigenvalue analysis. Results obtained from this analysis are presented in Table 6.5. As can be seen from the variation of the modal periods, the period affected by each event, resulted in softening of the system. In case of the synthetic ground motion, the first mode period reached a value of about 1 s at the end of the second event (Düzce earthquake), whereas it is 0.81 s during the single ground motion. Prior earthquake damage reduces the lateral stiffness of the structure significantly; letting the structure take less lateral load. This accompanies with increase in the fundamental period. The softening of the systems can be observed also from the distances in between the tips of the roof drift ratio and base shear ratio traces given in Figure 6.42.

6.5.1.2.2 Longitudinal (North-South) Direction of Building

2D models of the frames in the longitudinal direction of the building are shown in Figure 6.44. Damage distribution in the frames after the first and second events are presented in Figures 6.45 and 6.46, respectively.

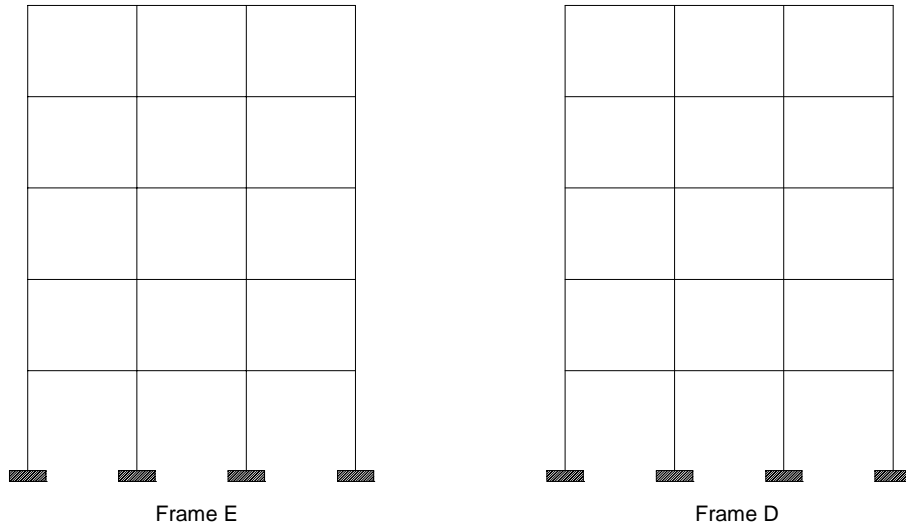


Figure 6.44 2D Frame model used in the inelastic analyses in longitudinal (NS) direction

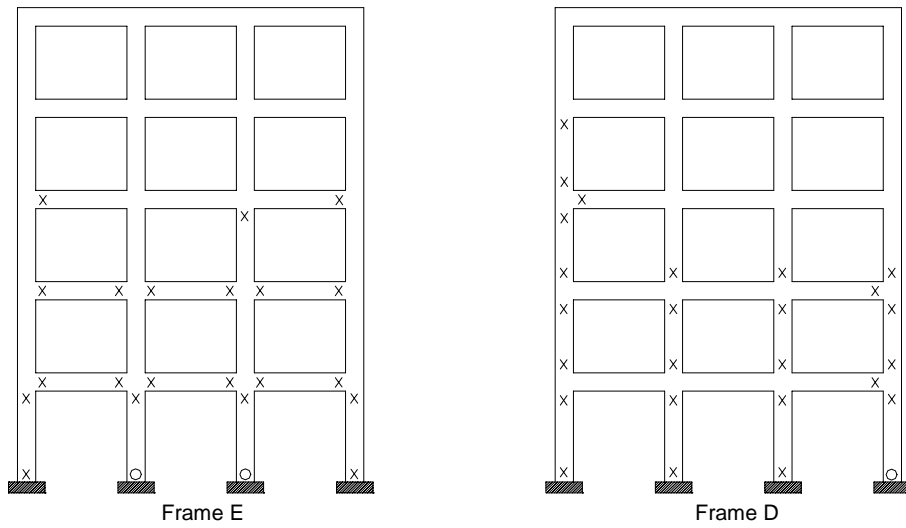


Figure 6.45 Damaged state of 2D Frame model used in the inelastic analyses in longitudinal (north-south) direction after Marmara earthquake (x : crack , o : yield, * : failure)

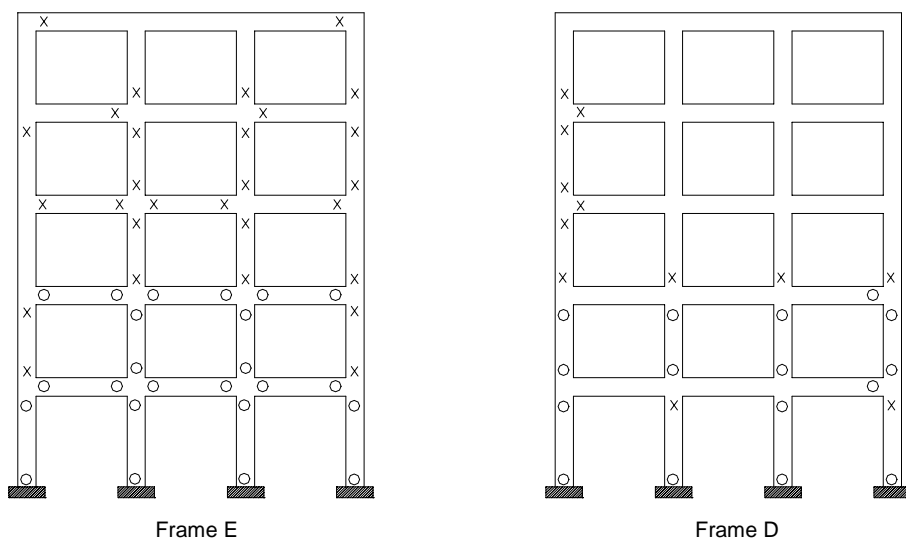


Figure 6.46 Damaged state of 2D frame model used in the inelastic analyses in longitudinal (north-south) direction after Düzce earthquake (x : crack , o : yield, * : failure)

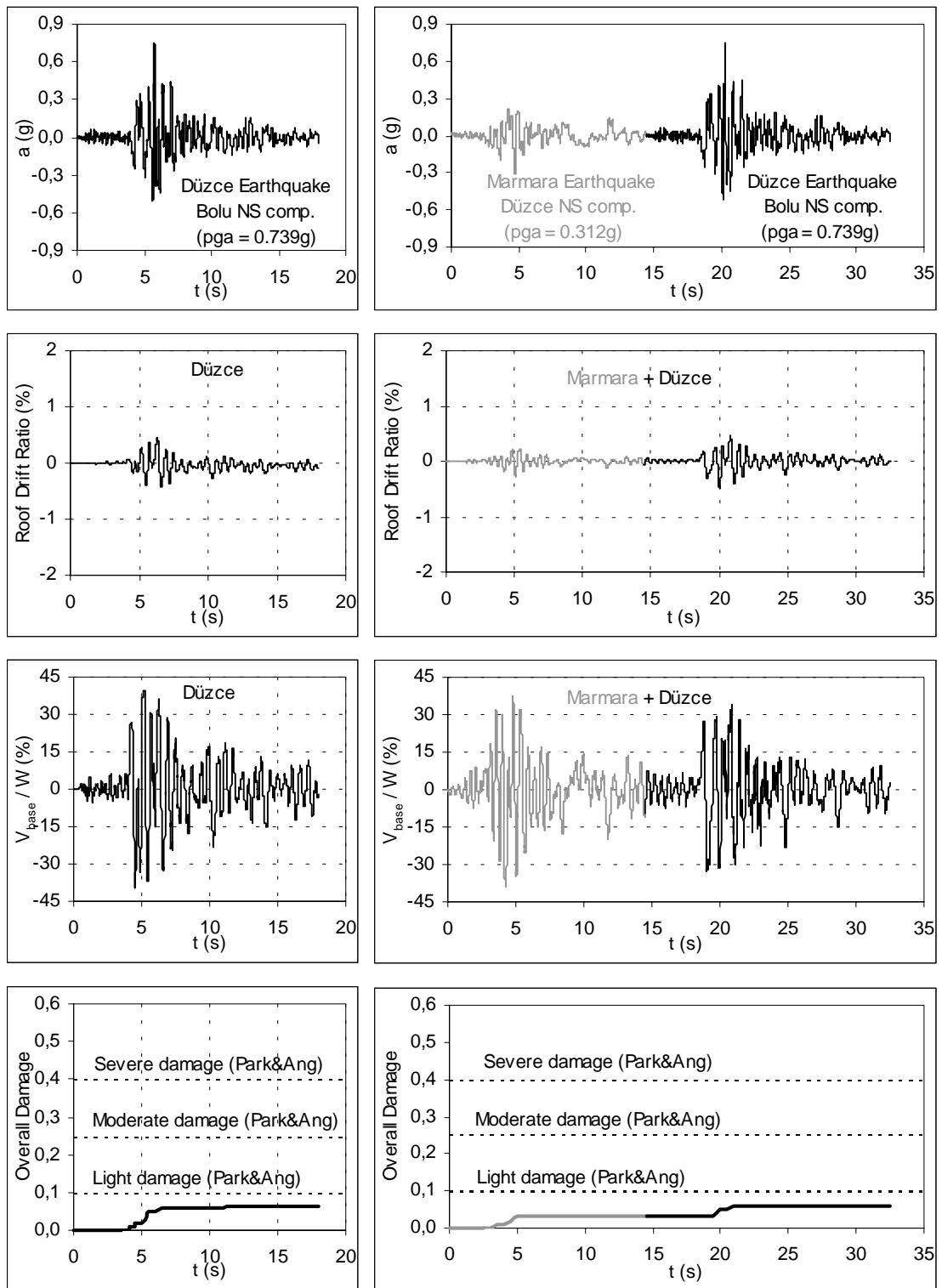


Figure 6.47 Ground acceleration histories, roof drift ratio variations, base shear ratio variations and damage curves for longitudinal (north-south) direction model of the building located at Bolu

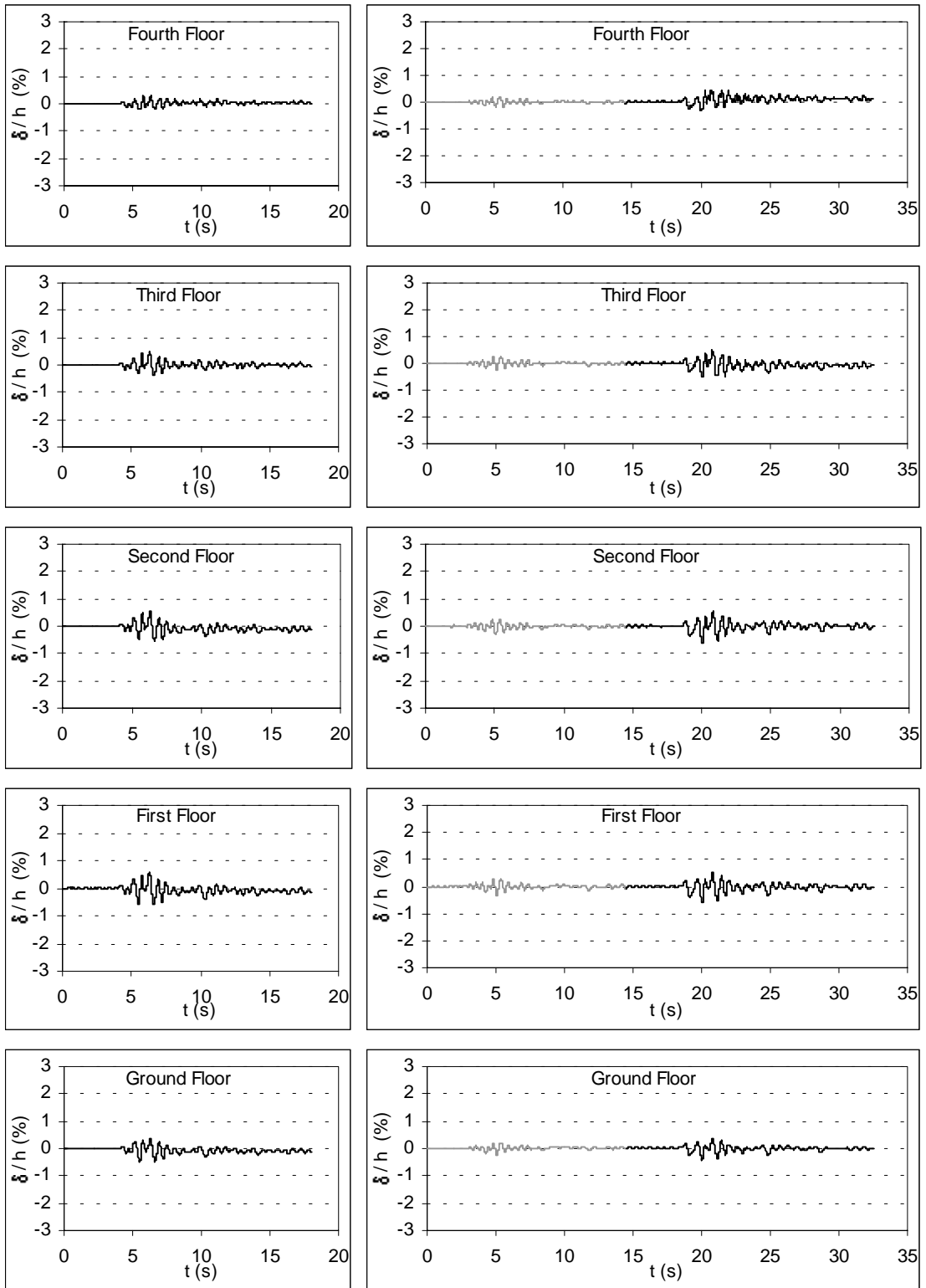


Figure 6.48 Interstory drift ratio histories for longitudinal (north-south) direction model of the building located at Bolu

In addition to the synthetic ground acceleration history used in the analysis, the roof drift ratio, base shear ratio variation and overall damage progression curve, are presented in Figure 6.47. The topmost figure indicates the synthetic ground acceleration histories used in the analysis. The gray parts of these relationships are belonging to the first event, the Marmara earthquake. Maximum response values obtained at the ends of the single and synthetic ground motions for the longitudinal (north-south) direction of the building are tabulated in Table 6.6.

Table 6.6 Maximum response values for the longitudinal (NS) direction of the building

Ground Motion	PGA (g)	Roof Drift Ratio (%)	V_{base} / W (%)	Overall Damage
Düzce	0.739	0.44	39.6	0.06
Marmara+Düzce [1] [2]	0.312[1], 0.739[2]	0.24[1], 0.45[2]	38.3[1], 33.9[2]	0.06 (0.03+0.03)

Table 6.7 Maximum drift response in the longitudinal (NS) direction of the building

Story	Düzce Earthquake		Marmara + Düzce Earthquakes	
	Interstorey Drift (mm)	Drift Ratio (%)	Interstorey Drift (mm)	Drift Ratio (%)
5	9	0.28	10	0.45
4	15	0.46	16	0.50
3	17	0.55	19	0.60
2	19	0.59	19	0.61
1	18	0.47	16	0.42

Figure 6.47 reveals that sudden increases in the reversals cause to rapid increases in the roof drift ratio, base shear ratio and damage. At the end of the first event, the overall damage of the system remains below the light damage level, meaning that no damage would occur at this stage of the history. The overall damage caused by the succeeding Düzce earthquake is also negligibly small. The overall damage index, obtained at the end of the synthetic ground motion history, does not reach the light damage level specified for modified Park and Ang damage model.

The roof drift ratio history is shown in Figure 6.47. In this direction, maximum roof drift ratio of 0.446 percent was obtained at 20 s, during the second event of the synthetic ground motion. The story drift histories in the longitudinal direction of the building are shown in Figure 6.48. The peak response values (roof drift ratio, base shear, overall damage index and inter-story peak drift ratios) are tabulated in Tables 6.6 and 6.7. Inter-story peak drift ratios obtained for all floor levels did not reach the drift limit of 1.0 percent given by ATC 40 (1996) for *immediate occupancy* performance level.

Calculated base shear ratio history in the transverse direction of the building is presented in Figure 6.47. Base shear is quite high between 4-7 s of the single ground motion, and 3-7 s during the first event and between 18-23 s during the second event of the synthetic ground motion. The base shear reaches to 39.6 percent when the undamaged system exposed to the single ground motion. It attains its peak values of 38.3 percent and 33.9 percent of the total building weight for the first and second events of the synthetic ground motion. (Figure 6.47 and Table 6.6). Reduction in the lateral load resistance apparently indicates the softening and deterioration of the system during the prior earthquake.

It can be shown that although the prior earthquake damage does not substantially affect the maximum drift response in future larger earthquakes, it has significant effects on the damage from succeeding earthquake. The structural system with a prior damage suffers less damage in an earthquake in comparison with the one without a prior damage (Figure 6.47).

Table 6.8 Modal Period variations in the longitudinal (NS) direction of the building

Mode	Undamaged State	Düzce Earthquake	Marmara + Düzce Earthquakes	
			End of first event (Marmara Earth.)	End of second event (Düzce Earth.)
1	0.38	0.54	0.48	0.68
2	0.11	0.17	0.15	0.20
3	0.06	0.08	0.07	0.10
4	0.03	0.05	0.04	0.06
5	0.02	0.03	0.02	0.03

Determination of structural response at instants during the time history and damage analysis is optional in IDARC. Hence, response snapshots are requested during the analysis to determine the variation of the fundamental vibration period at the ends of the successive motions. The first five vibration modes are obtained for the state of the longitudinal direction of the building. The vibration periods are found for the undamaged state and end of the first and second events, respectively. Results obtained are presented in Table 6.8. As can be seen from the variations in the modal periods, the system affected by both events. The first mode period of the undamaged state of the building in this direction is 0.38 s. It is 0.54 s at the end of the single ground motion. During the synthetic ground motion, it rises up to 0.48 s at the end of the Marmara earthquake and increases further at the end of the succeeding Düzce earthquake, reaching a peak value of 0.68 s. Increase in the fundamental stems from degradation in the lateral stiffness of the structure caused by sustained certain level of damage. Deterioration in the system lets the structure to take less lateral load. The variation of the fundamental vibration period of the structure can be observed from variation of distance between the tips of each two successive cycles shown in the roof drift ratio trace (Figure 6.47).

6.5.1.3 Discussions on Calculated and Observed Damages

Reliable information about the damage state of the building after the Marmara earthquake, 17 August 1999, was unavailable. The damage state due to the first event, found analytically, dominated of cracks (Figures 6.40 and 6.45). This refers to non-damage or minor damage state according to the damage classification specified for IDARC. Comparison of the observed and the analytically found damage could not be performed, since there is no available information about the observed damage state of the building after the Marmara earthquake.

However, it was determined that during the 12 November 1999 Düzce earthquake, the case study building sustained severe damage including column shear failures at the top of the columns at various locations of the ground and first floors. Main structural damage was concentrated in the first three floors. Damage consisted primarily of shear failures. Crushing of concrete was accompanied with buckling of

longitudinal steel bars. Diagonal shear cracks, which are indicative of shear distress, were also observed in many columns. Flexural cracks were visible in almost all beams. Some of the ground floor beams had diagonal shear cracks. Damage distribution was recorded throughout the building carefully and presented in Figures 6.8 to 6.38. Analytically computed damage results due to the synthetic ground motions are shown in Figures 6.41 and 6.46 for both transverse and longitudinal directions of the building.

It should be emphasized that a good match was observed between the damage states found analytically and observed after the Düzce earthquake, especially in the first two stories that suffered heavy damage. At the ground and first stories of the transverse (east-west) direction of the building suffered severe damage due to excessive drifts exceeding limit of 2.0 percent given by ATC 40 (1996) for *life safety* performance level (Figure 4.42). The damage sustained includes beam failures at the ground floor and is captured analytically. Consequently, on the basis of the damage analyses and evaluation of damage distribution in both directions of the building, the case study building is judged as being severely damaged.

6.5.2 Five-Story Private Building in Düzce

The selected case study building is a five story, reinforced concrete building located in Düzce, nearly 8 km away from the epicenter of the 12 November 1999 Düzce earthquake. The general view of the building can be seen from the photographs shown in Figure 6.49. The distance between the location of the case study building and the strong motion record station is about 250 m as shown in Figure 6.50. A simple key plan showing location of the building is given in Figure 6.51.

The building was designed and constructed in 1991, and it has been used for residential purposes. The structure experienced the two successive major earthquakes. Seismic performance of this structure during the 12 November 1999 Düzce earthquake was evaluated by Bayılı (2002).



Figure 6.49 General views of the building after Düzce earthquake
(Photographs taken by Bayılı, 2002)

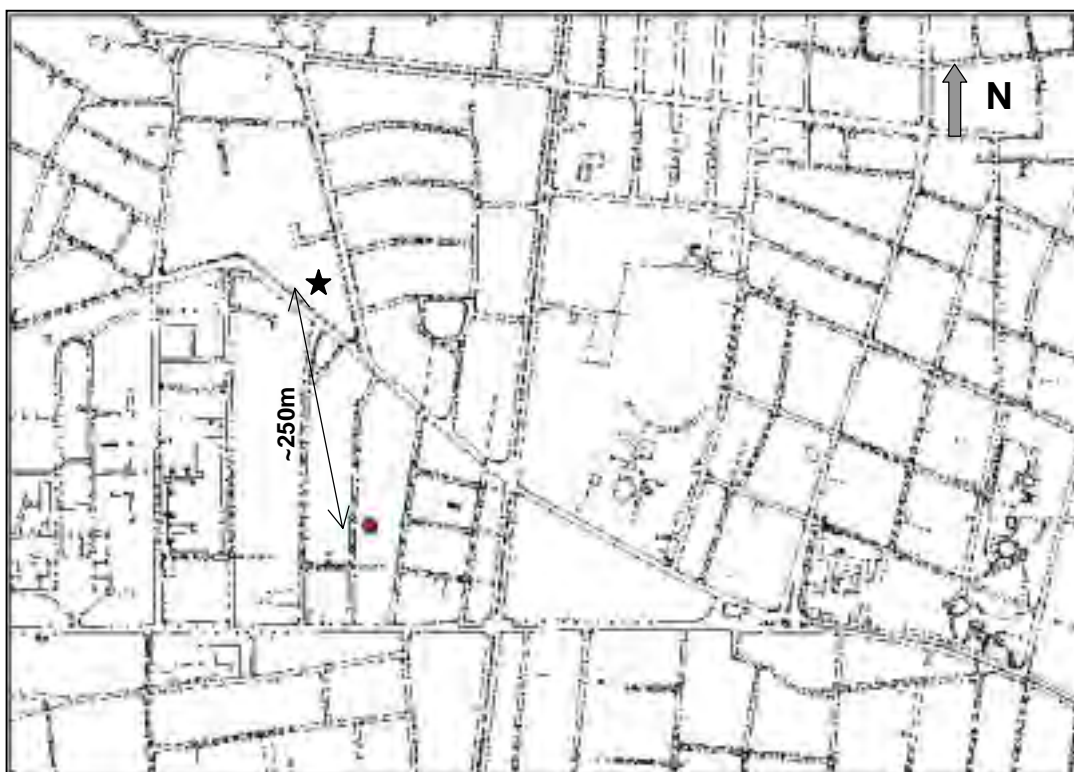


Figure 6.50 Location of the strong motion record station (solid star) and the investigated building (solid circle)

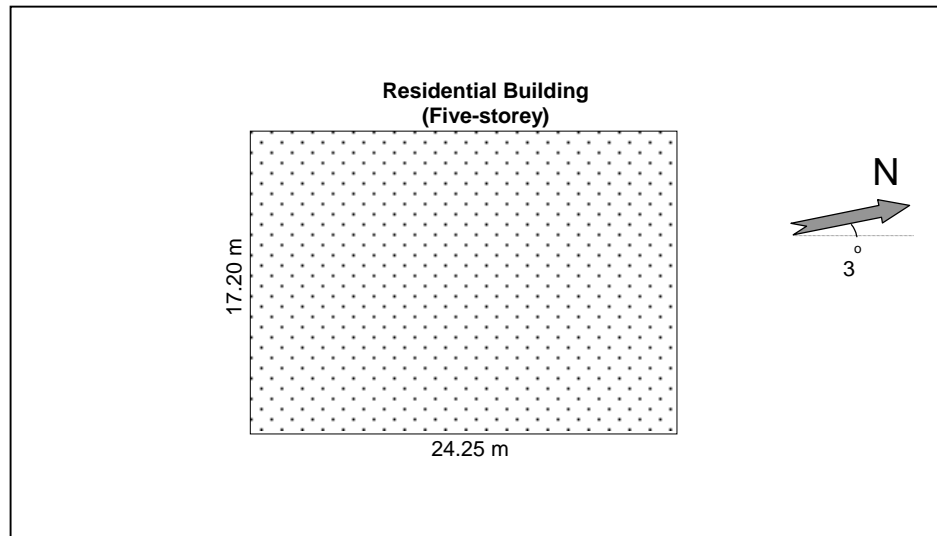


Figure 6.51 Key plan showing location of building

The structural system of the building was composed of reinforced concrete shear walls and moment resisting frames. Poor concrete strength and inadequate transverse reinforcement are the main deficiencies in the building. The concrete strength used in the building and considered in the analyses is 12 MPa. Steel yield strength is taken as 191 MPa.

The building was rectangular in plan and the dimensions measured from out to out are 24.25 by 17.20 meters. The floor plan area is 417 m². It has four bays in the transverse (east-west) direction and six bays in the longitudinal (north-south) direction of the building. As indicated in Figure 6.51, the east-west and north-south directions are slightly deviated from the longitudinal and transverse directions of the building. Inclination effect is ignored in the analyses.

The height of all stories was 2.80 m. The load carrying system was composed of frames and shear walls. The U-shaped shear walls were present around the two staircases. Column and shear wall locations were fixed, but column cross-sectional dimensions were reduced at the upper stories. In general, dimensions of beams and amount of longitudinal reinforcement in them do not vary from story to story. Slab thickness was 12 cm. Sample ground story plan of the building is given in Figure 6.52.

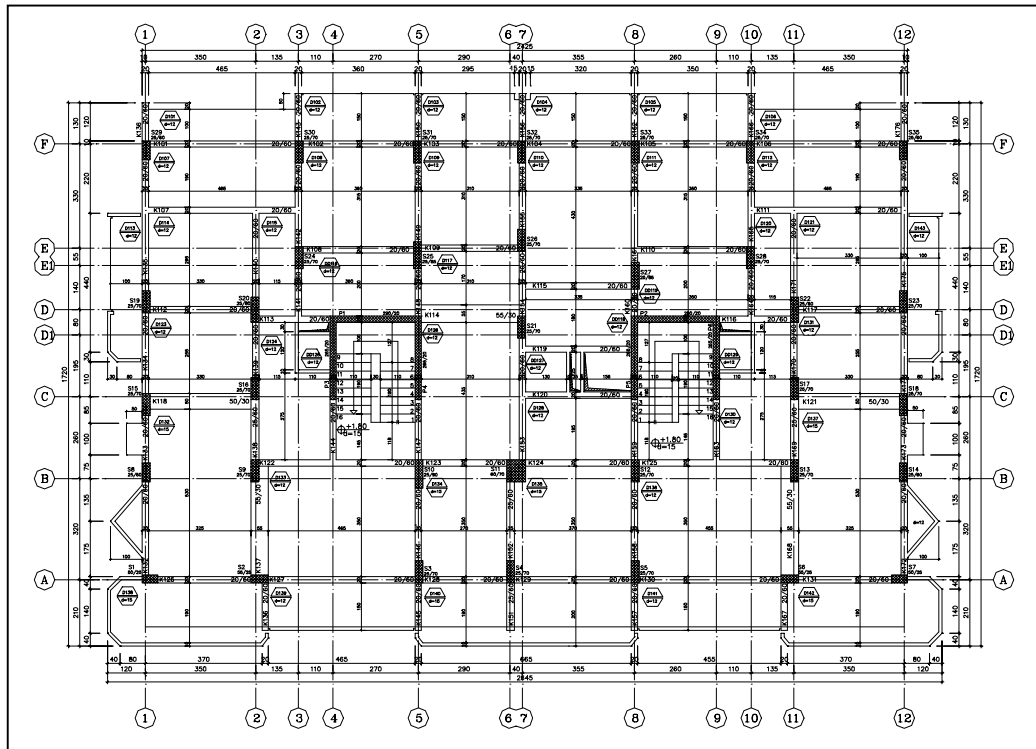


Figure 6.52 Ground floor plan

6.5.2.1 Observed Damage

The case study building was used for residential purposes only. After Marmara earthquake it was still in service. After the Düzce earthquake, the building was evacuated. Damage state of the structure after the Marmara earthquake is not available. Damage state of the building was recorded first after the Düzce earthquake. After this earthquake, damage distribution was recorded carefully throughout the building (Bayılı, 2002). Majority of the beams were observed to be without damage. Flexural and diagonal shear cracks were visible in some of the beams at the ground story. However shear walls of the structure exhibited flexural and shear cracks. After detailed inspections on structural members, the columns were discovered to sustain almost no damage. Distributions of the recorded damage are illustrated in the following photographs of the building taken after the Düzce earthquake (Figures 6.53 to 6.68). Considering the amount of damage observed throughout the Düzce city and the magnitude of the earthquake, damage level of the case study building was quite acceptable.



Figure 6.53 Rear elevation of the building after Düzce earthquake of 12 November 1999



Figure 6.54 Columns F3 and F5 at the ground story



Figure 6.55 Columns F8 and F10 at the ground story



Figure 6.56 Cracking on the second story exterior infill wall at the back side (east-west direction) of the building



Figure 6.57 Cracking on of the second story exterior infill walls at the right-side (south) of the building



Figure 6.58 Diagonal cracks on the web portion of the shear wall P1 at the ground story



Figure 6.59 Diagonal cracks on the web portion of the shear wall P2 and horizontal crack along the slab level of the ground story



Figure 6.60 Diagonal crack about 60 cm away from the end of beam spanning between E5 and E6 at the ground story



Figure 6.61 Diagonal crack in the beam spanning between B2 and C2 at the ground story



Figure 6.62 Flexural crack at the end of the beam spanning between A6 and B6 at the ground story



Figure 6.63 Flexural crack at the end of the beam spanning between B8 and C8 at the ground story



Figure 6.64 Flexural crack at the end of the beam spanning between B9 and C9, where it spans into the shear wall P2, at the ground story



Figure 6.65 Flexural crack, about 80 cm away from the end of the beam spanning between A8 and A11 at the ground story



Figure 6.66 Flexural crack, about 30 cm away from the end of the beam spanning between D12 and F12 at the ground story



Figure 6.67 Flexural crack, about 50 cm away from the left end of the beam spanning between B7 and B8 at the ground story



Figure 6.68 Flexural crack at the right end of the beam spanning between B7 and B8 at the ground story

6.5.2.2 2D Modeling and Inelastic Time History and Damage Analyses

At this stage of the research, the inelastic time history and damage analyses of this building were performed using synthetic ground motions comprising the damageable (strong) parts of the ground motions experienced in 1999 in Marmara region, Turkey. The synthetic ground motion acceleration histories used in these analyses can be seen in Figure 6.4.

The system is almost symmetric in plan in both directions as shown in Figure 6.51. The building is modeled as a series of plane frames linked by rigid horizontal elements. Setting the hinge moment to zero and condensing out the corresponding degree of freedom model the rigid link member hinges. Each frame is in the same vertical plane, and no torsional effects are considered. Since the floors are considered infinitely rigid, identical frames are simply lumped together. Input data is only prepared for each of the typical frames. Two-dimensional frame models of the building were prepared in both longitudinal and transverse directions for the inelastic time history and damage analyses. The structural system having ordinary properties is evaluated as moderately deteriorating system (MOD). Hence the hysteretic model deterioration parameter values proposed for such systems in the third chapter have been used in the analyses.

6.5.2.2.1 Transverse (East-West) Direction of Building

The 2D models composed of frames in transverse (east-west) direction of the building used in the analyses are presented in Figure 6.69. Damage states of these frames reported after the Marmara and Düzce earthquakes are given mutually in Figures 6.70 and 6.71, respectively.

The roof drift ratio, base shear ratio variation and overall damage progression curve, which were computed by applying only the transverse component of the synthetic ground acceleration, are presented in Figure 6.72. The topmost figure indicates the synthetic ground acceleration history used in the analysis. The gray parts of these relationships are those caused by the Marmara earthquake. Maximum

response values of both events obtained for the transverse (east-west) direction of the building are given in Table 6.9.

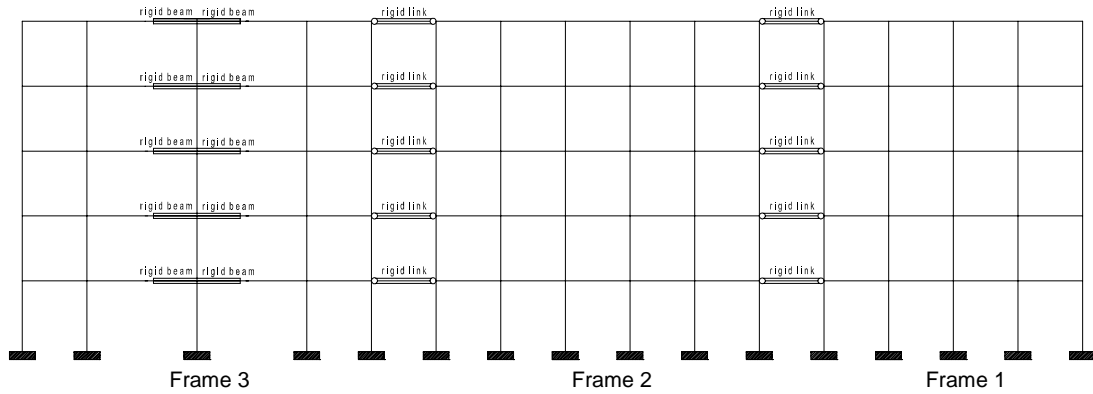


Figure 6.69 2D Frame model used in the inelastic analyses in transverse (EW) direction

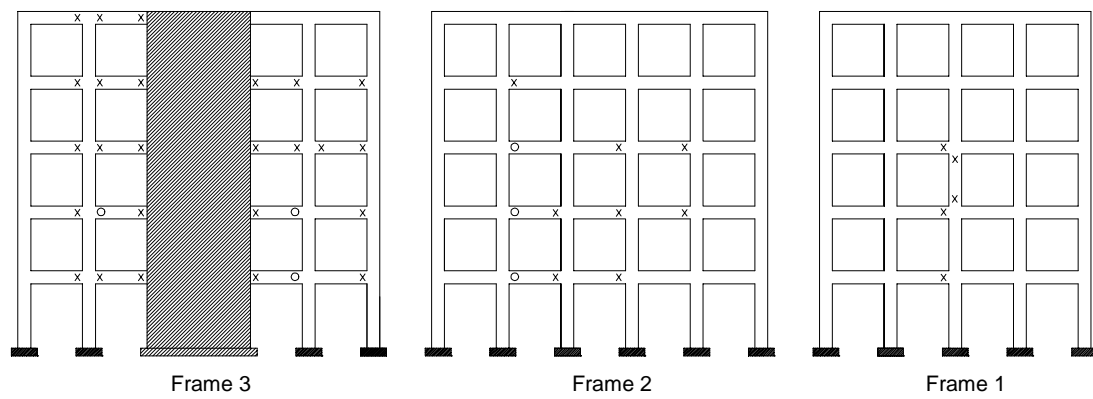


Figure 6.70 Damaged state of 2D Frame model used in the inelastic analyses in transverse (EW) direction after Marmara earthquake (x : crack , o : yield)

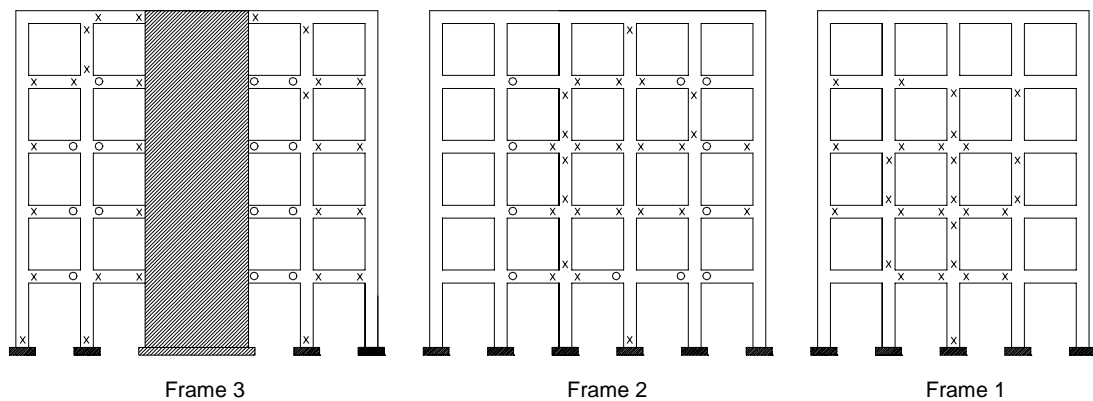


Figure 6.71 Damaged state of 2D frame model used in the inelastic analyses in transverse (EW) direction after Düzce earthquake (x : crack , o : yield, * : failure)

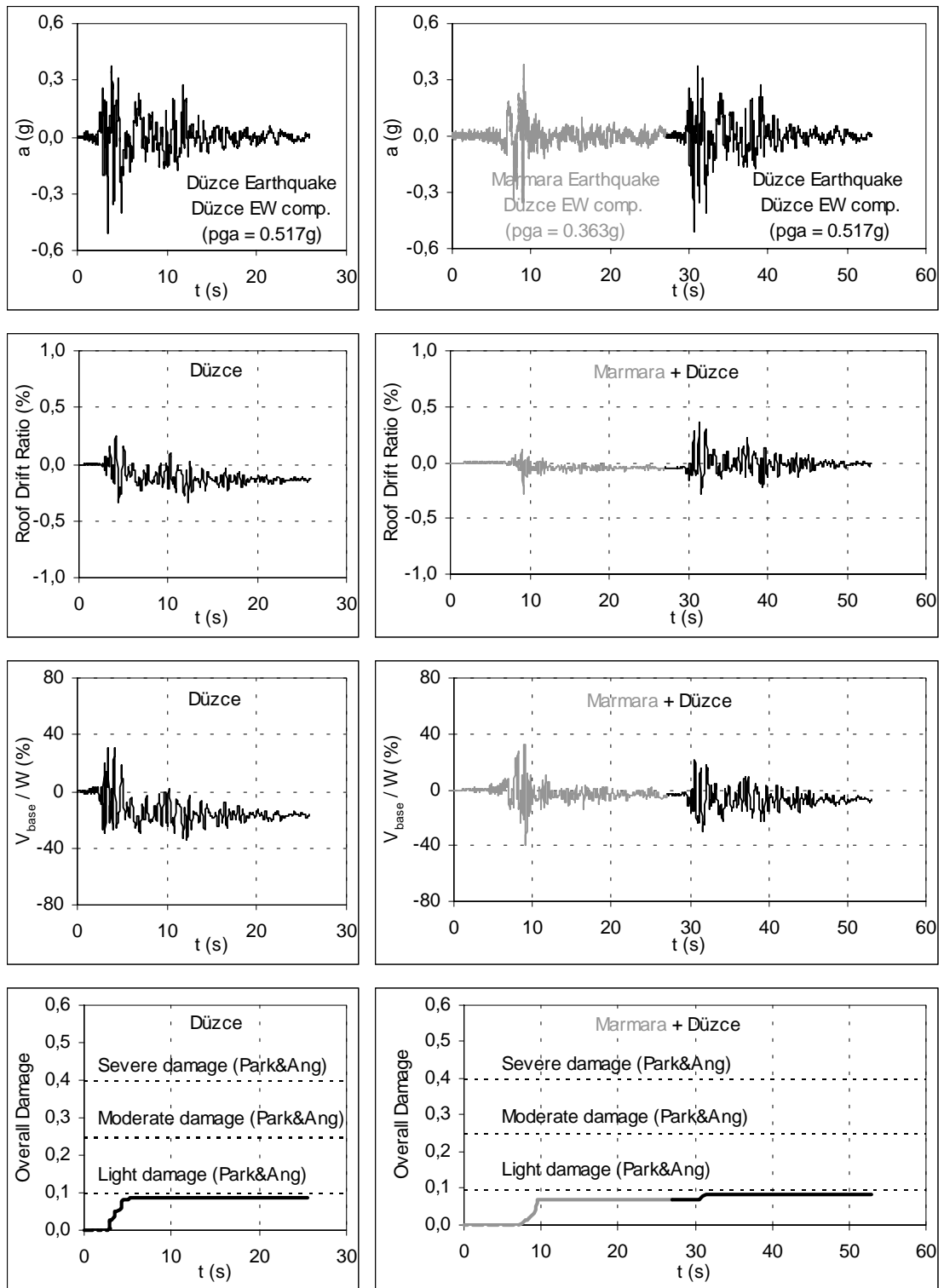


Figure 6.72 Ground acceleration histories, roof drift ratio variations, base shear ratio variations and damage curves for transverse (east-west) direction model of the building located at Düzce

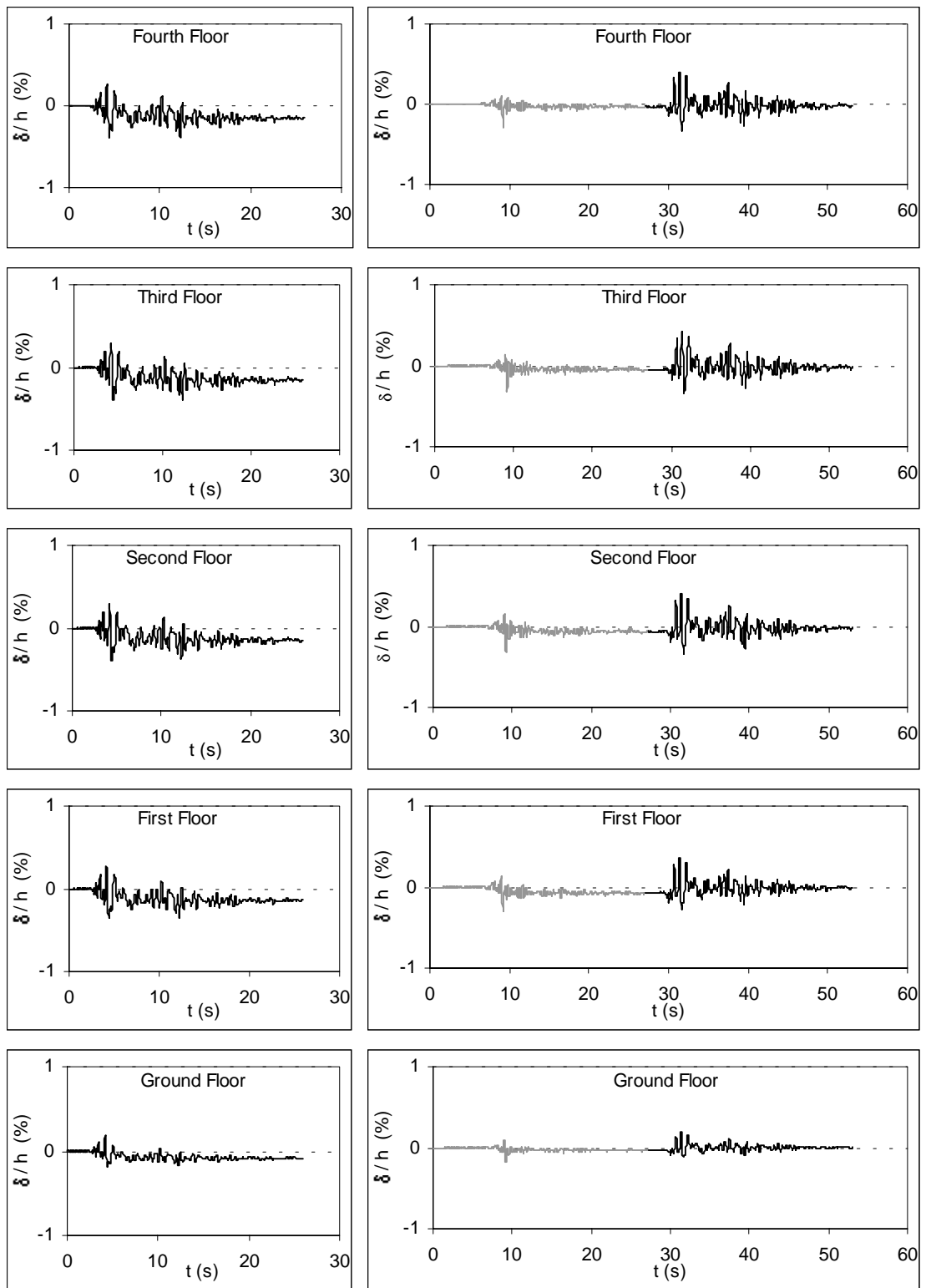


Figure 6.73 Interstory drift ratio histories for transverse (east-west) direction model of the building located at Düzce

Table 6.9 Maximum response values for the transverse (EW) direction of the building

Ground Motion	PGA (g)	Roof Drift Ratio (%)	V_{base} / W (%)	Overall Damage
Düzce	0.517	0.34	34.4	0.087
Marmara+Düzce [1] [2]	0.363 [1], 0.517 [2]	0.29 [1], 0.35[2]	40.1 [1], 29.9 [2]	0.085 (0.072+0.013)

Table 6.10 Maximum drift response in the transverse (EW) direction of the building

Story	Düzce Earthquake		Marmara + Düzce Earthquakes	
	Interstorey Drift (mm)	Drift Ratio (%)	Interstorey Drift (mm)	Drift Ratio (%)
5	11	0.39	11	0.40
4	11	0.41	12	0.41
3	11	0.40	11	0.41
2	10	0.36	10	0.37
1	5	0.18	6	0.21

The roof drift ratio, base shear ratio and damage increase rapidly at times corresponding to sudden increases in the single and synthetic ground motion traces, as shown in Figure 6.72. At the end of the first event, the overall damage of the system remains below the light damage level, meaning that non-damage would occur at this stage of the history. However, although the ground motion intensity of the Düzce earthquake is relatively larger than that of Marmara earthquake, Düzce earthquake does not cause substantial damage compared to Marmara earthquake (Table 6.9). The overall damage index obtained at the end of the second event, Düzce earthquake, which is representative of the cumulative damage, is 0.085 remaining below the light damage level of 0.1. This means that non-damage would occur in this direction of the case study building.

Maximum roof drift ratio of 0.351 percent was obtained during the second event at 30 s. The inter-story drift histories in the transverse direction of the building are shown in Figure 6.73. Peak values of inter-story drift and peak story drift ratios obtained for both single and synthetic ground motions are summarized in Table 6.10. Inspection on the inter-story drift ratio histories revealed that the peak story drift

ratios obtained for all floor levels did not reach the drift limit of 1 percent given by ATC 40 (1996) for *immediate occupancy* performance level. Calculated base shear ratio history in the transverse direction of the building is presented in Figure 6.72. Base shear is quite high between 7-9 s during the first event and between 30-33 s during the second event of the synthetic ground motion. It attains peak values of 40.1 percent and 29.9 percent of the total building weight for the first and second events, respectively (Table 6.9).

It has been demonstrated that although the prior earthquake damage does not substantially affect the maximum drift response in future larger earthquakes, it has significant effects on the damage from succeeding earthquake. The structural system with a prior damage suffers less damage in an earthquake in comparison with the one without a prior damage (Figure 6.72).

Table 6.11 Modal Period variations in the transverse (EW) direction of the building

Mode	Undamaged State	Düzce Earthquake	Marmara + Düzce Earthquakes	
			End of first event (Marmara Earth.)	End of second event (Düzce Earth.)
1	0.21	0.47	0.36	0.49
2	0.06	0.09	0.08	0.10
3	0.03	0.04	0.04	0.04
4	0.02	0.02	0.02	0.02
5	0.02	0.02	0.02	0.02

The variation of the fundamental period is determined via snapshots at the end of the two ground motions. The first five vibration modes are obtained for the state of the transverse direction of the building. The vibration periods are found for the undamaged state and end of the first and second events, respectively. Results obtained are presented in Table 6.11. As can be seen from the variation of the modal periods, the period affected by each event, resulted in softening of the system. The first mode period of the undamaged state of the building in this direction is 0.21 s. It rises up to 0.36 s at the end of the Marmara earthquake, and its increases further at the end of the Düzce earthquake reaching a peak value of 0.49 s. Sustaining a certain level of damage the lateral stiffness of the structure reduced significantly, and have increased the fundamental period; letting the structure take less lateral load.

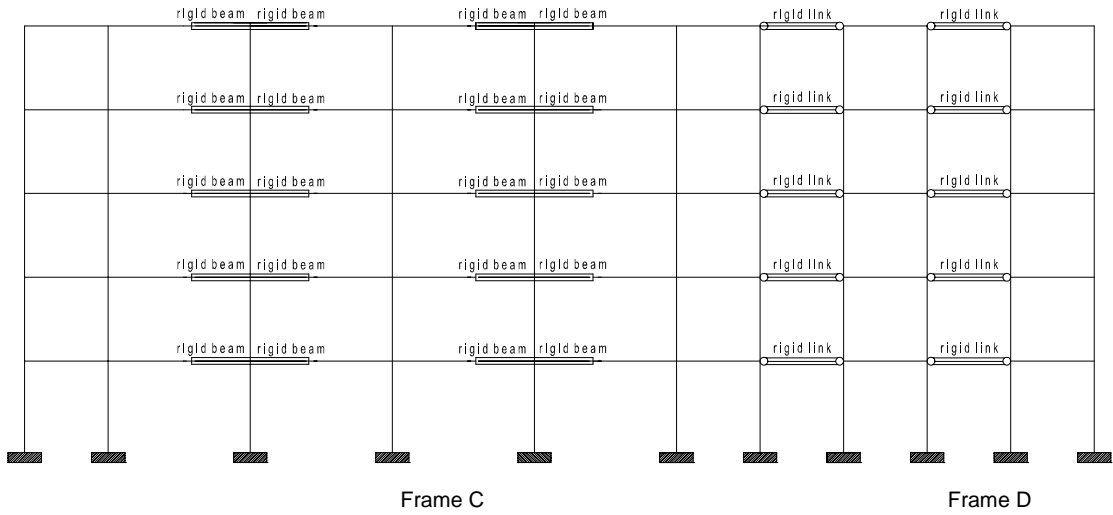


Figure 6.74 2D Frame model used in the inelastic analyses in longitudinal (NS) direction

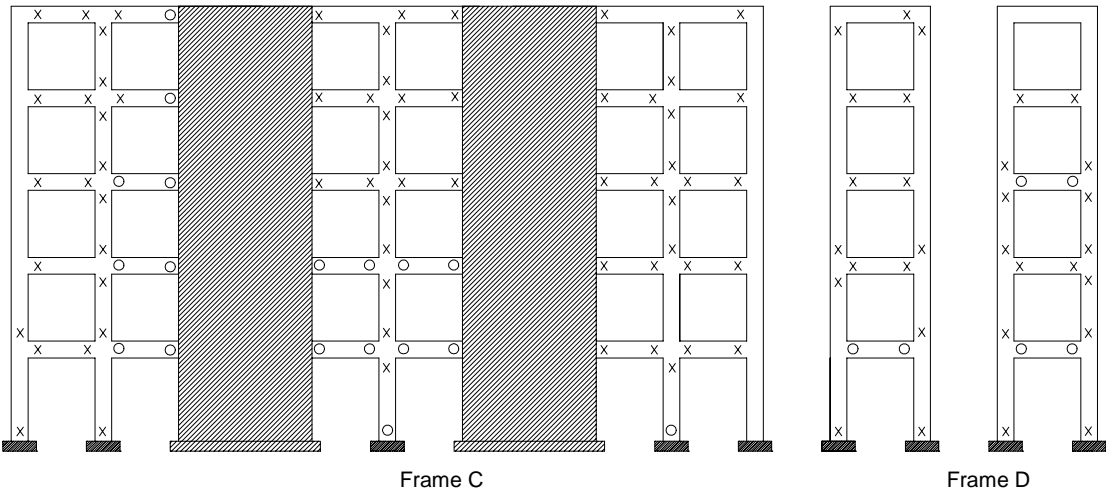


Figure 6.75 Damaged state of 2D frame model used in the inelastic analyses in longitudinal (NS) direction after Marmara earthquake (x : crack , o : yield)

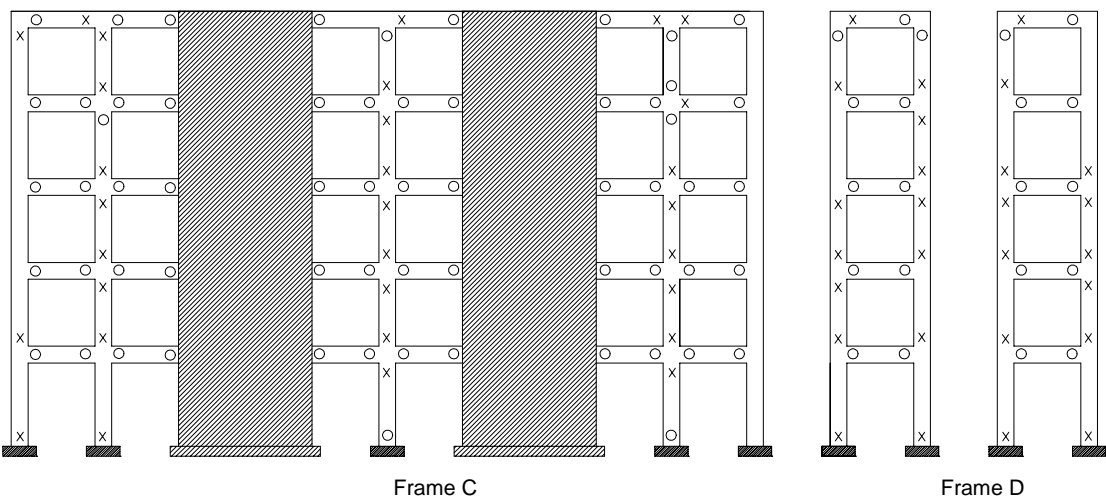


Figure 6.76 Damaged state of 2D frame model used in the inelastic analyses in longitudinal (NS) direction after Düzce earthquake (x : crack , o : yield , * : failure)

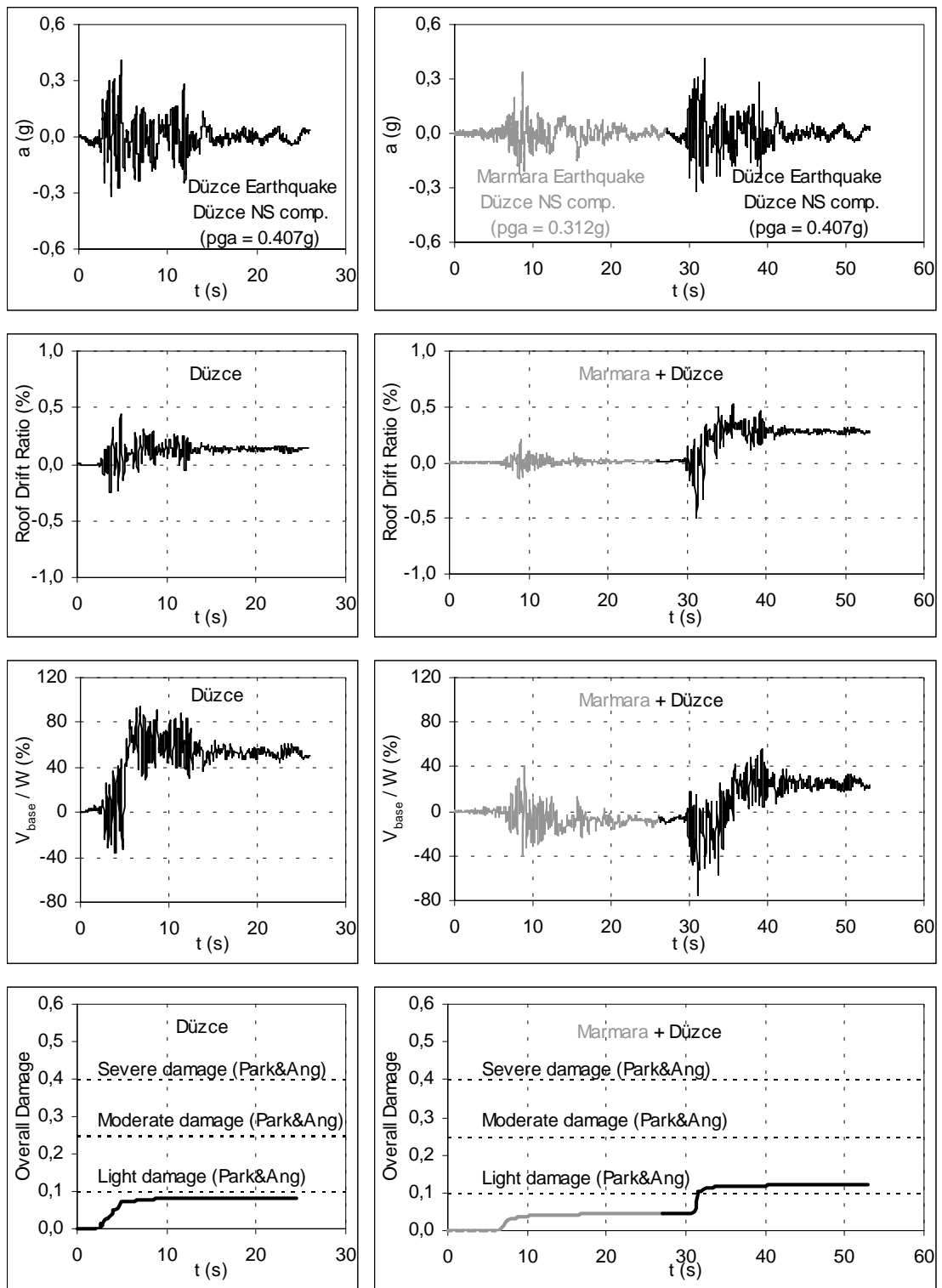


Figure 6.77 Ground acceleration histories, roof drift ratio variations, base shear ratio variations and damage curves for longitudinal (north-south) direction model of the building located at Düzce

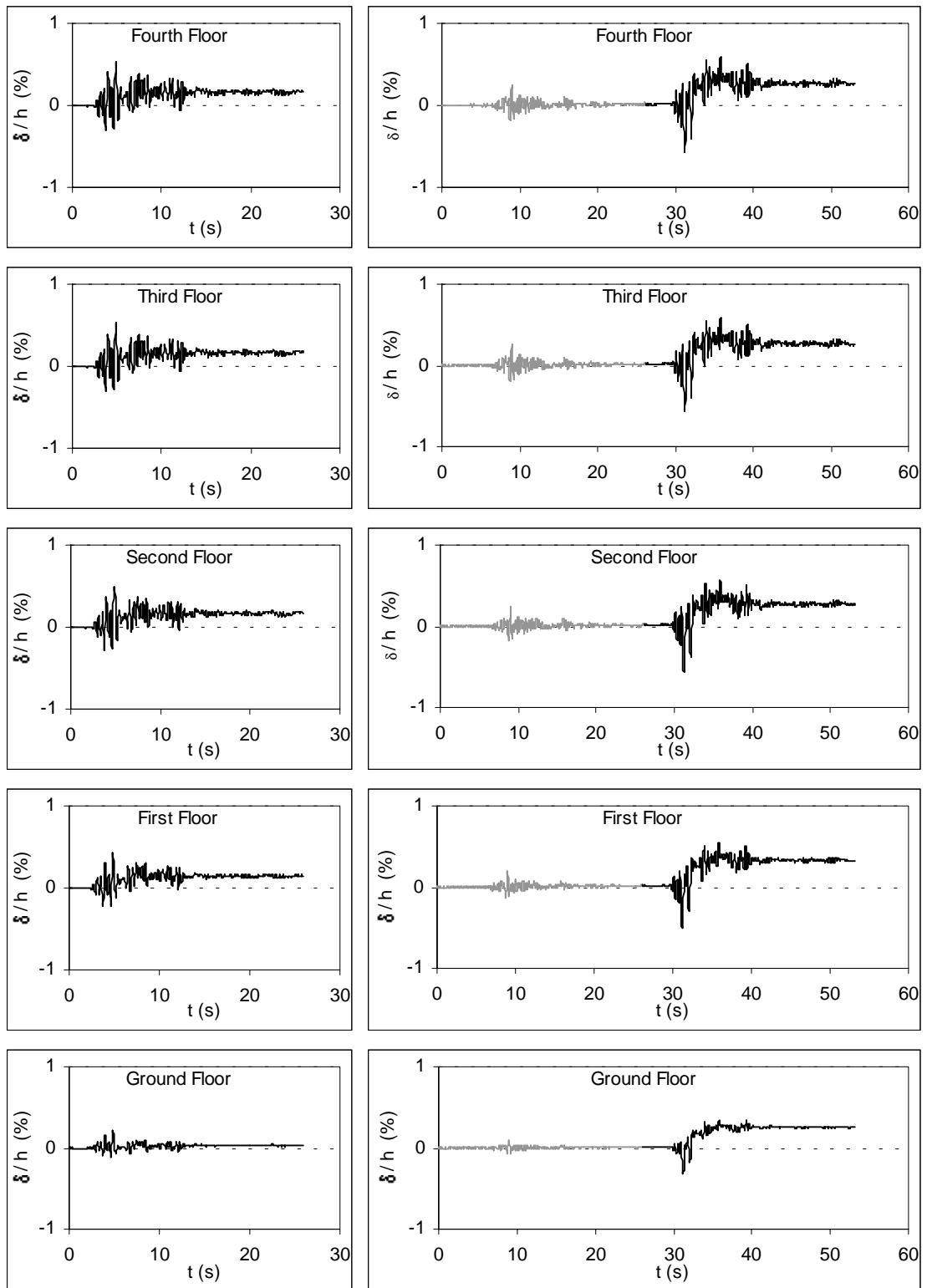


Figure 6.78 Interstory drift ratio histories for longitudinal (north-south) direction model of the building located at Düzce

6.5.2.2.2 Longitudinal (North-South) Direction of Building

The models of the frames in this direction of the building are presented in Figure 6.74. Figures 6.75 and 6.76 show the damage state of the frames after the Marmara and Düzce earthquakes, respectively.

The roof drift ratio, base shear ratio and overall damage progression curves, obtained by applying the longitudinal components of the single and synthetic ground acceleration histories, are presented in Figure 6.77. The topmost figure indicates the single and synthetic ground acceleration histories used in the analyses. The Marmara earthquake causes the gray parts of these relationships.

Table 6.12 Maximum response values for the longitudinal (NS) direction of the building

Ground Motion	PGA (g)	Roof Drift Ratio (%)	V_{base} / W (%)	Overall Damage
Düzce	0.407	0.44	94.3	0.084
Marmara+Düzce [1] [2]	0.312[1], 0.407[2]	0.20[1], 0.53[2]	40.3[1], 75.2[2]	0.120 (0.043+0.077)

Table 6.13 Maximum drift response in the longitudinal (NS) direction of the building

Story	Düzce Earthquake		Marmara + Düzce Earthquakes	
	Interstorey Drift (mm)	Drift Ratio (%)	Interstorey Drift (mm)	Drift Ratio (%)
5	15	0.55	16	0.59
4	15	0.54	17	0.59
3	15	0.52	16	0.58
2	13	0.45	15	0.55
1	6	0.22	10	0.34

Maximum response values of obtained during both single and each event of the synthetic ground motion for the longitudinal (north-south) direction of the building are given in Table 6.12.

Figure 6.77 reveals that the roof drift ratio, base shear ratio and damage increase suddenly at some time values corresponding to strong pulses in the ground acceleration reversals. The overall damage index obtained at the end of the first event remains below the light damage level. This means that no damage would occur during the Marmara earthquake. The overall damage caused by the succeeding Düzce earthquake is 0.077. The cumulative damage attained at the end of the second event exceeded the light damage level.

Figure 6.77 contains the roof drift ratio history obtained for this direction of the building. The roof drift ratio attained its first peak value of 0.20 percent during the first event at 9 s. In this direction, maximum roof drift ratio of 0.53 percent was obtained during the second event at 36 s. The stories peak response values (peak story shear, peak displacement, peak inter-story drift and peak story drift ratios) are tabulated in Table 6.13. The story drift histories in the longitudinal direction of the building are shown in Figure 6.78. Peak story drift ratios obtained for all floor levels did not reach the drift limit of 1.0 percent given by ATC 40 (1996) for *immediate occupancy* performance level. As seen in Figures 6.77 and 6.78 the structure was observed to undergo significant permanent sway in the transverse direction. At all floors the permanent drift was about 0.4 percent, and it was less than 1.0 percent, which is commonly accepted as the permanent drift ratio about which significant structural strength deterioration and stiffness degradation occurs and second order effects become significant. It is shown that prior damage does not have substantial effect on maximum drift response in future larger earthquakes.

Calculated base shear ratio history in the transverse direction of the building is presented in Figure 6.77. Base shear is quite high between 7-13 s during the first event and between 30-40 s during the second event. During the first and second events, the base shear reaches its peak values of 40.3 percent and 75.2 percent of the total building weight, respectively.

Determination of structural response at instants during the time history and damage analysis is optional in IDARC. Hence, response snapshots are requested

during the analysis to determine the variation of the fundamental vibration period at the ends of the successive motions.

Table 6.14 Modal Period variations in the longitudinal (NS) direction of the building

Mode	Undamaged State	Düzce Earthquake	Marmara + Düzce Earthquakes	
			End of first event (Marmara Earth.)	End of second event (Düzce Earth.)
1	0.29	0.36	0.32	0.38
2	0.06	0.06	0.06	0.06
3	0.03	0.03	0.03	0.03
4	0.02	0.02	0.02	0.02
5	0.01	0.01	0.01	0.01

The first five vibration modes are obtained for the state of the longitudinal direction of the building. The vibration periods are found for the undamaged state and end of the first and second events, respectively. Results obtained are presented in Table 6.14. As can be seen from the variation of the first mode period, the system affected by both events. The first mode period of the undamaged state of the building in this direction is 0.29 s. It rises up to 0.32 s at the end of the Marmara earthquake, and its increases further at the end of the Düzce earthquake reaching a peak value of 0.38 s. Sustaining a certain level of damage the lateral stiffness of the structure reduced significantly, and have increased the fundamental period; letting the structure take less lateral load. As seen in Figure 6.77 and Table 6.12, although the intensity of the second event is larger than that of first event, the maximum lateral load resisted during the second event (40.1 percent of the total building weight) is considerably smaller than that of the first event (29.9 percent of the total building weight).

It should be noted that although the prior earthquake damage does not have substantial effects on the maximum drift response in future larger earthquakes, it significantly affects the damage due to the succeeding earthquake (Figure 6.77).

6.5.2.3 Discussions on Calculated and Observed Damages

The case study building was used for residential purposes only. After Marmara earthquake, as it was still in service, the damage state of the building was expected to be very little. The building was evacuated after the Düzce earthquake. Damage state of the building was recorded first in July 2000. Observed damage distribution was recorded throughout the building by Bayılı (2002) and presented in Figures 6.53 to 6.68. After detailed inspections on structural members it was seen that majority of the beams were undamaged. However shear walls of the structure exhibited flexural and shear cracks. The columns were discovered to sustain almost no damage. Considering the amount of damage observed throughout the Düzce city and the magnitude of the earthquake, the damage state level of this case study building was quite acceptable (Bayılı, 2002).

After the Marmara earthquake, almost no damage was found analytically especially in the transverse (east-west) direction of the building. As inspected from the analytical damage distribution given in Figures 6.70 and 6.75, only sparsely distributed cracking damages were observed. Localized minor cracking refers to non-damage state level according to the damage classification specified for IDARC's damage model. Comparison of observed and analytically found damage could not be performed, since there is no available information about the observed damage state of the building after the Marmara earthquake. Analytically computed damages caused by the synthetic ground motions are presented in Figures 6.71 and 6.76 for both transverse and longitudinal directions of the building.

It should be noted that a good match was observed between the damage states found analytically and observed after the Düzce earthquake. In both transverse and longitudinal directions of the building, peak story drift ratios obtained for all floor levels are about 0.5 percent at most and do not reach the drift limit of 1.0 percent, given by ATC 40 (1996) for *immediate occupancy* performance level (Figures 6.73 and 6.78). As a result, on the basis of the damage analyses and evaluation of damage distribution in both directions of the building, the case study building is judged to have been suffered only minor damage.

CHAPTER 7

CONCLUSIONS

7.1 Summary

In modern building codes, structures are designed so that they would not collapse during design-level earthquakes likely to occur at the site of the building. In many cases, structures would not experience an earthquake with equivalent magnitude to the design-level earthquake during their lifetime. However, it is possible that structures, built in seismic zone where earthquakes occur quite often, may be subjected to several smaller-magnitude earthquakes. After being subjected to one or more of such earthquakes neither structural damage nor non-structural damage may occur and the structure could still retain its integrity. Although no visible damage may occur during such repeated earthquakes, structures subjected to them may experience degradation in structural characteristics due to residual deformations from previous ones.

If a structure undergoes successive earthquakes, and does not collapse, the residual deformations may build up. This build-up will result in accumulation of overall reduction of available structural attributes, such as stiffness, strength, ductility, energy dissipation capacity etc., during subsequent earthquakes.

The accumulated damage sustained under earthquake excitations with milder intensities may significantly affect the response of a building to design-level earthquakes. Observations of the behavior of reinforced concrete structures subjected to successive earthquakes, analytical studies and laboratory experiments have all contributed toward placing the accumulated damage due to low cycle fatigue on a firm rational basis and specifying this phenomenon in building seismic codes.

This study addresses the problem of estimating the prior earthquake damage effects on the response of reinforced concrete structures subjected to future design-level earthquakes. The motivation has arisen from the heavy damages or collapses of many reinforced concrete structures that experienced two major earthquakes recently in the Marmara Region, Turkey.

Comprehensive reviews of many of the damage models proposed by several researchers indicate that the main drawback of most damage models is the need of tuning their coefficients for a particular structural component and the lack of calibration against varying degrees of damage observed after actual earthquakes or laboratory tests (Williams and Sexsmith, 1995). The more rational prediction of cyclic response and damage for a particular structural type can be provided on the condition of fine-tuning of hysteretic model deterioration parameters. In this study attempts have been made to calibrate the deterioration parameters of IDARC hysteretic model. Deterioration (stiffness degradation, strength deterioration and pinching) parameters of IDARC's model have been calibrated to assess their most suitable combination providing more realistic damage prediction. Calibration of the parameters has been carried out by using a gradient search method via minimization of the difference between the amounts of experimentally and analytically computed dissipated hysteretic energy. In the calibration process the experimental database belonged to a total of twenty-two beam and column model tests, drawn from two sources. It has been demonstrated that fine-tuning of the hysteretic model deterioration parameters is essential for more realistic predictions about inelastic behavior and structural damage. In addition, sensitivities of the damage index and dissipated hysteretic energy to both IDARC's hysteretic model deterioration parameters and some of the principal structural characteristics have been designated. Three ranges of parameters are proposed for three deterioration levels of structural components in order to provide more rational structural damage prediction. Effects of some principal structural parameters, such as axial load level, concrete strength, reinforcement yield strength and cross-sectional area, on structural damage have been investigated.

The underlying general objective of this study has been the quantitative prediction of the intermediate and the resultant damage levels in a structure subjected to successive earthquake ground motions. To meet the objective inelastic time history and damage analyses of numerous SDOF systems have been carried out to determine whether the loading history has an effect on dissipated hysteretic energy and structural damage. Then this emphasis is directed to the analyses of MDOF systems. The importance of the effects of prior damage induced in reinforced concrete structures on their response to future earthquakes is widely recognized.

In addition to various constant and variable amplitude inelastic displacement reversals with increasing and decreasing order, synthetic ground motions composed one of the four earthquake records preceded or followed by its various times amplitude-compressed record acting as a prior earthquake and successive earthquake have been used in the inelastic time history and damage analyses of numerous SDOF systems.

An inelastic time history and damage analyses of two reinforced concrete buildings are performed to assess the prior earthquake damage effects on the structural response of damaged buildings. One of the buildings was located in Bolu, and the other was in Düzce city. The first building is a public building whereas the second is a private one. The analyses have been carried out using the created synthetic accelerograms comprised of base input provided by these two recorded ground motions. Effects of vertical components of ground motions and infill walls are not addressed. The overall structural damage caused by the subsequent (Düzce) earthquake has been quantified using the overall structural damage index of the previous (Kocaeli) destructive ground motion. The analytical damage results are compared with the observed structural damage. It has been demonstrated that the inelastic time history and damage analysis is competent to indicate the damage state of the structural systems. A good match was observed between the damage states found analytically and observed after the Düzce earthquake.

7.2 Conclusions

On the basis of the observations and results achieved in this study the following conclusions are drawn:

- The deterioration parameters of IDARC's hysteretic model have been calibrated by minimization of the differences between the amounts of experimentally and analytically computed dissipated hysteretic energy. Dissipated hysteretic energy and damage index of a reinforced concrete member are quite sensitive to selection of the hysteretic model deterioration parameters. Realistic damage predictions of structures and members strongly depend on the appropriate selection of the stiffness degradation (α), strength deterioration (β) and pinching (γ) parameters. A random selection of these parameters result in a considerable error in the damage index and energy dissipation, thus may cause to serious mislead in damage prediction. The most effective parameters are pinching and strength deterioration, whereas stiffness degradation parameter has less effect. In order to get reasonable, accurate estimates of cyclic response and damage for a prescribed path, fine-tuning of the parameters, especially γ and β , is highly essential.
- Structural characteristics of reinforced concrete members (axial load level, concrete strength, amount of transverse reinforcement, etc.,) influence the stiffness degradation, strength deterioration and pinching parameters of the hysteretic behavior, also have substantial effects on energy dissipation characteristics and damage index. Hence, for reasonable, accurate predictions of structural damage and energy dissipation, deterioration parameters of the hysteretic model should be selected attentively, considering the structural properties of the reinforced concrete members.
- For a successful prediction of structural damage, firstly the hysteretic model deterioration parameters should be selected so as to the hysteretic behavior in 'reality' is captured. The importance of the fine-tuning of deterioration

parameters, especially for β and γ , to permit more rational damage predictions, is demonstrated. As a result of extensive parametric analyses and evaluation of experimental data of reinforced concrete specimens subjected to constant and variable amplitude displacement cycles, three ranges of parameters are proposed, constituting the most suitable combination of parameters for deterioration levels of reinforced concrete members. These classes are defined as mildly deteriorating (MLD) systems, moderately deteriorating (MOD) systems and severely deteriorating (SVD) systems. A different combination of low cycle fatigue parameters (α , β , γ) is assigned to each class. For MLD systems $\alpha=10$, $\beta=0.1$, and $\gamma=0.8$ are assigned as the low cycle fatigue parameters. The values of the parameters α , β and γ for MOD systems are taken as 6.0, 0.3 and 0.5, respectively and deterioration parameters of SVD systems are proposed as $\alpha=3$, $\beta=0.6$, and $\gamma=0.3$.

- There is a large difference between the damage predictions from the modified Park and Ang damage model incorporated into IDARC and damage model proposed by Erberik and Sucuođlu (2004). The damage index implemented in IDARC is closely related to the hysteretic behavior of the reinforced concrete member being studied. The hysteresis model is controlled by three parameters, namely stiffness degradation (α), strength deterioration (β) and pinching (γ) parameters. The formulation of the model is as follows:

$$D = \frac{\mathbf{f}_m - \mathbf{f}_y}{\mathbf{f}_u - \mathbf{f}_y} + \mathbf{b} \frac{\int dE}{M_y \mathbf{f}_u}$$

h

degradation, but not on pinching. The model expresses the total damage at the n^{th} full-cycle as follows;

$$D_{e,n} = \frac{\mathbf{m} - 1}{\mathbf{m} - 1} + \left(\frac{\mathbf{m}}{\mathbf{m} - 1} \right) \cdot \left(\frac{4}{5\overline{E}_{n,n}} - 1 \right)$$

It should be noted that there is a similarity in between the first components of both models, but the second components are based on different concepts. The inspected difference may be attributed to the philosophy of both concepts

followed by the models and omits of the pinching effect by Erberik and Sucuođlu model.

- The damage model incorporated in IDARC is composed of two parts: deformation and strength. The deformation damage is comprised of the first term, whereas the strength damage stems from the energy term of the damage model. Since the enclosed area of moment-curvature hysteresis loops is a measure of the accumulated dissipated hysteretic energy of reinforced concrete components, the variables affecting the energy dissipation of the structural members are the same as those affecting their damage level attained in the end. Seismic structural damage and energy dissipation capacity of reinforced concrete members depend on the axial load level, amount of confinement reinforcement, concrete strength, amount and yield strength of longitudinal reinforcement and cross-sectional area.
- Increase in the axial load level to balanced level leads to stiffening and strengthening of the cross section, accompanying reduction in ductility. This effect is more striking for the sections containing low longitudinal reinforcement ratios. In case of axial load levels equal or greater than the balanced failure load, the amount of ductility is almost negligible. The axial load level has a substantial effect on the energy dissipation capacity and thus the deterioration level. The smaller the axial load level the larger is the amount of hysteretic energy dissipated before failure. However, the axial load does not affect significantly the number of constant amplitude cycles that can be sustained before failure. It has been inspected that the higher the axial load, the more abrupt is the failure. When the axial load capacity of a column member is 6~8 times the design axial load, i.e., when the column is proportioned almost as a girder, the frame action is greatly improved. The revision of the building or seismic codes should be based on firm bases of the effective parameters resulting from evidences of both extensive experimental and analytical research and observations on the structural behavior after actual earthquakes, laboratory tests. Experimental and analytical evidence indicate that, under reversals of displacement into the nonlinear range, a

factored axial compressive force exceeding $0.20f_cA_g$ acting on column members causes an abrupt failure process. However, structural design close to the limits of the code provisions is a tradition in Turkey. In order to address this and defuse the deficiencies commonly observed after earthquakes (especially inadequate concrete strength leading to increase in axial load level and thus expected behavior) in reinforced concrete buildings, the limitation related to axial load level specified in the national building and earthquake codes, TS 500 (2000) and TEC (1998), should be reduced to one-fourth or one-fifth of the limits currently in force.

- Concrete strength does not have substantial effect on the lateral load capacity of the framing systems. However, increase in concrete strength leads to a significant decrease in deformation of the framing systems. Hence, deterioration level of the structural system affected significantly by the variations in concrete strength.
- Concrete strength has a substantial effect on damage and damageability of structural systems. Specimens with relatively higher concrete strengths exhibited considerably larger energy dissipation capacity. The higher the concrete strength the larger was the amount of hysteretic energy dissipated before failure. The system with low concrete strength seems to undergo relatively more damage, due to excessive drifts and low lateral load capacity. The system with 15 MPa or lower concrete strength is a candidate to undergo significant damage. Due to the lack of good care and supervision, significant variations in concrete strength are observed during the construction, and the concrete strength in the structural components is found to be much lower than the strength of the selected concrete grade. If there is a doubt in providing the required sufficient concrete strength, the cross-sectional dimensions should be kept larger deliberately.
- The energy dissipation capacity and thus the deterioration level of the structural system are affected significantly by the ratio of transverse reinforcement. The specimens with transverse reinforcement ratios exceeding

one percent exhibited considerably larger energy dissipation capacity with slight changes in deterioration parameters. It should be stated that the smaller the hoop spacing the larger was the amount of hysteretic energy dissipated before failure.

- The number of load cycles has an effect on the level of damage sustained by a reinforced concrete component. Increase in the amplitude of the constant amplitude cycles diminishes the number of cycles up to failure.
- Both damage progression and accumulation of dissipated hysteretic energy follows different paths in variable amplitude loading histories. Hence, damage and cumulative hysteretic energy dissipated along a path seem apparently to depend on the number and amplitude of cycles constituting the path. However, resultant damage attained in the end of the loading history and accumulated hysteretic energy dissipated along the loading path are independent from the ordering of the same number and amplitude cycles along the path. The damage levels attained in the end of the different paths with the same number and amplitude cycles are almost equal. The same interpretation is valid for dissipated energy.
- Structural damage depends on the ductility level of constant amplitude reversals. Damage rapidly increases during the first pulse of the constant amplitude loading history. Regardless of ductility, this damage constitutes the major part of the total damage. Later, damage progression seems to follow almost a linear path with relatively very small rates. Damage increases almost in proportion to the increase in the cycle amplitudes. In this respect, the damage rule developed by Miner (1945) fails for reinforced concrete members as it assumes that the accumulation of damage is linear and independent of load path.
- There is a nonlinear relationship between the earthquake excitation intensity and the resultant damage attained in the end. Increase in the amplitude leads to exponential increase in damage.

- The prior earthquake damage has significant effect on the SDOF system response to subsequent future earthquakes. Increase of the prior earthquake intensity causes reduction in the damage from the succeeding main earthquake. Damage from prior earthquakes of one-fourth and one-third amplitude of the main earthquake record is negligibly small compared to the damage caused by the main earthquake.
- A definite ground motion record acting as prior earthquake and successive earthquake leads to substantially different amounts of damage. In comparison with the total damage, damage caused by such ground motion acting as prior earthquake is two-times of the damage resulted by the same ground motion acting as subsequent earthquake.
- The same or smaller amplitude intensity successive earthquakes cause damage ranging up to about 60 percent of the main earthquake damage. Successive earthquakes with intensities ranging from one to one-fourth of the main earthquake intensity cause to damages ranging from about 58 percent to 2 percent of the main earthquake damage.
- Prior earthquake damage does not substantially affect the maximum drift response in future larger earthquakes. The two-dimensional models of two five-story reinforced concrete frame-wall structures are exposed to single (Düzce) and synthetic (Marmara and Düzce) ground motions. Each of the synthetic ground motions consists of two different-intensity ground motions that are sequenced in increasing order. The peak drift response at each story and at the top of buildings was slightly affected by the previous (Marmara) shakes of smaller intensities. Synthetic ground motions caused peak drifts that ranged from 0 to 25 percent larger than those obtained in single (Düzce) ground motions.
- The prior earthquake damage significantly influences the damage of MDOF frame type structures from succeeding earthquakes. Although it seems

illogical, a structural system with a prior damage suffers less overall damage in an earthquake in comparison with the one without a prior damage.

7.3 Possible Future Work

The research conducted in this dissertation can be extended in the future as explained below:

- This study can be repeated by using three-dimensional nonlinear analyses tool. Such a study would enable comparison of efficiency and accuracy of the two nonlinear analyses tools used.
- The more reasonably accurate estimation of cyclic response is essential for damage assessment. The calibration process of hysteretic model deterioration parameters (stiffness degradation, strength deterioration and pinching parameters) has been performed using experimental database belong to twenty-two beam and column test specimens drawn from two sources. Dissipated hysteretic energy and damage index are quite sensitive to selection of the deterioration parameters, so fine-tuning is indispensable. Therefore in the future, it is possible to calibrate the deterioration parameters using the test data of a large number of different sets of specimens with various structural properties to determine more suitable combination of parameters including additional ones for a particular structural component with pre-identified material properties, axial load, and geometry.
- The inelastic time history and damage analyses conducted to understand the effects of loading history on seismic performance and damage given in Chapter 5 may be carried out with a large number of real earthquake records to make more definite conclusions.
- In this dissertation inelastic time history and damage analyses of two reinforced concrete buildings have been performed without considering the infill walls. It is believed that effective infill walls without windows, doors or

openings contribute to the framing systems in resisting the lateral force induced by earthquake forces in some degree. Hence, these analyses may be repeated for several other reinforced concrete buildings considering the efficient infill walls.

- In the inelastic time history and damage analyses performed in this study 'soil structure interaction (SSI)' effects are not taken into account. Consideration of SSI effects in the models is believed to be essential for more rational damage prediction. SSI effects would cause reductions in seismic demands and structural damage. Extending the scope of this study by considering SSI effects would be highly useful.

APPENDIX A

TABLES OF HYSTERETIC MODEL PARAMETERS TABULATED SEARCH STUDY RESULTS

Appendix A contains the sample table of the hysteretic model deterioration (stiffness degradation, strength deterioration and pinching) parameters search study results of the two sets of beam and column test specimens. The first set of the specimens was tested at Purdue University and the second set specimens were tested at METU Structural Mechanics Laboratory.

Table A.1 Analytical results of dissipated hysteretic energy and damage index for varied values of Hysteretic Model Parameters α , β and γ - Pujol column test specimen **C10-2-3N**

$$(E_{\text{exp}} = 20514 \text{ kNmm})$$

a	b	g	E_{ana} (kNmm)	$E_{\text{exp}} - E_{\text{ana}}$ (kNmm)	$ E_{\text{exp}} - E_{\text{ana}} $ (kNmm)	$\frac{ E_{\text{exp}} - E_{\text{ana}} }{E_{\text{exp}}}$	D_i	$ D - D_i $
5.0	0.80	0.50	11352	-9162	9162	0.447	0.856	0.186
5.0	0.70	0.50	16442	-4072	4072	0.198	0.994	0.048
5.0	0.61	0.50	20247	-266	266	0.013	1.041	0.001
5.0	0.60	0.50	20514	0	0	0.000	1.042	0.000
5.0	0.50	0.50	23627	3113	3113	0.152	1.009	0.033
5.0	0.40	0.50	25841	5327	5327	0.260	0.924	0.118
5.0	0.30	0.50	27483	6970	6970	0.340	0.803	0.239
5.0	0.20	0.50	28728	8214	8214	0.400	0.660	0.382
5.0	0.10	0.50	29713	9199	9199	0.448	0.501	0.541
5.0	0.00	0.50	30498	9985	9985	0.487	0.330	0.712
5.0	0.60	0.00	5445	-15068	15068	0.735	0.547	0.495
5.0	0.60	0.10	7607	-12906	12906	0.629	0.618	0.424
5.0	0.60	0.20	11560	-8953	8953	0.436	0.747	0.295
5.0	0.60	0.30	14981	-5533	5533	0.270	0.859	0.183
5.0	0.60	0.40	18028	-2486	2486	0.121	0.958	0.084
5.0	0.60	0.50	20514	0	0	0.000	1.042	0.000
5.0	0.60	0.60	22823	2310	2310	0.113	1.113	0.071
5.0	0.60	0.70	24681	4167	4167	0.203	1.174	0.132
5.0	0.60	0.80	26383	5869	5869	0.286	1.229	0.187
5.0	0.60	0.90	27821	7307	7307	0.356	1.275	0.233
5.0	0.60	1.00	29150	8636	8636	0.421	1.318	0.276
5.0	0.00	1.00	5777	-14737	14737	0.718	0.330	0.712
5.0	0.00	0.00	60352	39839	39839	1.942	0.330	0.712
5.0	0.80	1.00	4831	-15683	15683	0.764	0.584	0.458
5.0	0.80	0.00	11627	-8887	8887	0.433	0.836	0.206
1.0	0.60	0.50	14177	-6337	6337	0.309	0.831	0.211
2.0	0.60	0.50	17288	-3226	3226	0.157	0.933	0.109
3.0	0.60	0.50	18928	-1586	1586	0.077	0.987	0.055
5.0	0.60	0.50	20514	0	0	0.000	1.042	0.000
7.0	0.60	0.50	21465	951	951	0.046	1.069	0.027
10.0	0.60	0.50	22211	1697	1697	0.083	1.094	0.052
20.0	0.60	0.50	23144	2630	2630	0.128	1.124	0.082
50.0	0.60	0.50	23809	3295	3295	0.161	1.146	0.104
100.0	0.60	0.50	24046	3532	3532	0.172	1.154	0.112

APPENDIX B

STRUCTURAL PROPERTIES AND ENGINEERING AND ARCHITECTURAL DRAWINGS OF THREE BUILDINGS

Appendix B contains the engineering drawings of the Çeltiksuyu Regional Primary Education School buildings which was located at Çeltiksuyu village, Bingöl and subjected to the May 1, 2003 Bingöl Earthquake. In addition to snapshots of the three dimensional elevations of these buildings, engineering drawings showing ground stories column, beam and slab dimensions of the are presented in Figures B.1 to B.5. Finally to give an opinion about the damaged state of the buildings, the photographs of the buildings taken right after the earthquake are presented in Figure B.6.

Although one of these buildings did not suffer any structural, the brittle failure of columns of the other two buildings resulted in their total collapse during the earthquake. The story mechanisms occurred in the five-story *dormitory building*, result in failure killing more than eighty students. Three-story *school building* also collapsed due to the story mechanism at the ground story. However, four-story *residential building* did not suffer any structural damage.

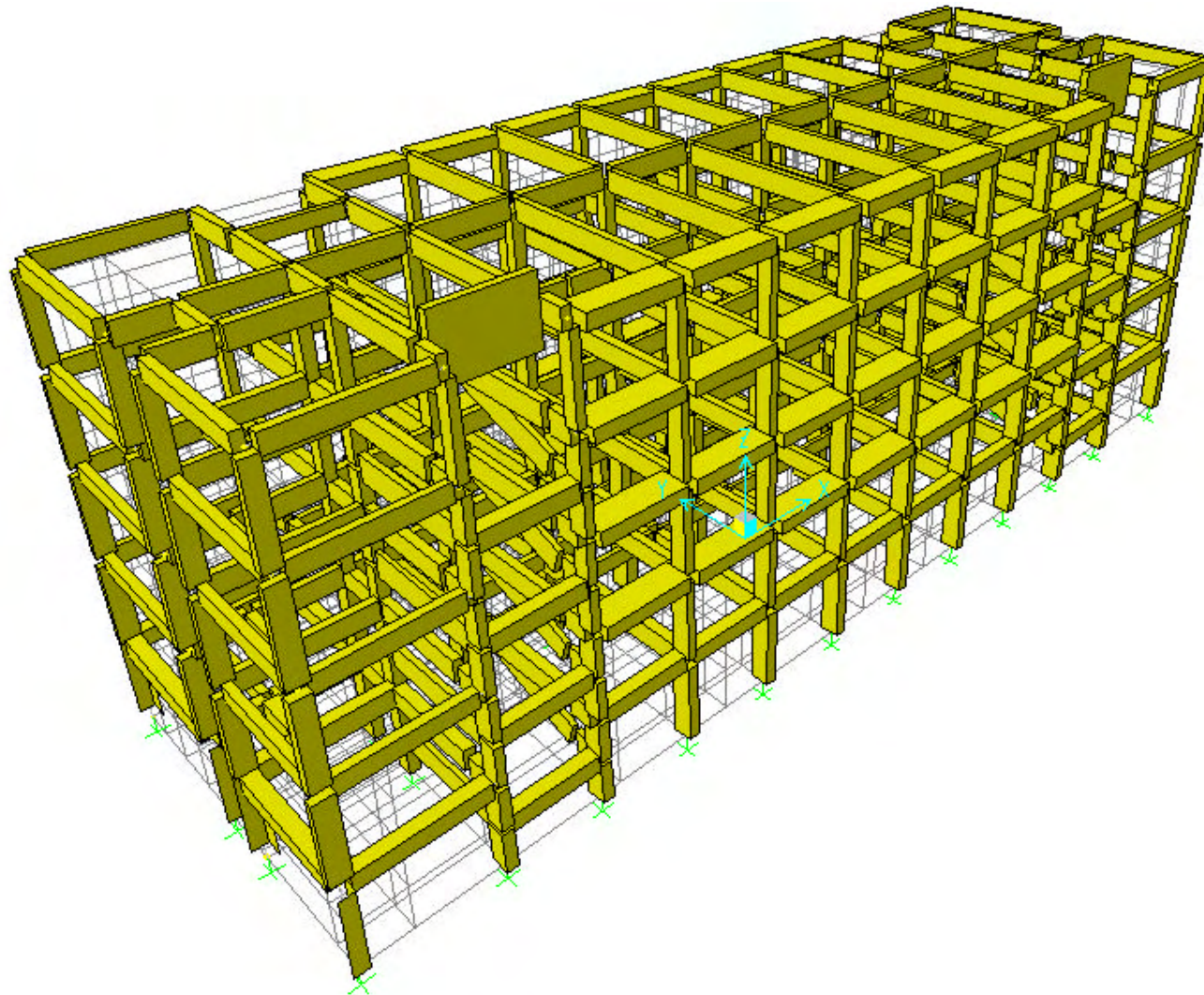


Figure B.1 Three dimensional elevation of the dormitory building

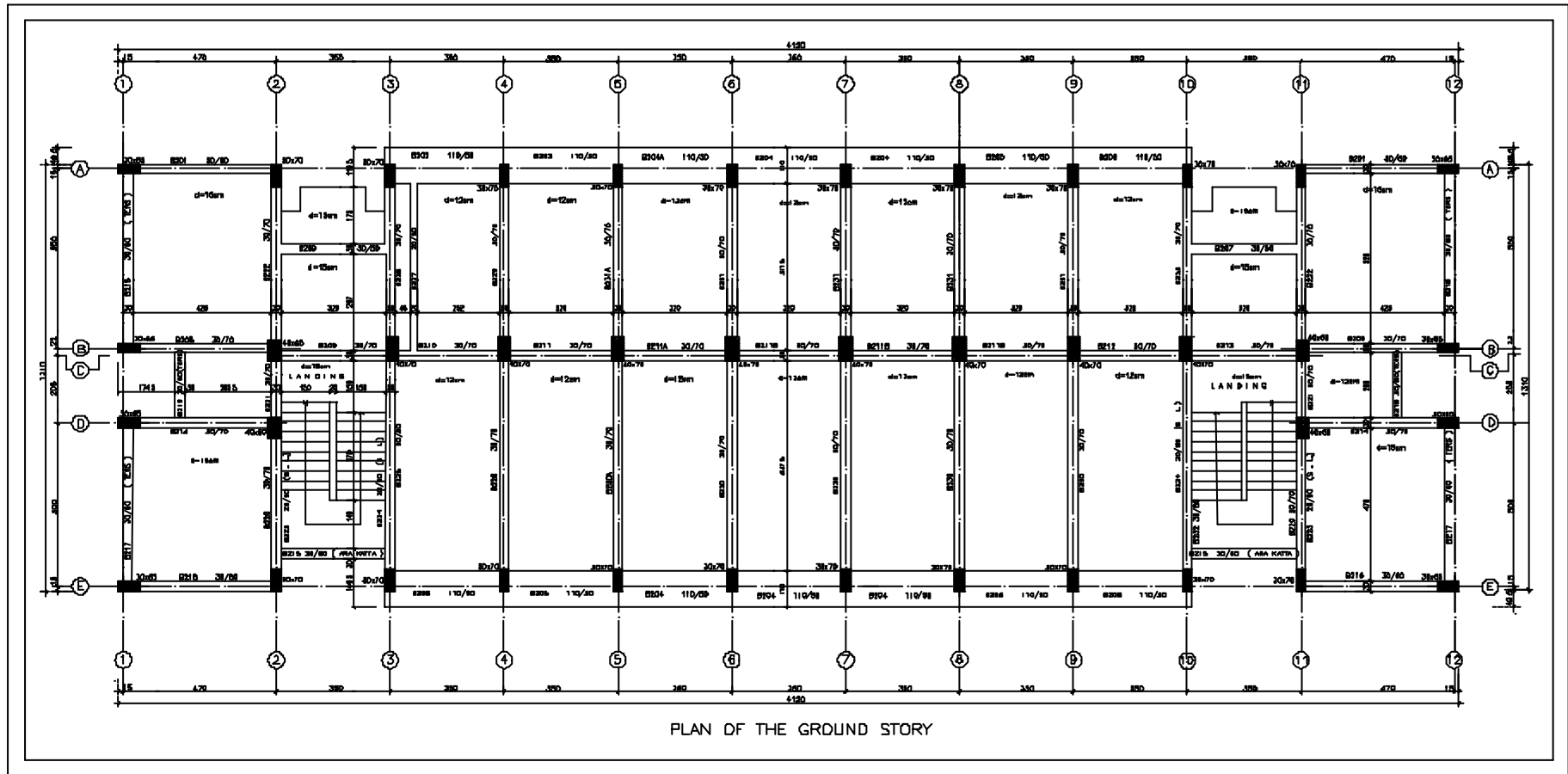


Figure B.2 Ground story plan of the dormitory building

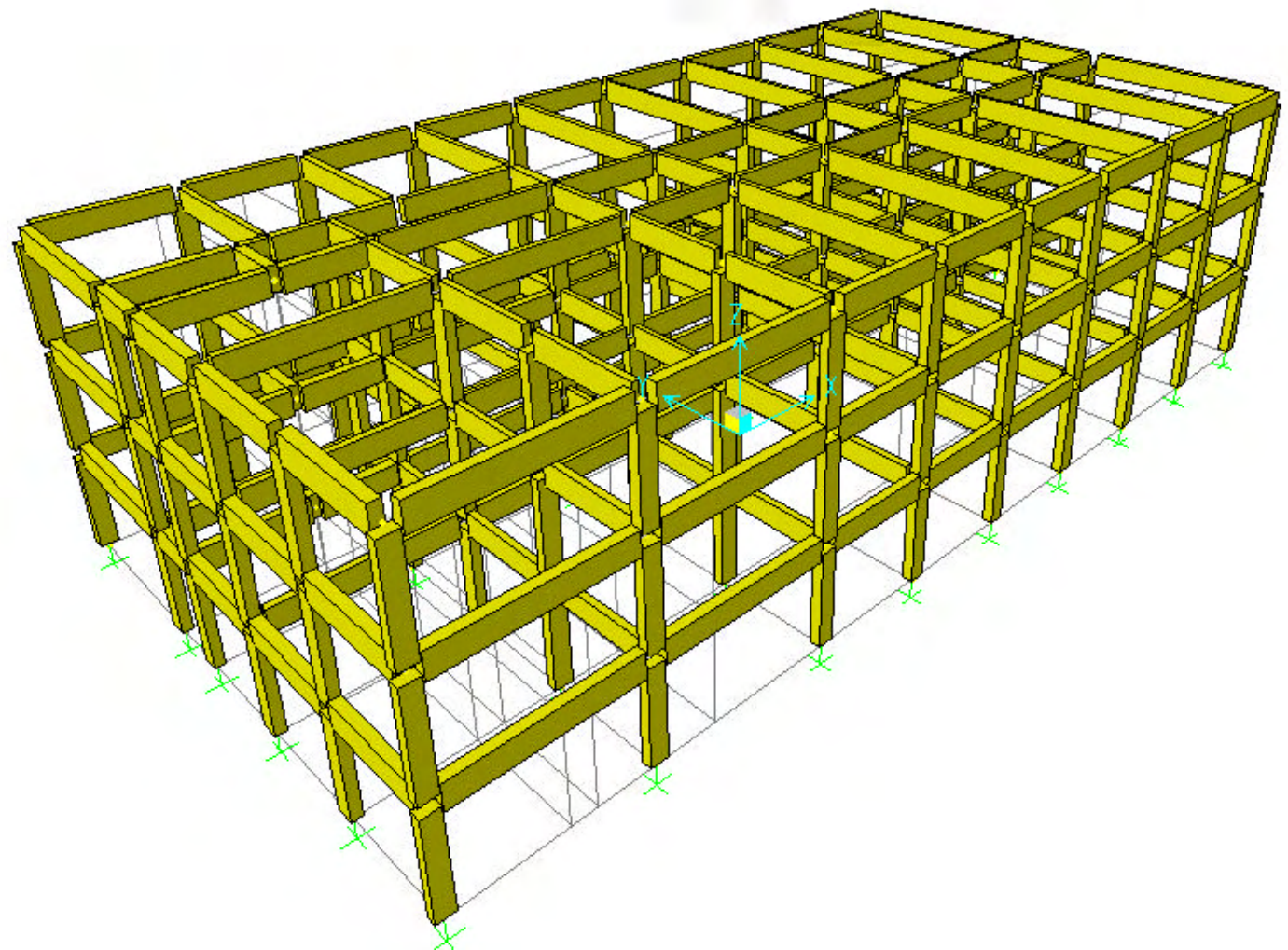


Figure B.3 Three dimensional elevation of the school building

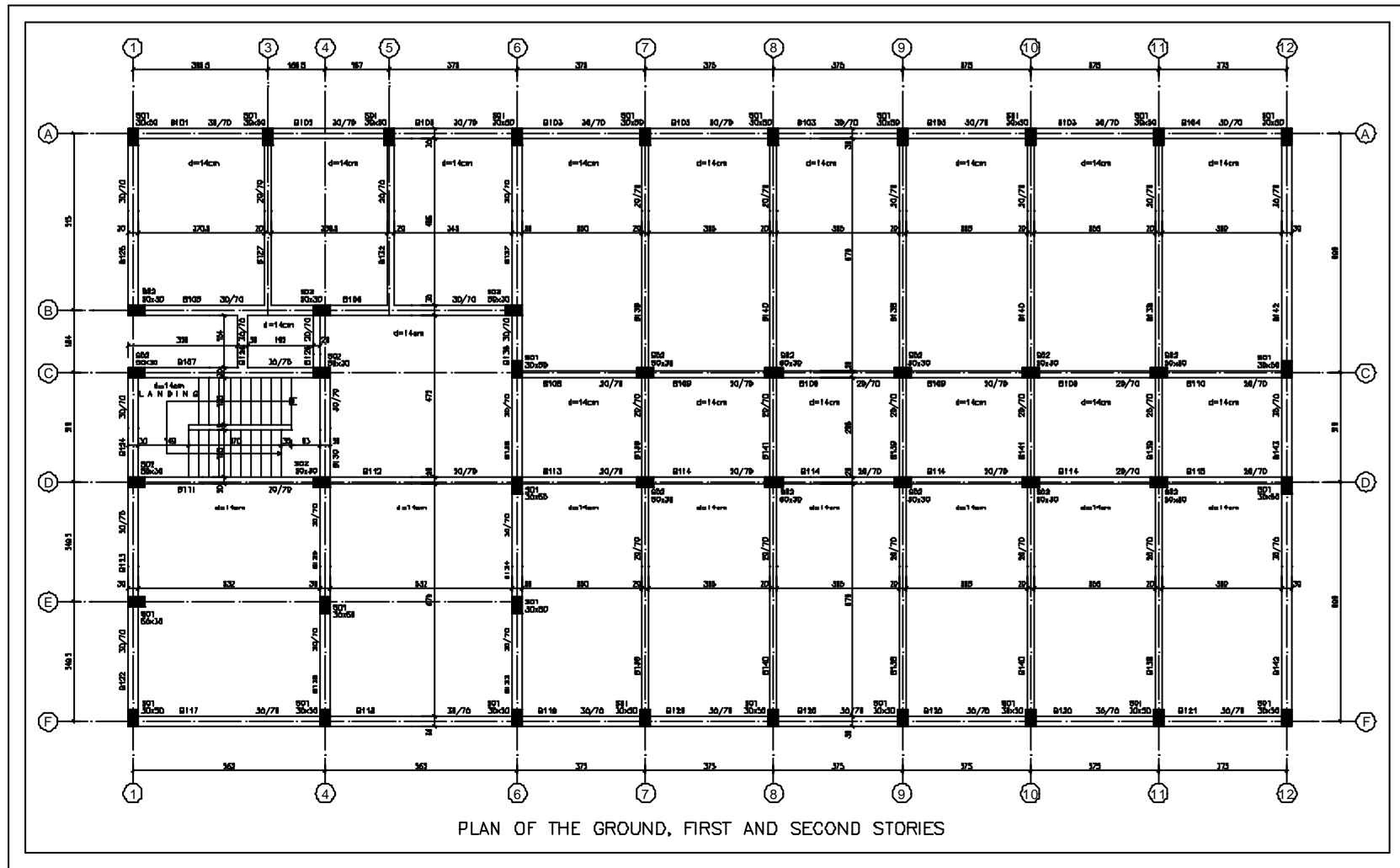


Figure B.4 Ground, first and second stories plan of the school building

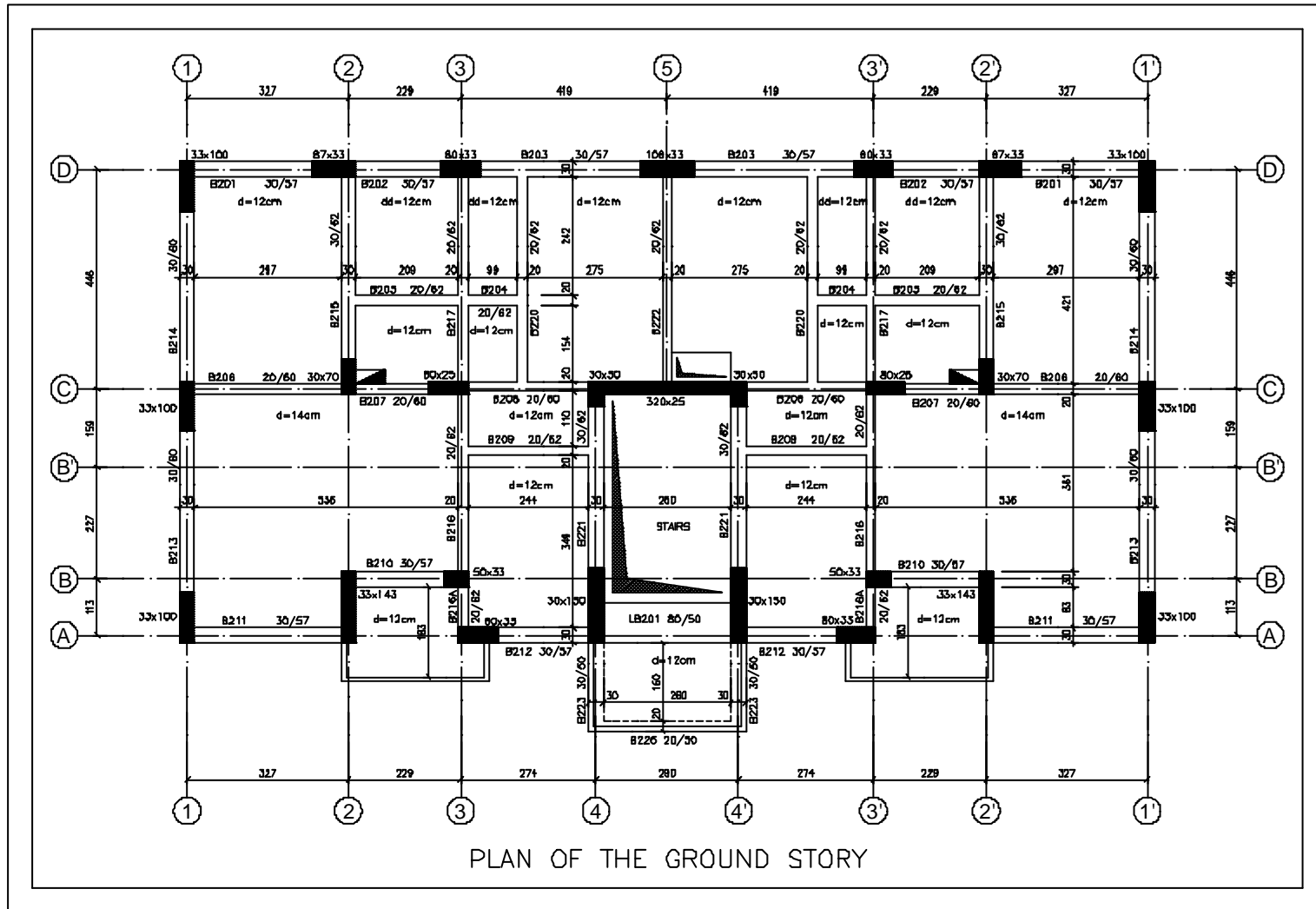
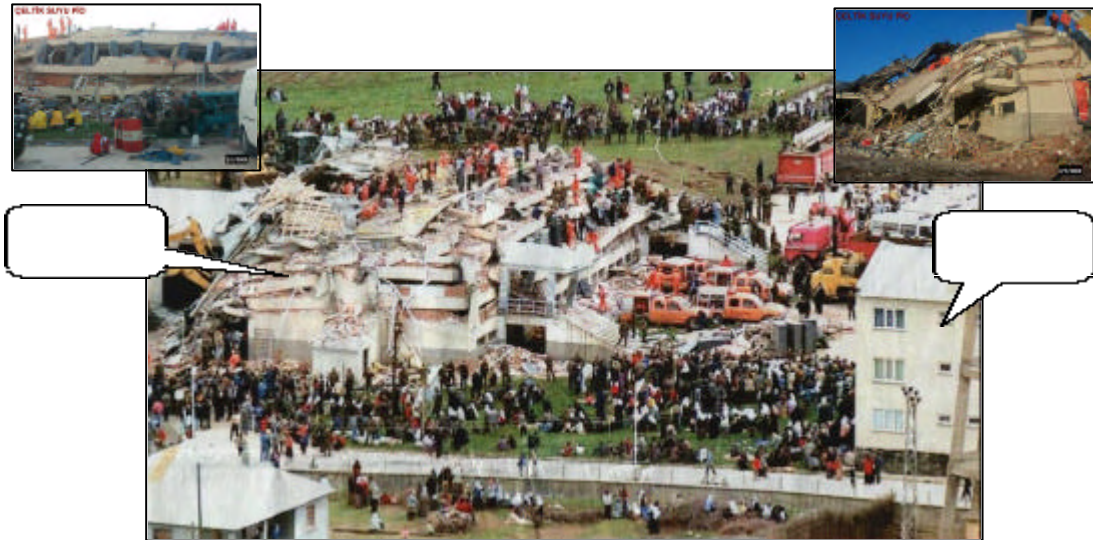


Figure B.5 Ground story plan of the residential building



(a) Dormitory building (Totally collapsed)



(b) School building (Fully collapse of ground story)



(c) Residential building (No damage)

Figure B.6 Photographs of the Çeltiksuyu Regional Primary Education School buildings after Bingöl earthquake of May 1, 2003

APPENDIX C

ENGINEERING AND ARCHITECTURAL DRAWINGS OF FIVE STORY BUILDING

Appendix C contains the three-dimensional model snapshot and engineering drawings of the branch office building of the Ministry of Public Works and Settlement located at Bolu, experienced the August 17, 1999 Marmara and November 12 1999 Düzce earthquakes. Three dimensional view of the building is shown in Figure C.1. Engineering drawings that are giving beam, slab and column details of the ground story are presented in Figures C.2 and C.3.

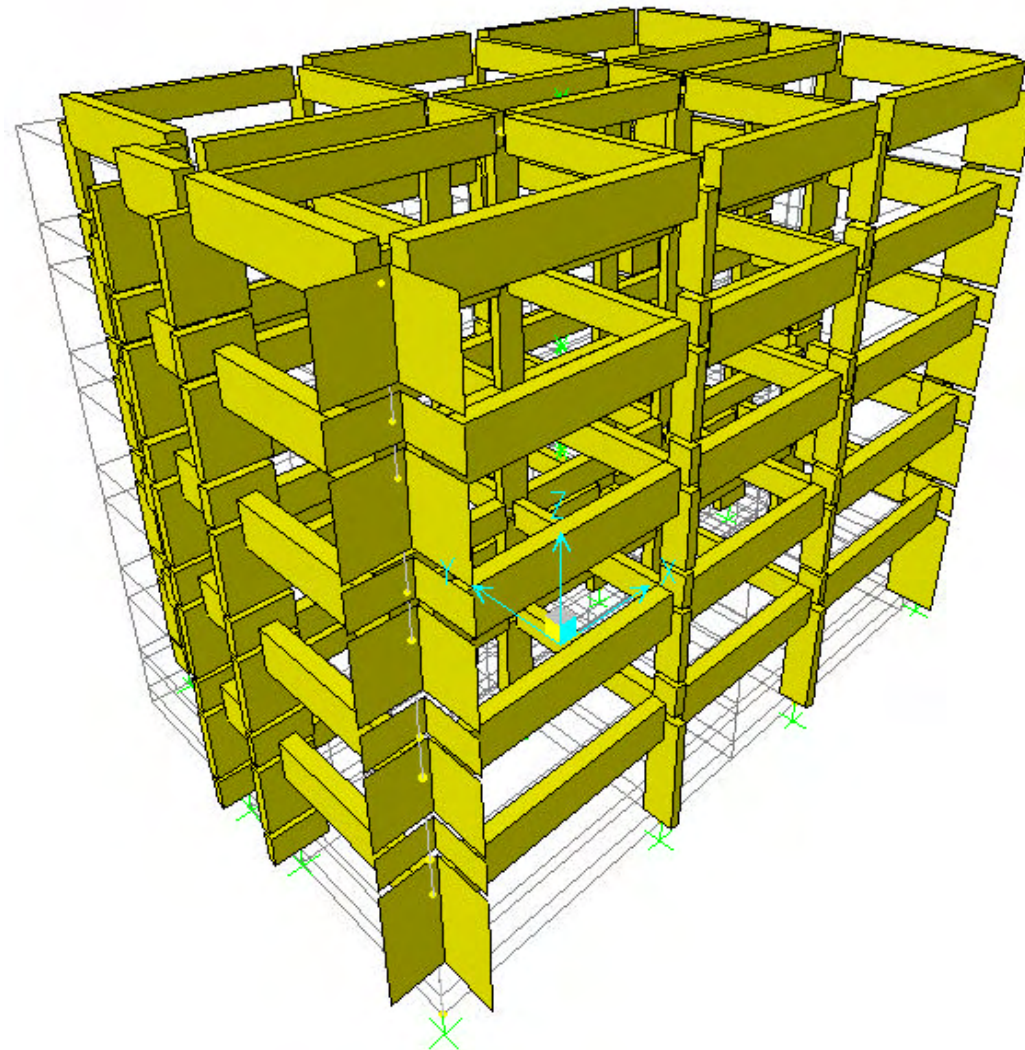


Figure C.1 Three Dimensional Elevation of The Building

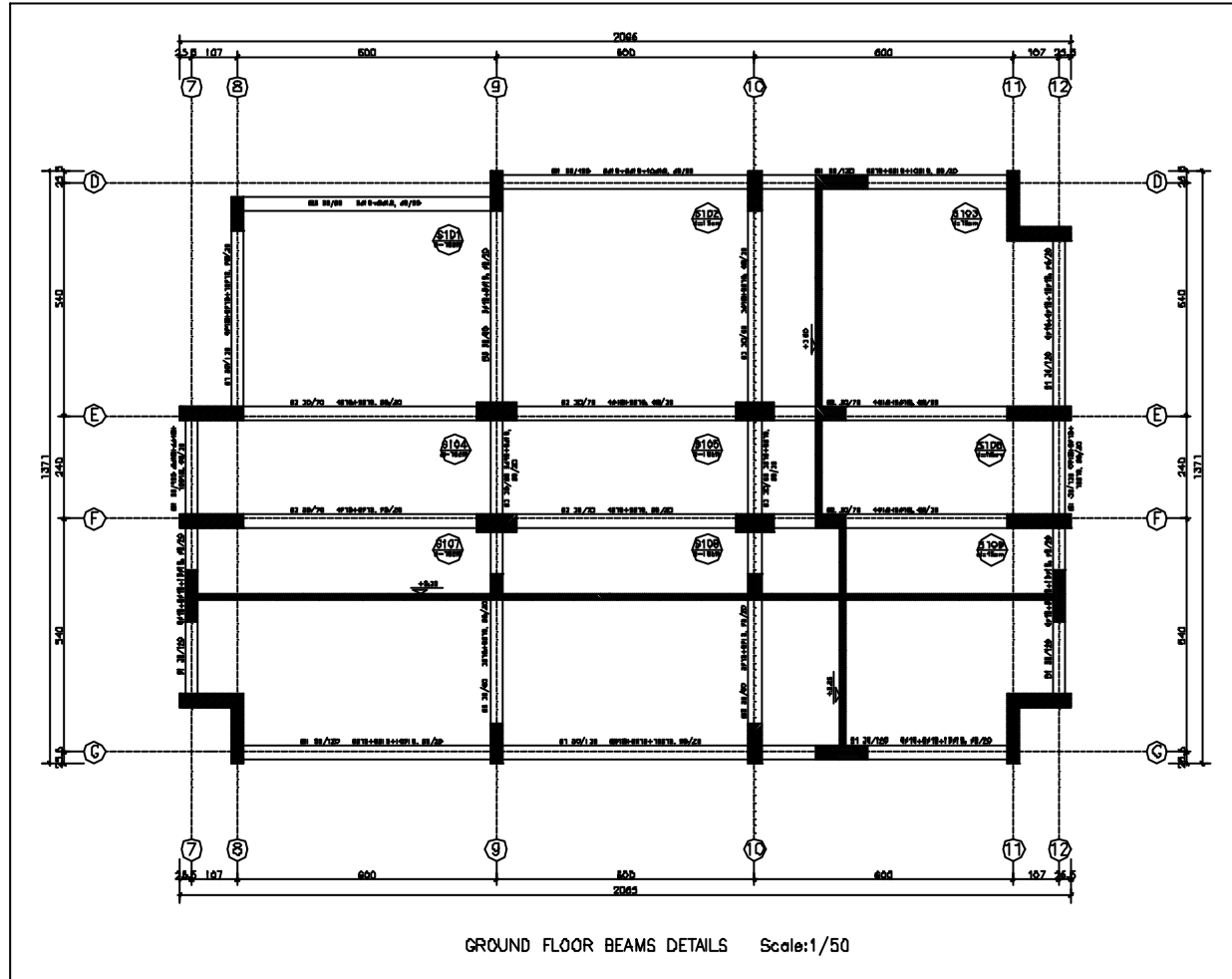


Figure C.2 Ground floor beams and slabs details

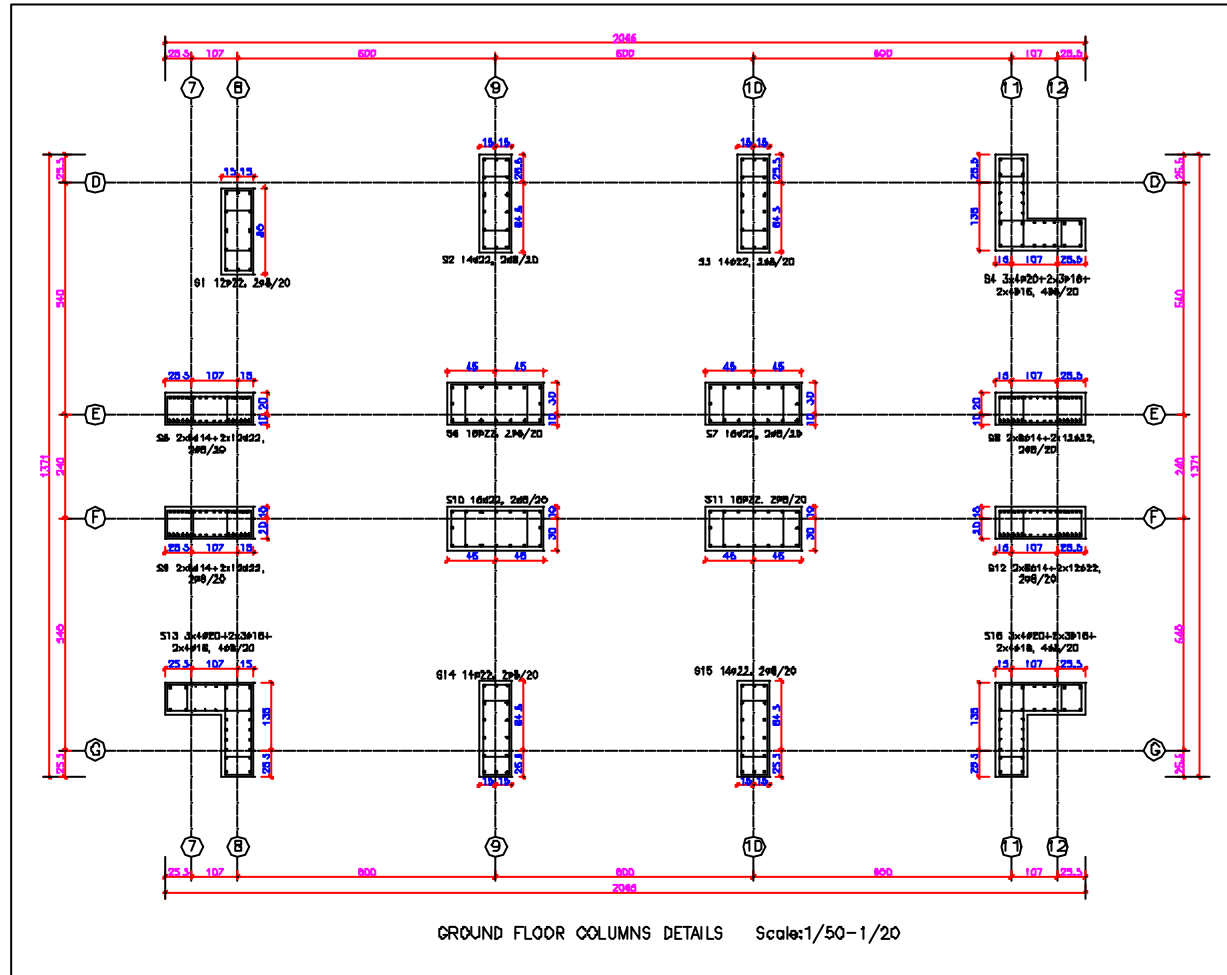


Figure C.3 Ground floor columns details

REFERENCES

1. Acar, F., Gülkan, P., 2003. "Low Cycle Fatigue and Seismic Structural Damage" Fifth National Conference on Earthquake Engineering, Paper No: AT-118, 26-30 May 2003, İstanbul, Turkey.
2. Boyutlandırma ve Malzeme Kalitesinin Önemi", Yapı Dünyası Dergisi, Ocak 2004, Vol. 94, s.19-28.
3. ATC, 1996. "Seismic Evaluation and Retrofit of Concrete Buildings", Applied Technology Council, ATC-40 Report, Volume I, Redwood City, California.
4. ATC, 1998a. "Evaluation of Earthquake Damaged Concrete and Masonry Wall Buildings, Basic Procedures Manual", Applied Technology Council (ATC-43 project), published by the Federal Emergency Management Agency, Report No. FEMA 306, Washington D.C.
5. ATC, 1998b. "Evaluation of Earthquake Damaged Concrete and Masonry Wall Buildings, Technical Resources", Applied Technology Council (ATC-43 project), published by the Federal Emergency Management Agency, Report No. FEMA 307, Washington D.C.
6. Araki, H., Shimazu, T., and Ohta, Kazuhiko, 1990. "On Residual Deformation of Structures after Earthquakes", Proceedings of the Eight Japan Earthquake Engineering Symposium-1990, Tokyo, Vol. 2, pp. 1581-1586. (In Japanese with English abstract)

7. Aschheim, M., Black, E., 1999. "Effects of Prior Earthquake Damage on Response of Simple Stiffness-degrading Structures", *Earthquake Spectra*, Vol.15, No. 1, pp. 1-24.
8. Banon, H., Biggs, J.M., Irvine, H.M., 1981. "Seismic Damage in Reinforced Concrete Frame", *Journal of Structural Engineering, ASCE*, Vol. 107, No. 9, pp. 1713-1729.
9. Düzce During The 12 November 1999 Düzce Earthquake", M.S. Thesis, Middle East Technical University, Department of Civil Engineering, Ankara, Turkey.
10. Bentz, E.C., and Collins, M.P., "RESPONSE 2000 - Reinforced Concrete Sectional Analysis" Department of Civil Engineering, University of Toronto.
11. Blume, J.A., Newmark, N.M., and Corning, L.H., " Design of Reinforced Concrete Buildings for Earthquake Motions" Portland Cement Association, Chicago 1961, 318 pp.
12. Building Code Requirements for Structural Concrete (ACI 318-1971)
13. Building Code Requirements for Structural Concrete (ACI 318-2002) and Commentary (ACI 318R - 2002)
14. Chai, Y. H., Romstad, K. M., 1997. "Correlation Between Strain Based Low Cycle Fatigue and Energy Based Linear Damage Models", *Earthquake Spectra*, Vol. 13, No. 2, pp. 191-209.
15. Chopra, A. K., 1995. *Dynamics of Structures : Theory and Applications to Earthquake Engineering*, Prentice-Hall Inc., New Jersey.
16. Chung, Y.S., Meyer, C., and Shinozuka, M., 1989. "Modeling of Damage", *ACI Structural Journal*, Vol. 86, No. 3, pp. 259-271.

17. Coffin, L.F., 1954. "A Study of Effects of Cyclic Thermal Stresses on Ductile
sactions of the American Society of Mechanical Engineers, Vol. 76,
pp. 931-950.
18. Collins, J.A., 1993. 'Failure of Materials in Mechanical Design : Analysis,
Prediction, Prevention' 2nd Ed. John Wiley, New York, 654 p.
19. Cosenza, E., Manfredi, G., 1992. "Seismic Analysis of Degrading Models by
means of Damage Functions Concept", Nonlinear Seismic Analysis and Design
of R/C Buildings, Elsevier Science Publishing Co., Inc., NY 10010, USA, pp. 77-
95.
20. Cosenza, E., Manfredi, G., 1996. "Seismic Design Based on Low Cycle Fatigue
Criteria", Eleventh World Conference on Earthquake Engineering, Paper
No.1141.
21.
Reinforced Concrete Frame Building in Bolu", M.S. Thesis, Middle East
Technical University, Department of Civil Engineering, Ankara, Turkey.
22. Çeçen, H., 1979. "Response of Ten-Story Reinforced Concrete Model Frames to
Simulated Earthquakes" Doctoral Thesis, Department of Civil Engineering,
University of Illinois at Urbana.
23. Dipasquale, E., Ju, J., Askar, A., Çakmak, A. S., 1990. "Relation Between Global
Damage Indices and Local Stiffness Degradation", Journal of Structural
Engineering, ASCE, Vol. 116, No. 5, pp. 1440-1456.
24. El-Bahy A., Kunnath, S.K., Stone, W.C., and Taylor, A.W., 1999. "Cumulative
Seismic Damage of Circular Bridge Columns: Benchmark and Low-cycle
Fatigue Tests", Proceedings, ACI Structural Journal, Vol. 96, No: 4, pp. 633-641.

25. El-Bahy A., Kunnath, S.K., Stone, W.C., and Taylor, A.W., 1999. "Cumulative Seismic Damage of Circular Bridge Columns: Variable Amplitude Tests", Proceedings, ACI Structural Journal, Vol. 96, No: 5, pp. 711-719.
26. Erberik, M.A., 2001. "Energy Based Seismic Evaluation of Degrading Systems", Ph.D. Thesis, Department of Civil Engineering, Middle East Technical University.
27. "Seismic Energy Dissipation in Deteriorating Systems Through Low-cycle Fatigue", Earthquake Engineering and Structural Dynamics, Vol. 33, pp. 49-67.
28. Erdik, M., Durukal, E., and Özbey, C., 2002. "Strong Ground Motion in 1999 Kocaeli and Düzce (Turkey) Earthquakes", Seventh U.S. National Conference on Earthquake Engineering, Boston.
29. Fajfar, P., 1992. "Equivalent Ductility Factors, Taking into Account Low-cycle Fatigue", Earthquake Engineering and Structural Dynamics, Vol. 21, pp. 837-848.
30. Ghobarah, A., Abou-Elfath, H., Biddah, A., 1999. "Response Based Damage Assessment of Structures", Earthquake Engineering and Structural Dynamics, Vol. 28, pp. 79-104.
31. Grzybowski, M., and Meyer, C., 1993. "Damage Accumulation in Concrete with and without Fiber Reinforcement" ACI Materials Journal, Vol.90, No.6, pp.594-604.
32. Gülkan, P., Sözen, M.A., 1999. "Procedure for Determining Seismic Vulnerability of Building Structures" Structural Journal, ACI, Vol.96, N.:3, pp.336-342.

33. Hanson, R.D., 1996. "The Evaluation of Reinforced Concrete Members Damaged by Earthquakes" *Earthquake Spectra*, Vol. 12, No. 3, Earthquake Engineering Research Institute, Oakland, California.
34. Hassiotis, S., and Jeong, G.D., 1993. "Assessment of Structural Damage from Natural Frequency Measurements", *Computers and Structures*, Vol. 49, pp. 679-691.
35. Kasiraj, I., and Yao, J.T.P., 1968, "Low-cycle Fatigue Failure of Seismic Structures", Technical Report, CE-11(68)NSF-065, University of New Mexico.
36. Krawinkler, H., and Zohrei, M., 1983. "Cumulative Damage in Steel Structures Subjected to Earthquake Ground Motions", *Computers and Structures*, Vol. 16, No.1-4, pp. 531-541.
37. Krawinkler, H., 1996. "Cyclic Loading Histories for Seismic Experimentation on Earthquake Spectra, Vol.12, No.1.
38. Kunnath, S.K., Reinhorn, A.M., and Park, Y.-J., 1990. "Analytical Modeling of Inelastic Seismic Response of R/C Structures", *Journal of Structural Engineering*, ASCE, Vol. 116, No. 4, Apr. 1990, pp. 996-1017.
39. Lew, H.S., 1997. "Evaluation of Seismic Performance Parameters" *Seismic Design Methodologies for the Next Generation of Codes*, Fajfar and Krawinkler (eds), Balkema, Rotterdam, pp.151-157.
40. Mahin, S.A., 1980. "Effects of Duration and Aftershocks on Inelastic Design Earthquakes", *Proceedings of the Seventh World Conference on Earthquake Engineering*, Vol. 5, pp. 677-679.
41. Manfredi, G., and Pecce, M., 1996. "Low Cycle Fatigue of RC Beams in NSC and HSC", *Engineering Structures*, Vol.19, No.3, pp. 217-223

42. Manson, S.S., 1953. "Behavior of Materials under Conditions of Thermal Stress", Heat Transfer Symposium, Engineering Research Institute, Ann Arbor, pp. 9-75.
43. McCabe, S.L., Hall, W.J., 1989. "Assessment of Seismic Structural Damage" Journal of Structural Engineering, ASCE, Vol. 115, No. 9, pp. 2166-2183.
44. Miner, M. A., 1945. "Cumulative Damage in Fatigue", Journal of Applied Mechanics, Vol.12, pp. 159-164.
45. -
dimensional Maximum Damage Indicators for Reinforced Concrete Structures under Seismic Excitation", Soil Dynamics and Earthquake Engineering, Vol. 1, pp. 435-443.
46. Park, P., and Paulay, T., 1975. "Reinforced Concrete Structures" John Wiley & Sons, New York.
47. Park, Y.-J., and Ang, A. H.-S., 1985. "Mechanistic Seismic Damage Model for Reinforced Concrete" Journal of Structural Engineering, ASCE, Vol. 111, No. 4, Apr. 1985, pp. 722-739.
48. Park, Y.-J., Ang, A. H.-S., and Wen, Y.K., 1985 "Seismic Damage Analysis of Reinforced Concrete Buildings" Journal of Structural Engineering, ASCE, Vol. 111, No. 4, Apr. 1985, pp. 740-757.
49. Pfrang, E.O., Siess, C.P. and Sözen, M.A. "Load-Moment-Curvature Characteristics of Reinforced Concrete Cross Sections" Journal ACI, Vol. 61, No.7, July 1964, pp.763-778.
50. Powell, G.H., Allahabadi, R., 1988. "Seismic Damage Prediction by Deterministic Methods: Concepts and Procedures" Journal of Earthquake Engineering and Structural Dynamics, Vol. 16, pp. 719-734.

51. Pujol, S., 2002, "Drift Capacity of Reinforced Concrete Columns Subjected to Displacement Reversals" Ph.D. Thesis, Purdue University, IN.
52. Saiidi, M., 1980. "Influence of Hysteresis Models on Calculated Seismic Response of R/C Frames", Proceedings of the Seventh World Conference on Earthquake Engineering, Vol. 5, pp. 423-430.
53. Sözen, M. A., 1981. "Review of Earthquake Response of R. C. Buildings with a View to Drift Control", State of the Art in Earthquake Engineering, State-of-the-Art Panel Reports Prepared for the Occasion of Seventh World Conference on Earthquake Engineering, İstanbul, Turkey, pp.383-418.
54. Sözen, M. A., 2000. "Measured Ground Shaking and Observed Damage: Do Recent Events Confirm a Direct Connection?", Earthquake Engineering Frontiers in the New Millennium : Proceedings of the China-US Millennium Symposium on Earthquake Engineering, 8-11 November 2000, Beijing, China, pp.43-56.
55. Specification for Structures to be Built in Disaster Areas (Afet Bölgelerinde Yapılacak Yapılar Hakkında Yönetmelik), (TEC) 1998. Ministry of Public Works and Settlement, Ankara, Turkey.
56. Stephens, J. E., Yao, J. T. P., 1987. "Damage Assessment Using Response Measurements", Journal of Structural Engineering, ASCE, Vol. 113, No. 4, pp. 787-801.
57. Stone, W.C., Taylor, A.W., 1993. "Seismic Performance of Circular Bridge Columns Designed in Accordance with AASHTO/CALTRANS standards, NIST Building Science Series 170, National Institute of Standards and Technology, Gaithersburg MD.

58. Sucuođlu, H., Erberik, M.A., 2004, "Energy-based Hysteresis and Damage Models for Deteriorating Systems", Earthquake Engineering and Structural Dynamics, Vol. 33, pp. 69-88.
59. Sucuođlu, H., Gülkan, P., Yılmaz, Ç., Bakýr, S., Özcebe, G., Ersoy, U., Tankut, T., Gür, T., Yılmaz, T., Erberik, A., Akkar, S., 2000, "Engineering Report of Marmara and Düzce Earthquakes", METU-EERC Report, Ankara, Turkey.
60. Sucuođlu, H., and Yılmaz, T., 2001. "Düzce, Turkey: A City Hiy by Two Major Earthquakes", Seismological Research Letters, Vol.72 No.6, pp. 679-689.
61. Suresh, S., 1991. Fatigue of Materials, Cambridge Solid State Science Series, pp. 2-13 and 126-140.
62. Tekada, T., Sözen, M. A., and Nielsen, N. N., 1970. "Reinforced Concrete Response to Simulated Earthquakes", Journal of the Structural Division, ASCE, No. ST12, pp. 2557-2573.
63. The Institute of Turkish Standards, 2000. Turkish Standards for Reinforced Concrete Structures (TS500), Ankara, Turkey.
64. Valles, R.E., Reinhorn, A.M., Kunnath, S.K., Li, C., and Madan, A., 1996. "IDARC 2D Version 4.0: A Program for the Inelastic Damage Analysis of Buildings", Technical Report NCEER-96-0010, State University of New York at Buffalo.
65. United States Geological Survey (USGS), 1999. "Implications for Earthquake Risk Reduction in The United States from the Kocaeli, Turkey, Earthquake of August 17, 1999", U.S. Geological Survey Circular 1193.
66. Wight, J. K., and Sözen, M. A., 1973. "Shear Strength Decay in Reinforced Concrete Columns Subjected to Large Deformation Reversals", Technical Report Structural Research Series No. 403, University of Illinois, Urbana, I11.

67. Williams, M.S., Sexsmith, R.G., 1995. "Seismic Damage Indices for Concrete Structures: A State-of-the-art Review", *Earthquake Spectra*, Vol. 11, No. 2, pp. 319-349.
68. Williams, M.S., Villemure, I., and Sexsmith, R.G., 1997. "Evaluation of Seismic Damage Indices for Concrete Elements Loaded in Combined Shear and Flexure", *ACI Structural Journal*, Vol. 94, Issue 3, pp. 315-322.
69. Wolschlag, C., 1993. "Experimental Investigation of the response of R/C Structural Walls Subjected to Static and Dynamic Loading", Doctoral Thesis, Department of Civil Engineering, University of Illinois at Urbana.
70. Xie, L.L., and Zhang, X., 1998, "Engineering Duration of Strong Motion and its Effects on Seismic Damage", *Proceedings of the Ninth World Conference on Earthquake Engineering*, Vol. 2, Paper : 3-2-7.

VITA

Fikri Acar was born in Midyat, on November 20, 1971. He received his B.S. degree, from Civil Engineering Department of Selçuk University in June 1993, as being the first student. He received his M.S. degree in Civil Engineering from the Middle East Technical University in August 1997. He worked as a research assistant in K y kkale University, Civil Engineering Department from 1994 to 2000. Since then he has been an Inspector in the Inspection Board of Ministry of Public Works and Settlement. His research interests include structural damage, inelastic behavior and damage-based design of concrete structural systems and seismic rehabilitation of damaged reinforced concrete and masonry buildings.